Quantitative MRI markers for the brain at risk

Lisa Annette van der Kleij

Quantitative MRI markers for the brain at risk

Lisa Annette van der Kleij

Quantitative MRI markers for the brain at risk
PhD Thesis, Utrecht University, the Netherlands

Cover and illustrations design:	Marleen van den End
Lay-out design:	Lisa Annette van der Kleij
Printed by:	Ridderprint
ISBN:	978-90-393-7194-7

This research is supported by the European Research Council.

Financial support for the publication of this thesis was generously provided by the Hartstichting and Alzheimer Nederland.

Financial support for the publication of this thesis from ChipSoft B.V. is gratefully acknowledged.

Quantitative MRI markers for the brain at risk

Kwantitatieve MRI markers voor het kwetsbare brein

(met een samenvatting het Nederlands)

Proefschrift

ter verkrijging van de graad van doctor aan de Universiteit Utrecht op gezag van de rector magnificus, prof.dr. H.R.B.M. Kummeling, ingevolge het besluit van het college voor promoties in het openbaar te verdedigen op donderdag 24 oktober 2019 des middags te 4.15 uur

door

Lisa Annette van der Kleij

geboren op 13 november 1990 te 's-Gravenhage

Promotor: Prof. dr. J. Hendrikse

Copromotoren: Dr. J.B. De Vis
Dr. E.T. Petersen

für Opa Josef Hüttner

mein Beispiel für die Freude am Lernen und die Kraft der Ausdauer
for showing me the joy of learning and the power of perseverence

25. Dezember 1924, Frühbuß (Přebuz) - 29. Dezember 2018, Coburg

Contents

Chapter 1

General introduction

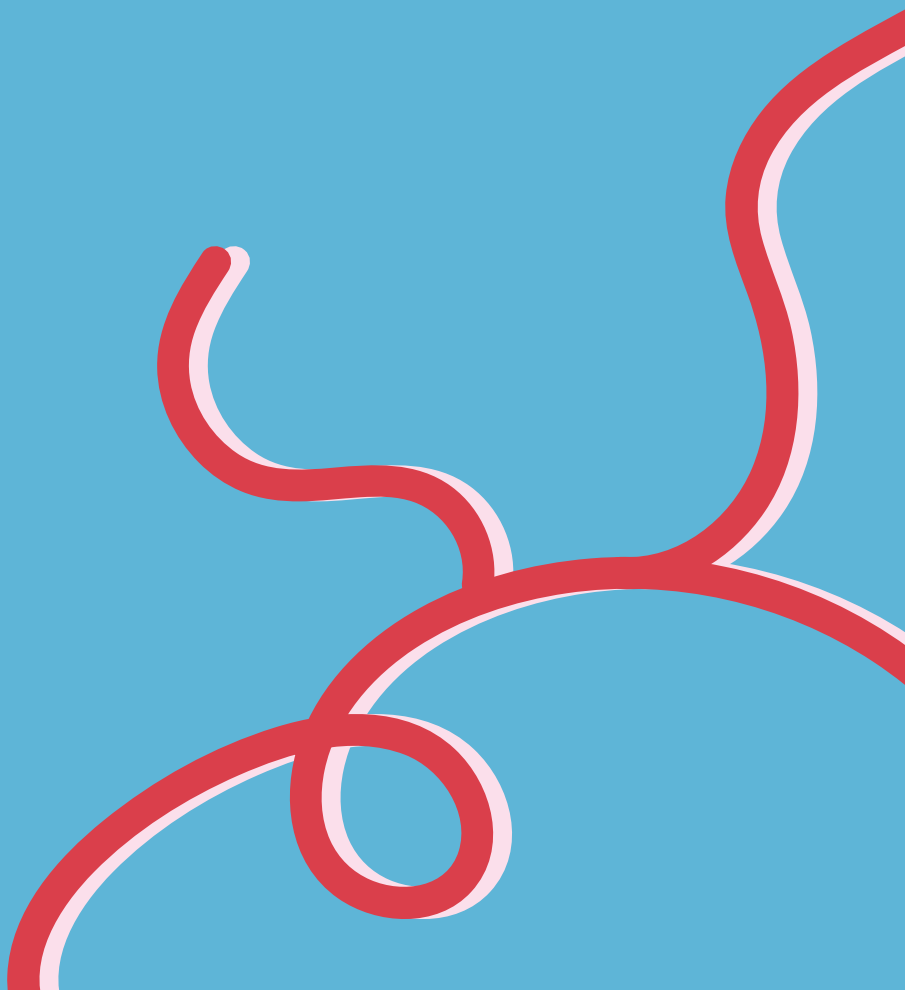

Since the publication of the first human magnetic resonance images in the late 1970s, the imaging modality has been established as a pillar of modern radiology. Improvements in hardware and sequence design continue to increase and optimize the possibilities of MRI; for example, they have enabled the imaging of brain function alongside structural images. This capability to analyze function and structure – with MRI's superior soft tissue contrast – opens doors to better diagnoses and a better understanding of brain pathologies.

MR images can be analyzed qualitatively or quantitatively. A qualitative approach carries the advantage of a relatively quick analysis without mandatory postprocessing. In a clinical setting, a qualitative image reading is generally adequate to identify salient pathology and abnormalities. Further, the use of rating scales allows semi-quantitative categorization of imaging characteristics, for instance the degree of white matter hyperintensity severity.[1] Nonetheless, qualitative readings are prone to inter- and intrarater variability, because they depend on a reader's interpretation and expertise. In comparison, a quantitative image analysis requires additional postprocessing, but it also facilitates an objective and more precise assessment, identification of subtle details, and pooling of data. In this thesis, I investigate the following quantitative MRI markers: cerebral blood flow (CBF), transverse relaxation time of peripheral cerebrospinal fluid ($T2_{pCSF}$) and brain volume measurements. All three markers can offer information on brain health and disease severity in cross-sectional and longitudinal studies. Brain volume and CBF are well-established MRI markers, whereas $T2_{pCSF}$ has not (yet) been established as a clinically relevant marker. I specifically focus on two pathologies marked by a considerable risk of future decline without a clear understanding of patient characteristics associated with poor outcome: subarachnoid hemorrhage and cognitive impairment/dementia. The investigated MRI markers may contribute to a better understanding of both pathologies and may characterize patients at risk for further decline. As well, I look at the use of cerebral blood flow measurements as an outcome measure in randomized trials.

Part 1: Identifying the impact of brain injury beyond conventional methods

Cerebral blood flow and structural brain injury in subarachnoid hemorrhage

Aneurysmal subarachnoid hemorrhage

The first part of this thesis focuses on the application of two markers in subarachnoid hemorrhage. Chapters 2 - 5 deal with aneurysmal subarachnoid hemorrhage (aSAH), which is a subtype of hemorrhage caused by rupture of a cerebral aneurysm. An aneurysm is a localized bulging of an artery due to a weakened vessel wall, which has

a berry-like shape in the majority of cases (Figure 1). aSAH affects a relatively young patient population with a median patient age of 55 years.[2] Moreover, the disease bears a poor prognosis; 70% of patients survive the first 90 days,[3] and only 60% of survivors can continue to function independently in daily live.[4] Even among survivors that regain functional independence, many experience long-term cognitive complaints and a decreased health-related quality of life.[5] Taken together this results in a large burden of aSAH on patients, their caregivers and society. Factors that can contribute to a poor prognosis are not always modifiable, such as patient age or the amount of extravasated blood on admission.[6] Yet the disease trajectory of aSAH provides an opportunity for preventative treatment for improved outcome even after aneurysm rupture.

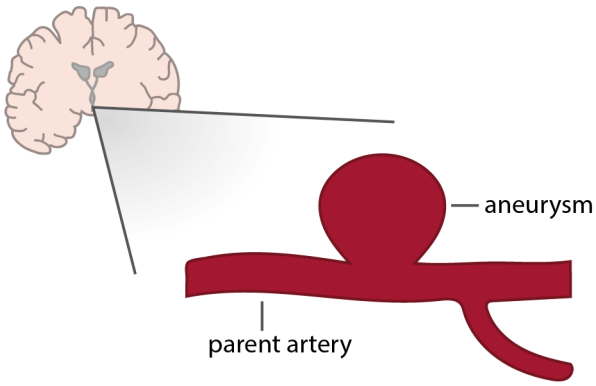

Fig. 1. Schematic illustration of a cerebral saccular (berry) aneurysm. Saccular aneurysms are typically located at the base of the brain around the circle of Willis.

The time trajectory after aSAH can be categorized in three stages: the acute stage, subacute stage and chronic stage. Before we look into the quantitative markers, systematic review chapters 2 and 3 provide an overview of brain injury throughout all disease stages. **Chapter 2** deals with brain injury on diffusion weighted imaging in the acute and subacute stages after aSAH. Diffusion weighted imaging is an MRI technique sensitive to early ischemia, because it detects the associated lower water mobility.[7] A review of cerebral infarction and volume changes in the chronic stage after aSAH is presented in **chapter 3**. Brain injury after aSAH can arise from (1) the initial insult, (2) the aneurysm securing procedure, and (3) delayed brain injury, which generally occurs between 4 and 14 days after ictus. Currently, delayed brain injury affects 1 in 4 patients and it is a major cause of poor outcome and death after aSAH.[8-10] Thus, additional treatment options are warranted.

The next three chapters in Part 1 focus on quantitative MRI markers in subarachnoid hemorrhage. The aim of **chapter 4** was to identify factors that carry a higher risk of long-term brain volume change. In the chapter, we explore the relationship between perfusion heterogeneity around day 14 post ictus, clinical characteristics and brain

volume changes after 6 and 18 months. The study is based on research that demonstrated a predictive value of perfusion heterogeneity for delayed brain injury and poor functional outcome after aSAH.[11, 12] The longitudinal study design in chapter 4 enabled a direct evaluation of the relationship between subacute perfusion heterogeneity and long-term brain volume changes. As perfusion heterogeneity is modifiable by pharmacological intervention, we interpreted the results of chapter 4 as an opportunity to possibly minimize long-term damage. **Chapter 5** describes the study protocol of the ongoing phase II trial, in which we evaluate the efficacy and safety of acetazolamide treatment after aSAH (ASH trial). We hypothesize that acetazolamide can benefit aSAH patients via three combined actions, as it can (1) increase cerebral blood flow through vasodilation, (2) reduce CSF production and (3) reduce cerebral edema.

Traumatic brain injury

Chapter 6 applies the findings from chapter 4 regarding perfusion and volume changes following aSAH to a different patient population: traumatic brain injury (TBI) patients. TBI and aSAH patients share some common characteristics, so we hypothesized that the observations from aSAH patients may apply to individuals suffering from TBI. First, TBI patients are relatively young with a mean age of 60 years in the United States although it affects people of all ages.[13] Second, TBI is also associated with a chronically decreased brain volume.[14, 15] Third, perfusion impairment is commonly observed in the acute and subacute phase after trauma, and a correlation has been found between perfusion impairment and decreased brain volume after TBI.[16, 17] Finally, subarachnoid hemorrhage due to trauma has been associated with poor functional outcome.[18] Yet, the relationship between SAH and brain volume change is unknown. As mild symptoms on admission are no guarantee of full functional recovery, the question arises which factors can distinguish patients at risk for poor outcome and future decline.[19] Chapter 6 evaluates whether cerebral perfusion and subarachnoid hemorrhage are associated with brain volume changes after TBI.

Part 2: vascular components in aging and dementia

Cerebral blood flow, T2 of peripheral CSF and brain volumetrics in healthy aging – mild cognitive impairment - dementia

Our increasingly aging population poses a big challenge for the 21^{rst} century.[20] To illustrate, the highest life expectancy for women increased from 45 years (Sweden) to 85 years (Japan) in only 160 years.[20, 21] Importantly, this increase in life expectancy does not automatically mean that age-related health is also increasing: among other pathologies, an increased life expectancy is also linked to an increase in dementia prevalence.[22, 23] The second part of this thesis investigates the three quantitative markers in

patients along the spectrum spanning healthy aging to dementia.

Age-related health is a continuum on which people with the least loss in function are referred to as the most successful agers.[24] Evidently, who is categorized as a successful ager depends on the observer and the criteria used. The concept of healthy aging – also dubbed successful aging – can be approached from various perspectives, such as the medical, psychological or societal perspective. From a medical perspective the concept of healthy aging is often tied to the avoidance of chronic illness, although in recent years it has been recognized that individuals with chronic illness can still consider themselves healthy.[25] Factors influencing healthy aging can be divided in three broad categories: physiological, cognitive/mental, and social/support.[25] The chapters in this thesis focus on the physiological factors associated with (healthy) aging. Over the life span, differences in these factors cause highly variable health levels between individuals with the same chronological age, which has been referred to as a difference in biological age.[26] Biological age is defined as the widely varying health and associated predicted mortality in individuals with the same chronological age.[27] Therefore, the recruited study population of **chapter 7** provided an exciting opportunity, because the participants were community-dwelling individuals between 62 to 70 years old.[28] The narrow age range allowed us to explore the relationship between cerebrovascular risk factors, physical fitness and cerebral blood flow – usually all associated with age – in a large cohort representative of the general population with a minimal expected contribution of age to the results.[29]

In the next two chapters we transition from a 'healthy' study population to study populations with cognitive impairment to investigate the three quantitative markers in a clinical setting. Cerebral blood flow, $T2_{pCSF}$ and brain volume could all provide additional information on brain health. Several studies have shown that cerebral atrophy and CBF are associated with disease severity as well as future cognitive decline.[30-32] We propose that, like CBF, $T2_{pCSF}$ could indicate a lower energy demand and cerebrovascular dysfunction. The hypothesis is based on a higher $T2_{pCSF}$ among demented elderly compared to healthy elderly in previous research from our group, which was attributed to lowered oxygenation of the peripheral subarachnoid space in the demented elderly group.[33] **Chapter 8** evaluates the additional value of the $T2_{pCSF}$ over atrophy and CBF to assess disease severity in a cohort of patients with varying levels of cognitive decline. The study sample was recruited from a memory clinic, and their disease severity ranged from subjective cognitive complaints to mild cognitive impairment and dementia.[34]

Finally, in **chapter 9** we investigate the effect of a moderate-to-high intensity aerobic exercise program on cerebral blood flow in patients with mild to moderate Alzheimer's disease. Physical exercise could be a non-pharmacological disease modifying treat-

ment, because it has been shown to both mitigate the effect of age on CBF and improve cognition in healthy individuals.[35-37] As part of the prospective, randomized ADEX trial,[38] Alzheimer's disease patients underwent MRI at baseline and after the 16 week exercise intervention program.

Part 3: methods

Arterial spin labeling, CSF MRI, and brain volumetric analysis

The chapters in part 3 describe the methods used in this thesis to explore quantitative markers of the brain at risk. **Chapter 10** can be used as a reference for cerebral blood flow measurements with arterial spin labeling (ASL) MRI. ASL is a non-invasive method to measure CBF by using blood water labeled at the neck level as an endogenous tracer.[39] The chapter offers a practical overview of ASL, and presents both research and clinical applications of the technique. **Chapter 11** can be used as a reference for the CSF MRI sequence and brain segmentation software used throughout this thesis. Other than the previously discussed $T2_{pCSF}$ measure, the one-minute CSF MRI sequence can also be used to simultaneously obtain intracranial volumes. In this chapter we investigate the precision of the CSF MRI cerebral volume measurements and validate the obtained volumes by comparison with conventional 3DT1w-based brain segmentation methods. **Chapter 12** explores the feasibility of structural MRI to detect adaptive cerebral volume changes during hypercapnia. Hypercapnia – increased blood CO_2 levels – causes vasodilation and thereby increased cerebral blood volume.[40] Burrow's correction of the Monro-Kellie doctrine states that an increase in cerebral blood volume is accompanied by an outflow of CSF to maintain a stable pressure within in fixed cranium.[41] Inspired by the Monro-Kellie hypothesis, we examine volume changes in gray matter, white matter and CSF in response to cerebral blood volume increases due to hypercapnia. The results could serve as a reference for the degree to which physiological changes can influence (our) volumetric MRI study results.

The results of this thesis are summarized and discussed in **chapter 13**.

References

1. Fazekas F, Chawluk JB, Alavi A, Hurtig HI, Zimmerman RA. Mr signal abnormalities at 1.5 t in alzheimer's dementia and normal aging. American journal of roentgenology. 1987;149:351-356
2. Anderson C, Hankey G, Jamrozik K, Dunbabin D. Epidemiology of aneurysmal subarachnoid hemorrhage in australia and new zealand: Incidence and case fatality from the australasian cooperative research on subarachnoid hemorrhage study (across). Stroke. 2000;31:1843-1850
3. Vergouwen MDI, Jong-Tjien-Fa AV, Algra A, Rinkel GJE. Time trends in causes of death after aneurysmal subarachnoid hemorrhage. A hospital-based study. 2016;86:59-63
4. Zacharia BE, Hickman ZL, Grobelny BT, DeRosa P, Kotchetkov I, Ducruet AF, et al. Epidemiology of aneurysmal subarachnoid hemorrhage. Neurosurgery Clinics. 2010;21:221-233
5. Passier P, Visser-Meily J, van Zandvoort M, Rinkel G, Lindeman E, Post M. Predictors of long-term health-related quality of life in patients with aneurysmal subarachnoid hemorrhage. NeuroRehabilitation. 2012;30:137-145
6. Rosengart Axel J, Schultheiss Kim E, Tolentino J, Macdonald RL. Prognostic factors for outcome in patients with aneurysmal subarachnoid hemorrhage. Stroke. 2007;38:2315-2321
7. Gass A, Ay H, Szabo K, Koroshetz WJ. Diffusion-weighted mri for the "small stuff": The details of acute cerebral ischaemia. The Lancet Neurology. 2004;3:39-45
8. van Gijn J, Kerr RS, Rinkel GJE. Subarachnoid haemorrhage. The Lancet. 2007;369:306-318
9. Roos YBWEM, de Haan RJ, Beenen LFM, Groen RJM, Albrecht KW, Vermeulen M. Complications and outcome in patients with aneurysmal subarachnoid haemorrhage: A prospective hospital based cohort study in the netherlands. Journal of Neurology, Neurosurgery & Psychiatry. 2000;68:337-341
10. Connolly ES, Rabinstein Alejandro A, Carhuapoma JR, Derdeyn Colin P, Dion J, Higashida Randall T, et al. Guidelines for the management of aneurysmal subarachnoid hemorrhage. Stroke. 2012;43:1711-1737
11. Mustonen T, Koivisto T, Vanninen R, Hänninen T, Vapalahti M, Hernesniemi J, et al. Heterogeneity of cerebral perfusion 1 week after haemorrhage is an independent predictor of clinical outcome in patients with aneurysmal subarachnoid haemorrhage. Journal of Neurology, Neurosurgery & Psychiatry. 2008;79:1128-1133
12. Lanterna LA, Lunghi A, Martchenko S, Gritti P, Bonaldi G, Biroli F. Cerebral watershed hypoperfusion in subarachnoid hemorrhage: Computed tomography perfusion analysis. 2011;114:961
13. DiMaggio C, Ayoung-Chee P, Shinseki M, Wilson C, Marshall G, Lee DC, et al. Traumatic injury in the united states: In-patient epidemiology 2000–2011. Injury. 2016;47:1393-1403
14. Irimia A, Chambers MC, Alger JR, Filippou M, Prastawa MW, Wang B, et al. Comparison of acute and chronic traumatic brain injury using semi-automatic multimodal segmentation of mr volumes. J Neurotrauma. 2011;28:2287-2306
15. MacKenzie JD, Siddiqi F, Babb JS, Bagley LJ, Mannon LJ, Sinson GP, et al. Brain atrophy in mild or moderate traumatic brain injury: A longitudinal quantitative analysis. American Journal of Neuroradiology. 2002;23:1509-1515
16. Bendinelli C, Cooper S, Evans T, Bivard A, Pacey D, Parson M, et al. Perfusion abnormalities are frequently detected by early ct perfusion and predict unfavourable outcome following severe traumatic brain injury. World Journal of Surgery. 2017;41:2512-2520
17. Xu Y, McArthur DL, Alger JR, Etchepare M, Hovda DA, Glenn TC, et al. Early nonischemic oxidative metabolic dysfunction leads to chronic brain atrophy in traumatic brain injury. J Cereb Blood Flow Metab. 2010;30:883-894
18. Wardlaw JM, Easton VJ, Statham P. Which ct features help predict outcome after head injury? Journal of Neurology, Neurosurgery & Psychiatry. 2002;72:188-192
19. McMahon P, Hricik A, Yue JK, Puccio AM, Inoue T, Lingsma HF, et al. Symptomatology and functional outcome in mild traumatic brain injury: Results from the prospective track-tbi study. J Neurotrauma. 2014;31:26-33
20. World Health Organization. World report on ageing and health. World Health Organization; 2015.
21. Oeppen J, Vaupel JW. Broken limits to life expectancy. Science. 2002;296:1029-1031

22. Prince M, Bryce R, Albanese E, Wimo A, Ribeiro W, Ferri CP. The global prevalence of dementia: A systematic review and metaanalysis. Alzheimer's & Dementia. 2013;9:63-75.e62
23. Ferrucci L, Giallauria F, Guralnik JM. Epidemiology of aging. Radiologic Clinics of North America. 2008;46:643-652
24. Schulz R, Heckhausen J. A life span model of successful aging. American psychologist. 1996;51:702
25. Hansen-Kyle L. A concept analysis of healthy aging. Nursing Forum. 2005;40:45-57
26. Mitnitski A, Howlett SE, Rockwood K. Heterogeneity of human aging and its assessment. Journals of Gerontology Series A: Biomedical Sciences and Medical Sciences. 2016;72:877-884
27. Chen BH, Marioni RE, Colicino E, Peters MJ, Ward-Caviness CK, Tsai P-C, et al. DNA methylation-based measures of biological age: Meta-analysis predicting time to death. Aging (Albany NY). 2016;8:1844
28. Eriksen CS, Garde E, Reislev NL, Wimmelmann CL, Bieler T, Ziegler AK, et al. Physical activity as intervention for age-related loss of muscle mass and function: Protocol for a randomised controlled trial (the lisa study). BMJ Open. 2016;6:e012951
29. Chen JJ, Rosas HD, Salat DH. Age-associated reductions in cerebral blood flow are independent from regional atrophy. NeuroImage. 2011;55:468-478
30. Jack Jr CR, Wiste HJ, Vemuri P, Weigand SD, Senjem ML, Zeng G, et al. Brain beta-amyloid measures and magnetic resonance imaging atrophy both predict time-to-progression from mild cognitive impairment to alzheimer's disease. Brain. 2010;133:3336-3348
31. Binnewijzend MA, Kuijer JP, Benedictus MR, van der Flier WM, Wink AM, Wattjes MP, et al. Cerebral blood flow measured with 3d pseudocontinuous arterial spin-labeling mr imaging in alzheimer disease and mild cognitive impairment: A marker for disease severity. Radiology. 2013;267:221-230
32. Chao LL, Buckley ST, Kornak J, Schuff N, Madison C, Yaffe K, et al. Asl perfusion mri predicts cognitive decline and conversion from mci to dementia. Alzheimer Dis Assoc Disord. 2010;24:19-27
33. De Vis J, Zwanenburg J, van der Kleij L, Spijkerman J, Biessels G, Hendrikse J, et al. Cerebrospinal fluid volumetric mri mapping as a simple measurement for evaluating brain atrophy. European radiology. 2016;26:1254-1262
34. Aalten P, Ramakers IH, Biessels GJ, de Deyn PP, Koek HL, OldeRikkert MG, et al. The dutch parelsnoer institute - neurodegenerative diseases; methods, design and baseline results. BMC Neurology. 2014;14:254
35. Ainslie PN, Cotter JD, George KP, Lucas S, Murrell C, Shave R, et al. Elevation in cerebral blood flow velocity with aerobic fitness throughout healthy human ageing. The Journal of physiology. 2008;586:4005-4010
36. Lucas SJ, Ainslie PN, Murrell CJ, Thomas KN, Franz EA, Cotter JD. Effect of age on exercise-induced alterations in cognitive executive function: Relationship to cerebral perfusion. Experimental gerontology. 2012;47:541-551
37. Groot C, Hooghiemstra A, Raijmakers P, Van Berckel B, Scheltens P, Scherder E, et al. The effect of physical activity on cognitive function in patients with dementia: A meta-analysis of randomized control trials. Ageing research reviews. 2016;25:13-23
38. Hoffmann K, Frederiksen KS, Sobol NA, Beyer N, Vogel A, Simonsen AH, et al. Preserving cognition, quality of life, physical health and functional ability in alzheimer's disease: The effect of physical exercise (adex trial): Rationale and design. Neuroepidemiology. 2013;41:198-207
39. Williams DS, Detre JA, Leigh JS, Koretsky AP. Magnetic resonance imaging of perfusion using spin inversion of arterial water. Proceedings of the National Academy of Sciences. 1992;89:212-216
40. Yoon S, Zuccarello M, Rapoport RM. Pco2 and ph regulation of cerebral blood flow. Frontiers in physiology. 2012;3:365
41. Burrows G. An disorders of the cerebral circulation; and on the connection between affections of the brain and diseases of the heart. Longman; 1846.

Part I

Identifying the impact of brain injury beyond conventional methods

Cerebral blood flow and structural brain injury in subarachnoid hemorrhage

Chapter 2

MRI and cerebral ischemia after aneurysmal subarachnoid hemorrhage: a systematic review and meta-analysis

L.A. van der Kleij[1], J.B. De Vis[1], J.M. Olivot[2], L. Calviere[2], C. Cognard[3], N.P.A. Zuithoff[4], G.J.E. Rinkel[5], J. Hendrikse[1], M.D.I. Vergouwen[5]

[1] Department of Radiology, University Medical Center Utrecht, The Netherlands
[2] Department of Neurology, University of Toulouse, France.
[3] Department of Radiology, University of Toulouse, France.
[4] Julius Center for Health Sciences and Primary Care, University Medical Center Utrecht, the Netherlands.
[5] Department of Neurology and Neurosurgery, Brain Center Rudolf Magnus, University Medical Center Utrecht, The Netherlands.

Stroke 48.1(2017): 239-245.

Introduction

The prognosis of aneurysmal subarachnoid hemorrhage (aSAH) has improved over the last decades. However, a recent hospital-based study showed that 90-day case-fatality is still 30%.[1] Determinants of functional outcome after aSAH may include the severity of the initial hemorrhage, rebleeding of the aneurysm, and cerebral ischemia which can be distinguished into: (1) acute ischemia at the time of bleeding when intracranial pressure rises and cerebral perfusion pressure drops; (2) procedure-related ischemia from endovascular or neurosurgical treatment of the aneurysm; and (3) delayed cerebral ischemia (DCI) which can occur between days 4 and 14 after the hemorrhage.[2, 3]

Magnetic resonance diffusion weighted imaging (MRI-DWI) is increasingly used for the evaluation of ischemia after aSAH. The aims of the present review were: 1) to analyze the proportion of patients with MRI-DWI lesions within 72 hours after aSAH, both before and after aneurysm treatment; 2) to study determinants of MRI-DWI lesions within 72 hours after aSAH; 3) to analyze the proportion of patients with MRI-DWI lesions between 72 hours and 21 days after aSAH; 4) to investigate the predictive value of MRI-DWI lesions within 72 hours for the development of DCI; and 5) to investigate if MRI-DWI can be used for the diagnosis of DCI in patients with clinical deterioration.

Methods

Search strategy

We searched the PUBMED, EMBASE, and Web of Science databases with the following combination of variables: (MRI OR magnetic resonance) and (subarachnoid hemorrhage OR SAH OR DCI OR delayed cerebral ischemia OR DIND). The last search was performed June 28, 2016. Only studies published after 01/01/2000 were included to assure a similar degree of image quality given the technical developments in MRI hardware and sequences. Both prospective and retrospective studies were included. Eligible articles were identified according to the PICO criteria. Type of patient population (P): 1) >95% of patients had aneurysmal SAH, defined as the presence of subarachnoid blood as shown by CT or lumbar puncture and the presence of an aneurysm on CT angiography, magnetic resonance angiography, or digital subtraction angiography; and 2) ≥10 patients had MRI-DWI performed <72 hours or between 72 hours and 21 days after ictus. Intervention (I): MRI scan performed ≤21 days after SAH. The MRI protocol included Diffusion Weighted Imaging (DWI). Comparator (C): N/A. Outcomes (O): MRI-DWI lesions assessed either <72 hours or between 72 hours and 21 days after ictus. Exclusion criteria were: 1) Manuscript written in another language than English, French, German, Spanish, Italian, Portuguese, or Dutch; 2) Conference abstract; 3) Animal study; 4) MRI was performed after elimination of the aneurysm with carotid artery occlusion

and subsequent bypass surgery; 5) MRI-DWI lesions were only presented for patients with angiographic vasospasm. Two authors (J.D.V. and L.v.d.K) screened the articles by title and abstract. Disagreement was resolved by consensus. One author (L.v.d.K.) performed the screening of the full article. The exclusion of articles in this phase was performed in consensus with two other authors (J.D.V. and M.D.I.V.). If more than one manuscript used the same or overlapping patient populations, we only included the report with the largest population or with the most relevant information for our review. If manuscripts reported on MRI findings, but timing of imaging could not be categorized into image acquisition <72 hours after ictus or between 72 hours and 21 days after ictus, the corresponding authors of these articles were contacted for additional information. In case the authors did not respond, the article was excluded. References of included articles were hand searched for additional eligible articles.

Data extraction

From included studies we retrieved data on age, sex, clinical condition on admission, amount of subarachnoid blood on admission CT, type of aneurysm treatment, MRI sequence, and MRI hardware information. We extracted data on MRI-DWI lesions within 72 hours after ictus, either before or after aneurysm treatment, and between 72 hours and 21 days after SAH. In studies investigating the relationship between MRI-DWI lesions and DCI, we decided a priori to include the following terms as an outcome measure reflecting DCI: delayed ischemic neurologic deficit, delayed ischemic deficit, delayed neurologic deficit, secondary cerebral ischemia, clinical vasospasm, symptomatic vasospasm, symptomatic ischemia, and cerebral infarction. The definition of DCI or a similar term needed to include clinical deterioration or cerebral infarction. Studies with 'vasospasm' as an outcome measure were only included if it was defined as any kind of clinical deterioration.

Quality assessment and risk of bias assessment

Quality assessment of the included articles was based on a previously used scoring system,[4, 5] which was adapted to fit the studies within the scope of this review (Table 1). Two authors (L.v.d.K. and J.D.V.) performed the assessment independently. Disagreement was solved in a consensus reading between both authors. The score ranged from 0-14, and a high quality paper was predefined as a score of 9-14. Risk of bias was assessed by L.v.d.K. and J.D.V. through a consensus reading using a tool developed to assess risk of bias in prevalence studies.[6]

Table 1. Quality Assessment

Criterion		Points
Design	Prospective cohort or prospective case-control	3
	Retrospective from prospective database or trial cohort	2
	Retrospective cohort, or unclear	1
Population	Representative for all SAH patients[a]	3
	In all patients an aneurysm was identified	1
	Baseline characteristics (age, sex, clinical condition, amount of subarachnoid blood on admission CT, type of aneurysm treatment) were described for all patients	1
	Arrival in hospital within 72 hours after ictus	1
Aim	Primary aim was to investigate the relationship between SAH and brain lesions on MRI	1
Size	Number of patients ≥ 100	1
MRI	The timing of MRI after ictus was predefined	1
Outcome	The primary outcome measure was an MRI-DWI lesion	1
Data analysis and presentation	Number of patients with MRI lesions were analyzed for each time frame separately[b]	1
Total score	*< 9 = low quality study; 9 -14 = high quality study*	*14*

[a]A study population was considered not representative if a patient selection was made on age, sex, clinical condition on admission, location of the aneurysm, or treatment method of the ruptured aneurysm.
b<72 hours after ictus, 72 hours –21 days

Analyses

First, we analyzed the proportion of patients with MRI-DWI lesions within 72 hours after aSAH, both before and after aneurysm treatment. Second, we studied if the following variables were determinants of MRI-DWI lesions prior to aneurysm treatment within 72 hours after ictus: age, sex, clinical condition on admission, and amount of subarachnoid blood on CT classified by the (modified) Fisher scale. Third, we examined the proportion of patients with MRI-DWI lesions between 72 hours and 21 days after ictus. Fourth, we analyzed the proportion of patients with and without MRI-DWI lesions within 72 hours who later on developed DCI, and calculated positive- and negative predictive values. And fifth, we analyzed the proportion of patients with clinical deterioration due to DCI with compatible MRI-DWI lesions. For the analyses in which the proportion of patients with MRI-DWI lesions was investigated within 72 hours or between 72 hours and 21 days, a separate sensitivity analysis was performed for lesions with both a high signal on DWI and low signal on ADC. Statistical analyses were performed in R (version 3.2.3) with the lme4 package.[7,8] We pooled proportions across studies using a generalized lin-

ear mixed-effects model for dichotomous outcomes, allowing for between-study heterogeneity. Besides the pooled proportion estimates, we report prediction intervals for the evaluation of between-study heterogeneity.[9] Subsequently, risk ratios with 95% confidence intervals were calculated where appropriate using the epitools package.[10] If zero events occurred in one group of a study, ½ was added to each cell of the table.[11] We included clinical grade on admission into the model to evaluate its impact on the prevalence of MRI-DWI lesions within 72 hours. For MRI-DWI lesions between 72 hours and 21 days, we included clinical grade on admission, aneurysm treatment, and day of scanning after ictus into the model (see Appendix, 'Metaregression'). Interrater agreement was assessed with Cohen's kappa.

Results

Our search strategy yielded a total of 7299 articles of which 13 were included with 522 SAH patients (Figure 1; Tables 2 and 3).[12-24] Additional data were obtained on request from 2 studies.[17, 23] Characteristics of the included studies are shown in Table 2. The median number of patients per study was 32 (range 11-100). Five studies provided data on MRI within 72 hours after ictus,[12, 14, 17, 19, 23] and 6 studies on MRI between 72 hours and 21 days after SAH.[15, 16, 18, 21, 22, 24] Two studies performed sequential imaging within both time categories.[13, 20] Six studies fulfilled the criteria for high-quality studies.[12-14, 16, 20, 24] Two out of 13 studies had a low risk of bias (Appendix, Table S1).

MRI-DWI lesions within 72 hours

Diffusion weighted imaging was performed within 72 hours after ictus in 302 patients from seven studies.[12-14, 17, 19, 20, 23] Four studies were considered a high-quality study.[12-14, 20] The median number of patients per study was 38 (range 15-85). MR imaging was performed before aneurysm treatment in 264 patients,[12-14, 17, 19, 20, 23] and after treatment in 38 patients.[13, 23] For one study with 15 patients, the corresponding author supplied additional data so that distinction could be made between pre- and post-treatment lesions.[23] Four studies defined a lesion as a hyperintense b1000-signal on DWI with a corresponding low ADC signal.[12, 13, 20, 23] Two studies defined lesions as high-intensity areas on DWI,[17, 19] and one study defined a lesion as an abnormal signal intensity on DWI.[14] In one study a comparison of DWI with CT was made to differentiate a lesion signal from a subarachnoid clot.[19]

Table 2. Study Characteristics

Study	N	Age	Sex, F	SAH severity
De Marchis et al (2015)	27	55 (45 - 74)	59%	HH I 37% IV 15% II 19% V 15% III 15%
Frontera et al (2015)	61 <72h 49 follow-up	55 (25 - 80)	67%	HH Median III (I-V)
Hadeishi et al (2002)	32 (57 included)	59 (35 - 85)	72% of 57	WFNS I 63% IV 19% II 16% V 3% III 0%
Leclerc et al (2002)	11	44 (28-61)	64%	HH I-II 100%
Liu et al (2007)	100 SAH	SAH 52±12 (19-81)	SAH 52%	HH I 14% IV 11% II 49% III 26%
Nagahata et al (2014)	52	Median 71 (39-87)	73%	-
Naidech et al (2010)	44	57	75%	WFNS I 43% IV 16% II 20% V 14% III 7%
Sanborn et al (2012)	22 SAH	SAH 51 (26-67)	SAH 77%	HH I 23% IV 23% II 27% V 14% III 14%
Sato et al (2010)	38	64	71%	H&K IV 47% V 53%
Shimoda et al (2010b)	85	58	60%	WFNS I-III 69% IV-V 31%
Siman et al (2011)	23	51	72%	HH I 22% IV 13% II 30% V 22% III 13%
Vatter et al (2011)	25	50±10 (27-66)	64%	HH I 4% IV 28% II 28% III 40%
Wartenberg et al 2011	15	62±16	-	HH IV 40% V 60%

Legend: HH = Hunt & Hess grade; WFNS = World Federation Neurosurgical Societies grade; Mod. Fisher =

Amount of SAH		Aneurysm treatment	Timing of MRI	DWI-MRI sequences	Field strength
Mod. Fisher I 37% II 11% III 26%	IV 26%	-	<48h, before aneurysm securing	b0, b1000, ADC maps	1.5 or 3
Mod. Fisher Median with/without lesion 4/3 (range 0-4)		-	<72h, both before and after aneurysm securing ≥4 days	b0, b1000, b2000, ADC maps	1.5 1.5
-		-	<72h, before aneurysm securing	b1100	1.5
-		Endovascular 64% Surgery 36%	Median 6 days (4-9)	b0, b1000, ADC maps	
Mod. Fisher II 26% III 48%	IV 26%	Endovascular 30% Surgery 70%	9±3 days (5-19)	b0, b1000, ADC maps	1.5
-		-	Median 16 hours (4-63)	-	3
Mod. Fisher II 2% III 82% IV 16%		Endovascular 25% Surgery 75%	At 14 days	b1000, ADC maps	1.5
Mod. Fisher III 68% IV 32%		Endovascular 59% Surgery 41%	At 14 days	-	-
Fisher III 100%		Endovascular 42% Surgery 32% Trap/bypass 5% None 21%	<24h, before aneurysm securing	b0, b1000	1.5
Fisher I-II 24% III 64%	IV 13%	Endovascular 11% Surgery 89%	<72h, before aneurysm securing ~7-10 days after admission	b0, b1000, ADC maps	1.5
Mod. Fisher II 4% III 65%	IV 30%	Endovascular or surgery	At 14 days	-	-
Fisher III 92% IV 8%		Endovascular 56% Surgery 40% None 4%	9±3 days	-	1.5
Mod. Fisher II 13% III 20%	IV 67%	-	Median 1 day (range 0-3), mixed before and after aneurysm securing	ADC maps	1.5

modified Fisher scale; DWI = diffusion weighted imaging; ADC = apparent diffusion coefficient

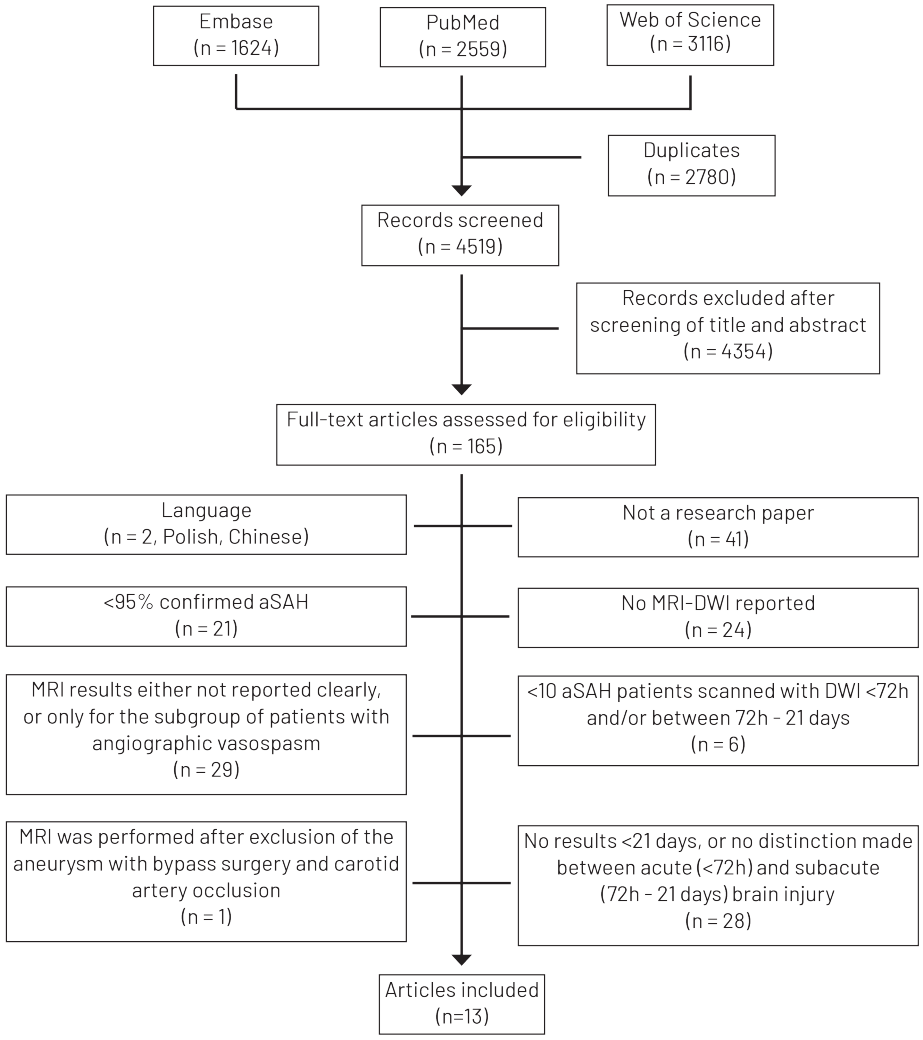

Fig. 1. Flowchart. aSAH indicates aneurysmal subarachnoid hemorrhage; DWI, diffusion weighted imaging; and MRI, magnetic resonance imaging

Table 3. Interrater agreement for studies screened by title and abstract

		Screen for full text?	
Rater		*JDV*	
		Yes	No
LvdK	Yes	95	81
	No	53	4290

κ = 0.57 (*P* <0.001).
Absolute agreement was observed for 95% of the screened papers (4290 of 4519).

Pre-treatment DWI lesions were reported in 105 of 264 patients (pooled proportion 51%; 95% CI 24-77%) (Figure 2). The 95% prediction interval was 4-96% (Figure 2). The two studies with the highest proportion of patients with pre-treatment DWI lesions only included patients with a poor clinical condition on admission (Hunt&Hess (H&H) / Hunt&Kosnik IV-V).[19, 23] In a sensitivity analysis with four studies and 150 patients in which lesions were defined as a hyperintense b1000-signal on DWI with a corresponding low ADC signal, the pooled proportion of lesions was 57% (95% CI 19-88%; 95% prediction interval 3-98%).[12, 13, 20, 23] Post-treatment DWI lesions were investigated in two studies and found in 26 of 38 patients (pooled proportion 68%; 95% CI 52-81%; 95% prediction interval 52-81%).[13, 23]

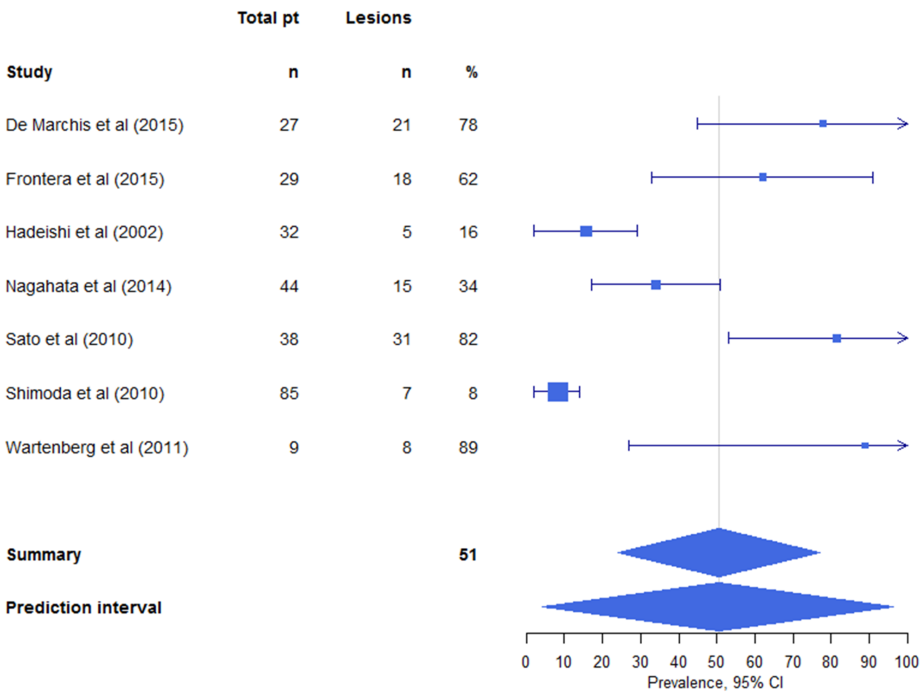

Fig. 2. Forest plot of pretreatment diffusion weighted imaging lesions <72 h after ictus. CI indicates confidence interval.

Determinants of pre-treatment MRI-DWI lesions within 72 hours

Three studies investigated determinants of pre-treatment MRI-DWI lesions within 72 hours after aSAH.[14, 19, 20]

Age

Two studies with a total of 123 patients investigated the relationship between age and DWI lesions.[19, 20] In a high-quality study with 85 patients, the mean age of patients with DWI lesions was 62 (±14) years versus 58 (±13) years in those without lesions.[20] In a low-quality study with 38 patients, the median age in patients with lesions >10 mm was 63 (IQR 54-73) years and in patients with lesions <10 mm 67 (IQR 55-76) years, compared with 60 (IQR 52-73) years in patients without lesions.[19] Since no individual patient data were available, data on age could not be pooled and therefore a potential relationship between age and presence of DWI lesions remains unclear.

Sex

One high-quality study and a low-quality study with a total of 123 patients investigated the relationship between sex and DWI lesions.[19, 20] DWI lesions were observed in 9 of 45 male patients and in 29 of 78 female patients (RR 0.54; 95% CI 0.28-1.03).

Clinical condition on admission

One high-quality study investigated the relationship between clinical condition on admission and presence of pre-treatment DWI lesions.[14] DWI lesions were observed in 5 of 7 patients with H&H grade IV-V on admission compared with 0 of 25 patients with H&H grade I-III (RR 35.8; 95% CI 2.2-578.9).[14] Clinical grade on admission was associated with lesion prevalence prior to aneurysm treatment (Appendix, 'Metaregression'). In a cohort with 75% of patients presenting with a good clinical grade (WFNS or H&H grade I-III) on admission, 30% (95% CI 10-62%) of patients are expected to present with pre-treatment DWI lesions <72 hours. In a cohort with 75% of patients presenting with a poor clinical grade (WFNS or H&H grade IV-V) on admission, 73% (95% CI 42-91%) of patients are expected to have MRI-DWI lesions before aneurysm treatment.

Amount of subarachnoid blood

One high quality study studied the relationship between the amount of subarachnoid blood, as measured with the modified Fisher score, and pre-treatment DWI lesions.[20] A median Fisher score of 3 (range 1-4) was reported in both the 7 patients with lesions and in the 78 patients without pre-treatment lesions.[20]

DWI lesions between 72 hours and 21 days

Eight studies with 346 patients reported on DWI-MRI between 72 hours to 21 days after ictus.[13, 15, 16, 18, 21-24] Four studies were high-quality studies.[13, 16, 20, 24] The median number of patients per study was 34 (range 11-100).

DWI lesions were assessed in 8 studies and reported in 173 out of 346 patients (47%; 95% CI 35-59% (Figure 3).[13, 15, 16, 18, 20-22, 24] The 95% prediction interval was 20-76% (Figure

3). The study with the lowest proportion of DWI lesions only included patients with a good clinical condition on admission (H&H I-II).[15] In none of the studies was a lesion defined as a hyperintense b1000-signal on DWI with a corresponding low ADC signal.

A high-quality study with 61 patients performed MRI within 72 hours and at a median follow-up time of 7 days from ictus.[13] Twelve patients were lost to follow-up. New DWI lesions were observed in 25 of 49 patients (51%, 95% CI 31-71%).

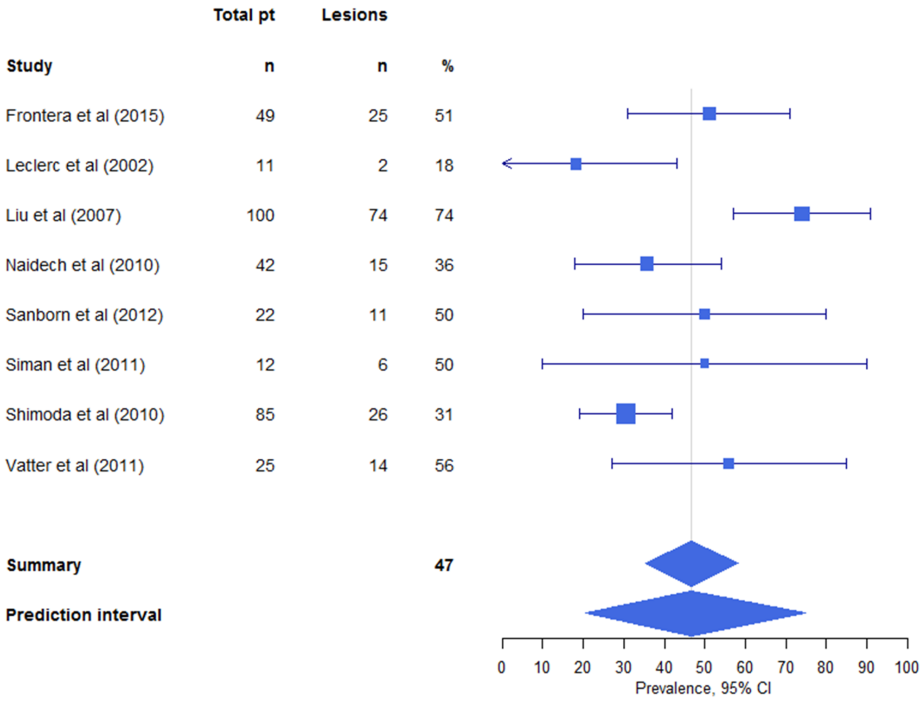

Fig. 3. Forest plot of diffusion weighted imaging lesions between 72 h and 21 d after ictus. CI indicates confidence interval.

Determinants of DWI lesions between 72 hours and 21 days

Clinical grade on admission did not influence the prevalence of MRI-DWI lesions between 72 hours and 21 days after ictus (Appendix, 'Metaregression'). The modality of aneurysm treatment slightly impacted the pooled prevalence. If 75% of patients underwent endovascular coiling, the expected lesion prevalence was 50% (95% CI 30-69%). If 25% underwent endovascular coiling, the expected lesion prevalence was 45% (95% CI 30-61 %). In addition, the pooled lesion prevalence was slightly affected by including day of scanning as a dichotomous determinant. The pooled lesion prevalence was 48%

(95% CI 34-63%) in a model with studies that on average scanned before day 14, compared to 44% (95% CI 26-64%) in a model in which all patients were scanned on day 14 post ictus.

Predictive value of MRI-DWI lesions within 72 hours for the development of DCI

In a high-quality study with 85 patients, clinical deterioration due to DCI developed in 6 of 7 patients with DWI lesions within 72 hours, and in 8 of 78 patients of patients without DWI lesions within 72 hours.[20] The positive predictive value of pre-treatment DWI lesions within 72 hours for developing clinical deterioration due to DCI was 86% (95% CI 17-100%) and the negative predictive value was 90% (95% CI 69-100%).

MRI-DWI in patients with clinical deterioration due to DCI

No studies were performed that investigated the proportion of patients with clinical deterioration due to DCI with compatible MRI-DWI lesions.

Discussion

In this systematic review we found that the proportion of patients with MRI-DWI lesions, both pre-treatment within 72 hours as between 72 hours and 21 days after ictus, differed widely between studies. This heterogeneity was somewhat wider in the analysis on MRI-DWI lesions pre-treatment with 72 hours compared with the analysis on lesions between 72 hours and 21 days. The wide 95% prediction intervals indicate that for a new, individual study the estimate of the proportion of patients with lesions carries a high level of uncertainty. Metaregression analyses identified clinical condition on admission as a determinant for pre-treatment lesions with 72 hours, and aneurysm treatment modality and day of MR imaging as determinants for lesions between 72 hours and 21 days.

One high-quality study showed that MRI-DWI lesions within 72 hours predict the later development of DCI. This supports the concept that processes involved in early brain injury after aSAH, such as increased intracranial pressure, microvascular alterations, platelet aggregation, acute vasospasm and reperfusion injury, induce the development of DCI.[25-28]

No studies are available that directly compare CT and MRI for the evaluation of cerebral ischemia after SAH. Nevertheless, it is plausible that MRI is the preferred method for the detection of cerebral ischemia after SAH because MRI is more sensitive for the detection of small cortical lesions, which have an important effect on outcome after SAH

according to autopsy studies.[29, 30]

Interestingly, clinical grade on admission only affected lesion prevalence in the model for DWI lesions with 72 hours. Between 72 hours and 21 days no such effect was found. The reason for this contrasting finding remains unclear. The model that included the day of MR imaging indicated that lesion prevalence is slightly lower in studies that assessed MRI-DWI lesions on day 14 compared with imaging between 72 hours and day 14. This finding is in accordance with the observation from human and animal studies that DWI hyperintensities may partially or fully reverse.[31, 32, 33] It has been found that even lesions with markedly decreased ADC normalize between day 1 and day 7 after stroke.[34]

A limitation of our study is that not all studies specified the evaluation of DWI lesions, which complicates interpretation of the results. The ADC value and DWI signal intensity at different b-levels are the most important features to distinguish various types of brain injury on DWI-MRI. Areas with a hyperintense signal on DWI in combination with a low ADC indicate cytotoxic edema in the acute stage which typically progress to infarction over time,[35] whereas a hyperintense signal on DWI with a normal ADC or a DWI lesion which decreases in signal intensity when going from b0 to b1000 images indicates vasogenic edema. Since the ADC value returns to normal around 1-4 weeks after ictus, vasogenic edema and ischemia due to cytotoxic edema cannot be distinguished after normalization on the ADC value.[35] Second, in the subacute stage blood products may complicate the characterization of DWI lesions.[35, 36] Finally, the number of patients available for analysis was low, both in individual studies and in total. Accordingly, outliers in an individual study may strongly impact its results, and subsequently the results of the meta-analysis. In addition, only two out of 13 studies had a low risk of bias. This limits the ability to identify determinants of DWI lesions and complicates the estimation of the true heterogeneity in lesion prevalence among studies.

Conclusion and future directions

Over the last 15 years, experience has been gained with the use of MRI in patients with aSAH. MRI is an imaging modality that can be used for diagnosing cerebral ischemia at different stages after SAH (Figure 4). More studies are needed to investigate if MRI is a useful diagnostic tool for the diagnosis of DCI in patients who have clinical deterioration between days 4 and 14 after ictus. Moreover, future MRI studies might challenge the current DCI definition.[2] Future research questions may include: 1) Does imaging performed within hours after DCI onset confirm the ischemic mechanism of clinical deterioration?; 2) What is the additional value of arterial spin labeling (ASL) and perfusion weighted imaging (PWI) besides DWI?; 3) Are MRI-DWI lesions on admission a risk factor for developing procedure-related ischemia from endovascular or neurosurgical treatment of the aneurysm?; and 4) Are MRI-DWI lesions on admission associated with

functional outcome in SAH patients who do not develop complications in the first three weeks after the hemorrhage?

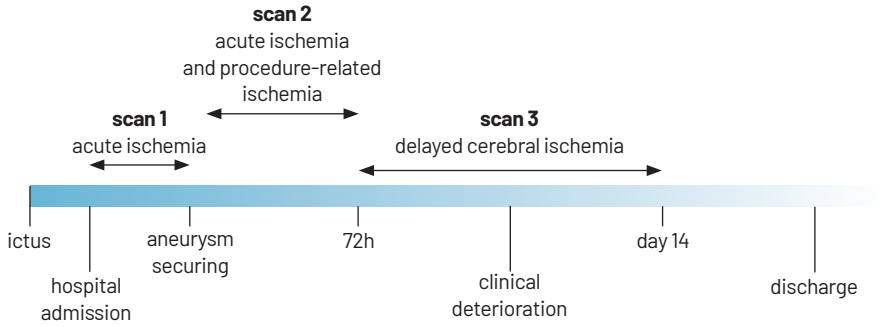

Fig. 4. Magnetic resonance imaging for diagnosing cerebral ischemia at different stages after aneurysmal subarachnoid hemorrhage.

We suggest well-designed prospective, longitudinal studies in unselected patient cohorts with large numbers of patients, detailed descriptions of the results, and MRI at predefined days to establish the proportion of patients with DWI-lesions, study determinants of lesions, and to investigate the evolution of cerebral ischemia and the impact of complications and interventions on cerebral ischemia after aSAH.

References

1. Vergouwen MD, Jong-Tjien-Fa AV, Algra A, Rinkel GJ. Time trends in causes of death after aneurysmal subarachnoid hemorrhage: A hospital-based study. Neurology. 2016;86:59-63.
2. Vergouwen M, Vermeulen M, van Gijn J, Rinkel G, Wijdicks E, Muizelaar J, et al. Definition of delayed cerebral ischemia after aneurysmal subarachnoid hemorrhage as an outcome event in clinical trials and observational studies: Proposal of a multidisciplinary research group. Stroke. 2010:2391-2395.
3. van Gijn J, Kerr RS, Rinkel GJ. Subarachnoid haemorrhage. Lancet. 2007;369:306-318.
4. de Rooij NK, Rinkel GJ, Dankbaar JW, Frijns CJ. Delayed cerebral ischemia after subarachnoid hemorrhage: A systematic review of clinical, laboratory, and radiological predictors. Stroke. 2013;44:43-54.
5. Boluijt J, Meijers JC, Rinkel GJ, Vergouwen MD. Hemostasis and fibrinolysis in delayed cerebral ischemia after aneurysmal subarachnoid hemorrhage: A systematic review. J Cereb Blood Flow Metab. 2015;35:724-733.
6. Hoy D, Brooks P, Woolf A, Blyth F, March L, Bain C, et al. Assessing risk of bias in prevalence studies: Modification of an existing tool and evidence of interrater agreement. J Clin Epidemiol. 2012;65:934-939.
7. R Core Team. R: A language and environment for statistical computing. Vienna, Austria: R Foundation for Statistical Computing; 2015.
8. Bates D, Mächler M, Bolker B, Walker S. Fitting linear mixed-effects models using lme4. 2015;67:48.
9. Higgins JP, Thompson SG, Spiegelhalter DJ. A re-evaluation of random-effects meta-analysis. J R Stat Soc Ser A Stat Soc. 2009;172:137-159.
10. Aragón TJ. Epitools: Epidemiology tools. 2012.
11. Higgins JPT, Green S. Measures of relative effect: the risk ratio and odds ratio. In: Cochrane handbook for systematic reviews of interventions. Version 5.1.0. The Cochrane Collaboration; 2011.
12. De Marchis GM, Filippi CG, Guo X, Pugin D, Gaffney CD, Dangayach NS, et al. Brain injury visible on early mri after subarachnoid hemorrhage might predict neurological impairment and functional outcome. Neurocrit Care. 2015;22:74-81.
13. Frontera JA, Ahmed W, Zach V, Jovine M, Tanenbaum L, Sehba F, et al. Acute ischaemia after subarachnoid haemorrhage, relationship with early brain injury and impact on outcome: A prospective quantitative mri study. J Neurol Neurosurg Psychiatry. 2015;86:71-78.
14. Hadeishi H, Suzuki A, Yasui N, Hatazawa J, Shimosegawa E. Diffusion-weighted magnetic resonance imaging in patients with subarachnoid hemorrhage. Neurosurgery. 2002;50:741-748.
15. Leclerc X, Fichten A, Gauvrit JY, Riegel B, Steinling M, Lejeune JP, et al. Symptomatic vasospasm after subarachnoid haemorrhage: Assessment of brain damage by diffusion and perfusion-weighted MRI and single-photon emission computed tomography. Neuroradiology. 2002;44:610-616.
16. Liu Y, Soppi V, Mustonen T, Kononen M, Koivisto T, Koskela A, et al. Subarachnoid hemorrhage in the subacute stage: Elevated apparent diffusion coefficient in normal-appearing brain tissue after treatment. Radiology. 2007;242:518-525.
17. Nagahata S, Nagahata M, Obara M, Kondo R, Minagawa N, Sato S, et al. Wall enhancement of the intracranial aneurysms revealed by magnetic resonance vessel wall imaging using three-dimensional turbo spin-echo sequence with motion-sensitized driven-equilibrium: A sign of ruptured aneurysm? Clin Neuroradiol. 2014:1-7.
18. Sanborn MR, Thom SR, Bohman LE, Stein SC, Levine JM, Milovanova T, et al. Temporal dynamics of microparticle elevation following subarachnoid hemorrhage: Laboratory investigation. J Neurosurg. 2012;117:579-586.
19. Sato K, Shimizu H, Fujimura M, Inoue T, Matsumoto Y, Tominaga T. Acute-stage diffusion-weighted magnetic resonance imaging for predicting outcome of poor-grade aneurysmal subarachnoid hemorrhage. J Cereb Blood Flow Metab. 2010;30:1110-1120.
20. Shimoda M, Hoshikawa K, Shiramizu H, Oda S, Yoshiyama M, Osada T, et al. Early infarction detected by diffusion-weighted imaging in patients with subarachnoid hemorrhage. Acta Neurochir (Wien). 2010;152:1197-1205.

21. Siman R, Giovannone N, Toraskar N, Frangos S, Stein SC, Levine JM, et al. Evidence that a panel of neurodegeneration biomarkers predicts vasospasm, infarction, and outcome in aneurysmal subarachnoid hemorrhage. PLoS One. 2011;6:e28938.
22. Vatter H, Guresir E, Berkefeld J, Beck J, Raabe A, du Mesnil de Rochemont R, et al. Perfusion-diffusion mismatch in mri to indicate endovascular treatment of cerebral vasospasm after subarachnoid haemorrhage. J Neurol Neurosurg Psychiatry. 2011;82:876-883.
23. Wartenberg KE, Sheth SJ, Michael Schmidt J, Frontera JA, Rincon F, Ostapkovich N, et al. Acute ischemic injury on diffusion-weighted magnetic resonance imaging after poor grade subarachnoid hemorrhage. Neurocrit Care. 2011;14:407-415.
24. Naidech A, Shaibani A, Garg R, Duran I, Liebling S, Bassin S, et al. Prospective, randomized trial of higher goal hemoglobin after subarachnoid hemorrhage. Neurocrit Care. 2010;13:S221.
25. Sehba FA, Hou J, Pluta RM, Zhang JH. The importance of early brain injury after subarachnoid hemorrhage. Prog Neurobiol. 2012;97:14-37.
26. Sehba FA, Mostafa G, Knopman J, Friedrich V, Jr., Bederson JB. Acute alterations in microvascular basal lamina after subarachnoid hemorrhage. J Neurosurg. 2004;101:633-640.
27. Bederson JB, Levy AL, Ding WH, Kahn R, DiPerna CA, Jenkins AL III, et al. Acute vasoconstriction after subarachnoid hemorrhage. Neurosurgery. 1998;42:352-360.
28. Claassen J, Carhuapoma JR, Kreiter KT, Du EY, Connolly ES, Mayer SA. Global cerebral edema after subarachnoid hemorrhage: Frequency, predictors, and impact on outcome. Stroke. 2002;33:1225-1232.
29. Dreier JP, Sakowitz OW, Harder A, Zimmer C, Dirnagl U, Valdueza JM, et al. Focal laminar cortical mr signal abnormalities after subarachnoid hemorrhage. Ann Neurol. 2002;52:825-829.
30. Weidauer S, Vatter H, Beck J, Raabe A, Lanfermann H, Seifert V, et al. Focal laminar cortical infarcts following aneurysmal subarachnoid haemorrhage. Neuroradiology. 2008;50:1-8.
31. Albach FN, Brunecker P, Usnich T, Villringer K, Ebinger M, Fiebach JB, et al. Complete early reversal of diffusion-weighted imaging hyperintensities after ischemic stroke is mainly limited to small embolic lesions. Stroke. 2013;44:1043-1048.
32. Kidwell CS, Alger JR, Di Salle F, Starkman S, Villablanca P, Bentson J, et al. Diffusion mri in patients with transient ischemic attacks. Stroke. 1999;30:1174-1180.
33. Hasegawa Y, Fisher M, Latour LL, Dardzinski BJ, Sotak CH. Mri diffusion mapping of reversible and irreversible ischemic injury in focal brain ischemia. Neurology. 1994;44:1484-1490.
34. Fiehler J, Foth M, Kucinski T, Knab R, von Bezold M, Weiller C, et al. Severe adc decreases do not predict irreversible tissue damage in humans. Stroke. 2002;33:79-86.
35. Schaefer PW, Grant PE, Gonzalez RG. Diffusion-weighted mr imaging of the brain. Radiology. 2000;217:331-345.
36. Kang BK, Na DG, Ryoo JW, Byun HS, Roh HG, Pyeun YS. Diffusion-weighted mr imaging of intracerebral hemorrhage. Korean Journal of Radiology. 2001;2:183-191.

Appendix

Table S1. Risk of bias

Item	Marchis (2015)	Frontera (2015)	Hadeishi (2002)	Leclerc (2002)	Liu (2007)
External validity					
1. Was the study's target population a close representation of the national population in relation to relevant variables, e.g., age, sex, occupation?	yes	yes	yes	yes	yes
2. Was the sampling frame a true or close representation of the target population?	yes	yes	no	no	yes
3. Was some form of random selection used to select the sample, OR, was a census undertaken?	yes	yes	yes	yes	yes
4. Was the likelihood of non-response bias minimal?	no	yes	yes	no	no
Internal validity					
5. Were data collected directly from the subjects (as opposed to a proxy)?	yes	yes	yes	yes	yes
6. Was an acceptable case definition used in the study?	yes	yes	yes	yes	yes
7. Was the study instrument that measured the parameter of interest (e.g., prevalence of low back pain) shown to have reliability and validity (id necessary)?	yes	yes	yes	yes	yes
8. Was the same mode of data collection used for all subjects?	yes	yes	no	yes	yes
9. Was the length of the shortest prevalence period for the parameter of interest appropriate?	yes	no	yes	no	no
10. Were the numerator(s) and denominators(s) for the parameter of interest appropriate?	yes	yes	yes	yes	yes
11. Summary item on the overall risk of study bias	moderate	low	low	high	moderate

	Naidech (2010)	Nagahata (2014)	Sanborn (2012)	Sato (2010)	Shimodal (2010)	Siman (2011)	Vatter (2011)	Warten-berg (2011)
	yes	yes	yes	yes	yes	yes	yes	yes
	no	no	no	no	yes	no	no	no
	yes	yes	no	yes	yes	no	yes	yes
	no	no	no	no	yes	no	no	no
	yes	yes	yes	yes	yes	yes	yes	yes
	yes	yes	yes	yes	yes	yes	yes	yes
	yes	yes	yes	yes	yes	yes	yes	yes
	yes	no	no	no	no	no	no	yes
	yes	yes	yes	yes	no	yes	no	no
	yes	yes	yes	yes	yes	yes	yes	yes
	moderate	moderate	high	moderate	moderate	high	high	high

Metaregression

Determinants for lesion prevalence were analyzed using metaregression, with the lme4 package in R. For MRI-DWI lesions within 72 hours, we included clinical grade on admission into the model. Aneurysm treatment was not taken into account for the metaregression of the MRI-DWI lesions within 72 hours, because only 38 patients from 2 studies underwent imaging after aneurysm securing <72 hours. For MRI-DWI lesions between 72 hours and 21 days, we included clinical grade on admission, aneurysm treatment, and whether patients were scanned before or on day 14 after ictus into the model. In terms of clinical grade on admission, we decided to combine the WFNS and the Hunt & Hess scale because of the small number of studies available for the analysis when separating both measurements. A good clinical grade was defined as grade I-III on the WFNS grading system or on the Hunt & Hess scale, and a poor clinical grade was defined as WFNS or Hunt & Hess grade IV-V (see "Methods"). Age and sex were not analyzed as a determinant, because the range of both the mean age and M/F ratios across studies was too narrow for a proper analysis. Mean age ranged from 44 to 64 years and the proportion of female patients was around 65% in each study (range 52-77%).

Acute stage (<72 hours after ictus)

Table S2. Lesion prevalence and clinical grade

Study	With lesion (n)	Total (n)	Proportion with lesions	H&H/WFNS grade I-III	Proportion grade I-III
Marchis	21	27	0.78	19	0.70
Frontera	18	29	0.62	18	0.62
Hadeishi	5	32	0.16	25	0.78
Sato	31	38	0.82	0	0.00
Shimoda	7	85	0.08	59	0.69
Nagahata	15	44	0.34	-	-
Wartenberg	8	9	0.89	0	0.00

Table S3. Metaregression of acute lesion prevalence

Determinant	Lesion prevalence w/o determinants	0% (95% CI)	25% (95% CI)	50% (95% CI)	75% (95% CI)	100% (95% CI)
Proportion H&H/ WFNS grade I-III	54%	87% (50-98%)	73% (43-91%)	52% (28-75%)	30% (10-62%)	15% (2-54%)

Table S3 displays the effect of clinical grade on lesion prevalence. The first column shows the lesion prevalence for the studies that were included in this model. The second column features the lesion prevalence for a model in which 0% of patients present-

ed with a H&H/WFNS grade of I-III. In columns 3 through 6, the expected lesion prevalence is presented for an increasing proportion of patients with H&H/WFNS grade I-III. As can be seen, the expected lesion prevalence is lower when there are relatively more patients with a good clinical grade (H&H/WFNS I-III) according to this model.

Subacute stage (72h – 21 days after ictus)

Table S4. Lesion prevalence, clinical grade, aneurysm treatment and timing of MRI

Study	With lesion (n)	Total (n)	Proportion with lesions	H&H/ WFNS grade I-III	Proportion grade I-III	Endovascular aneurysm securing	Proportion endovascular aneurysm securing	Scan on day 14 (1=yes)
Frontera	25	49	0.51	33	0.67	33	0.67	0
Leclerc	2	11	0.18	11	1,00	7	0.64	0
Liu	74	100	0.74	89	0.89	30	0.30	0
Naidech	15	42	0.36	-	-	11	0.26	1
Sanborn	11	22	0.50	14	0.64	13	0.59	1
Siman	6	12	0.50	7	0.58	9	0.75	1
Shimoda	26	85	0.31	59	0.69	9	0.11	0
Vatter	14	25	0.56	18	0.72	14	0.56	0

Table S5. Metaregression of subacute leion prevalence

Determinant	Lesion prevalence w/o determinants	0% (95% CI)	25% (95% CI)	50% (95% CI)	75% (95% CI)	100% (95% CI)
Proportion H&H/ WFNS grade I-III	49%	50% (3-97%)	50% (9-91%)	49% (23-76%)	49% (35-62%)	48% (20-78%)
Endovascular aneurysm securing	47%	43% (20-70%)	45% (30-61%)	47% (35-60%)	50% (30-69%)	52% (22-80%)
Scan on day 14 after ictus	47%	48% (34-63%)	47% (35-60%)	46% (34-59%)	45% (30-61%)	44% (26-64%)

Table S5 shows the lesion prevalence in a model with a varying proportion of patients with either a good clinical grade (row 2), endovascular aneurysm securing (row 3), or a scan on day 14 after ictus (row 4). The first column displays the lesion prevalence for the studies that were included in each model. The second column presents the lesion prevalence for a model in which 0% of patients presented with the determinant entered into the model. In column 3 through 6, the expected lesion prevalence is presented for an increasing proportion of patients with the determinant.

Chapter 3

Magnetic resonance imaging and brain injury in the chronic phase after aneurysmal subarachnoid hemorrhage; a systematic review

B.L. Stehouwer[1], L.A. van der Kleij[1], J. Hendrikse[1], G.J.E. Rinkel[2], J.B. De Vis[1,3]

[1] Department of Radiology, University Medical Center Utrecht, Utrecht, the Netherlands.
[2] Department of Neurology and Neurosurgery, Brain Center Rudolf Magnus, University Medical Center Utrecht, Utrecht, the Netherlands.
[3] Division of Magnetic Resonance Research, Russel H. Morgan Department of radiological science, Johns Hopkins University School of Medicine

International Journal of Stroke 13.1(2018): 24-34

Abstract

Background: Case-fatality rates after aneurysmal subarachnoid hemorrhage (aSAH) have decreased over the past decades. However, many patients who survive an aSAH have long-term functional and cognitive impairments.

Aims: We sought to review all data on conventional brain MRI obtained in the chronic phase after aSAH to (1) analyze the proportion of patients with cerebral infarction or brain volume changes; (2) investigate baseline determinants predictive of MRI detected damage; and (3) assess if brain damage is predictive of patient outcome.

Summary of review: All original data published between 01/01/2000 and 04/10/2017 was searched using the PUBMED, EMBASE, and Web of Science databases. Based on preset inclusion criteria, 15 from 5200 articles were included with a total of 996 aSAH patients. Quality assessment, risk of bias assessment, and level of evidence assessment was performed. The results according to aim, with levels of evidence, were: (1) 25 to 81% of aSAH patients show infarcts (strong); there is a higher ratio of cerebrospinal fluid-to-intracranial volume in patients compared to controls (strong); (2) there is a negative relation between age (moderate), DCI (low) and brain volume measurement outcomes; (3) lower brain parenchymal volume (strong) and the presence of infarcts or infarct volumes (moderate) are associated with a worse outcome.

Conclusion: Patients after aSAH may demonstrate brain infarcts and decreased brain parenchyma, which is related to worse outcome. Thereby, both brain infarcts and brain parenchyma volumes could be used as outcome markers in pharmaceutical trials.

Introduction

Case-fatality rates after aneurysmal subarachnoid hemorrhage (aSAH) have decreased over the past decades. Today, approximately one-third of patients die within three months after the event.[1] Of the patients who survive, many have long-term functional and cognitive impairments.[2,3]

Common determinants of poor functional outcome are the impact of the acute hemorrhage, also known as early brain injury (EBI),[4,5] bleeding related acute ischemia,[6,7] and complications such as rebleeding of the aneurysm, procedure-related complications,[8,9] delayed cerebral ischemia,[10–13] and hydrocephalus.[14] It remains unclear however, how these events lead to MRI changes in the chronic phase after aSAH, and how the MRI changes relate to adverse functional outcome.

Previous MRI research has focused on the assessment of focal brain injury or brain volume changes occurring after aSAH. As well, the relation between brain injury and clinical- or neuropsychological outcome has been investigated. In the present review we grouped the results of studies performed in this area with the purpose to provide insight for future research. The following aims were formulated: (1) to analyze the proportion of aSAH patients with cerebral infarction or brain volume changes in the chronic phase; (2) to investigate baseline determinants predictive of MRI detected damage; and (3) to assess if MRI detected damage is predictive of patient outcome.

Methods

Search strategy

A literature search was conducted using the PUBMED, EMBASE, and Web of Science databases and included articles published between 01/01/2000 and 04/10/2017. The search variables were: (magnetic resonance OR MRI) AND (subarachnoid hemorrhage OR SAH) OR (delayed cerebral ischemia OR DCI OR DIND). Eligible articles were identified according to PICO criteria. Patient population (P): (1) ≥10 patients included with aSAH, defined as the presence of subarachnoid blood shown by CT or lumbar puncture and the presence of an aneurysm on CT angiography, magnetic resonance angiography, or digital subtraction angiography; (2) MRI scans performed >21 days after aSAH. Intervention (I): imaging sequences were either T1-weighted imaging, T2-weighted imaging, Proton Density-weighted imaging (PD), and/or fluid-attenuated inversion recovery (FLAIR). Comparator (C): N/A. Outcomes (O): MRI brain damage, either infarcts or brain volume change, >21 days after aSAH. Exclusion criteria were (1) article not reporting original data; (2) article written in another language than English, French, German, or Dutch; (3) conference abstract; (4) cause of the hemorrhage unknown or other than an-

eurysmal in >5% of patients; (5) animal study. Two authors (J.D.V. and L.v.d.K) screened on title and abstract. In case of disagreement a consensus reading was performed. Subsequent full text screening was conducted by B.S., and exclusion was performed in consensus with J.D.V. If more than one article used the same or overlapping patient population and the same outcome measures, only the report with the largest patient population was included. If an article reported on MRI findings but the timing of imaging was unclear, the corresponding author was contacted for additional information. In case of no response, the article was excluded. The reference lists of included articles were hand-searched for additional eligible articles. A flowchart of the screening process can be found in Figure 1. The review methodology was published in the PROSPERO database (CRD42016040095). The PRISMA 2009 checklist for transparent reporting of systematic reviews and meta-analyses was applied.

Quality assessment, risk of bias assessment, and level of evidence assessment

Quality assessment was conducted based on a previously published scoring system[15,16] adapted to fit the studies within the scope of this review (Table 1). Two authors (B.S. and J.D.V.) conducted the assessment independently, and disagreement was resolved by consensus. A high-quality article was predefined as a score between 12 and 18. A score below 12 was considered to reflect a low quality article.

Risk of bias assessment was performed by two authors (B.S and J.D.V.) to evaluate external validity, internal validity, and overall risk of study bias (Appendix, Table I).[17] The level of evidence (strong, moderate, weak, low, or inconsistent) for a certain finding was determined based on study quality and number of studies supporting the finding (Figure 1).

Data extraction and analyses

The following baseline characteristics were extracted: number of patients who received MR imaging, age, sex, clinical condition at admission, i.e., Hunt and Hess scale (H&H)[18] or World Federation of Neurosurgical Societies SAH grading system (WFNS),[19] amount of blood on admission CT, i.e. Hijdra scale[20] or Fisher grade,[21] type of aneurysm treatment, the timing of the MRI, MRI sequences, and field strength.

To address the first aim, data on the number of patients with a cerebral infarct were extracted, and the proportion (with 95% CI) of patients with an infarct was calculated. Additionally, the number of infarcts per patient and infarct size was extracted. As well, brain volume measurement results were extracted. Due to the heterogeneity of the used measurements, it was chosen to focus on the cerebrospinal fluid / intracranial

volume ratio (CSF/ICV) or measures related to it, and on the ventricular-to-intracranial-width ratio (VIWr). The incorporated measures related to the CSF/ICV were brain parenchymal volume (BPV), lateral ventricle volume, and peripheral CSF volume.

Table 1. Scoring sheet for Quality Assessment

Criterion		Points
Design	Prospective cohort or prospective case-control (3)	3
	Retrospective from prospective database or trial cohort (2)	
	Retrospective cohort, or unclear (1)	
Population	Representative for all aSAH patients*	2
	In all patients an aneurysm was identified	1
	Baseline characteristics (age, sex, clinical condition, amount of subarachnoid blood on admission CT, type of aneurysm treatment) were described for all patients	1
Aim	Primary aim was to investigate the relationship between aSAH and brain damage†	2
	Primary aim was to investigate the relation between MRI findings and neuropsychological or clinical outcome	2
Size	Number of patients ≥ 100	1
MRI	Field strength and MRI sequences were described	1
Data	Number of patients with MRI lesions are presented	2
	Neuropsychological status is presented‡	2
	Clinical outcome is presented§	1
Total score		*18*

*A study population was considered not representative if a patient selection was made on sex, age, clinical condition on admission, location of the aneurysm, or treatment method of the ruptured aneurysm.
† Brain damage was considered not only ischemic but also volumetric changes due to aSAH
‡ Neuropsychological status was considered battery tests including multiple domains of functioning
§ Clinical outcome was considered the Glasgow Outcome Scale (GOS) or modified Ranking Scale (mRS)

To address the second aim, data on determinants and their relation to cerebral infarct or brain volume changes were extracted. The parameters investigated were; age, the clinical condition on admission, and the amount of extravasated blood on admission CT. For brain volume changes, two additional determinants could be investigated; preoperative- or symptomatic hydrocephalus, and delayed cerebral ischemia (DCI). To address the third aim, data describing the relation between brain damage and neuropsychological or clinical outcome were extracted.

Statistical analyses were performed using SPSS Statistics (SPSS, Inc., Chicago, IL, version 22).

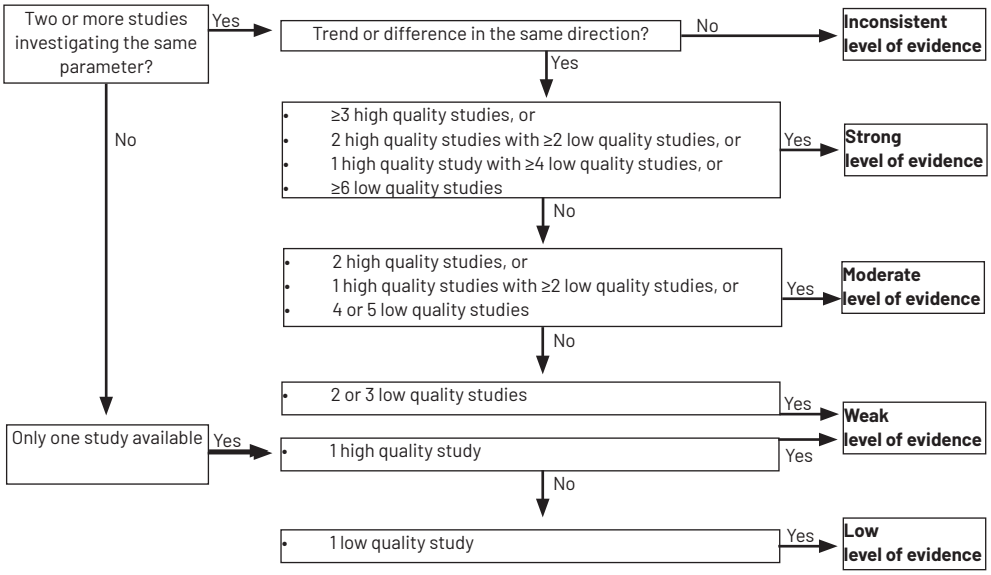

Fig. 1. Level of evidence scoring system

Results

The search strategy yielded 5200 unduplicated articles of which 15 were included (Figure 2). Of these 15 articles, two had an overlapping patient population, but different outcome measures.[22,23] The articles totaled 996 aSAH patients with a median number of 55 per study (range 20 - 138). Four articles included control subjects with a mean number of 30 subjects (range 25-30).[22–25] For each study, study characteristics are presented in Table 2. Seven out of the 15 articles fulfilled the criteria for high-quality studies.[22–24,26–29] Levels of evidence of the findings described below are presented in Table 3.

Proportion of aSAH patients with cerebral infarction or brain volume changes

Cerebral infarction

Twelve studies, with a median number of 50 patients per study (range 20-138), reported on the presence of cerebral infarcts.[24–28,30–36] Of 791 patients, 372 showed a cerebral infarct. The percentage of patients with an infarct ranged between 25 and 81 percent between studies (Table 2). The included studies varied in patient disease severity between WFNS I or II at admission or H&H grade 1 up to 4.[31,36]

One study reported on the number of infarcts detected in the patients who demonstrated infarcts: 152 infarcts in 84 patients.[31] Six studies reported on the size of the infarcts.[25,26,28,29,32,35] Three studies used a volume measurement (ml or cm^3) and found

a mean volume of 8.6 - 43.4 ml in a total of 108 patients.[25,28,35] The other three studies reported the mean diameter of the deficit, which ranged from 19 mm to 57 mm in a total of 102 patients.[26,29,32] These results are shown in Table 4.

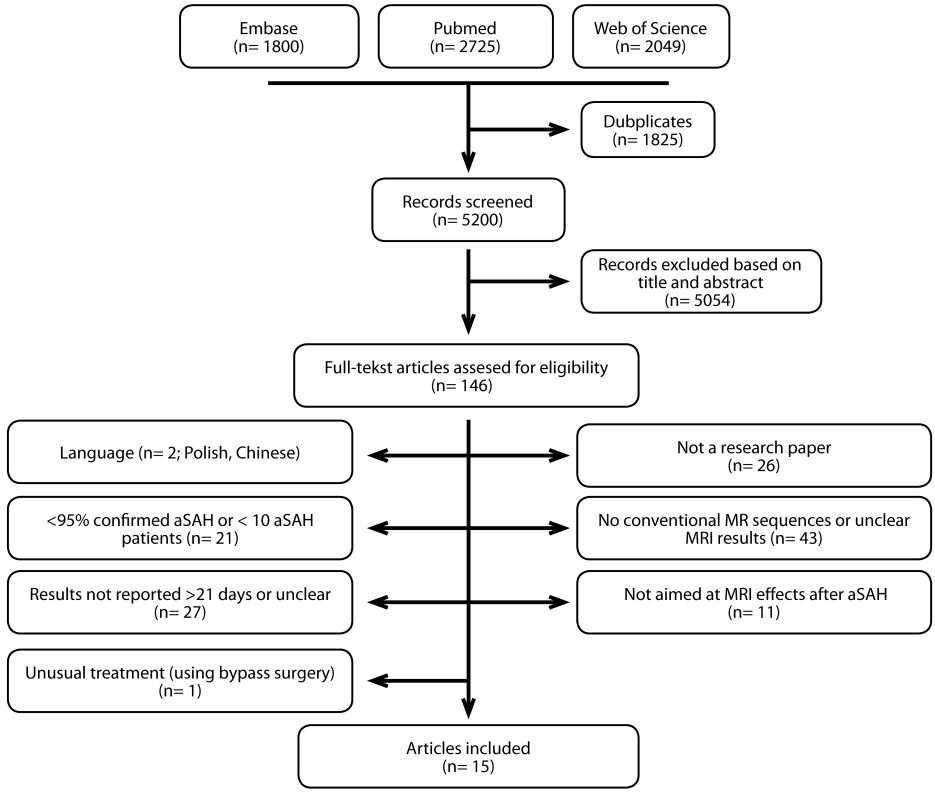

Fig. 2. Flowchart

Brain volume changes

Six articles, with a median number of 65.5 patients per study (range 38-88), reported on this brain volume changes.[22–25,29,35] In four of the six articles patients were compared to age- and sex-matched controls.[22–24,35] Two articles reported on the CSF/ICV ratio,[22,24] and in two other articles the CSF/ICV could be calculated.[25,35] The results (Table 5) show that CSF/ICV ratios were significantly higher in patients compared to controls for two out of three studies,[22,24] whilst there was no difference in the third.[35] The third studies' control group partly consisted of individuals who underwent endovascular intervention for a non-ruptured aneurysm.[35] Three articles reported the VIWr (Table 5).[23,24,29] Two studies found a significant higher mean ratio in aSAH patients compared to controls.[23,24] The third study reported results found in endovascular- and surgical treated patients.[29]

Table 2. Study Characteristics

Study	N	Age	Sex, F	SAH severity
Bendel 2006	77 aSAH 30 control	50.2±14.8 aSAH 54.1±15.5 control	57%	HH I,II 71.4% IV,V 6.5% III 22.1 %
Bendel 2008	138 aSAH	50±13 endo 51±13 surg	54.3%	HH I,II 68.1% IV,V 8.7% III 23.2%
Bendel 2009	37 aSAH 30 control	48.0±14.3 endo 50.1±13.5 surg 54.1±15.5 contr	48%	HH I-II 78.4% IV-V 5.4% III 16.2%
Bendel 2010	76 aSAH 30 contr	50.2± 14.9 54.1±15.5	56%	HH I-II 72% III-V 28%
De Bresser 2012	55 aSAH 25 contr	50.9±12.0 50.6± 9.0	70%	WFNS I-III 85% IV-V 15%
De Bresser 2015	38 aSAH	53.2±12.7	71%	WFNS I-III 84% IV-V 16%
Hadjivassiliou 2001	80 aSAH* 46 MRI	49.8 surg* 51.9 endo	70%	WFNS* 1 58.8% 4 10% 2 18.8% 3 12.5%
Kivisaari 2001	104 aSAH	45.5	52%	HH I 20% IV 10% II 40% III 30%
Koivisto 2000	109 aSAH* 88 MRI	*49 (16-73) endo 50 (14-75) surg	53%*#	HH* I-II 61.5% IV-V 13.8% III 23.9% N/A 1.1%
Koivisto 2002	46 aSAH* 40 MRI	*49 (24-72) endo 52 (24-75) surg	48%*	HH* I-II 63% IV-V 10.9% III 26.1%
Kronvall 2009	106 aSAH* 74 MRI	*54±15 (oral) 58±11 (iv)	76.4%*	HH* I 8.5% IV 9.4 % II 43.4% V 4.7% III 34%
Mustonen 2008	49 aSAH* 42 MRI	52 (14-75)*	57%*	HH II-II 63% IV-V 10% III 27%
Pyysalo 2011	32 aSAH	53	56.3%	HH I 31.3% IV 12.5% II 37.5% III 18.8%
Sencer 2008	20 aSAH	median 52 (10 - 73)	55%	WFNS I 65% II 35%
Soppi 2012	171 aSAH 126 MRI	*57.5,12.2 (enteral) 56.9, 12.8 (IV)	57.9%*	HH* I-II 56.7% IV 19.9% III 19.2% V 2.3%

No = number of patients and controls who underwent MRI examinations; * Baseline characteristics presented of all patients included in the paper, not only patients who underwent an MRI examination; MRI timing = timing of the MRI of which the data is included in this review; Contr = controls;

Amount of SAH		Aneurysm treatment	Timing of MRI	MRI sequences	Field strength	No. pt with infarct (%)
Fisher 1-2 36.4% 3-4 63,6%		42.9% endo 46.8% surg 10.4% combined	12 months	T1, T2, PD	1.5T	-
Mod.Fisher 0-2 36.2% 3-4 63.8%		48.6% endo 51.4% surg	15.8 months±8.5 (range, 9-64 months	T1, T2, PD	1.5T	56 (41)
Fisher 1-2 3.5% 3-4 64.9%		54.1% endo 45.9% surg	12 months	T1, T2, PD	1.5T	-
Fisher 1-2 36% 3-4 64%		52.6% endo 47.4% surg	12 months	T1, T2	1.5T	30 (39)
-		100% endo	6 ± 2 months	T1, T2	3T	26 (47)
-		100% endo	18 months	T1, T2	3T	16 (42)
Fisher* 1 8.8% 2 20% 3 21.3%	4 45% N/A 5%	50% endo 50% surg	12 months	T1, T2. PD	1.5T	33 (72)
Fisher 1 0% 2 31% 3 51%	4 18%	100% surg	2.1-5.6 yr, mean 3.3 yr	T1, T2, T1-Gd, - FLAIR only at 1.5T	N = 40 1.0T N = 64 1.5T	84 (81)
Mod. Fisher* 0-2 38.5% 3-4 61.5%		45.5% endo 53.4% surg	12 months	T2, PD	-	-
Mod. Fisher* 1-2 41.3% 3-4 58.7%		47.5% endo 52.5% chir	12 months	T2, PD	1.5T	13 (33)
Fisher* 1 1.9% 2 8.5% 3 43.4%		*81.1% endo 17.9 % surg 1% cons	3 months	T2, FLAIR	-	32 (43)
Fisher* 1 8% 2 35%	3 41% 4 16%	41% endo* 59% surg	12 months	-	1.5T	20 (48)
Fisher 1 9.4% 2 3.1% 3 28.1 %	4 31.3% N/A 28.1%	100% endo	>9 years	FLAIR, T2*	1.5T	14 (34)
-		35% endo 65% chir	2 – 20 months, median 4	T1, T2, FLAIR, DWI	1.5T	5 (25)
Fisher* I 0% II 17.5%	III 46.2% IV 36.3%	*29.8% endo 69.6% chir 0.6% cons	12 months	T1, T2, DWI	-	43 (34)

WFNS = World Federation Neurosurgical Societies grade; Mod. Fisher = modified Fisher scale; endo = endovascular treated patients; surg = surgically treated patients HH = Hunt and Hess grade.

Table 3. Level of evidence

Statement	Level of evidence
Brain damage – Cerebral infarct	
25-81% of patients showed an cerebral infarct on MRI in the chronic phase after aSAH	strong
Brain damage – Volume measurements	
There was a significant difference in brain volume measurements between patients and controls	strong
Determinants of volume changes	
Patient age was significantly correlated with a higher CSF/ICV and VIWr	moderate
DCI was found to be related to smaller brain parenchymal volumes and lateral ventricle enlargement	low
Brain damage and clinical or neuropsychological outcome - Cerebral infarct	
The presence of infarcts or infarct volumes was significantly correlated with clinical and neuropsychological outcome	moderate
Brain damage and neuropsychological or clinical outcome – Volume measurements	
Brain parenchymal volume measurements and VIWr were related to clinical and neuropsychological outcome	strong

Baseline determinants predictive of MRI detected damage

Determinants of cerebral infarction

Table 6 summarizes the results found on this topic. In short, two studies, with 38 and 88 patients, addressed this subject.[25,29] Clinical condition at admission was found not to relate to presence of cerebral infarct or infarct volumes (descriptive analysis).[25] One study found no relation between the amount of extravasated blood on admission CT and the presence of cerebral infarcts or infarct volumes (descriptive analysis),[25] whilst the second study did find a significant association with a higher Fisher grade. More specifically, a higher Fisher grade was associated with an increased number of infarcts outside the territory of the parental artery of the aneurysm (p=0.001).[29]

Determinants of brain volume changes

Table 6 summarizes the results found on this topic. In short, three studies, with a median of 76 patients (range 38 - 77), reported on this subject.[23–25] A significant correlation of age with brain volume changes was found in two studies (CSF/ICV: r=0.718, p<0.001; CSF/ICV: r=0.416, p<0.001; VIWr: r=0.366, p=0.001).[23,24] No relation between clinical grade at admission and brain volume changes was found in two studies (CSF/ICV: p=0.239; BPV: B (95%CI); 3.2 (-5-12.1)).[24,25] One study on the other hand, did find more brain atrophy in patients with higher H&H grade (VIWr: p<0.001).[24]

The amount of extravasated blood on admission CT was found to be associated with brain atrophy in one study (CSF/ICV: p=0.014; VIWr: p=0.001),[24] whereas another did not find a relation (BPV: B (95%CI); 0.38 (-0.71-1.46)).[25] One research group reported that patients with hydrocephalus on admission CT tended to have lower brain volumes (CSF/ICV: p=0.51; VIWr: p<0.001).[24] Another study reported that symptomatic hydrocephalus was not related to volume measurements (BPV: B (95%CI); -14 (-38—10); lateral ventricle volume: B (95%CI) 0.18 (-0.29—0.66)).[25] Lastly, it was reported that DCI is related to lower BPVs and lateral ventricle enlargement, which would result in a higher CSF/ICV (B (95%CI): -38 (-66- -9); B (95%CI): 0.80 (0.26-1.35)).[25]

Table 4. Size of the deficits in patients with a cerebral infarct

Study	No	Mean volume of infarct (ml / cm^3)	SD	Mean diameter of infarct (mm)	SD
Bendel[28]	15/67‡	17.6	35.8		
	33/71	20.9	46.5		
	7/67	27.6	26.3		
	11/71	43.4	69.7		
De Bresser[35]	26/55	8.7*	0.4 - 61.3*		
De Bresser[25]	16/38	8.6*	1.1 - 80.9*		
Koivisto[29]	8/40‡			43	40
	21/47			36	31
	9/40			30	29
	8/47			52	30
Koivisto[32]	6/19§			19†	13
	7/21			57	42
Soppi[26]	21/62||			39.3	27
	22/64			34.3	28

In the articles it was not specified if, in case of multiple infarcts, a summation of the volumes or sizes was given or the only results of the largest infarct, unless stated otherwise. No = number of patients with infarct / total MR population; * median and 10^{th} – 90^{th} percentile; † size of infarction is size of largest deficit in case of multiple deficits; ‡ results were presented based on vascular territory and treatment method (i.e. coiling or clipping), in descending order; infarcts in parental artery territory in coiled aSAH patients, infarcts in parental artery territory in clipped aSAH patients, infarct in vascular territories other than the parental territory in coiled aSAH patients, and infarcts in vascular territories other than the parental territory in clipped aSAH patients; § patients presented by treatment method; surgical and endovascular; || patients presented by treatment strategy; enteral and intravenous administration of nimodipine

Table 5. Brain volume measurement outcomes

CSF/ICV ratio	No patients	mean ± sd	No controls	mean ± sd	p-value
Bendel et al (2009)[22]	37	0.41 ± 0.036	30	0.38 ± 0.033	0.003
Bendel et al (2010)[24]	76	0.36 ± 0.07	30	0.30 ± 0.063	0.001
De Bresser et al (2012)[35]	55	0.21 ± 0.025	25	0.21 ± 0.029	0.681
De Besser et al (2015)[25]	38	0.21 ± 0.034			
VIW ratio	**No patients**	**mean ± sd**	**No controls**	**mean ± sd**	**p-value**
Bendel et al (2006)[23]	77	0.23 ± 0.06	30	0.20 ± 0.04	0.021
Bendel et al (2010)[24]	76	0.23 ± 0.06	30	0.20 ± 0.038	0.020
Koivisto et al (2000)[29]					
endovascular patients	40	0.24 ± 0.07			
surgical patients	47	0.24 ± 0.08			

CSF/ICV; cerebrospinal fluid / intracranial volume; VIW: ventricular-to-intracranial width.

Damage detected on MRI predictive of patient outcome

Clinical or neuropsychological outcome - Cerebral infarct

Table 7 shows all results on this topic. Two studies, with 32 and 88 patients, reported on the relation between presence of a cerebral infarct and clinical outcome.[29,34] An infarct ($p<0.05$),[34] an infarct in the parental artery territory of the aneurysm ($p<0.003$)[29] or in another vascular territory ($p=0.003$)[29] was associated with worse clinical outcome. Logistic regression analysis proved an infarct in the parental artery territory of the ruptured aneurysm to be an independent predictor of poorer clinical outcome (OR 6.20; 95% CI 1.67-23.05; $p=0.006$).[29] Two studies, with 88 and 138 patients, reported on the relation of infarct size and outcome.[28,29] Size of infarcts in the parental artery territory ($p<0.001$) or in another vascular territory ($p=0.001$), was significantly associated with poorer clinical outcome.[29] A significant relation between infarct volume and deficits in several tests of visual reproduction, delayed story recall, performance intelligent quotient and verbal intelligence quotient was reported (most p-values <0.01).[28]

Clinical or neuropsychological outcome – Brain volume measurements

Table 7 shows all results on this topic. In short, four studies with a median of 65.5 patients (range 38-88) reported on correlations between brain volume measurements and clinical outcome.[24,25,29,35] The reported relations were as follows; a positive relation for BPV (at 6±2months OR 38.8, 95% CI 4.6-329.0; and at 18 months OR 91.2, 95% CI 2.5-3395.1),[25,35] a positive relation for VIWr (GOS 2-4 vs 5; 0.28±0.06 vs 0.23±0.06, $p=0.028$ and univariate analysis, $p=0.04$),[24,29] a positive relation for lateral ventricle volume (OR 7.4, 95% CI 1.6-33.5),[35] no relation for lateral ventricle volume (OR 1.1; 95% CI 0.2-5.1),[35] and no relation for peripheral CSF volume (OR 2.3, 95% CI, 0.6-8.0).[35]

Table 6. Determinants of cerebral infarcts and brain volume measurements

Determinant – cerebral infarcts			
	Study		Outcome (statistics)
Age	-	-	-
Clinical condition at admission	De Bresser[25]		Not related to the presence of infarcts or infarct volumes (descriptive analysis)
Amount of extravasated blood	De Bresser[25]		Not related to the presence of infarcts or infarct volumes (statistics not given)
	Koivisto[29]		Higher Fisher grade is associated with increased number of infarcts outside the territory of the parental artery of the aneurysm (p=0.001)

Determinant – brain volume measurement			
	Study	Measure	Outcome (statistics)
Age	Bendel[24]	CSF/ICV	Significant correlation with a higher ratio (r=0.781, p<0.001)
	Bendel[24]	VIWr	Significant correlation with a higher ratio (r=0.416, p<0.001)
	Bendel[23]	VIWr	Significant correlation with a higher ratio (r=0.366, p=0.001)
Clinical condition at admission	Bendel[24]	CSF/ICV	No relation at 12 months (H&H grade 1-2: 43.98±7.54 vs H&H grade 3-5: 37.15±5.18; p=0.239)
	De Bresser[25]	BPV	No relation at 18 months (B, 95%CI; 3.2, -5-12.1)
	De Bendel[24]	VIWr	Higher H&H grade is related to higher ratio (H&H 1-2: 0.21±0.06 vs H&H 3-5: 0.29±0.05, p<0.001)
Amount of extravasated blood	Bendel[24]	CSF/ICV	Associated with a higher ratio (Fisher grade 0-2: 32.75±7.75 vs Fisher grade 3-4: 37.13±6.10, p=0.014)
	Bendel[24]	VIWr	Associated with a higher ratio (grade 0-2: 0.20±0.06 vs grade 3-4: 0.25±0.06, p=0.001).
	De Bresser[25]	BPV	No relation with Hijdra score (B, 95% CI: 0.38, -0.71-1.46)
Hydrocephalus	Bendel[24]*	CSF/ICV	Tends to be related (hydrocephalus: 34.44±7.57 vs no hydrocephalus: 37.64±5.35, p=0.51)
		VIWr	Significant correlation (hydrocephalus: 0.28±0.06 vs no hydrocephalus: 0.21±0.06, p<0.001)
	De Bresser[25]†	BPV	Not related (B, 95%CI: -14, -38—10)
		Lateral ventricle volume	Not related (B, 95%CI: 0.18, -0.29—0.66)
DCI‡	De Bresser[25]	BPV	Related to smaller volumes (B, 95%CI: -38 -66- -9)
	De Bresser[25]	Lateral ventricle enlargement	Related to lateral ventricle enlargement (B, 95%CI: 0.80, 0.26-1.35)

* preoperative hydrocephalus on admission CT; † symptomatic hydrocephalus defined as a decreased level of consciousness with increased bicaudate index that was larger than the upper 95th percentile for age; ‡ defined as new focal deficits during admission or decreasing level of consciousness with new infarcts on CT; CSF/ICV; cerebrospinal fluid/intracranial volume; VIWr: ventricular-to-intracranial width ratio; BPV: brain parenchymal volume; DCI: delayed cerebral ischemia.

Table 7. MRI damage predictive of patient outcome

Infarction and patient outcome		
	Study	Outcome (statistics)
Infarct presence	Pyysalo[34]	Infarct presence was related to poorer clinical outcome (p<0.05)
	Koivisto[29]	Infarct presence within (p<0.003) or outside the parental artery territory (p=0.003) was associated with poorer clinical outcome Infarct in the parental artery territory of the aneurysm was an independent predictor of poorer clinical outcome (OR 6.20; 95% CI 1.67-23.05; p=0.006, logistic regression*)
Infarct volume	Bendel[28]	Relation between infarct volumes and tests of visual reproduction, delayed story recall, performance intelligent quotient and verbal intelligence quotient (13 of 17 tests showed significant correlation, with most p-values <0.01.)
	Koivisto[29]	Size of infarct within (p<0.001) or outside the parental artery territory (p=0.001) was associated with poorer clinical outcome

Brain volume measures and patient outcome		
Measure	Study	Outcome (statistics)
CSF/ICV	Bendel[24]	A significant higher ratio was found in patients with a neurologic deficit (present: 37.45±6.13 vs absent: 32.66±7.25, p=0.003)
	Bendel[22]	In patients with at least one neuropsychological deficit, there was a trend towards a slightly higher ratio compared to patients without a deficit (present: 42.0±3.6 vs absent: 40.4±3.5, non-significant)
VIWr	Bendel[24]	A higher ratio was found in patients with a lower GOS or patients with a neuropsychological deficit (GOS 2-4 vs 5: 0.28±0.06 vs 0.23±0.06, p=0.028 and deficit present vs absent: 0.25±0.07 vs 0.21±0.05, p=0.028) Especially with a deficit in general intellectual functioning (present vs absent: 0.30±0.04 vs 0.22±0.06, p<0.001)
	Koivisto[29]	Relation between higher ratio and poorer clinical outcome (GOS)(p=0.04)
BPV	De Bresser [35]	Lower volume 6 months after ictus was associated with worse outcome (mRS)(OR 38.8, 95% CI 4.6-329.0)
	De Bresser[25]	Lower BPV at 18 months after ictus was associated with worse outcome (mRS)(OR 91.2, 95% CI 2.5-3395.1)
Ventricle volume	De Bresser[35]	Higher lateral ventricle volume 6 months after ictus was associated with worse clinical outcome (mRS)(OR 7.4, 95% CI, 1.6-33.5)
	De Bresser[25]	No association was found between lateral ventricle volume at 18 months after ictus and outcome (mRS)(OR 1.1, 95% CI 0.2-5.1)
Peripheral CSF volume	De Bresser[35]	Higher peripheral CSF volume 6 months after ictus was not associated with outcome (mRS)(OR, 2.3, 95% CI 0.6-8.0)

* variables used in the model: size of the ischemic lesion in the parental artery territory or in any other location; presence of an ischemic lesion in the parental artery territory or in any other location; deficit due to preoperative intracerebral hematoma and higher VIWr

Sample size differences between the studies investigating the relation between lateral ventricle volume and outcome may have contributed to conflicting differences; the sample size was 55 in the study where a positive relation was found compared to 38 in the negative study. Two studies, with 37 and 76 patients, reported on brain volume measures and neuropsychological outcome.[22,24] In short, there was a positive relationship and a tendency towards a positive relationship between CSF/ICV and neurologic deficits (present vs absent; 37.45±6.13 vs 32.66±7.25, p=0.003 and 42.0±3.6 vs 40.4±3.5, non-significant).[22,24] A higher VIWr was found in patients with any neuropsychological deficit (present vs absent; 0.25±0.07 vs 0.21±0.05, p=0.028), especially with a deficit in general intellectual functioning (present vs absent; 0.30±0.04 vs 0.22±0.06, p<0.001).[24]

Discussion

The following findings, summarized according to the aims of the review, were found: (1) 25- 81% of aSAH patients show infarcts; there is a higher ratio of cerebrospinal fluid-to-intracranial volume in patients compared to controls; (2) there is a negative relation between age and DCI versus brain volume measurement outcomes; (3) lower BPV and the presence of infarcts or infarct volumes are associated with a worse outcome.

The wide range (25-81%) in aSAH patients demonstrating brain infarcts (strong level of evidence) underscores the heterogeneity of patient populations in the included articles. Regarding brain volume changes, it was found that aSAH patients have a lower brain volume compared to controls (strong level of evidence).[22–24] Unfortunately, due to the continuous nature of a volume measurement and the effect of age on such a measurement, a cut-off value for presence or absence of brain volume loss could not be established. Therefore, the proportion of aSAH patients with brain volume loss could not be calculated. However, in general, the decreased brain volume in aSAH patients as compared to controls does bring support for the EBI theory. Further support for the EBI theory is found in two of the studies included in this review. One study found brain atrophy independent of infarct presence,[22] and a second study quantified global ventricular and sulcal enlargement.[24]

Regarding the question whether there are determinants predictive of MRI detected damage, our search taught us that a patient's age is negatively related to brain volume (moderate level of evidence), and that DCI relates to smaller BPV and lateral ventricle enlargement (low level of evidence). The first, although yielding limited evidence, is not surprising. It is well known that some quantity of brain volume loss is encountered with increasing age.[37] The second finding could be attributed to two things. One, in the study investigating this topic, the presence of new infarcts was included in their DCI definition.[25] Logically, this would lead to a negative relation of DCI with brain volume due to volume loss within the infarcted area. Two, pronounced EBI, resulting in an increase

of global parenchymal loss, may increase the likelihood of developing DCI. Besides the relation of age and DCI with MRI detected damage, we were not able to identify any other positive or negative determinant. In fact, most investigated determinants produced conflicting results. This may be due to heterogeneity of the used research methods. Across studies, different tools or scoring systems were used for both determinants and outcome measures which made the results difficult to summarize and may have introduced inadequacies. For example, two scoring methods were used to assess the amount of extravasated blood, i.e. Fisher grade and Hijdra scale. Of these two, the Hijdra score is thought to be more precise since it takes into account specific anatomic locations and it is shown to have a better interobserver agreement than the Fisher scale.[38] The same accounts for the discrepancies in findings between CFS/ICV and VIWr. In general the laborious volume measurements are thought to be more precise than the simple planimetric measure of the VIWr.

Our assessment of the relationship between MRI detected damage and patient outcome, resulted in the findings that BPV and VIWr are related to clinical- and neuropsychological outcome (strong level of evidence), and that the presence of infarcts or infarct volumes are significantly correlated with clinical or neuropsychological outcome (moderate level of evidence). This latter finding is not surprising, since neurologic deficits are expected when infarcts occur in critical brain areas. It is known that tests may be difficult to perform in aSAH patients due to test difficulty, poor clinical condition, or severe headache during mental exercise.[3] Therefore, studies investigating these properties may be skewed towards patients with better clinical outcome due to selection bias. Futhermore, a simple clinical tool such as the GOS can underappreciate the neuropsychological impact due to the gross subdivision into categories. For instance, patients with GOS '5' (i.e. mild or no disability) might still have subtle cognitive deficits and a need to apply adaptive strategies in daily life.[3,27,39]

A limitation of this review is that only cerebral infarcts and brain volume changes were investigated. Not only infarcts but also many different focal injury entities can occur, including white matter lesions, superficial siderosis, and leukoaraiosis. Taking these lesions into account might lead to stronger levels of evidence. However, the manner of data presentation in the included studies did not allow for a thorough evaluation of this.

Another limitation is that most studies showed skewedness towards a good recovery for the included patients. This is probably caused by the fact that patients had to endure scanning sessions and other follow-up investigations to be able to participate. Moreover, a few studies used data of MRI-sequences which were only obtained when the patient voluntarily stayed longer in the scanner, resulting in selection bias.[22–24] As well, a few studies even stated a good clinical condition or functional recovery as a inclusion criterium.[25,35] Thereby, it is likely that the general patient outcome in clinical

practice, and thereby most likely the MRI results, is worse than the presented results.

Future directions

The findings of this review are relevant as they underscore that not only focal brain injury plays an important role in the course of the disease, but presumably EBI also attributes significantly to brain damage as was proven by brain volume loss irrespective of brain infarcts. The results regarding possible determinants of infarct development or brain volume loss, and the relation between brain damage and neuropsychological or clinical outcome, however, were scarce and heterogeneous of character. On the one hand this shows the complexity of the effects of the disease with research focusing on different parameters, while on the other hand it emphasizes the need to conduct research on a uniform basis to be able to draw solid conclusions.

Therefore, in future work the entity of EBI, its effect on volume changes and, in continuation, its effect on patient outcome should be investigated. Of equal importance is the question how to intervene in this process to constrain global neuronal loss. In addition, standardized research needs to be conducted to draw rigid conclusions regarding determinants of brain injury and / or brain volume measurement outcomes, and the relation with clinical- or neuropsychological outcome. Only when understanding the source of the damage and the subsequent effects on patient level, therapies can be targeted to prevent any additional damage and with that improve patient outcome.

References

1. Vergouwen MD, Jong-Tjien-Fa AV, Algra A, Rinkel GJ. Time trends in causes of death after aneurysmal subarachnoid hemorrhage: A hospital-based study. Neurology. 2016;86:59–63.
2. Rinkel GJ, Algra A. Long-term outcomes of patients with aneurysmal subarachnoid haemorrhage. Lancet Neurol. 2011;10:349–356.
3. Al-Khindi T, MacDonald RL, Schweizer TA. Cognitive and functional outcome after aneurysmal subarachnoid hemorrhage. Stroke. 2010;41:519-536.
4. Cahill J, Zhang JH. Subarachnoid Hemorrhage: is it time for a new direction? Stroke. 2009;40:86–87.
5. Sehba FA, Pluta RM, Zhang JH. Metamorphosis of subarachnoid hemorrhage research: from delayed vasospasm to early brain injury. Mol Neurobiol. 2011;43:27–40.
6. Friedrich V, Flores R, Muller A, Sehba FA. Luminal platelet aggregates in functional deficits in parenchymal vessels after subarachnoid hemorrhage. Brain Res. 2010;1354:179–187.
7. Frontera JA, Ahmed W, Zach V, et al. Acute ischaemia after subarachnoid haemorrhage, relationship with early brain injury and impact on outcome: a prospective quantitative MRI study. J Neurol Neurosurg Psychiatry. 2015;86:71–78.
8. Grunwald IQ, Papanagiotou P, Politi M, Struffert T, Roth C, Reith W. Endovascular treatment of unruptured intracranial aneurysms: occurrence of thromboembolic events. Neurosurgery. 2006;58:612–617.
9. Kang DH, Kim BM, Kim DJ, et al. MR-DWI-positive lesions and symptomatic ischemic complications after coiling of unruptured intracranial aneurysms. Stroke. 2013;44:789–791.
10. Vergouwen MD, Vermeulen M, van Gijn J, et al. Definition of delayed cerebral ischemia after aneurysmal subarachnoid hemorrhage as an outcome event in clinical trials and observational studies: proposal of a multidisciplinary research group. Stroke. 2010;41:2391–2395.
11. Leclerc X, Fichten A, Gauvrit JY, et al. Symptomatic vasospasm after subarachnoid haemorrhage: Assessment of brain damage by diffusion and perfusion-weighted MRI and single-photon emission computed tomography. Neuroradiology. 2002;44:610–616.
12. Liu Y, Soppi V, Mustonen T, et al. Subarachnoid hemorrhage in the subacute stage: elevated apparent diffusion coefficient in normal-appearing brain tissue after treatment. Radiology. 2007;242:518–525.
13. Vatter H, Güresir E, Berkefeld J, et al. Perfusion-diffusion mismatch in MRI to indicate endovascular treatment of cerebral vasospasm after subarachnoid haemorrhage. J Neurol Neurosurg Psychiatry. 2011;82:876–883.
14. Bederson JB, Connolly ES Jr, Batjer HH, et al. Guidelines for the management of aneurysmal subarachnoid hemorrhage: A statement for healthcare professionals from a special writing group of the stroke council, American heart association. Stroke. 2009;40:994–1025.
15. de Rooij NK, Rinkel GJ, Dankbaar JW, Frijns CJ. Delayed cerebral ischemia after subarachnoid hemorrhage: a systematic review of clinical, laboratory, and radiological predictors. Stroke. 2013;44:43–54.
16. Boluijt J, Meijers JC, Rinkel GJ, Vergouwen MD. Hemostasis and fibrinolysis in delayed cerebral ischemia after aneurysmal subarachnoid hemorrhage: a systematic review. J Cereb Blood Flow Metab. 2015;35:724–733.
17. Hoy D, Brooks P, Woolf A, et al. Assessing risk of bias in prevalence studies : modification of an existing tool and evidence of interrater agreement. J Clin Epidemiol. 2012;65:934–939.
18. Hunt WE, Hess RM. Surgical risk as related to time of intervention in the repair of intracranial aneurysms. J Neurosurg. 1968;28:14–20.
19. Teasdale G, Drake CG, Hunt W, et al. A universal subarachnoid hemorrhage scale: report of a committee of the World Federation of Neurosurgical Societies. J Neurol Neurosurg Psychiatry. 1988;51:1457.
20. Hijdra A, Brouwers PJ, Vermeulen M, van Gijn J. Grading the amount of blood on computed tomograms after subarachnoid hemorrhage. Stroke. 1990;21:1156–1161.
21. Fisher CM, Kistler JP, Davis JM. Relation of cerebral vasospasm to subarachnoid hemorrhage visualized by computerized tomographic scannin. Neurosurgery. 1980;6:1–9.
22. Bendel P, Koivisto T, Niskanen E, et al. Brain atrophy and neuropsychological outcome after treatment of ruptured anterior cerebral artery aneurysms: a voxel-based morphometric study. Neuroradiology.

2009;51:711–722.
23. Bendel P, Koivisto T, Hänninen T, et al. Subarachnoid hemorrhage is followed by temporomesial volume loss: MRI volumetric study. Neurology. 2006;67:575–582.
24. Bendel P, Koivisto T, Äikiä M, et al. Atrophic enlargement of CSF volume after subarachnoid hemorrhage: Correlation with neuropsychological outcome. AJNR Am J Neuroradiol. 2010;31:370–376.
25. De Bresser J, Schaafsma JD, Luitse MJ, Viergever MA, Rinkel GJ, Biessels GJ. Quantification of structural cerebral abnormalities on MRI 18 months after aneurysmal subarachnoid hemorrhage in patients who received endovascular treatment. Neuroradiology. 2015;57:269–274.
26. Soppi V, Karamanakos PN, Koivisto T, et al. A randomized outcome study of enteral versus intravenous nimodipine in 171 patients after acute aneurysmal subarachnoid hemorrhage. World Neurosurg. 2012;78:101–109.
27. Hadjivassiliou M, Tooth CL, Romanowski CA, et al. Aneurysmal SAH: cognitive outcome and structural damage after clipping or coiling. Neurology. 2001;56:1672–1677.
28. Bendel P, Koivisto T, Könönen M, et al. MR Imaging of the Brain 1 Year after Aneurysmal Subarachnoid Hemorrhage: randomized study comparing surgical with endovascular treatment. Radiology. 2008;246:543–552.
29. Koivisto T, Vanninen R, Hurskainen H, Saari T, Hernesniemi J, Vapalahti M. Outcomes of early endovascular versus surgical treatment of ruptured cerebral aneurysms. A prospective randomized study. Stroke. 2000;31:2369–2377.
30. Kronvall E, Undrén P, Romner B, et al. Nimodipine in aneurysmal subarachnoid hemorrhage: a randomized study of intravenous or peroral administration. J Neurosurg. 2009;110:58–63.
31. Kivisaari RP, Salonen O, Servo A, Autti T, Hernesniemi J, Ohman J. MR imaging after aneurysmal subarachnoid hemorrhage and surgery: a long-term follow-up study. AJNR Am J Neuroradiol. 2001;22:1143–1148.
32. Koivisto T, Vanninen E, Vanninen R, Kuikka J, Hernesniemi J, Vapalahti M. Cerebral perfusion before and after treatment of acutely ruptured cerebral aneurysms: a 1-year prospective follow-up study. Neurosurgery. 2002;51:312–326.
33. Mustonen T, Koivisto T, Vanninen R, et al. Heterogeneity of cerebral perfusion 1 week after haemorrhage is an independent predictor of clinical outcome in patients with aneurysmal subarachnoid haemorrhage. J Neurol Neurosurg Psychiatry. 2008;79:1128–1133.
34. Pyysalo LM, Keski-Nisula LH, Niskakangas TT, Kähärä VJ, Ohman JE. Long-term MRI findings of patients with embolized cerebral aneurysms. Acta Radiol. 2011;52:204–210.
35. De Bresser J, Vincken KL, Kaspers AJ, Rinkel GJ, Viergever MA, Biessels GJ. Quantification of cerebral volumes on MRI 6 months after aneurysmal subarachnoid hemorrhage. Stroke. 2012;43:2782–2784.
36. Sencer S, Kiris T, Sencer A, et al. Diffusion and perfusion MRI findings with clinical correlation in patients with subarachnoid haemorrhage related vasospasm. Acta Neurochir Suppl. 2008;104:245–248.
37. Watanabe M, Liao JH, Jara H, Sakai O. Multispectral quantitative MR Imaging of the human brain: lifetime age-related effects. Radiographics. 2013;33:1305–19.
38. Van Norden AG, van Dijk GW, van Huizen MD, Algra A, Rinkel GJ. Interobserver agreement and predictive value for outcome of two rating scales for the amount of extravasated blood after aneurysmal subarachnoid haemorrhage. J Neurol. 2006;253:1217–1220.
39. Hütter BO, Gilsbach JM. Which neuropsychological deficits are hidden behind a good outcome (Glasgow = I) after aneurysmal subarachnoid hemorrhage?. Neurosurgery. 1993;33:999-1005.

Appendix

Table I. Risk of bias

Item	Bendel (2006)	Bendel (2008)	Bendel (2009)	Bendel (2010)	Bresser (2012)	Bresser (2015)
External validity						
1. Was the study's target population a close representation of the national population in relation to relevant variables, e.g., age, sex, occupation?	yes	yes	yes	yes	yes	yes
2. Was the sampling frame a true or close representation of the target population?	no	yes	no	no	no	no
3. Was some form of random selection used to select the sample, OR, was a census undertaken?	no	yes	no	no	yes	yes
4. Was the likelihood of non-response bias minimal?	no	yes	yes	yes	yes	yes
Internal validity						
5. Were data collected directly from the subjects (as opposed to a proxy)?	yes	yes	yes	yes	yes	yes
6. Was an acceptable case definition used in the study?	no	yes	yes	yes	yes	yes
7. Was the study instrument that measured the parameter of interest (e.g., prevalence of low back pain) shown to have reliability and validity (id necessary)?	yes	yes	yes	yes	yes	yes
8. Was the same mode of data collection used for all subjects?	yes	yes	yes	no	no	no
9. Was the length of the shortest prevalence period for the parameter of interest appropriate?	yes	yes	yes	yes	yes	yes
10. Were the numerator(s) and denominators(s) for the parameter of interest appropriate?	yes	yes	yes	yes	yes	yes
11. Summary item on the overall risk of study bias	high	low	high	high	moderate	moderate

	Hadjivassiliou (2001)	Kivisaari (2001)	Koivisto (2000)	Koivisto (2002)	Kronvall (2009)	Mustonen (2008)	Pyysalo (2011)	Sencer (2008)	Soppi (2012)
	yes	yes	yes	yes	yes	yes	yes	yes	yes
	yes	no	yes	yes	yes	yes	no	no	yes
	yes	yes	yes	yes	yes	yes	yes	no	yes
	no	yes	no	yes	no	no	yes	yes	no
	yes	yes	yes	yes	yes	yes	yes	yes	yes
	yes	yes	yes	yes	yes	yes	yes	yes	yes
	yes	no	no	yes	no	no	yes	yes	no
	no	yes	yes	yes	yes	no	yes	no	yes
	yes	yes	yes	yes	yes	yes	yes	yes	yes
	yes	yes	yes	yes	yes	yes	yes	yes	yes
	moderate	high	high	low	high	high	moderate	high	high

Chapter 4

Subacute perfusion impairment is related to long-term brain parenchymal volume loss after subarachnoid hemorrhage

L.A. van der Kleij[1], C. Lucci[1], T.D. Witkamp[1], M.D.I. Vergouwen[2], G.J.E. Rinkel[2], J. Hendrikse[1], E.T. Petersen[3,4], J.B. De Vis[5]

1 Department of Radiology, University Medical Centre Utrecht, Utrecht University, Utrecht, The Netherlands.
2 Department of Neurology and Neurosurgery, Brain Centre Rudolf Magnus, University Medical Centre Utrecht, Utrecht University, Utrecht, The Netherlands.
3 Danish Research Centre for Magnetic Resonance, Centre for Functional and Diagnostic Imaging and Research, Copenhagen University Hospital Hvidovre, Denmark
4 Centre for Magnetic Resonance, DTU Elektro, Technical University of Denmark, Kgs Lyngby, Denmark
5 National Institute of Neurological Disorders and Stroke, National Institutes of Health, Bethesda, Maryland, USA

Submitted manuscript

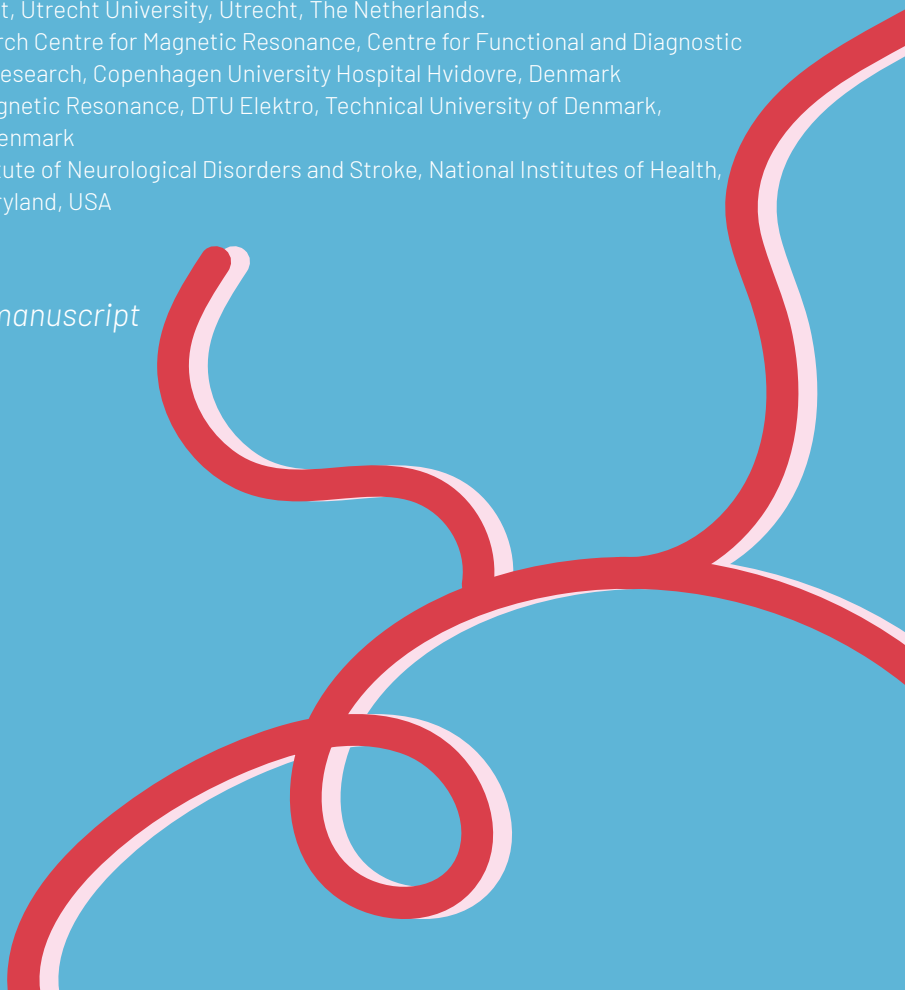

Abstract

A long-term decreased brain volume after aneurysmal subarachnoid hemorrhage is associated with worse clinical outcome. Evidence for clinical and imaging characteristics associated with a decreased brain volume is limited and based on cross-sectional studies. We hypothesized that perfusion impairment between days four to twenty-one after ictus is related to long-term brain volume loss. In this longitudinal study, clinical and imaging measures on admission were collected, and thirty-nine patients (72% female, 55±12 y.o.) underwent (3T) MRI around day fourteen, six months and eighteen months. Perfusion heterogeneity on ASL images was used as a measure for the degree of perfusion impairment. Brain parenchymal volume loss was obtained with automatic segmentation software. Median brain volume loss was 2.0% (IQR 0.7 - 3.7%) at six months and 3.3% (IQR 2.0 - 5.7%) at eighteen months. In the final, backward linear regression model (R^2=0.25, $R^2_{adjusted}$= 0.15), the degree of perfusion heterogeneity on day fourteen was related to brain volume loss (B = 11 (95%CI 1 – 21), P = 0.029). The amount of extravasated blood on admission CT and clinical condition on admission were not related to brain volume loss, but did contribute to the explained variance. In summary, perfusion heterogeneity in the subacute stage was associated with brain volume loss, independent from clinical and imaging measures on admission.

Introduction

A long-term decreased brain volume after aneurysmal subarachnoid hemorrhage (aSAH) is associated with worse clinical outcome [1-3] However, it is unclear which clinical and radiological markers are associated with this long-term brain parenchymal volume loss after aSAH: from previous studies limited evidence exists for clinical and imaging characteristics associated with a decreased brain volume.[4] A higher patient age (moderate level of evidence) and the occurrence of delayed cerebral ischemia (DCI)(low level of evidence) are associated with a smaller brain volumes a year after aSAH.[1, 2, 5] Conflicting results have been found on a possible association between decreased brain volume and either clinical condition on admission or the amount of extravasated blood on admission.[1, 2] Notably, the associations with decreased brain volume are drawn from cross-sectional data and no longitudinal MRI data yet exist to determine the degree of brain volume loss following aSAH.

Perfusion imaging in the subacute stage offers an advantage over structural imaging, because perfusion deficits often precede structural deficits and functional impairments. Perfusion measures are related to both diffuse and focal brain injury in the acute (first seventy-two hours) and subacute stages (day four to twenty-one) after aSAH.[6-9] Lower cerebral blood flow (CBF) values on computed tomography perfusion (CTP) in the subacute stage are seen in patients with DCI and poor neurological outcome.[6, 10] Abnormal mean transit time, time to peak, and bolus arrival time on perfusion-weighted MRI have been found to coincide with neurological deterioration after subarachnoid hemorrhage.[11] Perfusion impairment may be caused by micro- and macrovascular vasospasm.[12] Under normal conditions, a healthy brain has fairly homogeneous perfusion. Perfusion heterogeneity is a marker for perfusion impairment, because it reflects changes in arterial transit time and local perfusion changes, such as hypoperfusion due to vasospasm.[13] The occurrence of perfusion heterogeneity in the acute stage after aSAH was found to be a predictor of DCI.[14] On single-photon emission tomography (SPECT) images of aSAH patients, the coefficient of variation as a measure of perfusion heterogeneity was higher compared to controls.[15] More so, an increased perfusion heterogeneity was associated with poor outcome and chronic ischemic lesions.[7] These findings suggest that perfusion heterogeneity measures could be sensitive markers to identify individuals with a perfusion impairment who are, consequently, at risk for brain volume loss.

We hypothesized that a higher degree of perfusion heterogeneity is associated with (diffuse) brain volume loss, because of the association between perfusion impairment, DCI and poor outcome. For this, the relationship was investigated between perfusion impairment in the subacute stage and brain volume loss six and eighteen months after ictus, independently from age, clinical condition and the amount of extravasated blood on admission.

Methods

The research ethics board of the University Medical Centre Utrecht decided that no formal approval was needed for this study and no informed consent from patients, because it was a retrospective analysis of longitudinal study data collected as part of clinical care. We included patients who were admitted between December 2012 and February 2016. Inclusion criteria were: 1) confirmed aSAH; 2) endovascular coiling of the aneurysm; and 3) available MRI data from at least the scans around day fourteen and the scan at six months. Aneurysmal SAH was defined as the presence of subarachnoid blood on head CT or the presence of bilirubin in cerebrospinal fluid, and visualization of the aneurysm on either CT angiography, MR angiography or digital subtraction angiography. Exclusion criteria were: 1) contraindications for MRI; 2) a clinical condition which did not allow transportation to the MRI scanner; 3) age <eighteen years; and 4) neurosurgical clipping of the aneurysm. The first MRI scan was performed in the subacute stage between days four and twenty-one, and follow-up imaging was performed six months after ictus. All patients were scheduled for a second follow-up MRI scan at eighteen months. Functional outcome was assessed by the Barthel Activities of Daily Living index, which ranges from 0 to 20.[16]

Patient characteristics on admission

The following baseline characteristics were collected: age, sex, Prognosis on Admission of Aneurysmal Subarachnoid Hemorrhage (PAASH) score, and the Hijdra score. The PAASH scale describes the clinical condition on admission and it is based on the Glasgow Coma Scale (GCS). A score of 1 represents the best clinical status (GCS 15) and a score of 5 reflects the worst clinical status (GCS 3).[17] The Hijdra score represents the amount of extravasated blood on the admission head CT, and was rated by J.B.D.V. (4 years of experience).[18] The score ranges between 0 and 42. A higher score indicates a larger amount of blood present on the admission head CT.

Imaging protocol

Imaging was performed on a 3T Philips MR scanner with a SENSE 8-channel head receive coil and a body coil for transmission (Achieva, Philips Medical Systems, Best, The Netherlands). The imaging protocol included a T_2-fluid-attenuated inversion recovery (FLAIR) sequence, a Circle of Willis 3D time-of-flight magnetic resonance angiography (3D-TOF-MRA) sequence, and a diffusion weighted imaging (DWI) sequence. In addition, a pseudocontinuous arterial spin labeling (pCASL) sequence was performed in the scan around day fourteen after ictus. The scan parameters of the pCASL sequence were voxel size 3x3x7mm^3, FOV 240x119x240mm^3, TR/TE: 4000/14ms, and label duration 1650ms. A multislice EPI (echo planar imaging) readout was used with a 1525-2160ms

post label delay. The imaging parameters of the T_2-FLAIR sequence were TR/TI/TE = 10000/2800/120ms, voxel size 0.4x0.4x4mm^3, 1mm inter-slice gap), the parameters of the 3D-TOF-MRA sequence were TR/TE 22/3.45 ms, acquired voxel size 0.4x.0.7x1.0 mm^3, 0.5 mm inter-slice gap, reconstructed voxel size 0.36x0.36x0.50 mm^3, and the parameters of the DWI sequence were TR/TE 3015/68ms, b-factors = 2 (0 and 1000s/mm^2), voxel size= 0.5x0.5x4mm^3, 1mm inter-slice gap).

Image Analysis

Lesion and vasospasm assessment

An experienced neuroradiologist (T.D.W., 30 years of experience) assessed ischemic lesion occurrence and the number of ischemic lesions in each participant. This rating was performed on a joined reading of the T_2-FLAIR and DWI images, blinded for patient characteristics. Proximal vasospasm presence was scored on the MRA images. Ischemic lesion volume was obtained through manual segmentation (M.E.H.) while blinded for patient information in the Picture Archiving and Communication System (PACS) software IDS7 (Sectra AB, version 17.3, Linköping, Sweden).

ASL postprocessing

The pCASL data was processed using IDL 6.1 for Windows (ITT Visual Information Solutions, Boulder, C.O., U.S.A.). First, the label images were subtracted from the control images to remove stationary tissue signal. Subsequently, outliers in the control-label pairs were discarded after which the signal from the remaining label-control pairs was averaged.[19] All further analyses regarding the perfusion heterogeneity (see paragraph below) were performed on the resulting signal intensity maps. The images were purposely not quantified as we noticed a disruptive effect of blood on the M0 images which would have affected quantification. The quality of the pCASL images was assessed qualitatively (L.A.v.d.K.), and images of poor quality were excluded from further analysis.

Borderzone ratio and spatial coefficient of variation

Conventional ASL MRI images are acquired after a single, predefined PLD to ensure that the labeled protons have reached the tissue. This carries a disadvantage in clinical settings as the arterial transit time (ATT) may increase in disease-stages, which confounds the perfusion assessment. If the ATT exceeds the predefined post label delay (PLD), not all labeled spins will have reached the brain tissue at the time of image acquisition. This results in increased perfusion heterogeneity on the perfusion maps. In particular, a lower signal will arise in the borderzones (i.e., brain tissue around the utmost distal vasculature) along with an increased vascular signal in the proximal vasculature.[20] The degree of perfusion heterogeneity can be quantified with two distinct

methods: the borderzone ratio and coefficient of variation (CoV). The borderzone ratio is the perfusion in the borderzones expressed as a ratio against whole brain perfusion: [mean perfusion$_{\text{borderzone regions}}$] / [mean perfusion$_{\text{whole brain}}$].[21] Alternatively, global spatial CoV is the standard deviation relative to the mean whole brain perfusion: [standard devation$_{\text{perfusion, whole brain}}$] / [mean$_{\text{perfusion, whole brain}}$].[13] To obtain both measures, the obtained perfusion signal intensity maps were first aligned to Dartel space. Then, a whole brain mask was applied to obtain the mean and the standard deviation of global perfusion signal intensity. This whole brain mask excluded the bottom three slices to further circumvent the effect of blood on the quantitative analysis of the signal intensity maps. These bottom slices surround the circle of Willis, the structure around which most blood gathers after aSAH. To obtain the borderzone ratio, a borderzone region map was created based on territorial ASL data from individuals with steno-occlusive diseas.[22] These data were brought to standard space and mean perfusion territory maps were used to delineate the borderzone regions (Figure 1).

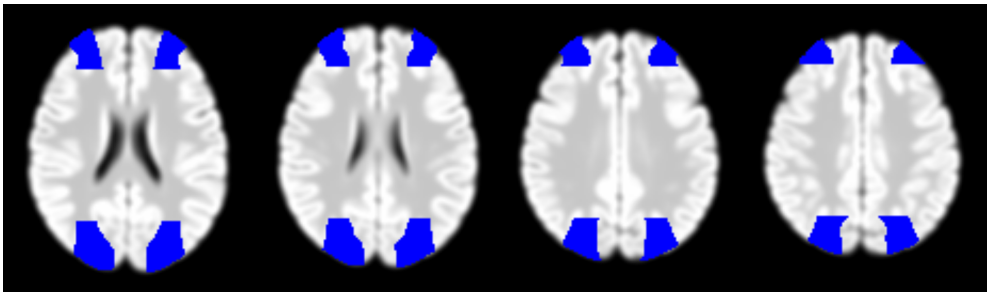

Fig. 1. Four axial slices showing the borderzone regions (blue) in standard space.

Brain volume measurements

Brain segmentation was performed using Statistical Parametric Mapping to obtain brain volume measurements (SPM12, Wellcome Department of Cognitive Neurology, Institute of Neurology, Queen Square, London) on the T_2-FLAIR images.[23, 24] The images were processed with the 'segment' function that combines the signal intensity of a voxel and its location to establish the probability of a voxel belonging to a particular tissue class, i.e., grey matter, white matter, cerebrospinal fluid, or skull. If lesions were not automatically excluded from the brain parenchymal tissue, they were segmented with the lesion prediction algorithm as implemented in the Lesion Segmentation Tool (LST) version 2.0.15 for SPM (www.statistical-modelling.de/lst.html) prior to brain segmentation.[25] The brain parenchymal volumes were calculated from the obtained grey matter and white matter volumes using MeVisLab (MeVis Medical Solutions AG, Bremen, Germany, version 2.7). If applicable, the lesion volume as found by the LST was subtracted from the brain parenchymal volume. To remove the effect of baseline brain volume on volume change, we used a relative brain volume loss measure: relative brain volume change (ΔBPV) = ($BPV_{\text{MRI 6/18 months}}$ - $BPV_{\text{MRI day 14}}$) / $BPV_{\text{MRI day 14}}$. The seg-

mentation quality was assessed qualitatively as either 'good', 'mediocre' or 'bad' (C.L.). Only segmentations that were considered to be of good quality were included in the final analysis.

Statistical analysis

Statistical analysis was carried out with R (R Foundation for Statistical Computing, Vienna, Austria). A multiple linear regression analysis was performed using a backward model.[26, 27] Variables included in the model were selected at a threshold of $P < 0.50$.[28] A p-value < 0.05 was considered statistically significant. The independent variables were age, Hijdra score, PAASH score, and either the borderzone ratio or the CoV. The dependent variable was relative brain volume change at either six or eighteen months. The assumption of linearity and homoscedasticity, normality of the residuals, and the influence of each observation through Cook's distance were tested for the resulting model. In addition, multicollinearity was evaluated through variance inflation factors (VIFs), where any factor above 4 was defined as 'requiring further investigation' and a VIF exceeding 10 as 'severe multicollinearity'. A spearman correlation was performed to investigate an expected correlation between the two measures of perfusion heterogeneity, and to investigate whether a correlation exists between DWI and T_2-FLAIR lesions or vasospasm in the subacute stage and brain volume loss. Mann-Whitney U and Wilcoxon signed-rank tests were performed to check for differences between and within groups. A Bonferroni corrected p-value of 0.006 was considered statistically significant for the 8 bivariate analyses regarding brain volume, and a corrected p-value of 0.008 was considered significant for the analyses regarding perfusion heterogeneity.

Results

Thirty-nine patients met the criteria of this study, and a follow-up scan at eighteen months was available in 27 patients (Figure 2). The first MRI scan was performed at a median of fourteen days (IQR 11 – 15) after ictus. The second MRI scan was obtained at a median of six months after ictus (IQR 6 – 6) and the third MRI scan at eighteen months (IQR 16 – 19) after ictus. Most patients (90 per cent) were in good clinical condition on admission. Baseline characteristics of the patients with one follow-up scan and those with two follow-up scans were similar (Table 1).

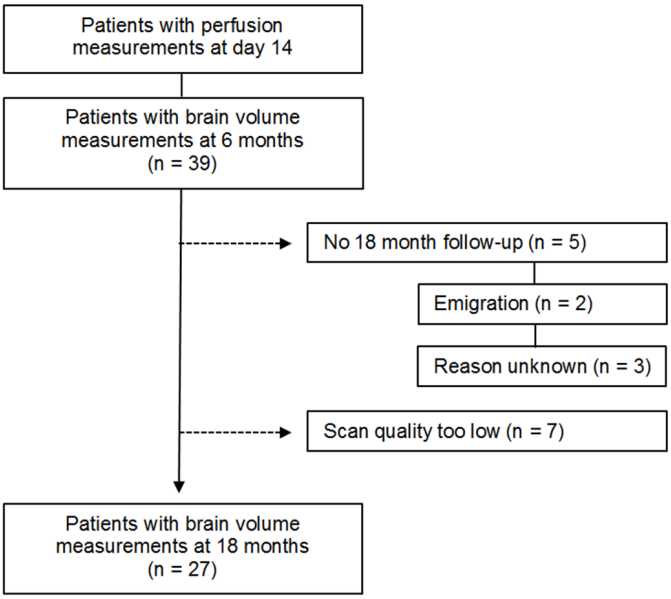

Fig. 2. Flowchart.

Table 1. Baseline parameters

		MRI 6 months (n = 39)	MRI 18 months (n = 27)
Age (mean)		55±12 (range 24-81)	56±12 (range 24-81)
Sex, n (%)		28 (72%)	21 (78%)
PAASH, n (%)	I II III IV V	I: 23 (59%) II: 12 (31%) III: 1 (3%) IV: 0 (0%) V: 3 (8%)	I: 15 (56%) II: 8 (30%) III: 1 (4%) IV: 0 (0%) V: 3 (11%)
Hijdra score (median)		25 (IQR 15-29)	24 (IQR 13-28)

PAASH = Prognosis on Admission of Aneurysmal Subarachnoid Hemorrhage; IQR = interquartile range.

The median brain volume change was 2.0 per cent (IQR 0.7 – 3.7 per cent) six months after ictus and 3.3 per cent (IQR 2.0 – 5.7 per cent) eighteen months after ictus (Table 2). Four patients (10 per cent) showed an elevated brain volume at six months with a mean increase of 1 per cent, and two patients (7 per cent) showed an elevated brain volume between day fourteen and eighteen months with a mean increase of 2 per cent. The additional median brain volume loss between six and eighteen months was 1.3 per cent (IQR -0.3 – 1.8 per cent) within the subgroup (P = 0.006).

No correlation was found between brain volume loss at six or eighteen months and total lesion volume ($\rho = 0.23$, P = 0.16 and $\rho = 0.12$, P = 0.57, respectively), number of lesions ($\rho = 0.23$, P = 0.17 and $\rho = 0.11$, P = 0.58, respectively) (Table 2). No difference was found

in the degree of brain volume loss at six or eighteen months between patients without lesions and patients with at least one ischemic lesion in the subacute stage (P = 0.22 and P = 0.68, respectively). Similarly, no difference was found between patients with and without vasospasm (P = 0.31 and P = 0.09, respectively). In addition, the degree of perfusion heterogeneity was not correlated with ischemic lesion presence in the subacute stage (all $\rho < 0.17$ and all $P > 0.29$). Age was also not correlated with the borderzone ratio ($\rho = 0.10$, P = 0.55) nor with the CoV ($\rho = -0.11$, P = 0.48). Lastly, vasospasm presence did not affect the borderzone ratio (P = 0.45) or CoV (P = 0.09). Functional outcome was available in 36 patients at 8.3±3.1 weeks from ictus. All patients showed good clinical outcome with a Barthel Index score of at least 18.

Table 2. Characteristics on MRI: perfusion heterogeneity, lesion presence, vasospasm and brain volume loss

		MRI 6 months (n=39)	**MRI 18 months (n=27)**
Borderzone ratio (median)	MRI day 14	0.95 (IQR 0.87-1.00)	0.93 (IQR 0.86-0.96)
CoV (median)	MRI day 14	0.58 (IQR 0.53-0.66)	0.59 (IQR 0.55-0.67)
Brain volume loss (median)	MRI 6 months MRI 18 months	2.0% (IQR 0.7-3.7%)	2.5% IQR (0.6-3.5%) 3.3% (IQR 2.0-5.7%)
Lesion presence, n (%)	MRI day 14	18 (46%)	13 (48%)
Total lesion volume (ml, median)	MRI day 14	0 (range 0-26)	0 (0-26)
Total number of lesions (median)	MRI day 14	0 (range 0-12)	0 (range 0-12)
Vasospasm presence, n (%)	MRI day 14	5 (13%)	2 (7%)

CoV = spatial coefficient of variation.

Multiple regression models: borderzone ratio

The median borderzone ratio was 0.95 (IQR 0.87 – 1.00) in all patients and 0.93 (IQR 0.85 – 0.97) in the subgroup. The final regression model included the borderzone ratio, the Hijdra score and the PAASH score for brain volume loss at six months ($R^2 = 0.16$, $R^2_{adjusted} = 0.09$) as well as at eighteen months ($R^2 = 0.25$, $R^2_{adjusted} = 0.15$) (Table 3). Age was excluded through backward selection due to P > 0.50 (Steyerberg et al., 2000). The borderzone ratio was the only variable associated with brain volume loss at six months (B = -7.7 (95% CI = -15.0 – -0.5), P = 0.037) and at eighteen months (B = -10.9 (95% CI = -20.7 – -1.2), P = 0.030). As an example, in the model a borderzone ratio of 0.70, a PAASH score of 1, and a Hijdra score of 20 were associated with a brain volume loss of 5.0 per cent at in eighteen months, whereas the associated volume loss was 2.0 per cent for a borderzone ratio of 1.00 and the same PAASH and Hijdra scores (Figure 3).

Table 3. Regression results

Volumes change day 14 – 6 months (n=39)

Model 1: Borderzone ratio, PAASH, Hijdra $R^2 = 0.16$ ($R^2_{ajd} = 0.09$)			Model 2: CoV, PAASH, Hijdra $R^2 = 0.19$ ($R^2_{ajd} = 0.13$)		
	B (95% CI)	p-value		B (95% CI)	p-value
Borderzone ratio	-7.74 (-14.99 – -0.48)	0.037*	CoV	8.27 (1.64 – 14.90)	0.016*
PAASH score	0.27 (-0.47 – 1.01)	0.466	PAASH score	0.38 (-0.35 – 1.12)	0.296
Hijdra score	0.04 (-0.04 – 0.13)	0.318	Hijdra score	0.03 (-0.06 – 0.12)	0.463

Volumes change day 14 – 18 months (n=27)

Model 3: Borderzone ratio, PAASH, Hijdra $R^2 = 0.25$ ($R^2_{ajd} = 0.15$)			Model 4: CoV, PAASH, Hijdra $R^2 = 0.25$ ($R^2_{ajd} = 0.15$)		
	B (95% CI)	p-value		B (95% CI)	p-value
Borderzone ratio	-10.94 (-20.72 – -1.16)	0.030*	CoV	10.92 (1.23 -20.61)	0.029*
PAASH score	0.44 (-0.47 – 1.35)	0.329	PAASH score	0.56 (-0.37– 1.49)	0.225
Hijdra score	0.05 (-0.07 – 0.16)	0.422	Hijdra score	0.04 (-0.08 – 0.16)	0.482

CoV = spatial coefficient of variation; PAASH = Prognosis on Admission of Aneurysmal Subarachnoid Hemorrhage; R^2_{ajd} = adjusted R^2. * P < 0.05

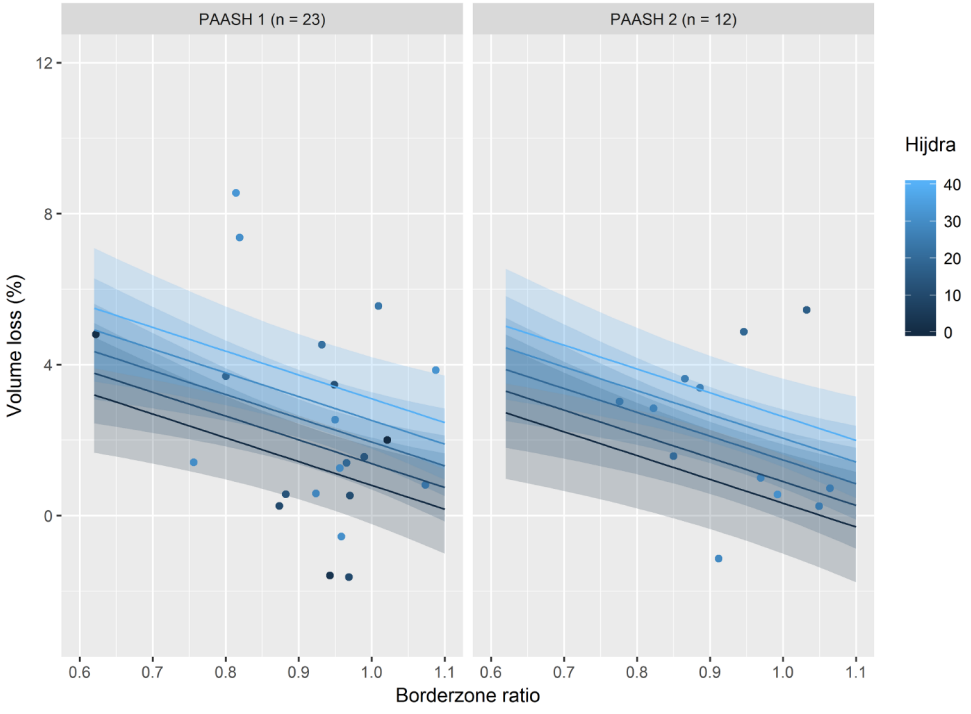

Fig. 3. A linear regression model of brain volume loss after 6 months based on the borderzone ratio. Multiple regression with brain volume loss at 6 months as the dependent variable and the borderzone ratio, PAASH, Hijdra as independent variables. The regression lines are dependent on the borderzone ratio along the x-axis; dependent on the Hijdra score as shown by the shade of blue with 95% confidence intervals, where a darker color represents a lower Hijdra score; and dependent on the PAASH score as shown in each subplot. A lower borderzone ratio is associated with a higher predicted brain volume loss (B = -7.74 (95% CI -14.99 – -0.48)). The Hijdra and PAASH scores are not significantly associated with brain volume loss (B = 0.04 (95% CI -0.04 – 0.13) and B = 0.27 (95% CI -0.47 – 1.01), respectively).

Multiple regression models: whole brain spatial coefficient of variation

The median CoV in all aSAH patients was 0.58 (IQR 0.53 – 0.66), and 0.59 (IQR 0.55 – 0.67) in the subgroup. The final regression model included the CoV, the Hijdra score and the PAASH score both for volume loss at six months (R^2 = 0.19, $R^2_{adjusted}$ = 0.13) and volume loss at eighteen months (R^2 = 0.25, $R^2_{adjusted}$ = 0.15) (Table 3).

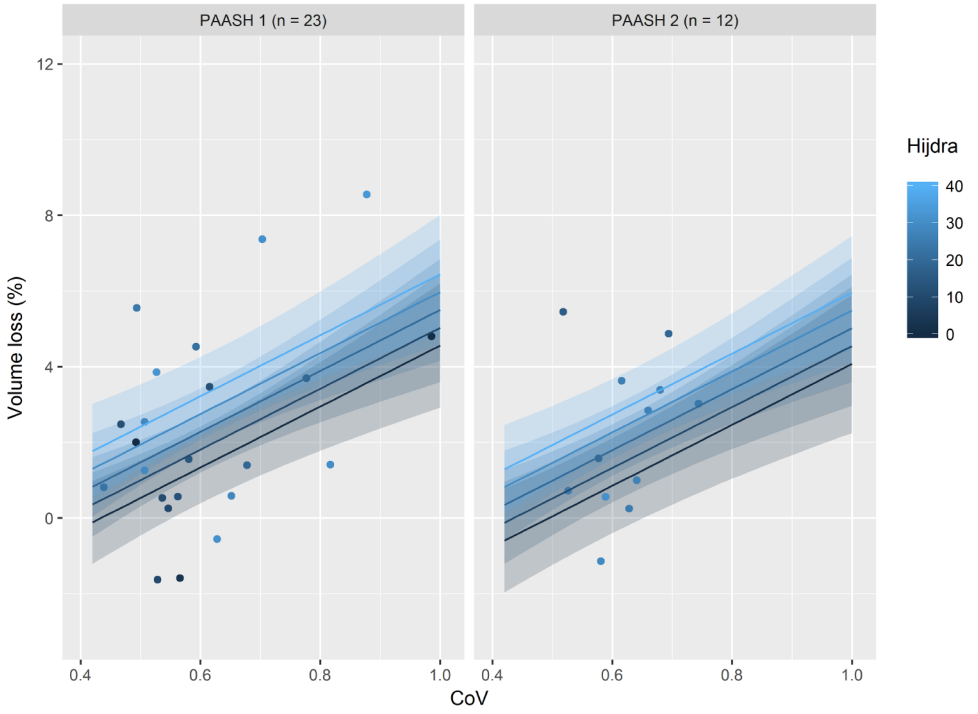

Fig. 4. A linear regression model of brain volume loss after six months based on the spatial coefficient of variation. Multiple regression with brain volume loss at six months as the dependent variable and the spatial coefficient of variation (CoV), PAASH, Hijdra as independent variables. The regression lines are dependent on the CoV along the x-axis; dependent on the Hijdra score as shown by the shade of blue with 95% confidence intervals, where a darker colour represents a lower Hijdra score; and dependent on the PAASH score as shown in each subplot. A higher CoV is associated with a higher predicted brain volume loss (B = 8.27 (95% CI 1.64 – 14.90). The Hijdra score and PAASH score are not significantly associated with the degree of brain volumes loss (B = 0.03 (-0.06 – 0.12) and B = 0.38 (-0.35 – 1.12), respectively).

The CoV was the only variable significantly associated with brain volume loss after six months (B = 8.3 (95% CI = 1.6 – 14.9), P = 0.016) and eighteen months (B =10.9 (95% CI = 1.2 – 20.6), P = 0.029). For instance, the associated volume loss was 2.1 per cent in the model for a CoV of 0.55, a PAASH score of 1, and a Hijdra score of 20, whereas the associated volume loss was 5.5 per cent for a CoV of 0.90 and the same PAASH and Hijdra scores (Figure 4).

The relationship between the borderzone ratio and the CoV

The borderzone ratio and the CoV showed a good correlation $\rho = -0.73$ ($P < 0.001$), which indicates that the CoV increases when the borderzone ratio decreases. Figure 5 displays the correlation plot of the borderzone ratio and CoV.

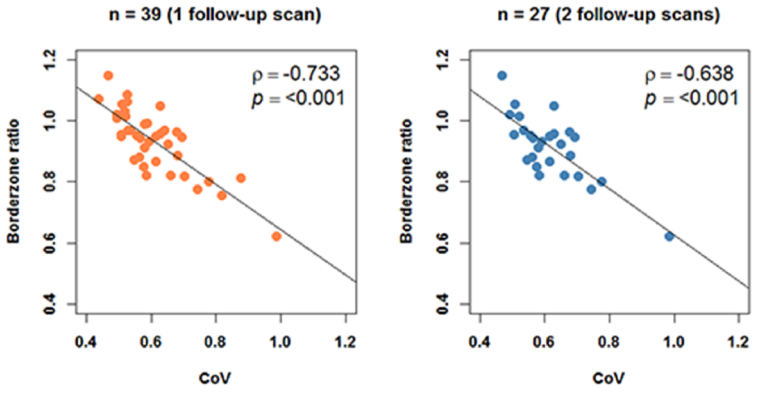

Fig. 4. Relationship between the CoV and the borderzone ratio. The left panel shows the relationship between the CoV and the borderzone ratio for all patients included in the study (n = 39). The right panel shows the relationship between the CoV and the borderzone ratio for the subgroup with a scan at eighteen months.

Discussion

The current study is the first to longitudinally track brain volume changes on brain MRI well into the chronic stage after aSAH. Perfusion heterogeneity partially explained the variance in brain volume loss after aSAH. This association was independent from clinical condition and the amount of extravasated blood on admission, characteristics that are often used as a measure for the severity of aSAH. As well, no correlation was found between long-term brain volume loss and ischemic lesion presence, volume, or number in the subacute stage. In one earlier study, brain volume changes after aSAH were tracked on CT. The median brain volume loss was 1.65 per cent between 24-48 hours after aneurysm securing and 1.5 months,[29] which is in line with the results from our

study. An increase in brain volume was noted in 1 in 3 patients,[29] which is considerably more frequent than the 1 in 10 patients at six months in our study.

Aneurysmal SAH places a large burden on surviving patients, their caregivers and society due to a relatively young patient age at ictus and a poor prognosis; 40 per cent of survivors remain functionally dependent,[30] and even those functionally independent after recovery from aSAH usually have persisting cognitive complaints and impairments.[31] No relationship has been observed between perfusion impairment <24h after ictus and cognitive functioning at 3 months after correction for age.[32] Yet, patients with perfusion impairment on SPECT as the CoV and CTP in the subacute stage are more likely to have impaired cognitive function a year after ictus and worse clinical outcome.[7, 10] In addition, subacute perfusion impairment was associated with chronic cerebral infarctio.[7, 10] Finally, perfusion impairment a year after aSAH was associated with the presence of cerebral infarction and cognitive impairment a year after aSAH.[33] No previous study has linked perfusion in the (sub)acute stage following aSAH to long-term brain volume changes.

Focal brain injury can be identified through a combined reading of DWI and T_2-FLAIR MR images. Studies on early, ischemic lesions (<72h) show a relationship between lesion presence, larger lesion volume and worse neurological outcome.[34-36] Diffuse injury, on the other hand, is not (as) apparent on structural images until the chronic stage, when it has manifested as a global decrease in brain volume. Similar to focal injury, diffuse injury as manifested in decreased brain volume is also associated with worse outcome.[1, 2, 37] Therefore, it is important to further identify factors associated with both focal and diffuse brain injury to aid clinical decision making and to find potential treatment targets. Cerebral perfusion heterogeneity measures contain the perfusion impairment caused both by focal and diffuse brain damage, because it is, for example, affected by globally increased arterial transit times, and perfusion deficits caused by ischemic lesions or vasospasm. As the borderzone ratio is defined anatomically, the borderzone ratio can change depending on the ischemic lesion location. If lesions are predominantly located outside of the borderzone regions, it could result in a relatively high borderzone ratio. For example, we observed borderzone ratios larger than 1. Alternatively, if lesions are predominantly located within the borderzone regions, a lower borderzone ratio is expected. Both lesion locations are common, as most lesions within 7 days of onset are found in either a territorial or a borderzone distribution on CT.[38] More specifically, in the absence of vasospasm, lesions are usually in the borderzone regions.[39] Spatial CoV on the other hand reflects global perfusion heterogeneity and, thus, depicts both delayed ATT and all ischemic lesions regardless of their location. On a group level, decreased perfusion in the subacute stage has been associated with brain injury after aSAH.[6, 9] However, on an individual level, quantitative perfusion values cannot be used to capture decreased cerebral perfusion as, even in normal subjects,

grey matter perfusion values can range between 40 – 100 ml/100g/min.[40] In addition, intrasubject variability is substantial with test-retest differences of up to 10 ml/100g/min on ASL MRI.[41] Both the borderzone ratio and the CoV offer the advantage of a relative measure whereby intersubject differences in mean global perfusion are neutralized.

Conceivably, perfusion heterogeneity can be modulated by various (interacting) factors through their effect on ATT or local perfusion, including edema, age, ischemic lesions and both proximal and distal vasospasm.[20, 42, 43] Therefore, a single factor may not be directly correlated with perfusion heterogeneity. In the current study we found no association between age and the borderzone ratio, despite the wide age range (24-81 years) of the included patients. In addition, no association was found between proximal vasospasm and perfusion heterogeneity. This suggests that the perfusion heterogeneity is tied to disease severity during the subacute stage in aSAH patients. Previous studies reported a positive association between age and decreased brain volume after subarachnoid hemorrhage.[1, 5] However, atrophy measures in these particular studies were cross-sectional in design, and thus the findings are in accordance with age-related decreased brain volume.[44] The mean annual brain volume loss was 0.32 per cent (95% CI 0.10 per cent - 0.54 per cent) in a group of healthy volunteers between 31 and 84 years old.[45] Therefore, it is unlikely that the brain volume changes found in our study with a similar age distribution can be attributed to normal ageing effects. Moreover, the brain parenchymal volume loss continued between six months and eighteen months, which demonstrates that the observed changes are not due to a normalization of edema.

This study has a few limitations. First, the population was in a relatively good clinical condition on admission compared to the overall aSAH population. This selection bias arose, because patients had to be able to undergo MR scanning. As a result, our models are limited in estimating the association between clinical condition on admission and brain volume loss given that limited data points are available for higher PAASH scores. This is also reflected in the good functional outcome of all patients, because of which we could not identify factors associated with outcome. In addition, the absence of a relationship between the PAASH score and brain volume loss might be due to the small range of PAASH scores investigated. Possibly, the observed relationship between perfusion heterogeneity and brain volume loss could be stronger in patients who present with a worse clinical status on admission. Second, segmentation was performed on 2D T_2-FLAIR images, because no 3D T_1-weighted images were obtained. Ideally, a 3D T_1-weighted sequence would have been used for optimal segmentation results of both grey and white matter, and volume changes within each tissue type could have been evaluated. However, a 2D sequence has the advantage of being less sensitive to patient motion, which is commonly seen in this patient population. Also, lesion volume could be obtained and subtracted from total brain volume because of the T_2-FLAIR images, allowing us to solely investigate diffuse brain damage. Our approach does allow us to

investigate brain volume changes resulting from Wallerian degeneration or neuronal degeneration in remote areas due to decreased connectivity.[46] To gain insight into a possible effect of focal lesions on a decrease in brain volume, we analyzed the correlation between presence volume, and number of DWI and T_2-FLAIR lesions and brain volume loss, but no correlations were found. The lack of a correlation with lesion volume and number may be explained by the little number and volume of lesions found: the median lesion volume was a multitude smaller than the observed brain volume changes.

In conclusion, we found an independent, positive association of perfusion heterogeneity with brain volume loss at six and eighteen months after aSAH. Consequently, perfusion heterogeneity may be used as a biomarker to identify patients at a higher risk of severe brain volume loss. Since volume loss is partially explained by perfusion heterogeneity, perfusion impairment could potentially be a therapeutic target to decrease the degree of brain atrophy.

Acknowledgements

We are grateful to M.E. Hendriks for the manual diffusion-weighted lesion segmentation as well as to N.S. Hartkamp for providing template territorial ASL maps in Dartel space. We also thank H.J.M.M. Mutsaerts for his advice on the analyses.

References

1. Bendel P, Koivisto T, Aikia M, Niskanen E, Kononen M, Hanninen T, et al. Atrophic enlargement of csf volume after subarachnoid hemorrhage: Correlation with neuropsychological outcome. American Journal of Neuroradiology. 2010;31:370-376
2. de Bresser J, Schaafsma JD, Luitse MJ, Viergever MA, Rinkel GJ, Biessels GJ. Quantification of structural cerebral abnormalities on mri 18 months after aneurysmal subarachnoid hemorrhage in patients who received endovascular treatment. Neuroradiology. 2015;57:269-274
3. Koivisto T, Vanninen R, Hurskainen H, Saari T, Hernesniemi J, Vapalahti M. Outcomes of early endovascular versus surgical treatment of ruptured cerebral aneurysms. Stroke. 2000;31:2369
4. Stehouwer BL, van der Kleij LA, Hendrikse J, Rinkel GJ, De Vis JB. Magnetic resonance imaging and brain injury in the chronic phase after aneurysmal subarachnoid hemorrhage: A systematic review. International journal of stroke : official journal of the International Stroke Society. 2018;13:24-34
5. Bendel P, Koivisto T, Hänninen T, Kolehmainen A, Könönen M, Hurskainen H, et al. Subarachnoid hemorrhage is followed by temporomesial volume loss: Mri volumetric study. Neurology. 2006;67:575-582
6. Cremers CHP, van der Schaaf IC, Wensink E, Greving JP, Rinkel GJE, Velthuis BK, et al. Ct perfusion and delayed cerebral ischemia in aneurysmal subarachnoid hemorrhage: A systematic review and meta-analysis. Journal of Cerebral Blood Flow & Metabolism. 2013;34:200-207
7. Mustonen T, Koivisto T, Vanninen R, Hänninen T, Vapalahti M, Hernesniemi J, et al. Heterogeneity of cerebral perfusion 1 week after haemorrhage is an independent predictor of clinical outcome in patients with aneurysmal subarachnoid haemorrhage. Journal of Neurology, Neurosurgery & Psychiatry. 2008;79:1128
8. Cahill J, Calvert JW, Zhang JH. Mechanisms of early brain injury after subarachnoid hemorrhage. Journal of Cerebral Blood Flow & Metabolism. 2006;26:1341-1353
9. Dankbaar JW, Rijsdijk M, van der Schaaf IC, Velthuis BK, Wermer MJ, Rinkel GJ. Relationship between vasospasm, cerebral perfusion, and delayed cerebral ischemia after aneurysmal subarachnoid hemorrhage. Neuroradiology. 2009;51:813-819
10. Sanelli PC, Anumula N, Johnson CE, Comunale JP, Tsiouris AJ, Riina H, et al. Evaluating ct perfusion using outcome measures of delayed cerebral ischemia in aneurysmal subarachnoid hemorrhage. American Journal of Neuroradiology. 2013;34:292
11. Hertel F, Walter C, Bettag M, Mörsdorf M, Macdonald RL, Schackert G, et al. Perfusion-weighted magnetic resonance imaging in patients with vasospasm: A useful new tool in the management of patients with subarachnoid hemorrhage. Neurosurgery. 2005;56:28-35
12. Aralasmak A, Akyuz M, Ozkaynak C, Sindel T, Tuncer R. Ct angiography and perfusion imaging in patients with subarachnoid hemorrhage: Correlation of vasospasm to perfusion abnormality. Neuroradiology. 2008;51:85
13. Mutsaerts HJ, Petr J, Vaclavu L, van Dalen JW, Robertson AD, Caan MW, et al. The spatial coefficient of variation in arterial spin labeling cerebral blood flow images. J Cereb Blood Flow Metab. 2017:271678X16683690
14. Lanterna LA, Lunghi A, Martchenko S, Gritti P, Bonaldi G, Biroli F. Cerebral watershed hypoperfusion in subarachnoid hemorrhage: Computed tomography perfusion analysis. Journal of Neurosurgery. 2010;114:961-968
15. Mustonen T, Koivisto T, Vanninen E, Vanninen R, Kuikka JT. Cerebral perfusion heterogeneity and complexity in patients with acute subarachnoid haemorrhage. Nuclear Medicine Communications. 2006;27:157-164
16. Collin C, Wade DT, Davies S, Horne V. The barthel adl index: A reliability study. International Disability Studies. 1988;10:61-63
17. Takagi K, Tamura A, Nakagomi T, Nakayama H, Gotoh O, Kawai K, et al. How should a subarachnoid hemorrhage grading scale be determined? A combinatorial approach based solely on the glasgow coma scale. Journal of Neurosurgery. 1999;90:680-687
18. Hijdra A, Brouwers PJ, Vermeulen M, van Gijn J. Grading the amount of blood on computed tomograms

after subarachnoid hemorrhage. Stroke. 1990;21:1156
19. Oguz KK, Golay X, Pizzini FB, Freer CA, Winrow N, Ichord R, et al. Sickle cell disease: Continuous arterial spin-labeling perfusion mr imaging in children. Radiology. 2003;227:567-574
20. Zaharchuk G, Bammer R, Straka M, Shankaranarayan A, Alsop DC, Fischbein NJ, et al. Arterial spin-label imaging in patients with normal bolus perfusion-weighted mr imaging findings: Pilot identification of the borderzone sign. Radiology. 2009;252:797-807
21. Hendrikse J, Petersen ET, van Laar PJ, Golay X. Cerebral border zones between distal end branches of intracranial arteries: Mr imaging. Radiology. 2008;246:572-580
22. Hartkamp NS, Petersen ET, Chappell MA, Okell TW, Uyttenboogaart M, Zeebregts CJ, et al. Relationship between haemodynamic impairment and collateral blood flow in carotid artery disease. Journal of Cerebral Blood Flow & Metabolism. 2017
23. Ashburner J, Barnes G, Chen C, Daunizeau J, Flandin G, Friston K, et al. Spm12 manual. 2014
24. Ashburner J. Computational anatomy with the spm software. Magnetic Resonance Imaging. 2009;27:1163-1174
25. Schmidt P, Gaser C, Arsic M, Buck D, Förschler A, Berthele A, et al. An automated tool for detection of flair-hyperintense white-matter lesions in multiple sclerosis. NeuroImage. 2012;59:3774-3783
26. Moon K-W. Ggiraphextra: Make interactive 'ggplot2'. Extension to 'ggplot2' and 'ggiraph'. 2016
27. R Core Team. R: A language and environment for statistical computing. 2017
28. Steyerberg EW, Eijkemans MJ, Harrell FE, Jr., Habbema JD. Prognostic modelling with logistic regression analysis: A comparison of selection and estimation methods in small data sets. Stat Med. 2000;19:1059-1079
29. Tam AK, Kapadia A, Ilodigwe D, Li Z, Schweizer TA, Macdonald RL. Impact of global cerebral atrophy on clinical outcome after subarachnoid hemorrhage. J Neurosurg. 2013;119:198-206
30. Zacharia BE, Hickman ZL, Grobelny BT, DeRosa P, Kotchetkov I, Ducruet AF, et al. Epidemiology of aneurysmal subarachnoid hemorrhage. Neurosurg Clin N Am. 2010;21:221-233
31. Passier PE, Visser-Meily JM, van Zandvoort MJ, Rinkel GJ, Lindeman E, Post MW. Predictors of long-term health-related quality of life in patients with aneurysmal subarachnoid hemorrhage. NeuroRehabilitation. 2012;30:137-145
32. Huenges Wajer IMC, Cremers CHP, van Zandvoort MJE, Vergouwen MDI, van der Schaaf IC, Velthuis BK, et al. Ct perfusion on admission and cognitive functioning 3 months after aneurysmal subarachnoid haemorrhage. Journal of Neurology. 2015;262:623-628
33. Egge A, Waterloo K, Sjøholm H, Ingebrigtsen T, Forsdahl S, Jacobsen EA, et al. Outcome 1 year after aneurysmal subarachnoid hemorrhage: Relation between cognitive performance and neuroimaging. Acta Neurologica Scandinavica. 2005;112:76-80
34. Frontera JA, Ahmed W, Zach V, Jovine M, Tanenbaum L, Sehba F, et al. Acute ischaemia after subarachnoid haemorrhage, relationship with early brain injury and impact on outcome: A prospective quantitative mri study. Journal of Neurology, Neurosurgery & Psychiatry. 2014;86:71-78
35. Sato K, Shimizu H, Fujimura M, Inoue T, Matsumoto Y, Tominaga T. Acute-stage diffusion-weighted magnetic resonance imaging for predicting outcome of poor-grade aneurysmal subarachnoid hemorrhage. Journal of Cerebral Blood Flow & Metabolism. 2010;30:1110-1120
36. De Marchis GM, Filippi CG, Guo X, Pugin D, Gaffney CD, Dangayach NS, et al. Brain injury visible on early mri after subarachnoid hemorrhage might predict neurological impairment and functional outcome. Neurocritical Care. 2015;22:74-81
37. Pyysalo LM, Keski-Nisula LH, Niskakangas TT, Kähärä VJ, Öhman JE. Long-term mri findings of patients with embolized cerebral aneurysms. Acta Radiologica. 2011;52:204-210
38. Rabinstein AA, Weigand S, Atkinson JLD, Wijdicks EFM. Patterns of cerebral infarction in aneurysmal subarachnoid hemorrhage. Stroke. 2005;36:992
39. Brown RJ, Kumar A, Dhar R, Sampson TR, Diringer MN. The relationship between delayed infarcts and angiographic vasospasm after aneurysmal subarachnoid hemorrhage. Neurosurgery. 2013;72:702-708
40. Alsop DC, Detre JA, Golay X, Günther M, Hendrikse J, Hernandez-Garcia L, et al. Recommended implementation of arterial spin-labeled perfusion mri for clinical applications: A consensus of the ismrm

perfusion study group and the european consortium for asl in dementia. Magnetic Resonance in Medicine. 2015;73:102-116
41. Gevers S, Osch MJv, Bokkers RP, Kies DA, Teeuwisse WM, Majoie CB, et al. Intra- and multicenter reproducibility of pulsed, continuous and pseudo-continuous arterial spin labeling methods for measuring cerebral perfusion. Journal of Cerebral Blood Flow & Metabolism. 2011;31:1706-1715
42. Liu Y, Zhu X, Feinberg D, Guenther M, Gregori J, Weiner MW, et al. Arterial spin labeling mri study of age and gender effects on brain perfusion hemodynamics. Magnetic Resonance in Medicine. 2012;68:912-922
43. Østergaard L, Aamand R, Karabegovic S, Tietze A, Blicher JU, Mikkelsen IK, et al. The role of the microcirculation in delayed cerebral ischemia and chronic degenerative changes after subarachnoid hemorrhage. Journal of Cerebral Blood Flow & Metabolism. 2013;33:1825-1837
44. Takao H, Hayashi N, Ohtomo K. A longitudinal study of brain volume changes in normal aging. European Journal of Radiology. 2012;81:2801-2804
45. Scahill RI, Frost C, Jenkins R, Whitwell JL, Rossor MN, Fox NC. A longitudinal study of brain volume changes in normal aging using serial registered magnetic resonance imaging. Archives of Neurology. 2003;60:989-994
46. Fornito A, Zalesky A, Breakspear M. The connectomics of brain disorders. Nature Reviews Neuroscience. 2015;16:159

Chapter 5

Acetazolamide in aneurysmal Subarachnoid Haemorrhage (ASH): study protocol of a phase II randomized controlled trial

L.A. van der Kleij[1*], M.D.I. Vergouwen[2], I.C. van der Schaaf[1], J.C.W. Siero[1,3], G.J.E. Rinkel[2], J.B. De Vis[4], J. Hendrikse[1]

[1] Department of Radiology, University Medical Center Utrecht, Utrecht University, Utrecht, The Netherlands.
[2] Department of Neurology and Neurosurgery, Brain Center Rudolf Magnus, University Medical Center Utrecht, Utrecht University, Utrecht, The Netherlands.
[3] Spinoza Center for Neuroimaging, Amsterdam, The Netherlands
[4] National Institute of Neurological Disorders and Stroke, National Institutes of Health, Bethesda, Maryland, USA

Submitted manuscript

Abstract

Introduction: Approximately 30% of patients with aneurysmal subarachnoid hemorrhage (aSAH) develop delayed cerebral ischemia (DCI), which increases the risk of poor functional outcome. Currently, the only drug proven to reduce the risk of DCI is the calcium antagonist nimodipine, but its effect is modest. Therefore, additional drugs to decrease the risk of DCI are needed. We hypothesize that acetazolamide (ACZ), a carbonic anhydrase inhibitor, is such a drug, by improving cerebral perfusion.

Methods and analysis: The Acetazolamide in Aneurysmal Subarachnoid Haemorrhage (ASH) study is a phase II study that evaluates the efficacy and safety of acetazolamide in patients with aSAH with a PROBE design (Prospective, Randomized, Open-label study with Blinded End-point assessment). Forty aSAH patients will be randomized within 5 days post-ictus to either the ACZ arm (500mg 3x/day iv, given from randomization through day 14 post-ictus) or the control group (care as usual without ACZ). The efficacy will be evaluated by comparing cerebral perfusion as assessed with cerebral blood flow MRI measurements performed 7±2 days after ictus in both groups, and safety by comparing the incidence of (serious) adverse events.

Status: currently recruiting patients.

Ethics and dissemination: The study protocol has been approved by the institutional review board of the University Medical Center Utrecht. The outcomes of the study will provide information on the efficacy and safety of acetazolamide when administered in the first two weeks after aSAH. The results of this phase II trial can inform larger, phase III trials and will be disseminated through publication in a peer-reviewed journal and by presentation at scientific conferences.

Trial registration number: Netherlands trial register NTR6680/ NL6493. Registered on 2 March 2017.

EudraCT: 2016-005151-25.

Protocol version 7, February 2019.

Article summary: strengths and limitations

- The acetazolamide dosage used in this study has been found safe for other, registered indications.
- The study will provide data on the efficacy of daily acetazolamide treatment in improving cerebral perfusion, a potential strategy to decrease the risk of DCI in patients with aneurysmal SAH.
- The study will provide data on the safety of daily acetazolamide treatment in patients with aneurysmal SAH.
- The study does not collect evidence on the mechanism by which acetazolamide affects aneurysmal subarachnoid haemorrhage patients.
- The control group will receive care as usual without a placebo treatment.

Introduction

The prognosis of aneurysmal subarachnoid hemorrhage (aSAH) is relatively poor. After 3 months, approximately one-third of the patients has died and one-third has long-term functional and/or cognitive impairments.[1,2] The most important determinants of poor functional outcome after aSAH are the initial bleeding, rebleeding of the aneurysm, delayed cerebral ischemia (DCI), and hydrocephalus.[3] DCI typically has a gradual onset between days 4 and 14 after the hemorrhage, and it affects 1 in 4 aSAH patients.[3-6] The interval between ictus and the onset of DCI provides an opportunity for preventive treatment. The only drug proven to reduce the risk of DCI is the calcium antagonist nimodipine. However, the effect of nimodipine is only modest. Therefore, additional treatment options are needed.

Acetazolamide (ACZ) is a carbonic anhydrase inhibitor used for various therapeutic indications, including the treatment of glaucoma,[7] idiopathic intracranial hypertension,[8] sleep apnoea, and high altitude sickness.[9,10] ACZ increases the cerebral blood flow (CBF) by inducing vasodilation.[11] In addition, ACZ can reduce cerebral oedema and cerebral spinal fluid (CSF) production.[12-16] These combined actions of ACZ make it a promising drug for the prevention of DCI in aSAH patients (Figure 1).

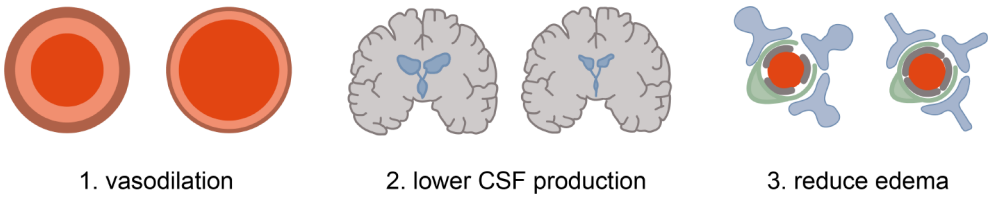

Fig. 1. The three potential effects of acetazolamide after aneurysmal subarachnoid hemorrhage. 1) Vasodilation; 2) Lower CSF production; 3) Reduction of cerebral oedema, and specifically cytotoxic oedema.[16] The illustration shows the two types of oedema present after aneurysmal subarachnoid hemorrhage on the left: cytotoxic oedema (intracellular swelling) and vasogenic oedema (disrupted tight junctions causing an enlarged extracellular compartment). On the right, a normalization of both oedema types is depicted.

To evaluate the efficacy in terms of improving cerebral perfusion and safety of ACZ on aSAH patients, we designed the Acetazolamide in aneurysmal Subarachnoid Hemorrhage (ASH) trial.

Study aims

The main goals of the ASH study are: 1) to investigate whether acetazolamide increases cerebral blood flow when administered for several days following aSAH, and 2) to investigate whether its use is safe in this patient population.

Methods and analysis

Study Setting

The ASH trial is a single-center study at the University Medical Center Utrecht, the Netherlands. Subjects are recruited within 5 days (120 hours) after ictus by a member of the study team.

Participants

Inclusion criteria are: 1) age 18 years or older; 2) admission within 120 hours after ictus; 3) confirmed aSAH by the presence of subarachnoid blood on computed tomography (CT) or lumbar puncture, and by visualization of the aneurysm on either CT angiography, MR angiography, or digital subtraction angiography; and 4) adequate occlusion of the ruptured aneurysm. Exclusion criteria are: 1) expected intensive care unit (ICU) admission for longer than the inclusion window (subjects are not recruited at the ICU); 2) perimesencephalic hemorrhage; 3) traumatic SAH; 4) any contra-indication for MRI; 5) severe liver or renal dysfunction; 6) pregnancy or breastfeeding; 7) diagnosis of Addison's disease; 8) pituitary insufficiency; or 9) use of phenytoin. Study duration for a participant is 10 weeks (Figure 2).

Design

The phase II ASH trial has a PROBE design (Prospective, Randomized, Open-label study with Blinded End-point assessment).

Informed consent and randomization

Informed consent will be obtained from patients after they have been informed about nature of the study, its purpose, associated procedures, the expected duration, and risks of participation. The patient will be assured that the choice for participation or non-participation in the trial will not affect the quality of care they receive. Informed consent by proxy will be obtained when a participant is incompetent to provide consent. After informed consent has been obtained, a web-based randomization procedure will be performed by the investigator. Patients will be randomized to either the intervention arm or the control arm in a 1:1 ratio. A digital randomization list has been prepared by an external party via ResearchOnline (www.researchonline.info). Randomization is stratified for type of aneurysm treatment (neurosurgical versus endovascular treatment).

Interventions

Patients randomized to the intervention arm will receive ACZ in addition to care as usual

from inclusion through day 14 after ictus. The ACZ dosage is 500 mg intravenously, three times daily dissolved in a 100 ml saline solution. This dosage corresponds with the recommended dose in the summary of product characteristics. If a patient is discharged from the hospital before day 14, ACZ treatment will be stopped at discharge. The treatment duration is chosen to cover the critical stage after ictus during which DCI may occur. Any other medication given to the patient as part of standard clinical care is allowed during the study, while no other study medication is allowed. The control group will receive care as usual without placebo.

Subjects can leave the study at any time for any reason if they wish to do so without any consequences. Also, the investigator can decide to withdraw a subject from the study for urgent medical reasons. If a participant in the intervention arm misses either one or both MRI scans, they will continue to receive ACZ. If ACZ treatment is discontinued, any remaining MRI scans are cancelled.

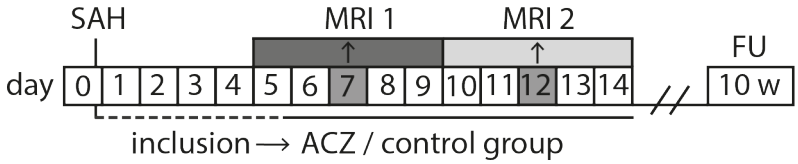

Fig. 2. Participant timeline. Participants with secured aneurysms are included within 5 days (120 hours) of ictus, after which they are randomized to the acetazolamide (ACZ) treatment or control group. The primary end-point, cerebral blood flow, is assessed on MRI 1 at day 7(±2). MRI 2 is performed at day 12(±2). At the 10 week follow-up, data on adverse events, the degree of disability, and quality of life are collected. Day 0 is the day of ictus. SAH = subarachnoid hemorrhage, day of ictus; FU = follow-up; 10 w = 10 weeks.

Outcomes

Table 1 displays an overview study outcomes.

Table 1. Outcomes

Parameter	Measurement instrument
CBF on day 7±2	ASL MRI
Safety until 10 weeks	(S)AEs in clinical record and questionnaire
Delayed Cerebral Ischemia	Clinical record(blinded assessment)
CBF on day 12±2	ASL MRI
CBF change between MRI 1 and MRI 2	ASL MRI
Hydrocephalus	Imaging records (blinded assessment)
Quality of life at 10 weeks	Short SS-QoL questionnaire[17]
Disability at 10 weeks	mRS questionnaire[18]

CBF = cerebral blood flow; ASL = arterial spin labeling; (S)AEs = (serious) adverse events; SS-QoL = stroke specific – quality of life; mRS= modified Rankin Scale.

Cerebral blood flow

MR Imaging will be performed at day 7±2 (MRI 1) for the primary outcome measure and at day 12±2 (MRI 2) after ictus for secondary outcome measures. CBF will be quantified non-invasively with arterial spin labeling (ASL) MRI.

Secondary outcome measures

Adverse events are defined as any undesirable experience occurring to a subject during the study, whether or not considered related to any study procedure. All (S)AEs reported spontaneously by the patient or observed by the investigator or staff from study inclusion until 10 weeks after ictus will be recorded in the case report form (CRF). This includes information from the medical chart, lab test results and imaging findings. AE's will be registered only if they are unrelated to the aSAH. Adverse events are classified as either unexpected or expected, and they are graded by severity. The (S) AEs occurring between hospital discharge and the 10 week follow-up will be recorded through a custom questionnaire (supplementary material). The questionnaire consists of questions on complaints the patient experienced and any hospital admissions after the initial discharge. Patients in the intervention arm will be asked whether they suspect a link between their complaints and acetazolamide.

DCI is defined as either clinical deterioration caused by delayed cerebral ischemia or cerebral infarction.[5] Clinical deterioration due to DCI is defined as "the occurrence of focal neurological impairment (such as hemiparesis, aphasia, apraxia, hemianopia, or neglect), or a decrease of at least 2 points on the Glasgow Coma Scale[; this] should last for at least 1 hour, is not apparent immediately after aneurysm occlusion, and cannot be attributed to other causes by means of clinical assessment, CT or MRI scanning of the brain, and appropriate laboratory studies".[5] The occurrence of DCI is assessed with a blinded reading of relevant information from the medical chart by two independent neurologists. Hydrocephalus will be determined by a blinded assessment of all available medical imaging (CT/MRI). It is defined based on the bicaudate index (BCI). First the width of the frontal horns at the level of the caudate nuclei is measured relative to corresponding brain diameter.[19] Subsequently, the relative BCI is obtained through division of the BCI by the normal upper limit (95th percentile) for age. [19] A relative BCI greater than 1 is defined as hydrocephalus.[20]

Third, the degree of disability and quality of life (QoL) will be assessed at 10 weeks. The degree of disability will be measured with the modified Rankin scale (mRS), which will be administered as part of standard clinical practice.[18 21] The quality of life (QoL) will be measured with a short, stroke specific QoL scale.[22] It assesses function on a five-point scale in 12 domains commonly affected by stroke: self-care, mobility, upper extremity function, language, vision, work, thinking, family roles, social roles, personality, mood and energy. The short stroke-specific QoL questionnaire used in this study was shown

to correspond well with the original stroke specific QoL scale with 49 items.[17 22]

Sample size

The study is powered on the primary objective of this study: CBF at day 7±2. The sample size calculation is based on a previous study in which the effect of ACZ on CBF was evaluated with ASL MRI in 16 healthy volunteers (mean age 56.5±6 years).[11] In that study, a single dose of ACZ (14 mg/kg with a maximum dose of 1200 mg) was used, which is comparable to the dosage in the ASH trial (i.e., 1500 mg per day, 3 doses of 500 mg). Baseline CBF was 50ml/min/100g in that study, which increased to 80 ml/min/100g after ACZ.[11] Therefore, the change in CBF induced by acetazolamide is expected to be a multitude larger than day-to-day fluctuations in CBF as measured with ASL MRI (around 3%±13% compared to 60%).[11 23]Based on this 60% CBF increase, an alpha of 5% and a beta of 80%, a minimum of 8 patients is needed for each study arm. As the effect on CBF in aSAH patients receiving ACZ for several days might be smaller compared to healthy controls after a single dose, we adopted a conservative estimate of 20 patients in both the ACZ and control group.

Data collection and management

After informed consent, subjects will be registered in the ASH study database using subject identification numbers. The key to the identification code is stored separately and is secured by the investigator. A study specific, secured database within OpenClinica (www.openclinica.com) is set up for this project. Study data collected will consist at least of: study identification number, age at inclusion, date and hour of ictus, date and hour of admission, date of inclusion, date and hour of treatment start, date of end-of-treatment, sex, medical history prior to SAH, Prognosis on Admission of Aneurysmal Subarachnoid Haemorrhage (PAASH)[24] score, the amount of extravasated blood scored on the admission head CT scan (Hijdra score[25]), location and size of the ruptured aneurysm, occurrence of rebleeding, DCI, hydrocephalus, timing of MRI imaging, timing of ACZ administration, CBF, quality of life,[17] (serious) adverse events, and modified Rankin Scale[18]. Data will be kept in storage for at least 15 years.

Data analysis

The primary outcome measurement will be analysed in a per-protocol analysis including all subjects in whom MRI 1 was performed. Patients without are MRI 1 are excluded from the per-protocol analysis. Both an intention-to-treat and per-protocol analysis will be carried out for the other study objectives. In the per-protocol analysis, only intervention arm subjects will be included that completed treatment, while all subjects of the control arm will be included. The intention-to-treat analysis includes all patients.

Table 2 provides an overview of the statistical tests used for each outcome measure. The ASL data will be analysed in accordance with the current guidelines.[26] Differences in CBF between the study arms will be evaluated for each imaging time point. Moreover, longitudinal changes in CBF within each group are compared. Good outcome on the mRS is defines as a score of 0 – 2.[19]

Table 2. Statistical analyses.

Type	Parameter	Unit	Statistical test
Primary	CBF on MRI 1[a]	Continuous	T-test (or Mann-Whitney U)
Secondary	Safety until 10 weeks	Count	Chi-square test
	Delayed Cerebral Ischemia	Count	Risk ratio
	CBF on MRI 2[b]	Continuous	T-test (or Mann-Whitney U)
	CBF between MRI 1 and 2	Continuous	T-test (or Wilcoxon signed-rank)
Tertiary	Hydrocephalus	Count	Risk ratio
	Quality of life at 10 weeks	Count (n/60)	Mann-Whitney U
	Disability at 10 weeks	Count	Risk ratio

[a]day 7±2; [b]day 12±2; CBF = cerebral blood flow.

Monitoring

An external, qualified monitor is appointed to assure the quality and validity of the research data and study procedures. The monitoring will be performed according to the NFU (Netherlands Federation of University Medical Centers) guidelines. In addition, an interim safety analysis will be performed by the in-house Data Safety Monitoring Board (DSMB), who can advise premature study termination. The DSMB will be blinded for group assignment, but de-blinding can occur if a difference in (S)AE prevalence is found between the two groups. If the study team decides not to implement the DSMB's advice, the institutional review board will be informed of the DSMB's advice along with the study team's reasoning to not follow it.

Ethics and dissemination

Research ethics approval

The ASH trial protocol has been approved by the institutional review board of the University Medical Center Utrecht. All substantial protocol modifications are to be communicated to the institutional review board, which are defined as changes that significantly affect: 1) the safety or physical or mental integrity of the subjects of the trial; 2) the scientific value of the trial; 3) the conduct or management of the trial; or 4) the

quality or safety of any intervention used in the trial. Non-substantial modifications should not be notified to the review board and the competent authority, but they should be recorded and filed by the study team. All individual subject data records will be collected on confidential basis and according to the applicable national data protection, privacy and secrecy laws.

Consent

Consent will be obtained by an ASH trial study team member trained in good clinical practice (GCP). If the treating neurologist or neurosurgeon considers a patient incapable to provide informed consent, the legal representative will be asked for permission on their behalf. Prior to providing consent, the participant or legal representative will be informed of the nature of the study, its purpose and associated procedures, the expected duration, and risks of participation. The patient will be assured that the choice for participation or non-participation in the trial will not affect the quality of care they receive. As the inclusion window is within 120 hours after ictus, the investigator will inform the patient or legal representative as soon as possible to ensure maximum consideration time. If the patient recovers to a state in which informed consent can be provided, the study information will be provided and a retrospective informed consent procedure will be started.

Safety

There are no risks related to the MRI in this patient population and no contrast agents are used. Severe side effects of ACZ are rare (1/100 – 1/10000). As patients only receive study medication during their hospital stay, they are closely monitored for any possible side effects throughout the entire treatment duration. The investigator and treating physician can decide to withdraw a subject from the study for urgent medical reasons.

Dissemination

The basic principles on public disclosure and publication policy as described in the Central Committee on Research Involving Human Subjects (CCMO) statement will be followed (english.CCMO.nl). This includes publication of study results within 12 months after study completion. In addition, results will be disseminated at scientific conferences and registered in the EudraCT database (2016-005151-25).

Discussion and conclusion

The ASH trial investigates the efficacy and safety of ACZ after aSAH. Acetazolamide is an inexpensive, commonly used carbonic anhydrase inhibitor. Currently approved applications include treatment of idiopathic intracranial hypertension and glaucoma. The study design has several advantages. First, the ACZ dosage used in this study has been found to be safe for other, registered indications. Second, the study will provide data on the efficacy of daily ACZ treatment in improving cerebral perfusion, a potential strategy to decrease the risk of DCI in patients with aneurysmal SAH. Third, acetazolamide can benefit aSAH patients via three different mechanisms, which makes it a promising candidate drug for subacute aSAH treatment. Finally, the study will provide data on the safety of daily ACZ treatment in patients with aneurysmal SAH. A limitation of the study is that only patients with a relatively good clinical status can undergo MRI, which means that ICU patients cannot be evaluated for the primary endpoint. As well, the control group will receive care as usual without a placebo treatment, which may affect subjective, non-MRI derived study parameters. Finally, the study does not collect evidence on the mechanism by which acetazolamide affects aneurysmal subarachnoid hemorrhage patients. The results of this study will be published in peer-reviewed journals and at scientific conferences. They can inform larger trials on the effect of acetazolamide on clinical outcome after aneurysmal subarachnoid hemorrhage.

References

1. Rinkel GJ, Algra A. Long-term outcomes of patients with aneurysmal subarachnoid haemorrhage. Lancet Neurol 2011;10(4):349-56. doi: 10.1016/S1474-4422(11)70017-5 [published Online First: 2011/03/26]
2. Zacharia BE, Hickman ZL, Grobelny BT, et al. Epidemiology of aneurysmal subarachnoid hemorrhage. Neurosurg Clin N Am 2010;21(2):221-33. doi: 10.1016/j.nec.2009.10.002 [published Online First: 2010/04/13]
3. van Gijn J, Kerr RS, Rinkel GJ. Subarachnoid haemorrhage. Lancet 2007;369(9558):306-18. doi: 10.1016/S0140-6736(07)60153-6 [published Online First: 2007/01/30]
4. Dorsch NW, King MT. A review of cerebral vasospasm in aneurysmal subarachnoid haemorrhage Part I: Incidence and effects. J Clin Neurosci 1994;1(1):19-26. [published Online First: 1994/01/01]
5. Vergouwen M, Vermeulen M, van Gijn J, et al. Definition of Delayed Cerebral Ischemia After Aneurysmal Subarachnoid Hemorrhage as an Outcome Event in Clinical Trials and Observational Studies: Proposal of a Multidisciplinary Research Group. Stroke; a journal of cerebral circulation 2010((Vergouwen M.; Vermeulen M.; van Gijn J.; Rinkel G.; Wijdicks E.; Muizelaar J.; Mendelow A.; Juvela S.; Yonas H.; Terbrugge K.; Macdonald R.; Diringer M.; Broderick J.; Dreier J.; Roos Y.)):2391-5.
6. Roos YB, de Haan RJ, Beenen LF, et al. Complications and outcome in patients with aneurysmal subarachnoid haemorrhage: a prospective hospital based cohort study in the Netherlands. J Neurol Neurosurg Psychiatry 2000;68(3):337-41. [published Online First: 2000/02/16]
7. Grant WM, Trotter RR. Diamox (acetazoleamide) in treatment of glaucoma. AMA Arch Ophthalmol 1954;51(6):735-9. [published Online First: 1954/06/01]
8. Wall M, McDermott MP, Kieburtz KD, et al. Effect of acetazolamide on visual function in patients with idiopathic intracranial hypertension and mild visual loss: the idiopathic intracranial hypertension treatment trial. Jama 2014;311(16):1641-51. doi: 10.1001/jama.2014.3312 [published Online First: 2014/04/24]
9. Gertsch JH, Basnyat B, Johnson EW, et al. Randomised, double blind, placebo controlled comparison of ginkgo biloba and acetazolamide for prevention of acute mountain sickness among Himalayan trekkers: the prevention of high altitude illness trial (PHAIT). BMJ 2004;328(7443):797. doi: 10.1136/bmj.38043.501690.7C [published Online First: 2004/04/09]
10. Nussbaumer-Ochsner Y, Latshang TD, Ulrich S, et al. Patients with obstructive sleep apnea syndrome benefit from acetazolamide during an altitude sojourn: a randomized, placebo-controlled, double-blind trial. Chest 2012;141(1):131-8. doi: 10.1378/chest.11-0375 [published Online First: 2011/06/11]
11. Bokkers RP, van Osch MJ, Klijn CJ, et al. Cerebrovascular reactivity within perfusion territories in patients with an internal carotid artery occlusion. J Neurol Neurosurg Psychiatry 2011;82(9):1011-6. doi: 10.1136/jnnp.2010.233338 [published Online First: 2011/03/10]
12. Bartsch P, Swenson ER. Clinical practice: Acute high-altitude illnesses. N Engl J Med 2013;368(24):2294-302. doi: 10.1056/NEJMcp1214870 [published Online First: 2013/06/14]
13. Jafarzadeh F, Field ML, Harrington DK, et al. Novel application of acetazolamide to reduce cerebrospinal fluid production in patients undergoing thoracoabdominal aortic surgery. Interact Cardiovasc Thorac Surg 2014;18(1):21-6. doi: 10.1093/icvts/ivt384 [published Online First: 2013/10/17]
14. Gao F, Zheng M, Hua Y, et al. Acetazolamide Attenuates Thrombin-Induced Hydrocephalus. Acta Neurochir Suppl 2016;121:373-7. doi: 10.1007/978-3-319-18497-5_64 [published Online First: 2015/10/16]
15. Faraci FM, Mayhan WG, Heistad DD. Vascular effects of acetazolamide on the choroid plexus. J Pharmacol Exp Ther 1990;254(1):23-7. [published Online First: 1990/07/01]
16. Sturdivant NM, Smith SG, Ali SF, et al. Acetazolamide Mitigates Astrocyte Cellular Edema Following Mild Traumatic Brain Injury. Scientific Reports 2016;6:33330. doi: 10.1038/srep33330
https://www.nature.com/articles/srep33330#supplementary-information
17. Post MW, Boosman H, van Zandvoort MM, et al. Development and validation of a short version of the Stroke Specific Quality of Life Scale. J Neurol Neurosurg Psychiatry 2011;82(3):283-6. doi: 10.1136/jnnp.2009.196394 [published Online First: 2010/08/31]
18. Rankin J. Cerebral vascular accidents in patients over the age of 60. II. Prognosis. Scott Med J 1957;2(5):200-15. [published Online First: 1957/05/01]

19. van Gijn J, Hijdra A, Wijdicks EF, et al. Acute hydrocephalus after aneurysmal subarachnoid hemorrhage. Journal of neurosurgery 1985;63(3):355-62.
20. van Asch CJJ, van der Schaaf IC, Rinkel GJE. Acute Hydrocephalus and Cerebral Perfusion after Aneurysmal Subarachnoid Hemorrhage. American Journal of Neuroradiology 2010;31(1):67. doi: 10.3174/ajnr.A1748
21. van Swieten JC, Koudstaal PJ, Visser MC, et al. Interobserver agreement for the assessment of handicap in stroke patients. Stroke 1988;19(5):604-7. [published Online First: 1988/05/01]
22. Williams LS, Weinberger M, Harris LE, et al. Development of a stroke-specific quality of life scale. Stroke 1999;30(7):1362-9. [published Online First: 1999/07/02]
23. Yen Y-F, Field AS, Martin EM, et al. Test-retest reproducibility of quantitative CBF measurements using FAIR perfusion MRI and acetazolamide challenge. Magnetic Resonance in Medicine 2002;47(5):921-28. doi: doi:10.1002/mrm.10140
24. van Heuven AW, Mees SMD, Algra A, et al. Validation of a prognostic subarachnoid hemorrhage grading scale derived directly from the Glasgow Coma Scale. Stroke 2008;39(4):1347-48. doi: 10.1161/Strokeaha.107.498345
25. Hijdra A, Brouwers PJAM, Vermeulen M, et al. Grading the Amount of Blood on Computed Tomograms after Subarachnoid Hemorrhage. Stroke 1990;21(8):1156-61.
26. Alsop DC, Detre JA, Golay X, et al. Recommended implementation of arterial spin-labeled perfusion MRI for clinical applications: A consensus of the ISMRM perfusion study group and the European consortium for ASL in dementia. Magnetic Resonance in Medicine 2015;73(1):102-16. doi: doi:10.1002/mrm.25197

Chapter 6

Subarachnoid hemorrhage and cerebral perfusion are associated with brain volume decrease in a cohort of predominantly mild traumatic brain injury patients

L.A. van der Kleij[1,2],J.B. De Vis[2], M.C. Restivo[3], L.C.Turtzo[2,4], J. Hendrikse[1], L.L. Latour[2,4]

[1] Department of Radiology, University Medical Center Utrecht, Utrecht, Netherlands
[2] Acute Cerebrovascular Diagnostics Unit, National Institute of Neurological Disorders and Stroke, National Institutes of Health, Bethesda, Maryland, USA
[3] Division of Intramural Research, National Heart Lung, and Blood Institute, National Institutes of Health, Bethesda, Maryland, USA
[4] Acute Studies Core, Center for Neuroscience and Regenerative Medicine, Bethesda, Maryland, USA

Submitted manuscript

Abstract

Biomarkers are needed to identify traumatic brain injury patients at risk for accelerated brain volume loss and its associated functional impairment. Subarachnoid hemorrhage (SAH) has been shown to affect cerebral volume and perfusion, possibly by induction of inflammation and vasospasm. The purpose of this study was to assess the impact of SAH due to trauma on cerebral perfusion and brain volume. For this, MRI was performed <48 hours and at 90 days after TBI. The <48h scan was used to assess SAH presence and perfusion. Brain volume changes were assessed quantitatively over time. Differences in brain volume change and perfusion were compared between SAH and non-SAH patients. A linear regression analysis with clinical and imaging variables was used to identify predictors of brain volume change. All patients had a relatively good status on admission, and 83% presented with the maximum Glasgow coma scale score. Brain volume decrease was greater in the 11 SAH patients (-3.2%, IQR -4.8 – -1.3%) compared to the 46 non-SAH patients (-0.4%, IQR -1.8 – 0.9%; P<0.001). Brain perfusion was not affected by SAH, but it was correlated with brain volume change (ρ=0.39; P<0.01). Forty-three percent of brain volume change was explained by SAH (ß -0.40, P=0.001), loss of consciousness (ß -0.24, P=0.035) and peak perfusion curve signal intensity height (ß 0.27, P=0.012). Subarachnoid hemorrhage and lower perfusion in the acute phase may identity traumatic brain injury patients at increased risk for accelerated brain volume loss, in addition to loss of consciousness occurrence. Future studies should determine whether the findings apply to TBI patients with worse clinical status on admission. SAH predicts brain volume decrease independent of brain perfusion. This indicates the adverse effects of SAH extend beyond vasoconstriction, and that hypoperfusion also occurs separately from SAH.

Introduction

One in two moderate traumatic brain injury (TBI) patients and one in five mild TBI patients is affected by long-term functional impairment.[1-3] Therefore, markers are needed to characterize patients at risk for long-term impairment despite a relatively good clinical status on admission. Accelerated brain volume loss following TBI has been linked to long-term functional status and cognition.[4, 5] In addition to being a resultant of the immediate brain injury, it is thought to reflect ongoing pathological processes, for it can occur beyond one year after TBI.[6-9] This illustrates the notion of TBI as a chronic rather than an acute disease.[9]

Subarachnoid hemorrhage (SAH) accompanies TBI in about 35% of patients, and an association between SAH and functional outcome has been found previously.[10] A possible explanation for this association is provided in evidence from pre-clinical studies. Herein, subarachnoid blood was shown to trigger oxidative stress and a dysregulated inflammatory response, which induced axonal injury and neuronal cell loss.[11-15] Thereby, traumatic SAH might provoke and exacerbate secondary injury after TBI. In support of this hypothesis, early anti-inflammatory and anti-apoptotic treatment resulted in decreased neural apoptosis following SAH in a rat model.[16] As well, subarachnoid blood might be related to perfusion impairment by promoting vasospasm.[17]

Early perfusion has also been shown associated with poor functional outcome independently from the effects of subarachnoid blood.[18, 19] The presence of perfusion impairment signals a mismatch in oxygen delivery and cerebral oxygen consumption. This may have lasting effects, as impaired perfusion in the first days post injury has been associated with brain volume loss.[6, 20] The watershed or borderzone regions are expected to be especially susceptible to this oxygen delivery mismatch as they have the lowest perfusion pressure.[21-24] Interestingly, a decreased borderzone perfusion has been found associated with long-term brain volume decreases after aneurysmal SAH.[25] Therefore, we suspect a similar relationship between borderzone perfusion and brain volume decrease after TBI, and SAH due to trauma in particular.

In this longitudinal study, we set out to evaluate the association of subarachnoid hemorrhage, perfusion parameters, and clinical characteristics on admission with brain volume change until 90 days post TBI. We hypothesize that SAH presence and altered (borderzone) perfusion within 48 hours after injury are associated with brain volume decrease following TBI. Lastly, we examine possible differences in perfusion between patients with and without SAH to investigate a possible link between SAH with vasoconstriction and hypoperfusion.

Methods

Participants

Seventy-two patients were selected for this retrospective analysis of data collected prospectively as part of the Traumatic Head Injury Neuroimaging Classification (THINC) study. Subjects presented to and were enrolled at Suburban Hospital (Bethesda, MD) or MedStar Washington Hospital Center (Washington, DC). This study was approved by the National Institutes of Health Intramural Institutional Review Board (NCT01132937). Patients who present to the emergency department with 1) a history of acute head injury, 2) are 18 years or older, and 3) are able to undergo MRI within 48 hours of injury, are approached and enrolled. Written informed consent was obtained from the patient or surrogate.

To be included in this analysis, subjects were required to have (1) 3DT1-weighted (3DT1w) imaging, T2*-weighted gradient echo (GRE) imaging, and T2-fluid-attenuated inversion recovery imaging (T2-FLAIR), dynamic susceptibility contrast (DSC) perfusion weighted imaging (PWI) within 48 hours, (2) 3DT1w at 90 days post injury, (3) imaging performed on the same MR system for both time points.

Clinical neurological status on admission was assessed with the Glasgow Coma Scale (GCS).[26] The scale ranges from 3 to 15, where a score of 3 represents full impairment and a score of 15 represents no impairment in the motor, eye and verbal response.

Injury severity was defined according to the United States Department of Defense / Veteran Affairs guidelines that include GCS score, loss of consciousness and post-traumatic amnesia duration, and imaging findings.[27] Mild/moderate/severe TBI was defined as GCS 13-15/9-12/3-8, loss of consciousness <30 minutes/30 minutes – 1 day/>1day, structural imaging normal/abnormal/abnormal, and post-traumatic amnesia <1 day/1 – 7 days/>7 days. The highest severity category is assigned when a patient meets the criteria of several categories. In addition to this classification, patients were classified as 'silent' TBI when they did not show either loss of consciousness, post-traumatic amnesia or an altered mental status. However, clinical concern in the 'silent' was sufficient to trigger an urgent CT of the head to rule out hemorrhage (Table 1).

Functional outcome at 90 days was assessed with the Extended Glasgow Outcome Scale (GOS-E).[28, 29] The GOS-E ranges from 1 to 8, where a score of 1 represents a patient's death and a score of 8 represents a patient's return to preinjury baseline.

Image protocol

Imaging was performed on 1.5T (Sigma, General Electric, Milwaukee,

WI, USA) and 3T (Philips, Cleveland, OH, USA; Siemens Healthcare, Malvern, PA, USA) MR systems. The imaging protocol at both time points included 3DT1w (1x1x1 mm voxels ~5.25 min) and T2-FLAIR (1x1x3.5 mm, ~2 min) sequences. At baseline (<48h) the protocol also included DSC PWI (2x2x7 mm, 1.5 min) during the bolus injection of a single dose of gadolinium based contrast agent, T2*-weighted GRE sequence (TE= 12ms, 0.75x0.75x3.5 mm, 2.25 min), and 3D-T2* susceptibility-weighted imaging (SWI, TE=27ms, ~1x1x1mm, 3.75 min). A board-certified radiologist performed a clinical interpretation of all MRI for medical records. Patients were stratified as positive or negative for subarachnoid hemorrhage based primarily on the appearance on T2-FLAIR and T2*-weighted GRE. Traumatic microbleeds (TMBs) were identified using the two T2*-weighted sequences and classified as punctate or having a linear appearance. To reduce the likelihood of false positive detection of TMBs from vasculature conspicuous on SWI, TMBs were only scored as positive if detectable on both T2* sequences. Hematoma presence was defined as the presence of subdural, intraventricular or intraparenchymal blood.

Image processing

The lesion prediction algorithm (LST, v.2.0.15) for statistical parametric mapping (SPM) was used to segment hyperintense lesions on T2-FLAIR images and correct the 3DT1w images for possible corresponding hypointensities.[23] Subsequently, brain volume was obtained with CAT12 (http://www.neuro.uni-jena.de/cat/) as the sum of the gray and white matter volumes, including the lesion volume. The intracranial volume was defined as the brain and cerebrospinal fluid (CSF) volumes combined, while global atrophy was defined as the CSF volume relative to intracranial volume. Segmentation quality was assessed as either "adequate" or "poor" on visual inspection (L.A.v.d.K.). Patients with a 'poor' brain segmentation quality rating were excluded from data analyses. Brain volume change was defined using the baseline as reference; negative values for brain volume change indicates a decrease in brain volume over time.

Perfusion analysis was performed on the motion corrected PWI using two methods: deconvolution-based analysis and temporal similarity perfusion analysis (TSP). Standard perfusion maps (CBF and Tmax) were extracted from the time-series PWI using a block-circulant singular value deconvolution (bSVD) approach.[30] A separate perfusion analysis was done using TSP, which is a model-free technique that assesses regional perfusion based on deviation from the whole-brain healthy tissue average.[31] Both perfusion analysis methods were performed using Matlab R2018a (The MathWorks, Inc., Natick, MA, USA).

TSP provides Pearson's r correlation maps, peak signal intensity (SI) maps (i.e., the maximum gadolinium-induced signal drop per voxel), and relative delay maps (i.e., the

time delay at which the voxel perfusion time course is most correlated with the whole-brain average).[31] The TSP peak signal intensity maps were inverted to obtain TSP peak height maps, in which a higher peak reflects a higher gadolinium concentration. Although TSP does not provide perfusion in absolute units, it makes it easier to identify regions where perfusion deviates from normal (e.g., lesions, ischemia) and it is even less sensitive to errors resulting from a poorly chosen arterial input function.

For both the bSVD and the TSP technique, the resulting perfusion maps were coregistered to a downsampled Dartel template (matrix size: 256x256x40, voxel size: 0.71x0.85x4.5 mm^3). Subsequently, a borderzone mask in Dartel space was created, where borderzone regions were defined as overlapping perfusion territories across subjects on previously obtained territorial arterial spin labeling maps (Figure 1).[32] Whole brain and borderzone perfusion values were retrieved, and the borderzone ratio relative to whole brain values was calculated separately for each perfusion parameter. The rationale behind this was that a lower borderzone ratio could signal subtle perfusion abnormalities, which cause reduced CBF or prolonged arterial transit times.[33]

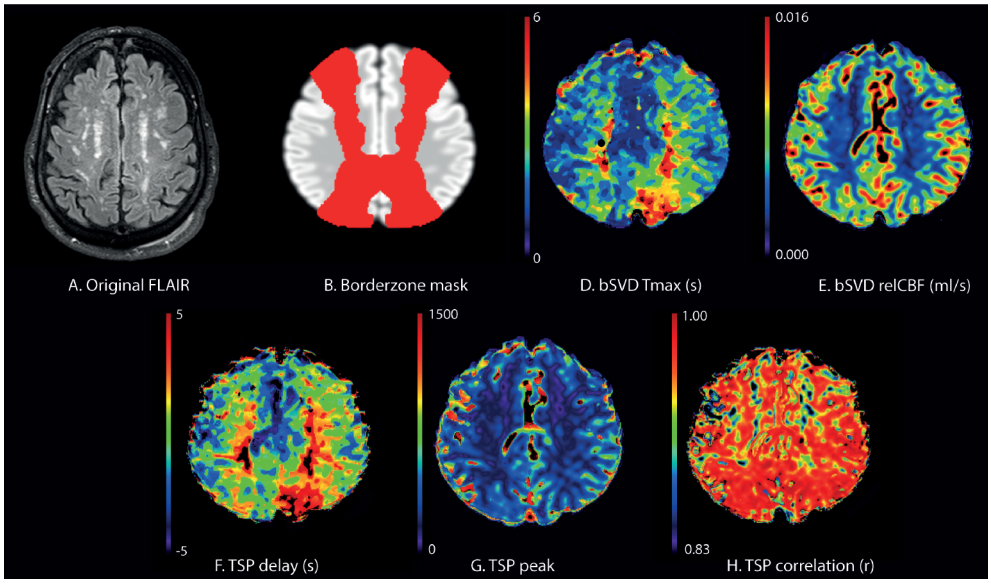

Fig. 1. The original FLAIR image (A), borderzone region mask (B) and resulting perfusion maps in Dartel space from a single patient (D - H). Images D and E show the perfusion parameters obtained from the model-based block-circulant singular value deconvolution (bSVD) analysis: Tmax and cerebral blood flow (CBF). Images F – H show the perfusion parameters obtained from the model-free temporal similarity perfusion (TSP) analysis: delay, peak height and correlation maps.

Statistical analysis

Statistical analyses were carried out in R 3.5.1.[34] Non-parametric tests were used to

account for non-normal distributions. Differences between groups were analyzed with a Mann-Whitney U, Kruskal-Wallis test or Chi-square test, and differences between baseline and 90 days were analyzed with a Wilcoxon signed-rank test. Correlations were tested with Spearman's rank correlation. Multiple linear regression with backwards selection ($P < 0.50$) was performed to identify the combination of variables associated with relative brain volume change. In the initial model, only variables at a P-value < 0.15 in bivariate analyses were entered in a regression model.

Results

Patient characteristics

Fifty-seven patients were included in this study after 15 subjects were excluded due to poor brain segmentation quality. Subject characteristics of the included patients are shown in Table 1. The 15 excluded subjects had a median age of 46 years (IQR 39 – 57 years), 47% were female and 20% received a diagnosis of either moderate or severe TBI.

Table 1. Baseline characteristics

Variable		Total n = 57	SAH positive n = 11 (19%)	SAH negative n = 46 (81%)	*P-value*[a]
Median (IQR) age (years)		49 (33 – 65)	66 (61 – 68)	46 (30 – 60)	0.005
Sex, female		15 (26%)	2 (18%)	13 (28%)	n.s.
TBI severity	*Silent*	13 (23%)	2 (18%)	11 (24%)	n.s.
	Mild	38 (67%)	8 (73%)	30 (65%)	
	Moderate	6 (11%)	1 (9%)	5 (11%)	
Hematoma (all)		14 (25%)	7 (64%)	7 (15%)	0.003
Subdural		14 (25%)	7 (64%)	7 (15%)	0.003
Intraventricular		2 (4%)	1 (14%)	1 (2%)	n.s.
Intraparenchymal		7 (12%)	4 (36%)	3 (7%)	0.028
Traumatic microbleed presence		21 (37%)	7 (64%)	14 (30%)	n.s.
GCS at admission	*13*	1 (2%)	0 (0%)	1 (2%)	n.s.
	14	9 (16%)	3 (27%)	6 (13%)	
	15	47 (82%)	8 (73%)	39 (85%)	
GOS-E at 90 days	*4*	1 (2%)	0 (0%)	1 (2%)	n.s.
	5	5 (9%)	1 (10%)	4 (9%)	
	6	5 (9%)	2 (20%)	3 (7%)	
	7	12 (21%)	2 (20%)	10 (22%)	
	8	33 (59%)	5 (50%)	28 (61%)	
Median (IQR) brain volume at baseline (ml)		1094 (1016 – 1182)	1090 (942 – 1207)	1097 (1029 – 1168)	n.s.
Median (IQR) brain volume at 90 days (ml)		1086 (1010 – 1156)	1087 (918 – 1137)	1084 (1015 – 1168)	n.s.
Median (IQR) brain volume change (ml)		-8[c] (-25 – 7)	- 32[d] (-50 – -13)	–5[e] (-19 – 8)	0.001

[a]Difference SAH positive and negative patients; [c]*P* = 0.002; [d]*P* < 0.001; [e]*P* = 0.097. N.s. = not significant; TBI = traumatic brain injury; GCS = Glasgow coma scale; GOS-E = Glasgow outcome scale extended.

The majority of patients were admitted with a good clinical status: 83% had the maximum GCS score. Median acute imaging time of the included patients was 17 hours (IQR: 7 – 25 hours) and median follow-up imaging time was 91 days (IQR: 76 – 110 days). Median brain volume change was -0.7% (IQR -2.1 – 0.6%). SAH due to trauma was identified in 11 of 57 patients (19%). Frequency of trauma-related findings are shown in Table 1.

SAH and brain volume decrease

Brain volume decrease was greater in patients with SAH (-3.2%, IQR -4.8 – -1.3%) compared to patients clear of SAH (-0.4%, IQR -1.8 – 0.9%; P < 0.001; Figure 2). In contrast, whole brain and borderzone ratio perfusion parameters did not significantly differ in patients with and without SAH (Figure 2).

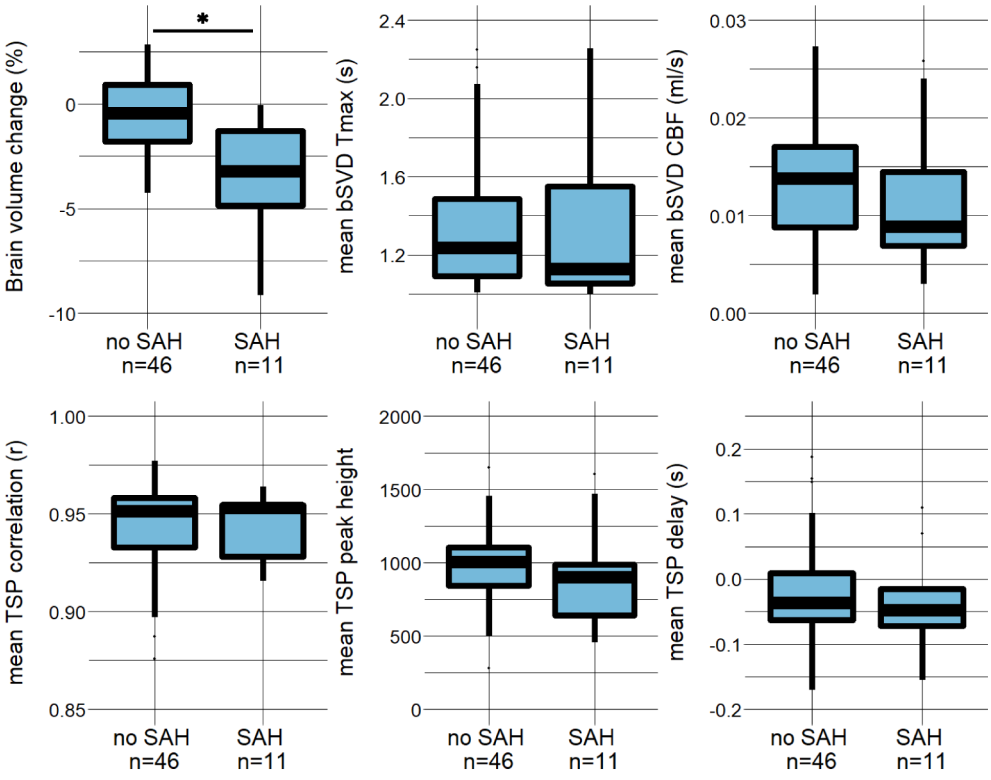

Fig. 2. Differences in brain volume change (%) and perfusion parameters for patients without (left boxplots) and with (right boxplots) subarachnoid hemorrhage (SAH) on MRI. The top left graph shows that brain volume decrease was greater for patients with SAH (P < 0.001). The middle and right top row graphs show no effect of SAH presence on Tmax and cerebral blood flow (CBF) obtained with block-circulant singular value deconvolution (bSVD). The bottom row shows that no effect of SAH presence was found on (from left to right) mean correlation, mean peak height and mean delay obtained with temporal similarity perfusion mapping (TSP). *P <0.05.

Perfusion parameters and brain volume decrease

Whole brain TSP peak height values were significantly associated with brain volume change: $\rho = 0.39$ (P = 0.003; Figure3), but there was no significant association found between whole brain bSVD CBF values and brain volume change: $\rho = 0.24$ (P = 0.079). Also, whole brain Tmax, TSP delay and TSP correlation were not associated with brain volume change. None of the borderzone ratios were associated with brain volume change.

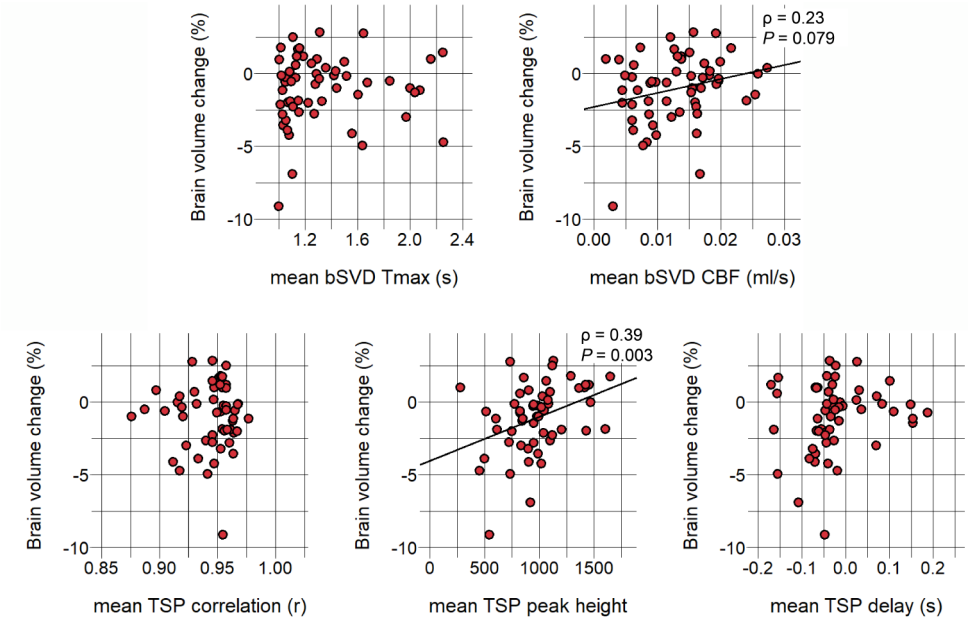

Fig 3. The association between perfusion measures and brain volume change (%). The top row displays Tmax and cerebral blood flow (CBF) obtained with block-circulant singular value deconvolution (bSVD) analysis. The bottom row shows the mean correlation, mean peak height and mean delay parameters obtained with temporal similarity perfusion mapping (TSP). Mean TSP peak height was the only perfusion parameter significantly associated with brain volume change (ρ = 0.39, P = 0.003).

Predictors of brain volume decrease

Brain volume decrease between 48 hours and 90 days after TBI was greater in those with loss of consciousness (-1.1% (IQR -2.7 – -0.1%)) compared to patients without loss of consciousness -0.2% (IQR -1.0 – 1.1%); P = 0.042). As well, a greater brain volume change was found in patients with hematoma compared to those without hematoma presence (-2.0% (IQR -4.6 – -0.5) compared to -0.4% (IQR -1.9 – 0.9); P = 0.013), and in patients with traumatic microbleeds (-2.0% (IQR -3.9 – -0.5%)) compared to those clear of traumatic microbleeds (-0.3% (IQR -1.2 – 0.7%); P = 0.018). Brain volume change did not differ depending on occurrence of post-traumatic amnesia (P = 0.119), relative brain

volume at baseline (P = 0.961), or admission GCS score (P = 0.261) in bivariate analyses, and neither depending on injury severity class (P = 0.152). Table 2 shows the final regression model (R^2 = 46%), which included SAH presence, mean TSP peak height value, loss of consciousness, hematoma presence, and traumatic microbleed presence. In this model, SAH presence and lower mean TSP peak height value were significantly associated with brain volume change.

Table 2. Linear model for relative brain volume change

Dependent variable: relative brain volume change (%)		
	ß	*P*
SAH presence	-0.35	0.005*
Mean TSP peak height	0.29	0.009*
Loss of consciousness	-0.20	0.067
Hematoma presence[a]	-0.18	0.172
Traumatic microbleed presence	-0.14	0.239

R^2 = 46%, F = 9.8.2 (*P* < 0.0001). [a]presence of subdural, intraparenchymal and/or intraventricular blood.
* *P* < 0.05.

Extended Glasgow Outcome Scale (GOS-E)

The level of disability at 90 days as measured by the Extended Glasgow Outcome Scale (GOS-E) was not different between those with and without subarachnoid hemorrhage (P = 0.507), nor was it related to hematoma presence (P = 0.846), TSP peak height values (P > 0.181), bSVD values (P > 0.146), FLAIR lesion volume (P = 0.282), or brain volume change (P = 0.184). Yet, GOS-E score was different between patients with loss of consciousness (7.5, IQR, 6.3 – 8) and patients without (8.0, IQR 8.0 – 8.0; P = 0.041).

Discussion

TBI patients with a relatively good clinical status upon admission showed pronounced brain volume decrease between the first day of injury and 90 days. Subarachnoid hemorrhage and lower perfusion (mean TSP peak height) in the acute phase may identity patients at increased risk for brain volume decrease in addition to the occurrence of loss of consciousness. SAH and perfusion appear to affect brain volume independently, as there was no difference in perfusion parameters depending on SAH presence.

Our reported volume changes are in line with various reports of regional and global brain volume changes after TBI.[5, 35-37] Specifically, we found 1% brain volume decrease in the whole group. This is similar to the decrease found at 6 weeks in a multi-time point, cross-sectional MRI study with primarily moderate-severe TBI patients as well as

to the decrease in cortical volume between 2 days and 1 month after mild TBI.[38, 39] One study found a 10% brain volume decrease between day 2 and day 200, which only corresponds to the greatest observed decreases in our study.[40] To compare, the normal annual brain volume decrease for a healthy adult is 0.32% (95% CI 0.10% - 0.54%).[41] These volume changes can affect daily life for patients, as brain abnormalities and increased atrophy have been related to impaired cognition.[42] In the current study, however, no association was found between brain volume decrease and functional outcome, which was good for the majority of patients (GOS-E ≥ 7). Importantly, long-term cognitive or behavioral problems are common even among those with good functional outcome.[3] Therefore, though the GOS-E enables identification of gross changes in functional impairment, it may not detect the complaints associated with brain volume decrease that affect everyday activities. Another explanation for the lack of an association between volume change and functional outcome is that brain volume changes following TBI may be confounded by cerebral edema. In the multi-time point, cross-sectional study, also an increase in brain volume of nearly 1% was found around day 13, which was ascribed to edema.[38] Consequently, the average volume change in our cohort could reflect a reduction of edema.

Cerebral edema following TBI is caused by various factors, including mechanical disruption of blood vessels and ischemia.[43] SAH could be associated with increased cerebral edema due to its pro-inflammatory effects. Nevertheless, the median volume decrease of 3% in SAH patients is over a threefold greater than reported changes based on edema reduction.[38] This points to true brain volume loss, at least in the patients with SAH, although cannot be confirmed by our data as no edema correction was performed. Brain volume loss following SAH can, in part, be explained by the activation of the immune system when blood is present in the CSF space.[44] The resulting, mainly pro-inflammatory effects,[44] can amongst other things evoke vasospasm.[45] Further, subarachnoid blood was found to induce spreading depolarizations in 76% of swine in a preclinical study, and these spreading depolarizations were found to incite early brain injury,[46] most likely due to their effect on inflammation as well as vasoconstriction.[47, 48] The combined effects of subarachnoid blood that provoke tissue ischemia can be widespread due to the circulating nature of CSF throughout the central nervous system.[17, 45, 46, 49, 50] Thereby, it could explain the pronounced effect of SAH on brain tissue volume. This may also explain why hematoma presence, a more localized pathology, had a weaker association with brain volume decrease in our study. Given that we did not find an effect between SAH presence and blood flow, we hypothesize that the effect of SAH on brain volume decrease in our study is mainly caused by dysregulated inflammation resulting in cell death rather than by vasoconstriction.

Earlier research has reported an association between decreased brain perfusion and brain volume loss. For example, a study in moderate-to-severe TBI patients observed

an association between CBF 5 days post TBI and brain volume loss at 6 months [6]. As well, in mild TBI patients, hypoperfusion on single-photon emission computed tomography (SPECT) was associated with increased cerebral atrophy 6 months after injury.[20] A lower CBF in TBI patients could be explained by cerebral edema, spreading depolarizations and vasospasm which are all caused by a predominantly pro-inflammatory state following TBI.[45, 46, 50, 51] Edema is a direct result of TBI and can lead to a decreased tissue perfusion due to microvascular compression.[51] Vasospasm, on the other hand, is an indirect effect resulting from the activation of the immune system as a response to subarachnoid blood.[17] In our study, we found a significant association between the TSP peak height parameter and brain volume change, but not between bSVD CBF and brain volume change. This dissociation is unexpected as previous studies in stroke patients have found the peak height measure to strongly correlate with relative CBF.[52] Noise in the CBF data related to model (fit) errors may have contributed to this discrepancy, or a relatively low sample size may have resulted in a false positive association between our peak height measurements and brain volume change. If any effect does exist, we could say it is more likely related to the presence of edema rather than vasospasm as we did not find lower peak height measurements in patients with SAH. In any case, we want to emphasize that the value of TSP peak height as an absolute parameter remains unclear. This because aside from perfusion, it can be affected by a patient's hydration status, contrast administration method, and contrast dose. Lastly, vasoconstriction of the major arteries typically occurs after day 2,[53] which is after imaging took place in the current study. Consequently, the found associations between perfusion parameters and brain volume changes are likely dependent on MRI timing. Possibly a stronger relationship between perfusion parameters and brain volume change can be found during the occurrence of vasoconstriction.

Limitations of the study include the absence of cognitive testing. We found no association between brain volume change and outcome on the GOS-E. Perhaps cognitive impairment is more sensitive to detect the effects of brain volume decrease on daily functioning. As neuropsychological testing was not part of this study, we could not link our findings to impaired cognitive performance following TBI. Another limitation of the study is that increased injury severity is associated with worse scan quality. Fifteen patients were excluded in the current study secondary to poor brain segmentation quality. Twenty percent of these patients were classified as moderate or severe. In comparison, 11% of the patients included in the final analysis carried a diagnosis of either moderate (or severe) TBI. In addition, the inclusion criteria of informed consent for a research MRI within 48 hours after injury may induce a bias towards patients with a good clinical status. As such, the associations found are largely reflective of mild TBI patients, and future research should elicit their application to the general TBI population.

Moreover, the imaging of TBI patients shortly after injury means that the images can include extravasated blood, edema and hyperemia. Volume changes do therefore not necessarily reflect atrophy but also may result from the recovery of the brain from injury-related phenomena. Interestingly, SAH was associated with greater brain volume decreases despite these confounding factors. Another limitation of the study is that we do not have a quantitative measure of extravasated blood volume, or a measure of the degree of inflammation. As such, we could not test whether increased extravasated blood volume increased inflammatory markers are associated with increased volume changes. For research settings, a quantitative measure can provide more insight into the mechanism by which SAH affect brain volume. In contrast, in clinical settings a qualitative assessment of SAH presence is a more useful measure than quantitative measures. Lastly, little data were available to calculate a meaningful sample size estimation to determine the relationship between loss of consciousness and brain volume change. Based on our data, a power of 0.8 and α of 0.05, a future study should include at least 138 patients to investigate differences in brain volume change depending on loss of consciousness.

The results of this study help us understand the causes of brain volume decrease associated with (mild) TBI, which may be the cause of functional impairment. Future studies should examine whether the findings can be generalized to TBI patients with worse clinical status on admission. Our findings show the potential of imaging markers related to vascular injury on acute MRI, especially subarachnoid blood, to identify patients at risk for long-term brain volume loss in addition to loss of consciousness as a clinical marker.

Acknowledgements

We are deeply appreciative of the patients and their families without whom this research would not be possible. We thank the investigators of the NINDS - Center for Neuroscience and Regenerative Medicine THINC Study, the staff at Suburban Hospital and Washington Hospital Center, and the NINDS Stroke Team.

References

1. Lundin, A., de Boussard, C., Edman, G. and Borg, J. (2006). Symptoms and disability until 3 months after mild TBI. Brain Injury 20, 799-806.
2. McMahon, P., Hricik, A., Yue, J.K., Puccio, A.M., Inoue, T., Lingsma, H.F., Beers, S.R., Gordon, W.A., Valadka, A.B., Manley, G.T., Okonkwo, D.O. and Investigators, T.-T. (2014). Symptomatology and functional outcome in mild traumatic brain injury: results from the prospective TRACK-TBI study. Journal of neurotrauma 31, 26-33.
3. Benedictus, M.R., Spikman, J.M. and van der Naalt, J. (2010). Cognitive and Behavioral Impairment in Traumatic Brain Injury Related to Outcome and Return to Work. Archives of Physical Medicine and Rehabilitation 91, 1436-1441.
4. Sidaros, A., Skimminge, A., Liptrot, M.G., Sidaros, K., Engberg, A.W., Herning, M., Paulson, O.B., Jernigan, T.L. and Rostrup, E. (2009). Long-term global and regional brain volume changes following severe traumatic brain injury: A longitudinal study with clinical correlates. NeuroImage 44, 1-8.
5. Tate, D.F., Khedraki, R., Neeley, E.S., Ryser, D.K. and Bigler, E.D. (2011). Cerebral volume loss, cognitive deficit, and neuropsychological performance: comparative measures of brain atrophy: II. Traumatic brain injury. Journal of the International Neuropsychological Society 17, 308-316.
6. Xu, Y., McArthur, D.L., Alger, J.R., Etchepare, M., Hovda, D.A., Glenn, T.C., Huang, S., Dinov, I. and Vespa, P.M. (2010). Early nonischemic oxidative metabolic dysfunction leads to chronic brain atrophy in traumatic brain injury. Journal of Cerebral Blood Flow and Metabolism: Official Journal of the International Society of Cerebral Blood Flow and Metabolism 30, 883-894.
7. Trivedi, M.A., Ward, M.A., Hess, T.M., Gale, S.D., Dempsey, R.J., Rowley, H.A. and Johnson, S.C. (2007). Longitudinal changes in global brain volume between 79 and 409 days after traumatic brain injury: relationship with duration of coma. Journal of neurotrauma 24, 766-771.
8. Green, R., Colella, B., Maller, J., Bayley, M., Glazer, J. and Mikulis, D. (2014). Scale and pattern of atrophy in the chronic stages of moderate-severe TBI. Frontiers in Human Neuroscience 8.
9. Masel, B.E. and DeWitt, D.S. (2010). Traumatic Brain Injury: A Disease Process, Not an Event. Journal of neurotrauma 27, 1529-1540.
10. Wardlaw, J.M., Easton, V.J. and Statham, P. (2002). Which CT features help predict outcome after head injury? Journal of Neurology, Neurosurgery & Psychiatry 72, 188-192.
11. Prunell, G.F., Svendgaard, N.-A., Alkass, K. and Mathiesen, T. (2005). Inflammation in the Brain after Experimental Subarachnoid Hemorrhage. Neurosurgery 56, 1082-1092.
12. Schneider, U.C., Davids, A.-M., Brandenburg, S., Müller, A., Elke, A., Magrini, S., Atangana, E., Turkowski, K., Finger, T., Gutenberg, A., Gehlhaar, C., Brück, W., Heppner, F.L. and Vajkoczy, P. (2015). Microglia inflict delayed brain injury after subarachnoid hemorrhage. Acta Neuropathologica 130, 215-231.
13. Murakami, K., Koide, M., Dumont, T.M., Russell, S.R., Tranmer, B.I. and Wellman, G.C. (2011). Subarachnoid Hemorrhage Induces Gliosis and Increased Expression of the Pro-inflammatory Cytokine High Mobility Group Box 1 Protein. Translational Stroke Research 2, 72-79.
14. Simard, J.M., Geng, Z., Woo, S.K., Ivanova, S., Tosun, C., Melnichenko, L. and Gerzanich, V. (2009). Glibenclamide Reduces Inflammation, Vasogenic Edema, and Caspase-3 Activation after Subarachnoid Hemorrhage. Journal of Cerebral Blood Flow & Metabolism 29, 317-330.
15. Loane, D.J. and Kumar, A. (2016). Microglia in the TBI brain: The good, the bad, and the dysregulated. Experimental Neurology 275, 316-327.
16. Li, J., Chen, J., Mo, H., Chen, J., Qian, C., Yan, F., Gu, C., Hu, Q., Wang, L. and Chen, G. (2016). Minocycline Protects Against NLRP3 Inflammasome-Induced Inflammation and P53-Associated Apoptosis in Early Brain Injury After Subarachnoid Hemorrhage. Molecular Neurobiology 53, 2668-2678.
17. Handa, Y., Kabuto, M., Kobayashi, H., Kawano, H., Takeuchi, H. and Hayashi, M. (1991). The Correlation between Immunological Reaction in the Arterial Wall and the Time Course of the Development of Cerebral Vasospasm in a Primate Model. Neurosurgery 28, 542-549.
18. Kaloostian, P., Robertson, C., Gopinath, S.P., Stippler, M., King, C.C., Qualls, C., Yonas, H. and Nemoto, E.M. (2012). Outcome Prediction within Twelve Hours after Severe Traumatic Brain Injury by Quantita-

tive Cerebral Blood Flow. Journal of neurotrauma 29, 727-734.
19. Bendinelli, C., Cooper, S., Evans, T., Bivard, A., Pacey, D., Parson, M. and Balogh, Z.J. (2017). Perfusion Abnormalities are Frequently Detected by Early CT Perfusion and Predict Unfavourable Outcome Following Severe Traumatic Brain Injury. World Journal of Surgery 41, 2512-2520.
20. Hofman, P.A.M., Stapert, S.Z., van Kroonenburgh, M.J.P.G., Jolles, J., de Kruijk, J. and Wilmink, J.T. (2001). MR Imaging, Single-photon Emission CT, and Neurocognitive Performance after Mild Traumatic Brain Injury. American Journal of Neuroradiology 22, 441-449.
21. Mangla, R., Kolar, B., Almast, J. and Ekholm, S.E. (2011). Border zone infarcts: pathophysiologic and imaging characteristics. Radiographics 31, 1201-1214.
22. Momjian-Mayor, I. and Baron, J.-C. (2005). The Pathophysiology of Watershed Infarction in Internal Carotid Artery Disease. Stroke 36, 567-577.
23. Schmid, S., Teeuwisse, W.M., Lu, H. and van Osch, M.J.P. (2015). Time-efficient determination of spin compartments by time-encoded pCASL T2-relaxation-under-spin-tagging and its application in hemodynamic characterization of the cerebral border zones. NeuroImage 123, 72-79.
24. Hendrikse, J., Petersen, E.T., Van Laar, P.J. and Golay, X. (2008). Cerebral border zones between distal end branches of intracranial arteries: MR imaging. Radiology 246, 572-580.
25. van der Kleij, L.A., Lucci, C., Petersen, E.T., Vergouwen, M.D.I., Rinkel, G.J.E., Hendrikse, J. and De Vis, J.B. (2017). Decreased borderzone perfusion is related to brain parenchymal volume loss after subarachnoid hemorrhage. In: ISMRM 25th Annual Meeting & Exhibition: Honolulu, HI, USA.
26. Teasdale, G. and Jennett, B. (1974). ASSESSMENT OF COMA AND IMPAIRED CONSCIOUSNESS: A Practical Scale. The Lancet 304, 81-84.
27. US Department of Veterans Affairs and Department of Defense (VA/DoD)(2009). VA/DoD clinical practice guideline for management of concussion/mild traumatic brain injury.
28. Wilson, J.T.L., Pettigrew, L.E.L. and Teasdale, G.M. (1998). Structured Interviews for the Glasgow Outcome Scale and the Extended Glasgow Outcome Scale: Guidelines for Their Use. Journal of neurotrauma 15, 573-585.
29. Jennett, B., Snoek, J., Bond, M.R. and Brooks, N. (1981). Disability after severe head injury: observations on the use of the Glasgow Outcome Scale. Journal of Neurology, Neurosurgery & Psychiatry 44, 285-293.
30. Wu, O., Østergaard, L., Weisskoff, R.M., Benner, T., Rosen, B.R. and Sorensen, A.G. (2003). Tracer arrival timing-insensitive technique for estimating flow in MR perfusion-weighted imaging using singular value decomposition with a block-circulant deconvolution matrix. Magnetic Resonance in Medicine 50, 164-174.
31. Song, S., Bokkers, R.P.H., Luby, M., Edwardson, M.A., Brown, T., Shah, S., Cox, R.W., Saad, Z.S., Reynolds, R.C., Glen, D.R., Cohen, L.G. and Latour, L.L. (2017). Temporal similarity perfusion mapping: A standardized and model-free method for detecting perfusion deficits in stroke. PLOS ONE 12, e0185552.
32. Hartkamp, N.S., Petersen, E.T., Chappell, M.A., Okell, T.W., Uyttenboogaart, M., Zeebregts, C.J. and Bokkers, R.P.H. (2017). Relationship between haemodynamic impairment and collateral blood flow in carotid artery disease. Journal of Cerebral Blood Flow & Metabolism 38, 2021-2032.
33. Zaharchuk, G., Olivot, J.M., Fischbein, N.J., Bammer, R., Straka, M., Kleinman, J.T. and Albers, G.W. (2012). Arterial Spin Labeling Imaging Findings in Transient Ischemic Attack Patients: Comparison with Diffusion- and Bolus Perfusion-Weighted Imaging. Cerebrovascular Diseases 34, 221-228.
34. R Core Team (2017). R: A Language and Environment for Statistical Computing: Vienna, Austria.
35. Wu, X., Kirov, I.I., Gonen, O., Ge, Y., Grossman, R.I. and Lui, Y.W. (2016). MR Imaging Applications in Mild Traumatic Brain Injury: An Imaging Update. Radiology 279, 693-707.
36. Maxwell, W.L., MacKinnon, M.-A., Stewart, J.E. and Graham, D.I. (2010). Stereology of cerebral cortex after traumatic brain injury matched to the Glasgow Outcome Score. Brain 133, 139-160.
37. MacKenzie, J.D., Siddiqi, F., Babb, J.S., Bagley, L.J., Mannon, L.J., Sinson, G.P. and Grossman, R.I. (2002). Brain Atrophy in Mild or Moderate Traumatic Brain Injury: A Longitudinal Quantitative Analysis. American Journal of Neuroradiology 23, 1509-1515.
38. Blatter, D.D., Bigler, E.D., Gale, S.D., Johnson, S.C., Anderson, C.V., Burnett, B.M., Ryser, D., Macnamara,

S.E. and Bailey, B.J. (1997). MR-based brain and cerebrospinal fluid measurement after traumatic brain injury: correlation with neuropsychological outcome. American Journal of Neuroradiology 18, 1-10.
39. Toth, A., Kovacs, N., Perlaki, G., Orsi, G., Aradi, M., Komaromy, H., Ezer, E., Bukovics, P., Farkas, O., Janszky, J., Doczi, T., Buki, A. and Schwarcz, A. (2013). Multi-Modal Magnetic Resonance Imaging in the Acute and Sub-Acute Phase of Mild Traumatic Brain Injury: Can We See the Difference? Journal of neurotrauma 30, 2-10.
40. Irimia, A., Chambers, M.C., Alger, J.R., Filippou, M., Prastawa, M.W., Wang, B., Hovda, D.A., Gerig, G., Toga, A.W., Kikinis, R., Vespa, P.M. and Horn, J.D.V. (2011). Comparison of Acute and Chronic Traumatic Brain Injury Using Semi-Automatic Multimodal Segmentation of MR Volumes. Journal of neurotrauma 28, 2287-2306.
41. Scahill, R.I., Frost, C., Jenkins, R., Whitwell, J.L., Rossor, M.N. and Fox, N.C. (2003). A longitudinal study of brain volume changes in normal aging using serial registered magnetic resonance imaging. Archives of Neurology 60, 989-994.
42. Shelli R. Kesler, H.F.A.E.D.B. (2000). SPECT, MR and quantitative MR imaging: correlates with neuropsychological and psychological outcome in traumatic brain injury. Brain Injury 14, 851-857.
43. Unterberg, A.W., Stover, J., Kress, B. and Kiening, K.L. (2004). Edema and brain trauma. Neuroscience 129, 1019-1027.
44. Moraes, L., Grille, S., Morelli, P., Mila, R., Trias, N., Brugnini, A., LLuberas, N., Biestro, A. and Lens, D. (2015). Immune cells subpopulations in cerebrospinal fluid and peripheral blood of patients with Aneurysmal Subarachnoid Hemorrhage. SpringerPlus 4, 195.
45. Bavbek, M., Polin, R., Kwan, A.-L., Arthur Adam, S., Kassell Neal, F. and Lee Kevin, S. (1998). Monoclonal Antibodies Against ICAM-1 and CD18 Attenuate Cerebral Vasospasm After Experimental Subarachnoid Hemorrhage in Rabbits. Stroke 29, 1930-1936.
46. Hartings, J.A., York, J., Carroll, C.P., Hinzman, J.M., Mahoney, E., Krueger, B., Winkler, M.K.L., Major, S., Horst, V., Jahnke, P., Woitzik, J., Kola, V., Du, Y., Hagen, M., Jiang, J. and Dreier, J.P. (2017). Subarachnoid blood acutely induces spreading depolarizations and early cortical infarction. Brain 140, 2673-2690.
47. Jander, S., Schroeter, M., Peters, O., Witte, O.W. and Stoll, G. (2001). Cortical Spreading Depression Induces Proinflammatory Cytokine Gene Expression in the Rat Brain. Journal of Cerebral Blood Flow & Metabolism 21, 218-225.
48. Bosche, B., Graf, R., Ernestus, R.-I., Dohmen, C., Reithmeier, T., Brinker, G., Strong, A.J., Dreier, J.P. and Woitzik, J. (2010). Recurrent spreading depolarizations after subarachnoid hemorrhage decreases oxygen availability in human cerebral cortex. Annals of Neurology 67, 607-617.
49. Ousman, S.S. and Kubes, P. (2012). Immune surveillance in the central nervous system. Nature Neuroscience 15, 1096.
50. Dreier, J.P., Ebert, N., Priller, J., Megow, D., Lindauer, U., Klee, R., Reuter, U., Imai, Y., Einhäupl, K.M. and Victorov, I. (2000). Products of hemolysis in the subarachnoid space inducing spreading ischemia in the cortex and focal necrosis in rats: a model for delayed ischemic neurological deficits after subarachnoid hemorrhage? Journal of Neurosurgery 93, 658-666.
51. Østergaard, L., Engedal, T.S., Aamand, R., Mikkelsen, R., Iversen, N.K., Anzabi, M., Næss-Schmidt, E.T., Drasbek, K.R., Bay, V., Blicher, J.U., Tietze, A., Mikkelsen, I.K., Hansen, B., Jespersen, S.N., Juul, N., Sørensen, J.C.H. and Rasmussen, M. (2014). Capillary Transit Time Heterogeneity and Flow-Metabolism Coupling after Traumatic Brain Injury. Journal of Cerebral Blood Flow & Metabolism 34, 1585-1598.
52. Liu, Y.-J., Chung, H.-W., Huang, I.-J., Wang, F.-N., Chin, S.-C., Lee, C.-S. and Chen, C.-Y. (2002). A Reinvestigation of Maximal Signal Drop in Dynamic Susceptibility Contrast Magnetic Resonance Imaging. Journal of Neuroimaging 12, 330-338.
53. Kramer, D.R., Winer, J.L., Pease, B., Amar, A.P. and Mack, W.J. (2013). Cerebral vasospasm in traumatic brain injury. Neurology research international 2013.

Part II

Vascular components in aging and dementia

Cerebral blood flow, T2 of peripheral CSF and brain volumetrics in healthy aging – mild cognitive impairment – dementia

Chapter 7

Is cerebral blood flow affected by preventable vascular risk factors and physical fitness level?

L.A. van der Kleij[1], N.L. Højland Reislev[2], C.S. Eriksen[3,4], H.R. Siebner[2], C.-J. Boraxbekk[2], E.L. Mortensen[4,5], M. Kjaer[3,4], E. Garde[2,4,5], E. T. Petersen[2,6]

[1] Department of Radiology, University Medical Center Utrecht, Utrecht, the Netherlands
[2] Danish Research Centre for Magnetic Resonance, Centre for Functional and Diagnostic Imaging and Research, Copenhagen University Hospital Hvidovre, Denmark
[3] Department of Orthopedic Surgery M, Institute of Sports Medicine Copenhagen, Bispebjerg and Frederiksberg University Hospitals, Copenhagen, Denmark
[4] Centre for Healthy Aging, Faculty of Health and Medical Sciences, Copenhagen University, Copenhagen, Denmark
[5] Department of Public Health, Copenhagen University, Copenhagen, Denmark
[6] Centre for Magnetic Resonance, DTU Elektro, Technical University of Denmark, Kongens Lyngby, Denmark

Manuscript in preparation (an extension of the 2019 ISMRM abstract)

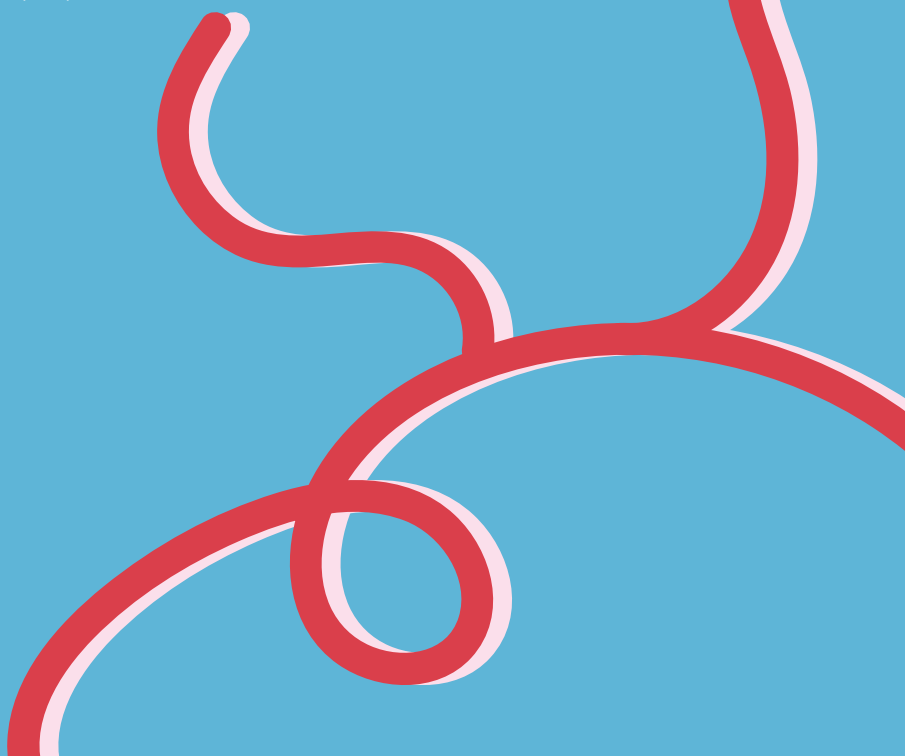

Abstract

The health-related effects of aging are highly variable across individuals with a similar chronological age, a phenomenon which is referred to as a difference in biological age due to lifestyle, environmental and genetic factors. Physical exercise has been shown to positively affect aging, for example by negating the age-related decrease in cerebral blood flow. In the present study, we investigated the relationship between vascular risk factors, physical fitness and whole-brain gray matter cerebral blood flow. The study population consisted of 300 home-dwelling volunteers between 62 and 70 years old, who were not currently participating in vigorous exercise and were clear of severe or dysregulated disease. They underwent a 3T MRI protocol that included structural and arterial spin labeling sequences to obtain gray matter cerebral blood flow. A linear regression analysis with vascular risk factors and physical fitness was used to identify determinants of cerebral blood flow. We found that preventable risk factors for neurovascular disease and physical fitness are associated with gray matter cerebral blood flow. In women, high mean arterial pressure, low bone mineral content in the leg, high gait speed and low hand grip strength were associated with lower gray matter cerebral blood flow. In men, high mean arterial pressure, high age, high HDL cholesterol and weak leg extensor power were associated with lower gray matter cerebral blood flow. Moreover, we found a lower cerebral blood flow in women than in men after correction for hematocrit in this cohort of elderly adults. Our results show the complex interaction between health and cerebral blood flow. Future analyses will include regional blood flow measures, and the effect of a 12-month exercise intervention on cerebral blood flow. This line of research provides insight into factors that explain CBF variability and into the expected effect of physical exercise interventions on CBF.

Introduction

When individuals reach the sixth decade in life, the accumulated health-related effects of environmental, socioeconomic and genetic factors, and their interactions, are highly variable.[1] In other words, people's health and associated predicted mortality differs, which can be referred to as a difference in 'biological' age.[2] Risk factors for vascular pathology, including hypertension and diabetes, are known to increase biological age.[3] Cerebral blood flow (CBF) has been proposed as a marker of cerebrovascular health, because it decreases with both age and cardiovascular risk factors.[4-6] Interestingly, cerebrovascular disease affects men and women differently. For example, the higher stroke incidence in men can be explained by sex-specific risk factors in conjunction with a higher prevalence of general risk factors such as hypertension.[7, 8]

Physical exercise may provide a mechanism to modulate the aging process. For example, life-long exercise has been proposed to negate the age-associated decrease in CBF.[9-11] A decreased cerebral blood flow has been associated with worse cognition, and predictive of future decline in individuals with cognitive impairment and dementia.[12, 13] Moreover, poor cardiovascular fitness in midlife has been associated with reduced brain volumes 20 years later.[14] Therefore, various – predominantly aerobic – exercise interventions have aimed at improving cognition and cerebral blood flow in older populations.[15-19] Physical activity also encompasses resistance or strength training aimed to increase muscular fitness. The importance of strength training is illustrated by the tight link between age-related decreases in skeletal muscle mass and muscle power and functional ability.[20, 21] This study aims at extending the previous research by examining the relationship between muscle power and CBF.

In the current study, we examine the relationship between vascular risk factors, physical fitness and CBF. A lower CBF was expected in participants with increased vascular risk factors and decreased physical fitness. We included community-dwelling adults within a narrow age range (62 – 70 years), to minimize the contribution of chronological age to the results. In addition, differences between male and female subjects were examined by means of separate analyses.

Methods

Participants

The LIve active Successful Aging (LISA) study investigates the relationship between physical fitness, cognition and mental health in volunteers around retirement age.[22] A detailed description of the study design can be found in Eriksen et al., 2016.[22] In the present study, data from 301 participants were included. Inclusion criteria required

participants to be 1) between 62 and 70 years old, 2) home dwelling and 3) functionally independent. After undergoing the measurements reported in the current sub study, participants were included in an exercise-related study. Therefore, exclusion criteria were participation in a regular exercise regime (>1 h strenuous exercise per week), presence of severe or dysregulated disease, musculoskeletal diseases impeding training ability, use of systemic glucocorticoids, androgens or antiandrogens and any contraindications for physical exercise or MRI.

Medical examination

Participants were fasting, and asked to refrain from alcohol, and caffeine from 10pm the evening before the assessments. A medical doctor obtained height, weight and blood samples as well as blood pressure in a seated position after at least 5 min rest with an automated oscillometric device. Mean arterial pressure was defined as (2*diastolic blood pressure + systolic blood pressure) / 3. Bone mineral content (BMC) in the leg, fat percentage and total lean body mass were measured with a whole body dual energy X-ray absorptiometry (DEXA)-scan (Lunar iDEXA, GE Medical Systems, Madison, Wisconsin, USA) using enCORE software, V.16 (see Eriksen et al. 2016[22] for details).

Physical tests

Physical fitness was assessed by both muscle strength and cardiorespiratory fitness. Upper limb and lower limb muscle strength were assessed with a grip strength measurement for each hand (DHD-1 Digital Hand Dynamometer, Saehan corporation, Seoul, South-Korea) and a leg extensor power test for each leg (Leg Extensor Power Rig, Queen's Medical Centre, Nottingham University, UK), respectively. Leg extensor power and hand grip measurements from the strongest limb were selected for the final analysis. Cardiorespiratory fitness was assessed with a 400 meter gait speed test, which has been established as an estimate for VO_2 peak in older adults.[23]

Image protocol and analysis

MRI was performed on a 3T system with a 32-channel head coil (Philips Medical Systems, Best, The Netherlands).

Structural MRI

The protocol included a 3D-T1w scan for structural imaging: TR/TE=6/2.7 ms, 288×288 matrix, 244 slices, isotropic voxels 0.85mm^3. Segmentation of gray matter, white matter and cerebrospinal fluid volumes was performed with the FAST[24] tool in FSL (FMBRIB, Oxford, United Kingdom).

Perfusion MRI

Arterial Spin Labeling (ASL) (EPI with SENSE factor 2.5, TR/TE=4610/13 ms, 80×80 matrix, 22 slices, 90 volumes, voxel size 3x3x6 mm3, labeling duration 1800 ms, post labeling delay=2000 ms; M0: TR/TE=9000/13 ms, 22 slices).

ASL quantification was performed with in-house software in Matlab (2014b). The T1 of blood used in the analysis was corrected individually per subject for hematocrit: $T_{1'blood}$ = 0.52 * hematocrit + 0.38.[25] The segmented gray matter map was registered to ASL space to obtain gray matter CBF using FSL's FLIRT tool for linear registration.

Statistical analyses

Female and male participants were analyzed separately to account for sex differences – as identified with independent t-tests – in physiology and performance on physical tests. First, selected vascular risk factors were tested in a bivariate Pearson correlation with gray matter CBF. Subsequently, subjects were assigned to one of three groups for each physical test based on their performance (lowest, middle and highest). Then, CBF differences between the different levels were tested using an ANOVA. Finally, variables identified at $P < 0.10$ were entered as independent variables into a multiple regression analysis with gray matter CBF as the dependent variable. Age was always included in the initial model, because of the strong evidence for its correlation with CBF.[26] Stepwise, backward elimination was performed at a *P*-level > 0.05 to yield the final model. A *P*-value ≤ 0.05 was considered significant.

Results

Three cases were excluded due to a mean gray matter CBF below 20 ml/100g/min. As such, the final analysis included 298 participants (Table 1). There was no difference in mean gray matter CBF between male (45±5.3 ml/100g/min) and female participants (45±6.4 ml/100g/min) before correction for hematocrit ($P = 0.708$). After hematocrit correction, gray matter CBF was lower in female subjects (43±6.0 ml/100g/min) than in male subjects (46±5.2; $P < 0.001$).

Female subjects

The following variables were selected for regression analysis from the bivariate correlations, because of a $P < 0.10$: waist circumference ($P = 0.063$), total muscle mass ($P = 0.001$), blood iron ($P = 0.071$), mean arterial pressure ($P = 0.036$), blood creatinine ($P = 0.0493$), leg BMC ($P = 0.001$), gait speed ($P = 0.041$), and hand grip strength ($P = 0.003$). After backward elimination, the final model included mean arterial pressure, leg BMC, gait speed and hand grip strength (Table 2). Here, mean arterial pressure and gait speed

were negatively associated with CBF, while leg BMC and hand grip were positively associated with CBF.

Table 1. Baseline characteristics.

	All (n = 298)	Female (n=173)	Male (n=125)	*P*-value
Age (years)	67±2.5	66±2.5	67±2.6	0.480
Hematocrit	0.42±0.04	0.41±0.03	0.44±0.03	<0.001*
BMI	26±4.0	25±4.3	26±3.5	0.053
Waist (cm)	92±11.9	88±11.2	98±10.0	<0.001*
Fat mass (%)	33±8.0	36±7.7	28±5.8	<0.001*
Muscle mass (kg)	48±9.1	41±4.3	57±5.4	<0.001*
BMC leg (g)	976±243	801±106	1218±154	<0.001*
MAP (mmHg)	105±11.7	103±12.9	107±9.7	0.014*
Iron (μmol/l)	19±5.2	18±4.6	20±5.6	<0.001*
Total cholesterol (mmol/l)	5.8±1.0	5.9±1.0	5.6±1.1	0.023*
LDL (mmol/l)	3.3±1.0	3.3±1.0	3.4±0.9	0.415
HDL (mmol/l)	2.0±0.5	2.1±0.5	1.7±0.5	<0.001*
eGFR (ml/min)	77±11.8	76±12.1	78±11.3	0.207
Creatinine (μmol/l)	77.2±15.8	69.7±11.0	87.6±15.4	<0.001*
Glucose mean (from HbA1c) (mmol/l)	6.2±0.7	6.2±0.7	6.3±0.7	0.157
400m gait (s)	238±30	247±27	225±30	<0.001*
Leg extensor power (Watt/kg)	2.7±0.7	2.4±0.5	3.1±0.7	<0.001*
Hand grip strength (kg)	36±11.1	28±4.9	47±7.4	<0.001*

BMI = body mass index; BMC = bone mineral content; MAP = mean arterial pressure; LDL = low-density lipoprotein; HDL = high-density lipoprotein; eGFR = estimated glomerular filtration rate; HbA1c = Hemoglobin A1c.

Table 2. Gray matter CBF and vascular risk factors in female subjects

	β	B (95% CI)	*P*
Mean arterial pressure	-0.17	-0.08 (-0.15 – -0.01)	0.020
BMC leg	0.19	0.01 (0.00 – 0.02)	0.011
Gait speed (ref slow)			
middle	-0.19	-2.46 (-4.57 – -0.35)	0.022
fast	-0.18	-2.28 (-4.4 – -0.15)	0.036
Hand grip strength (ref weak)			
middle	0.23	2.96 (0.86 – 5.1)	0.006
strong	0.20	2.56 (0.34 – 4.8)	0.024

Dependent variable = mean gray matter perfusion. R^2 = 17%; F = 5.4. *P* < 0.001.

Male subjects

The following variables were selected from the bivariate correlations, because of a $P < 0.10$: age ($P = 0.011$), mean arterial pressure ($P = 0.059$), total cholesterol ($P = 0.063$), high-density lipoprotein (HDL) cholesterol ($P = 0.041$), and leg extensor power ($P = 0.016$). After backward elimination, the final model included age, mean arterial pressure, HDL cholesterol, and leg extensor power (Table 3). Gray matter CBF was negatively associated with age, mean arterial pressure, and HDL cholesterol, whereas a positively relationship was found between CBF and leg extensor power.

Table 3. Gray matter CBF and vascular risk factors in male subjects

	β	B (95% CI)	*P*
Age	-0.19	-0.38 (-0.73 – -0.03)	0.034
Mean arterial pressure	-0.20	-0.11 (-0.20 – -0.02)	0.022
HDL cholesterol	-0.21	-2.31 (-4.21 – -0.42)	0.017
Leg extensor power (ref weak)			
middle	0.23	2.56 (0.41 – 4.70)	0.020
strong	0.21	2.31 (0.13 – 4.49)	0.038

Dependent variable = mean gray matter perfusion. R2 = 16%; F = 4.6. P < 0.001.

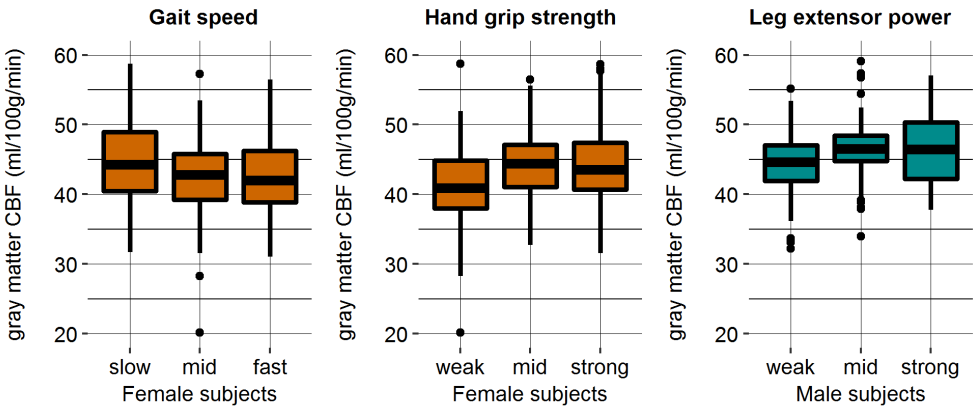

Fig. 1. Performance on physical fitness measures and gray matter CBF. Cerebral blood flow associated with gait speed and hand grip strength in female subjects (performance on x-axis). In male subjects, gray matter CBF was associated with leg extensor power. Mid = middle.

Discussion

We examined the relationship between vascular risk factors, physical fitness and CBF in home-dwelling, elderly participants. Preventable risk factors for vascular disease and physical fitness were found associated with cerebral blood flow. The majority of baseline characteristics varied between male and female subjects despite their similar age. After correction for different hematocrit levels, CBF was lower in female than in male subjects. Previous studies have found inconsistent results on the effect of blood pressure on CBF.[26] For both women and men, we found higher mean arterial pressure to be associated with lower gray matter CBF. In women, higher bone mineral content in the leg was associated with higher gray matter CBF. In men, on the other hand, higher HDL cholesterol was associated with lower gray matter CBF, which is in opposition with an earlier report.[5] The relationship between physical fitness measurements and CBF was discordant between the two sexes. A stronger hand grip and lower gait speed were associated with higher gray matter CBF in female volunteers, while greater leg extensor power was associated with gray matter perfusion in males (Figure 1).

Typically, a fixed T_1 of arterial blood is used for perfusion quantification. The recommended value of 1650 ms (3T MRI) from the ASL white paper corresponds with an average human hematocrit value of 0.42.[27, 28] Although this was true for our overall study sample, a significant difference in hematocrit was found between men and women. Whereas no CBF difference was observed before correction, it was significantly lower in women compared to men after the ASL quantification was corrected for hematocrit. The effect on hematocrit on CBF is in agreement with a recent study, in which the fixed hematocrit value from the white paper lead to particularly erroneous CBF for female and non-European subjects.[29] Contradictory findings are reported on the interaction between sex and cerebral blood flow, perhaps because hematocrit was not always accounted for in CBF quantification.[6, 26, 30] The results of this study emphasize that sex-related perfusion differences on ASL MRI cannot be understood without taking hematocrit into consideration, also in elderly men and (post-menopausal) women. Moreover, more subtle perfusion modifiers may be missed in cross-sectional studies without T_1 correction due to the substantial effect of hematocrit. Albeit weaker than hematocrit, HDL cholesterol has been positively associated with blood T_1 which would correspond to a negative association with quantified CBF from ASL MRI.[31] Indeed, in our male subjects we found an inverse relation between HDL cholesterol and CBF. This was an unexpected finding, as HDL cholesterol is protective for cardio- and cerebrovascular health.[32, 33] It is plausible that the T_1 effect could account for this negative association.

Typically, it is assumed that a higher CBF is indicative of better (cerebrovascular) health. Indeed, physical exercise has been shown to maintain CBF with aging. Contradicting evidence has also been found, where lower fitness levels are associated with a higher CBF.[34, 35] Also, mixed results have been reported on the effect of an physical

exercise intervention on CBF.[18, 36-38] In one study, hyperperfusion was observed in patients with mild cognitive impairment compared to control subjects.[39] Further, hyperperfusion was observed in the subjects with the lowest Mini Mental State Examination scores, which was hypothesized to signify compensatory mechanisms.[39] An intervention study found regional hyperperfusion in MCI patients compared to control subjects, which disappeared after a 12 week aerobic exercise regime.[40] CBF was reduced in former smokers compared to non-smokers, but no difference in CBF was found between current smokers and non-smokers.[41] Overall, increased CBF seems to signal good cerebrovascular health but can also function as a compensatory mechanism in poor cerebrovascular health states. [39, 41]

Our results are in contrast with research that found an positive association between estimated cardiorespiratory fitness and gray matter CBF in a mixed cohort of elderly men and women.[42] One could speculate that the observed inverse relationship between cardiorespiratory fitness and CBF in women may be driven by metabolic efficiency. The high energetic demand of neurons is met by oxidative phosphorylation in mitochondria. Mitochondrial functioning has been shown to decrease with aging, and is associated with neurodegeneration.[43] Individual differences exist regarding the energy (ATP) produced by the same amount of fuel – oxygen.[44] At the metabolic level, it has been suggested that increased fitness is linked to more efficient aerobic metabolism.[45, 46] It has been shown that physical exercise has a strong effect on mitochondrial function and the neurotrophin BDNF (brain derived neurotrophic factor), which also influences mitochondrial function.[45] Further, mitochondrial physiological processes have been proposed as a pathway by which physical exercise can modulate Alzheimer's disease.[47] These data point to physical exercise as a potential therapeutic strategy for this disease.[47] We speculate that a lower CBF in combination with high cardiorespiratory fitness could also be indicative of better brain health although it is unclear why this finding was only present in women and not in men. Even though we do not have direct data on oxygen consumption available, the longitudinal aspect of this study will allow us to shed some light on whether this group of subjects, that is low CBF but high fitness levels, perform better over the years. A limitation of the study is that gait speed was used as a proxy for VO_2 peak, so we do not have a clean measure of cardiorespiratory fitness. Also, the range in cardiorespiratory fitness is relatively narrow, because individuals who participated in regular physical exercise were excluded from study participation.

In summary, we observed an association between whole-brain gray matter CBF, preventable vascular risk factors and physical fitness, which differed between male and female subjects. Our results reiterate the relevance of hematocrit and $T_{1,blood}$ measurements, because correction for hematocrit significantly altered obtained gray matter CBF. Following the baseline measurements described here, the participants were randomized to (1) heavy or (2) moderate intensity resistance training or (3) habitual phys-

ical activity level (control group). Future analyses will focus on the effect of exercise intervention, in particular for the subjects with the lowest fitness scores and highest vascular risk factors at baseline. Nevertheless, these results provide insight into factors that explain individual CBF variability in older adults.

References

1. Mitnitski A, Howlett SE, Rockwood K. Heterogeneity of human aging and its assessment. *The Journals of Gerontology: Series A*. 2017;72:877-884
2. Chen BH, Marioni RE, Colicino E, Peters MJ, Ward-Caviness CK, Tsai P-C, et al. DNA methylation-based measures of biological age: Meta-analysis predicting time to death. *Aging (Albany NY)*. 2016;8:1844-1859
3. Pyrkov TV, Slipensky K, Barg M, Kondrashin A, Zhurov B, Zenin A, et al. Extracting biological age from biomedical data via deep learning: Too much of a good thing? *Scientific Reports*. 2018;8:5210
4. Chen JJ, Rosas HD, Salat DH. Age-associated reductions in cerebral blood flow are independent from regional atrophy. *NeuroImage*. 2011;55:468-478
5. Jennings JR, Heim Alicia F, Kuan Dora C-H, Gianaros Peter J, Muldoon Matthew F, Manuck Stephen B. Use of total cerebral blood flow as an imaging biomarker of known cardiovascular risks. *Stroke*. 2013;44:2480-2485
6. Parkes LM, Rashid W, Chard DT, Tofts PS. Normal cerebral perfusion measurements using arterial spin labeling: Reproducibility, stability, and age and gender effects. *Magnetic Resonance in Medicine*. 2004;51:736-743
7. Appelros P, Stegmayr B, Terént A. Sex differences in stroke epidemiology. *Stroke*. 2009;40:1082-1090
8. Poorthuis MHF, Algra AM, Algra A, Kappelle LJ, Klijn CJM. Female- and male-specific risk factors for stroke: A systematic review and meta-analysisassociations between sex-specific risk factors and strokeassociations between sex-specific risk factors and stroke. *JAMA Neurology*. 2017;74:75-81
9. Ainslie PN, Cotter JD, George KP, Lucas S, Murrell C, Shave R, et al. Elevation in cerebral blood flow velocity with aerobic fitness throughout healthy human ageing. *The Journal of Physiology*. 2008;586:4005-4010
10. Bailey Damian M, Marley Christopher J, Brugniaux Julien V, Hodson D, New Karl J, Ogoh S, et al. Elevated aerobic fitness sustained throughout the adult lifespan is associated with improved cerebral hemodynamics. *Stroke*. 2013;44:3235-3238
11. Boraxbekk C-J, Salami A, Wåhlin A, Nyberg L. Physical activity over a decade modifies age-related decline in perfusion, gray matter volume, and functional connectivity of the posterior default-mode network—a multimodal approach. *NeuroImage*. 2016;131:133-141
12. Binnewijzend MAA, Kuijer JPA, Benedictus MR, van der Flier WM, Wink AM, Wattjes MP, et al. Cerebral blood flow measured with 3d pseudocontinuous arterial spin-labeling mr imaging in alzheimer disease and mild cognitive impairment: A marker for disease severity. *Radiology*. 2013;267:221-230
13. Chao LL, Buckley ST, Kornak J, Schuff N, Madison C, Yaffe K, et al. Asl perfusion mri predicts cognitive decline and conversion from mci to dementia. *Alzheimer disease and associated disorders*. 2010;24:19
14. Spartano NL, Himali JJ, Beiser AS, Lewis GD, DeCarli C, Vasan RS, et al. Midlife exercise blood pressure, heart rate, and fitness relate to brain volume 2 decades later. *Neurology*. 2016;86:1313-1319
15. Akazawa N, Choi Y, Miyaki A, Sugawara J, Ajisaka R, Maeda S. Aerobic exercise training increases cerebral blood flow in postmenopausal women. *Artery Research*. 2012;6:124-129
16. Lautenschlager NT, Cox KL, Flicker L, Foster JK, van Bockxmeer FM, Xiao J, et al. Effect of physical activity on cognitive function in older adults at risk for alzheimer disease: A randomized trial. *JAMA*. 2008;300:1027-1037
17. Groot C, Hooghiemstra AM, Raijmakers PGHM, van Berckel BNM, Scheltens P, Scherder EJA, et al. The effect of physical activity on cognitive function in patients with dementia: A meta-analysis of randomized control trials. *Ageing Research Reviews*. 2016;25:13-23
18. Flodin P, Jonasson LS, Riklund K, Nyberg L, Boraxbekk CJ. Does aerobic exercise influence intrinsic brain activity? An aerobic exercise intervention among healthy old adults. *Frontiers in Aging Neuroscience*. 2017;9
19. Jonasson LS, Nyberg L, Kramer AF, Lundquist A, Riklund K, Boraxbekk C-J. Aerobic exercise intervention, cognitive performance, and brain structure: Results from the physical influences on brain in aging (phibra) study. *Frontiers in aging neuroscience*. 2017;8:336

20. Reid KF, Fielding RA. Skeletal muscle power: A critical determinant of physical functioning in older adults. *Exerc Sport Sci Rev*. 2012;40:4-12
21. Fielding RA, Vellas B, Evans WJ, Bhasin S, Morley JE, Newman AB, et al. Sarcopenia: An undiagnosed condition in older adults. Current consensus definition: Prevalence, etiology, and consequences. International working group on sarcopenia. *Journal of the American Medical Directors Association*. 2011;12:249-256
22. Eriksen CS, Garde E, Reislev NL, Wimmelmann CL, Bieler T, Ziegler AK, et al. Physical activity as intervention for age-related loss of muscle mass and function: Protocol for a randomised controlled trial (the lisa study). *BMJ Open*. 2016;6
23. Simonsick EM, Fan E, Fleg JL. Estimating cardiorespiratory fitness in well-functioning older adults: Treadmill validation of the long distance corridor walk. *Journal of the American Geriatrics Society*. 2006;54:127-132
24. Zhang Y, Brady M, Smith S. Segmentation of brain mr images through a hidden markov random field model and the expectation-maximization algorithm. *IEEE transactions on medical imaging*. 2001;20:45-57
25. Lu H, Clingman C, Golay X, van Zijl PCM. Determining the longitudinal relaxation time (t1) of blood at 3.0 tesla. *Magnetic Resonance in Medicine*. 2004;52:679-682
26. Clement P, Mutsaerts H-J, Václavů L, Ghariq E, Pizzini FB, Smits M, et al. Variability of physiological brain perfusion in healthy subjects – a systematic review of modifiers. Considerations for multi-center asl studies. *Journal of Cerebral Blood Flow & Metabolism*. 2017;38:1418-1437
27. Lu H, Clingman C, Golay X, Van Zijl PC. Determining the longitudinal relaxation time (t1) of blood at 3.0 tesla. *Magnetic Resonance in Medicine: An Official Journal of the International Society for Magnetic Resonance in Medicine*. 2004;52:679-682
28. Alsop DC, Detre JA, Golay X, Günther M, Hendrikse J, Hernandez-Garcia L, et al. Recommended implementation of arterial spin-labeled perfusion mri for clinical applications: A consensus of the ismrm perfusion study group and the european consortium for asl in dementia. *Magnetic Resonance in Medicine*. 2015;73:102-116
29. Smith LA, Melbourne A, Owen D, Cardoso MJ, Sudre CH, Tillin T, et al. Cortical cerebral blood flow in ageing: Effects of haematocrit, sex, ethnicity and diabetes. *European Radiology*. 2019
30. Liu W, Lou X, Ma L. Use of 3d pseudo-continuous arterial spin labeling to characterize sex and age differences in cerebral blood flow. *Neuroradiology*. 2016;58:943-948
31. Rosmini S, Bulluck H, Treibel TA, Bhuva AN, Abdel-Gadir A, Culotta V, et al. Hematocrit, iron and hdl-cholesterol explain 90% of variation in native blood t1. *Journal of Cardiovascular Magnetic Resonance*. 2016;18:O86
32. Assmann G, Gotto Antonio M. Hdl cholesterol and protective factors in atherosclerosis. *Circulation*. 2004;109:III-8-III-14
33. Amarenco P, Goldstein LB, Callahan A, Sillesen H, Hennerici MG, O'Neill BJ, et al. Baseline blood pressure, low- and high-density lipoproteins, and triglycerides and the risk of vascular events in the stroke prevention by aggressive reduction in cholesterol levels (sparcl) trial. *Atherosclerosis*. 2009;204:515-520
34. Intzandt B, Sabra D, Foster C, Desjardins-Crépeau L, Hoge R, Steele CJ, et al. Enhanced fitness relates to reduced cerebrovascular reactivity and perfusion in a sample of very healthy older adults. *bioRxiv*. 2018:444208
35. Thomas BP, Yezhuvath US, Tseng BY, Liu P, Levine BD, Zhang R, et al. Life-long aerobic exercise preserved baseline cerebral blood flow but reduced vascular reactivity to co2. *Journal of Magnetic Resonance Imaging*. 2013;38:1177-1183
36. Chapman SB, Aslan S, Spence JS, DeFina LF, Keebler MW, Didehbani N, et al. Shorter term aerobic exercise improves brain, cognition, and cardiovascular fitness in aging. *Frontiers in aging neuroscience*. 2013;5:75
37. Murrell CJ, Cotter JD, Thomas KN, Lucas SJE, Williams MJA, Ainslie PN. Cerebral blood flow and cerebrovascular reactivity at rest and during sub-maximal exercise: Effect of age and 12-week exercise

training. *AGE*. 2013;35:905-920
38. Chapman SB, Aslan S, Spence JS, Keebler MW, DeFina LF, Didehbani N, et al. Distinct brain and behavioral benefits from cognitive vs. Physical training: A randomized trial in aging adults. *Frontiers in Human Neuroscience*. 2016;10
39. Luckhaus C, Flüß MO, Wittsack H-J, Grass-Kapanke B, Jänner M, Khalili-Amiri R, et al. Detection of changed regional cerebral blood flow in mild cognitive impairment and early alzheimer's dementia by perfusion-weighted magnetic resonance imaging. *NeuroImage*. 2008;40:495-503
40. Alfini AJ, Weiss LR, Nielson KA, Verber MD, Smith JC. Resting cerebral blood flow after exercise training in mild cognitive impairment. *Journal of Alzheimer's Disease*. 2019:1-14
41. Elbejjani M, Auer R, Dolui S, Jacobs DR, Haight T, Goff DC, et al. Cigarette smoking and cerebral blood flow in a cohort of middle-aged adults. *Journal of Cerebral Blood Flow & Metabolism*. 2018:0271678X18754973
42. Zimmerman B, Sutton B, Low K, Fletcher M, Tan CH, Schneider-Garces N, et al. Cardiorespiratory fitness mediates the effects of aging on cerebral blood flow. *Frontiers in Aging Neuroscience*. 2014;6
43. Grimm A, Eckert A. Brain aging and neurodegeneration: From a mitochondrial point of view. *J Neurochem*. 2017;143:418-431
44. Salin K, Auer Sonya K, Rey B, Selman C, Metcalfe Neil B. Variation in the link between oxygen consumption and atp production, and its relevance for animal performance. *Proceedings of the Royal Society B: Biological Sciences*. 2015;282:20151028
45. Marques-Aleixo I, Oliveira PJ, Moreira PI, Magalhães J, Ascensão A. Physical exercise as a possible strategy for brain protection: Evidence from mitochondrial-mediated mechanisms. *Progress in Neurobiology*. 2012;99:149-162
46. Itoh K, Nakamura K, Iijima M, Sesaki H. Mitochondrial dynamics in neurodegeneration. *Trends Cell Biol*. 2013;23:64-71
47. Bernardo TC, Marques-Aleixo I, Beleza J, Oliveira PJ, Ascensão A, Magalhães J. Physical exercise and brain mitochondrial fitness: The possible role against alzheimer's disease. *Brain Pathology*. 2016;26:648-663

Chapter 8

Transverse relaxation time of CSF in the peripheral subarachnoid space reflects cognition in a memory clinic cohort

L.A. van der Kleij[1], E.T. Petersen[2,3], J.H. Verwer[4], J. Hendrikse[1], G.J. Biessels[4], J.B. De Vis[5]

[1] Department of Radiology, University Medical Center Utrecht, Utrecht University, Netherlands
[2] Danish Research Centre for Magnetic Resonance, Centre for Functional and Diagnostic Imaging and Research, Copenhagen University Hospital Hvidovre, Denmark
[3] Centre for Magnetic Resonance, DTU Elektro, Technical University of Denmark, Kongens Lyngby, Denmark
[4] Department of Neurology and Neurosurgery, Brain Center Rudolf Magnus, University Medical Center Utrecht, Utrecht University, Netherlands.
[5] Acute Cerebrovascular Diagnostics Unit, National Institute of Neurological Disorders and Stroke, National Institutes of Health, Bethesda, Maryland, USA

Manuscript in preparation

Abstract

Introduction: Dementia research has shifted focus towards the early stages of cognitive decline, which has increased the demand for imaging markers that can predict conversion to dementia. We evaluated the added value of the T2 of peripheral cerebrospinal fluid ($T2_{pCSF}$) over established imaging markers of global atrophy and cerebral blood flow for disease severity in cognitive impairment.

Methods: Twenty-seven patients with varying levels of cognitive impairment were included after referral to a memory clinic. All patients underwent a 3T MRI protocol, which consisted of structural imaging for brain volume segmentation, pCASL for cerebral blood flow measurement and a CSF sequence to obtain $T2_{pCSF.}$ Multiple linear regression with cognition as the dependent variable was performed to evaluate the contribution of $T2_{pCSF}$ over global atrophy and cerebral blood flow to the proportion of explained variance.

Results: Verbal memory showed a strong association with $T2_{pCSF}$, where addition of the MRI contributed to 16% of the explained variance in a model with global atrophy and cerebral blood flow. The final verbal memory models for immediate (R^2 0.57) and delayed recall (R^2 0.62) included $T2_{pCSF}$ (ß -0.56, *P*=0.008; ß -0.55, *P*=0.010), global atrophy (ß -0.41, *P* = 0.033; ß -0.41, *P*=0.033) and cerebral blood flow (ß -0.51, *P*=0.005; ß -0.19, *P*=0.246). In contrast, global atrophy was the strongest determinant in the final models for verbal fluency (R^2 0.53) and mini-mental state examination score (R^2 0.62) at baseline.

Conclusion: $T2_{pCSF}$, global atrophy and gray matter cerebral blood flow explained over 50% of variance in cognitive performance at baseline. The $T2_{pCSF}$ marker showed a strong relationship with verbal memory in the regression model that also included global atrophy and CBF. Future studies in larger cohorts should elicit whether it is also predictive of disease progression.

Introduction

Dementia is a widespread disease that affects 6% of people above the age of 60.[1] Despite many clinical trials in patients with mild cognitive impairment (MCI) and dementia, no disease modifying treatment has been found. In response, the focus of dementia research has shifted towards a younger population and the earlier stages of cognitive decline.[2] This means, however, that a more heterogeneous group is studied as only a subset of patients with cognitive complaints and MCI will convert to dementia.[3] Therefore, it is important to establish biomarkers that can reliably differentiate between different subsets of patients and reflect the earliest stages of pathology and disease processes.

Imaging parameters may provide early markers as well as reveal the pathogenetic mechanisms underlying dementia before clinical manifestation.[4] Accordingly, they can aid in categorizing the heterogeneous group of individuals with cognitive impairment, and can help us in making informed decisions on when and in which patients to test a particular treatment.[2] Imaging markers can be roughly classified as either structural or functional. Conventionally used structural makers are qualitative atrophy rating scales and quantitative measures of (regional) atrophy.[5, 6] The degree of atrophy is known to be associated with disease severity, and it can predict conversion from MCI to Alzheimer's disease (AD).[7] A well-studied functional imaging marker is cerebral blood flow (CBF), which is decreased throughout all disease stages, including the early, mild cognitive impairment stage of disease.[8-10] CBF has been associated with global cognitive function, and it was found predictive of cognitive decline in healthy, elderly individuals.[11, 12] Ongoing research is aimed at establishing which imaging markers best reflect clinical symptoms and which imaging markers are predictive of cognitive decline.

Aside the more common, structural and functional biomarkers, recent work has aimed to identify novel biomarkers.[13-17] One such marker is the transverse relaxation rate of CSF ($T2_{CSF}$). The $T2_{CSF}$ was found to be higher in dementia patients compared to healthy, elderly controls.[18] However, the explanation behind this difference is not clearly understood. As T2 values are known to be dependent on the degree of oxygenation,[19] one could hypothesize that the peripheral $T2_{CSF}$ ($T2_{pCSF}$) reflects oxygen diffusion due to its proximity to the major cerebral arteries.[20] As such, it could provide information on cerebrovascular health. This hypothesis finds further support in recent observations that cerebrovascular dysfunction and cerebrovascular disease do not only often co-occur with dementia, but are involved in the pathogenesis of dementia.[21, 22]

The purpose of this study was to investigate the added value of $T2_{pCSF}$ over atrophy and CBF measurements for disease severity. For this, we considered memory clinic

patients with subjective cognitive complaints, mild cognitive impairment and dementia. We first evaluated the relationship between CBF and $T2_{pCSF}$ in the peripheral subarachnoid space to gain insight into the association behind increased T2 values in dementia patients. Subsequently, we investigated the relationship between atrophy, CBF, and cognitive functioning with or without $T2_{pCSF}$ to establish the added value of $T2_{pCSF}$ in estimating disease severity.

Methods

Population

Thirty-five subjects were recruited at the Neurology department of the University Medical Center Utrecht as a substudy of the prospective, multi-center cohort study *The Pearl Neurodegenerative Diseases*.[23] The study was approved by the Medical Ethical Committee of the University Medical Center Utrecht. Included patients were referred to a memory clinic for the evaluation of cognitive problems. Exclusion criteria were normal pressure hydrocephalus, morbus huntington, recent transient ischemic attack (TIA) or cerebrovascular accident (CVA) (<2 years), TIA/CVA followed by cognitive decline (within three months), history of schizophrenia, bipolar disorder or psychotic symptoms not otherwise specified or previous treatment for these diseases, current major depressive disorder (DSM V), cognitive problems due to alcohol abuse, brain tumor, epilepsy, encephalitis, mental incompetence for deciding participation, or absence of a reliable informant.

Cognitive and functional assessment

The clinical dementia rating (CDR) scale was administered to stage the severity of cognitive and functional impairment.[24] The scale ranges from 0 (no impairment) to 0.5, 1, 2, and 3 (severe dementia). General cognitive function was assessed with the mini-mental state evaluation (MMSE).[25] The MMSE score ranges between 0 and 30, where lower scores indicate worse cognition. Verbal fluency was assessed with the 60 second animal naming task. The score was the total of correct animals named within 60 seconds.[26] Verbal memory was assessed with an immediate and delayed recall of 15 Word-Auditory Verbal Learning Test.[27] The immediate recall test consisted of five trials, and the delayed recall test of one trial. The total number of correct answers was recorded. Verbal memory and semantic fluency were investigated, because a recent meta-analysis identified them as good predictors of future decline in MCI.[28]

Imaging protocol

MR imaging was performed on a 3T system (Philips Medical Systems, Best, the Netherlands). The protocol consisted of structural 3DT1-weighted (3DT1w) imaging (FOV = 232x256x192, voxels = 1x1x1mm^3, TR/TE = 8187/4.5ms), a T2-FLAIR sequence (TR/TI/TE = 11000/2800/125ms, voxels = 1x1x3mm^3), a pseudocontinuous Arterial Spin Labeling (pCASL) EPI sequence to obtain CBF (voxels=3x3x7mm^3, FOV=240x119x240mm^3, TR/TE4000/14ms, post label delay=1525-2160ms), and a CSF MRI sequence to obtain $T2_{pCSF}$ (FOV=240x240x161mm^3, voxels=3x3x7mm^3 0:57min).

Image analysis

Structural

Tissue volumes and gray matter maps were obtained by segmentation of the T2-FLAIR and 3DT1w images. First, the lesion prediction algorithm (L.S.T., v 2.0.15) was used as a tool in SPM12 (Wellcome Department of Cognitive Neurology, Institute of Neurology, London) to segment hyperintense lesions on the T2-FLAIR images.[29, 30] Then, corresponding hypointensities on the 3DT1w images were corrected. The corrected 3DT1w images were provided as input to the CAT12 toolbox for SPM (http://www.neuro.uni-jena.de/cat/) for tissue volume segmentation.[31] Global atrophy was defined as the relative CSF volume compared to the intracranial volume (the sum of CSF, gray and white matter). The resulting gray matter probability maps were coregistered in SPM12 to the pCASL images for gray matter perfusion analyses.

Functional: perfusion-weighted image analysis

The pCASL data was processed using IDL 6.1 for Windows (ITT Visual Information Solutions, Boulder, C.O., U.S.A.). After subtraction of the label-control pairs, outliers were discarded and the averaged label-control pairs were quantified.[32, 33] Partial volume correction was performed by applying the segmented gray matter map at a 50% threshold to the perfusion maps in native space. To evaluate CBF in dementia-related brain structures, CBF in the precuneus and the posterior cingulate were obtained by normalization of the perfusion maps to Montreal Neurological Institute (MNI) space.[34-36]

The quality of the pCASL images was assessed qualitatively (L.A.v.d.K. and J.B.D.V.) and images of poor quality were excluded from further analysis.

Functional: T_2 of peripheral CSF analysis

The CSF MRI data was processed using IDL 6.1 for Windows (ITT Visual Information Solutions, Boulder, C.O., U.S.A.). The CSF MRI sequence is a one-minute scan that is based on the distinctively long T_2 of CSF compared to other tissues. The sequence

includes a T_2 preparation scheme with refocusing pulse trains of varying length (0, 4, 8 or 16) in a Malcolm Levitt's CPD (MLEV) scheme to generate varying effective echo times (TEs) (0, 280, 560 and 1120 ms, respectively).[37, 38, 39] Image processing was as follows: first, the T_2 in each voxel was estimated by fitting the signal decay curves.[18] Second, CSF partial volume of each voxel was obtained by generating the M_0 of each voxel based on an extrapolation of the data to the intersect at eTE = 0ms. For this, only the last three eTEs were used to exclude signal from the brain parenchyma, and the resulting M_0 map was smoothed with a 7mm Gaussian filter. The partial volume was obtained by comparing the M_0 in each voxel to M_0 reference voxels (for a more detailed description see *van der Kleij et al., 2018*).[38]

To obtain the T_2 of peripheral CSF voxels, we excluded the ventricles and applied a partial volume threshold. The partial volume threshold was decided based on an evaluation of the effect of different thresholds (15%, 50% and 75%) on obtained peripheral CSF volume, the obtained $T2_{pCSF}$ value, and the association between $T2_{pCSF}$ and global atrophy. As shown in the last paragraph of the results section, we established a 50% threshold as the optimal between balance partial volume errors and errors introduced by outlier voxels.

Statistical analysis

Statistical analyses were carried out in R (v. 3.5.3).[40] Differences between disease stages (i.e., subjective complaints, MCI and dementia) regarding $T2_{pCSF}$, global atrophy or CBF were tested using an ANOVA with a post-hoc Tukey test. Bivariate regression was used to test the relationship between CBF and either age, global atrophy or $T2_{pCSF}$. Next, multiple linear regression analysis with backward selection ($P < 0.50$) was performed to investigate variables associated with cognitive functioning.[41] To examine the added value of $T2_{pCSF}$ in estimating symptom severity, the initial models with cognition as the dependent variable either in- or excluded $T2_{pCSF}$ as an independent variable along global atrophy and gray matter CBF. A *P*-value <0.05 was considered significant.

Results

Eight out of thirty-five patients were excluded due to motion-corrupted pCASL image data. Excluded patients were 76±7 years old, 43% were female, one patient was diagnosed with subjective cognitive complaints, four with MCI, and three with dementia. Twenty-seven participants were included in the final analysis (mean age 75±7.0 years, 41% female). Five subjects were diagnosed with subjective cognitive complaints (median age 70 (IQR 66 – 75) years, 0% female, median CDR 0.5 (IQR 0.5 – 0.5)), fifteen with MCI (median age 75 (IQR 70 – 78) years, 47% female, median CDR 0.5

(IQR 0.5 – 0.5)), and seven with dementia (median age 80 (IQR 75 – 85) years, 57% female, median CDR 1.0 (IQR 1.0 – 1.0)). Within the dementia group, five were diagnosed with probable Alzheimer's disease (including one patient with posterior cortical atrophy), two with mixed Alzheimer's and vascular dementia.

Differences per disease stage

The mean $T2_{pCSF}$ was 1.67±0.13s, and it differed between subjects with subjective cognitive complaints (1.51±0.13s) and patients with either dementia (1.74±0.10s; P = 0.003) or MCI (1.69±0.10s; P = 0.007), but not between the MCI and dementia groups (P = 0.551; Figure 1). The mean degree of global atrophy was 31.1±3.7%, and it differed between subjects with dementia (35.4±1.8%) and patients with either subjective cognitive complaints (28.0±2.7%; P < 0.001) or MCI (30.4±3.0%; P = 0.001), but not between the MCI and subjective cognitive complaints groups (P = 0.224; Figure 1). Gray matter CBF (mean 48±14 ml/100g/min) was not different between disease stages (P = 0.942, P = 0.978, P = 0.990; Figure 1). Similarly, CBF in the posterior cingulate cortex (46±15 ml/100g/min) and precuneus (42±12 ml/100g/min) did not differ according to disease stage (all P > 0.116).

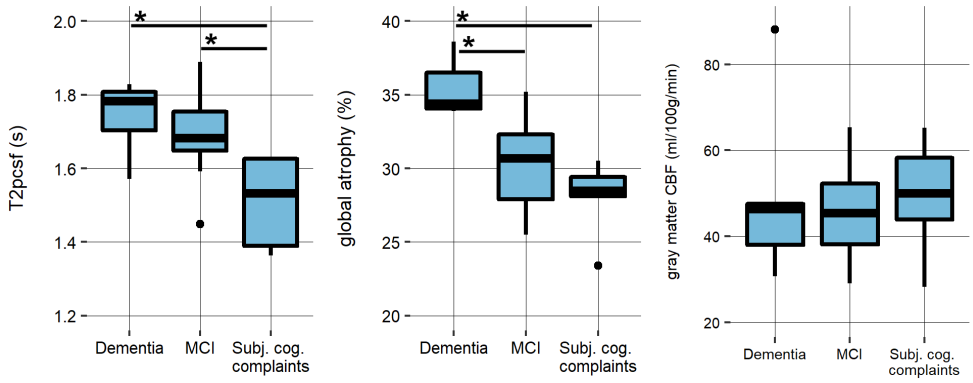

Fig. 1. The T2 of peripheral CSF, atrophy and gray matter perfusion per disease stage. MCI = mild cognitive impairment; subj. cog. complaints = subjective cognitive complaints; CBF = cerebral blood flow;* = P < 0.05.

The relationship between T2, age and atrophy and perfusion

In bivariate associations, partial volume corrected cortical gray matter CBF was associated with both $T2_{pCSF}$ (R^2 = 0.27, P = 0.006) and global atrophy (R^2 = 0.15, P = 0.044), but not with age (P = 0.779; Figure 2). Precuneus CBF was also associated with $T2_{pCSF}$ (R^2 = 0.33, P = 0.002) and global atrophy (R^2 = 0.24, P = 0.010), but not with age (P = 0.534; Figure 2). Lastly, CBF in the posterior cingulate was associated with $T2_{pCSF}$ (R^2

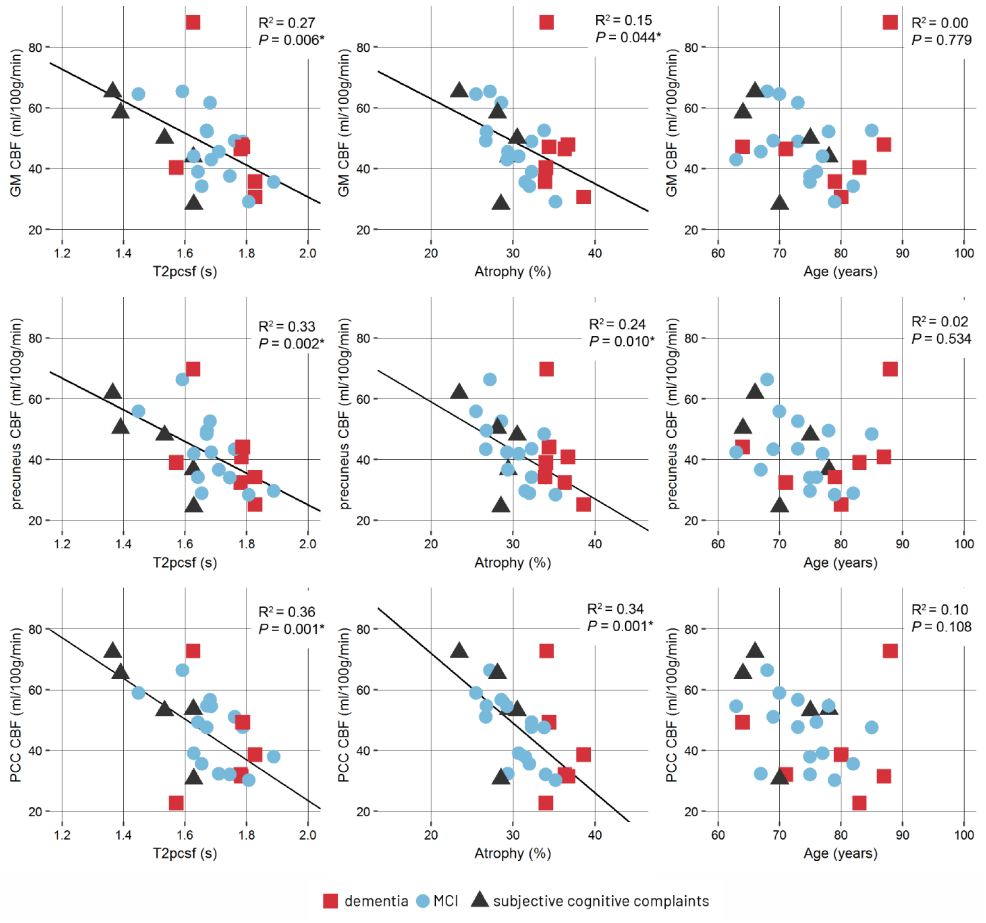

Fig. 2. The relationship between gray matter (GM) CBF (top row), precuneus CBF (middle row), posterior cingulate (PCC) CBF (bottom row) and $T2_{pCSF}$ (left column), global atrophy (middle column), and age (right column).

The relationship between $T2_{pCSF}$, perfusion and atrophy and cognition at baseline

Median total immediate recall was 23 IQR 20 – 31 (maximum score 75), median delayed recall was 2 IQR 0 – 5 (maximum score 15), and median number of animals named correctly was 14 IQR 11 – 20 (no set maximum score). Figure 3 shows scatterplots of performance on the verbal memory tests and $T2_{pCSF,}$ gray matter CBF, and global atrophy.

Tables 1 and 2 present the final multiple regression models with performance on the memory and verbal fluency tests as dependent variables. Table 1 presents the regression models with $T2_{pCSF}$ entered as an independent variable, whereas Table 2 displays the models without $T2_{pCSF}$ to compare the additional value of $T2_{pCSF}$ in explaining the

observed variance in cognitive function. $T2_{pCSF}$ increased the explained variance of all models, except for the model with MMSE as the dependent variable. Table 3 displays the regression models without global atrophy. $T2_{pCSF}$ increased the explained variance on the immediate recall test by 16% to 57%, on the delayed recall test by 16% to 62%, and on the verbal fluency task by 5% to 53%. $T2_{pCSF}$ ($P = 0.008$), GM CBF ($P = 0.005$) as well as global atrophy ($P = 0.033$) were significantly associated with performance on the immediate recall test, while only $T2_{pCSF}$ and global atrophy were significantly associated with a subject's delayed recall ability ($P = 0.010$; $P = 0.033$; Figure 3). In contrast, only global atrophy was significantly associated with performance on the verbal fluency task ($P = 0.007$). Further, global atrophy ($P < 0.001$) was associated with general cognition represented by the MMSE score together with GM CBF ($P = 0.017$).

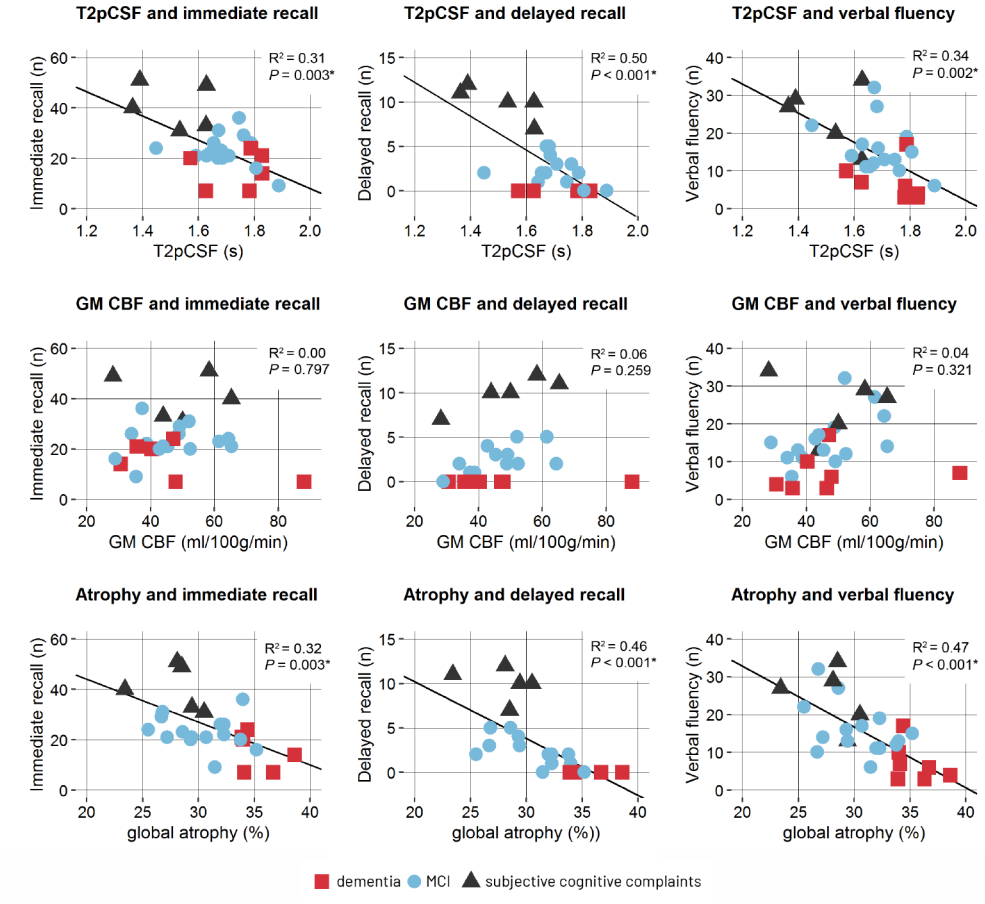

Fig 3. The relationship between $T2_{pCSF}$ (top row), gray matter (GM) CBF (middle row), atrophy (bottom row) and performance on the verbal memory and verbal fluency tests. The left column presents the relationship with immediate recall, the middle column the relationship with delayed recall, and the right column with verbal fluency.

Table 1. Final regression models including $T2_{pCSF}$ with cognition as the dependent variable

	Immediate recall		Delayed recall		Verbal fluency		MMSE	
Independent variable	β	*P*	β	*P*	β	*P*	β	*P*
$T2_{pCSF}$	-0.56	0.008*	-0.55	0.010*	-0.31	0.134	-	-
GM CBF	-0.51	0.005*	-0.19	0.246	-0.18	0.190	-0.36	0.017*
Global atrophy	-0.41	0.033*	-0.41	0.033*	-0.56	0.007*	-0.86	<0.001*

Explained variance full model: Immediate: $R^2 = 0.57$; F = 9.9 (*P* < 0.001); Delayed: $R^2 = 0.62$. F = 10.8 (*P* < 0.001); Verbal fluency: $R^2 = 0.53$. F = 8.6 (*P* < 0.001); MMSE (mini-mental state examination): $R^2 = 0.62$. F = 18.8 (*P* < 0.001).

Table 2. Regression models excluding $T2_{pCSF}$ with cognition as the dependent variable

	Immediate recall		Delayed recall		Verbal fluency	
Independent variable	β	*P*	β	*P*	β	*P*
GM CBF	-0.33	0.070	-0.01	0.946	-0.08	0.609
Global atrophy	-0.70	<0.001*	-0.69	<0.001*	-0.72	<0.001*

Immediate: $R^2 = 0.41$; F = 8.0 (*P* = 0.002); Delayed: $R^2 = 0.46$. F = 9.0 (*P* = 0.001); Verbal fluency: $R^2 = 0.48$. F = 11.0 (*P* < 0.001).

Table 3. Regression models excluding global atrophy with cognition as the dependent variable

	Immediate recall		Delayed recall		Verbal fluency	
Independent variable	β	*P*	β	*P*	β	*P*
GM CBF	-0.47	0.014*	-0.17	0.351	-0.14	0.481
$T2_{pCSF}$	-0.80	<0.001*	-0.79	<0.001*	-0.65	0.002*

Immediate: $R^2 = 0.47$; F = 10.3 (*P* < 0.001); Delayed: $R^2 = 0.52$. F = 11.3 (*P* < 0.001); Verbal fluency: $R^2 = 0.35$; F = 6.4 (*P* = 0.006). *$P < 0.05$

The influence of partial volume on obtained $T2_{pCSF}$

We compared the number, total volume and median partial CSF volume of included peripheral CSF voxels at minimum thresholds of 15%, 50% and 75% CSF volume (Figure 3). The median volume of included voxels decreased with an increasing partial volume threshold. A threshold of 15% yielded a peripheral CSF volume of 589 cc (IQR 529 – 636 cc, range 413 – 784 cc), a 50% threshold 246 cc (IQR 190 – 318 cc, range 79 – 400 cc) and a 75% threshold 105 cc (IQR 67 – 139 cc, range 20 – 192 cc; *P* < 0.001) (Figure 3). Then, the obtained $T2_{pCSF}$ and its association with global atrophy were compared for different thresholds (Figure 3). The obtained $T2_{pCSF}$ was 1.52s (IQR 1.39 – 1.57s), 1.67s (IQR 1.63 - 1.78s), and 1.74s (IQR 1.69 – 1.86s) for a threshold of 15%, 50% and 75%, respectively. The $T2_{pCSF}$ value was different between a threshold of 15% and 50% (*P* < 0.001) as well as

between a threshold of 50% and 75% ($P = 0.026$). The correlation between global atrophy and $T2_{pCSF}$ did not differ depending on the partial volume threshold (15%: $\beta = 0.57$, $P = 0.002$; 50%: $\beta = 0.57$, $P = 0.002$; 75%: $\beta = 0.53$, $P = 0.004$). Similarly, the association of $T2_{pCSF}$ with verbal fluency and verbal memory remained stable across each threshold. In the final analysis, we decided on a 50% threshold to maintain sufficient voxels for $T2_{pCSF}$ quantification while minimizing partial volume.

Discussion

The results of this study show an association between the T2 of peripheral CSF and disease severity in patients from a memory clinic. In a regression model with global atrophy and gray matter CBF, the $T2_{pCSF}$ showed a strong association with verbal memory – immediate and delayed recall of a word list. In contrast, global atrophy showed a strong association with verbal fluency and MMSE score in the respective regression models. Gray matter CBF was associated with immediate recall alongside $T2_{pCSF}$ and global atrophy.

The current study is inspired by the theory that poor cerebrovascular health can cause or aggravate disease severity along the dementia spectrum.[21] For example, decreased CBF has been proposed as a marker of cerebrovascular health, because it has been found associated with disease severity in AD.[42] However, a more comprehensive imaging biomarker reflective of cerebrovascular health is desired. The $T2_{pCSF}$ was hypothesized to reflect oxygenation in the peripheral CSF space in a previous study.[18] As oxygen can only enter the CSF space through diffusion along vessel walls, we speculate that $T2_{pCSF}$ would reflect cerebrovascular health, i.e., both cerebral perfusion and diffusion of nutrients. Capturing a measure of diffusion in addition to tissue perfusion could be of importance, because previous work has shown that Alzheimer's patients demonstrate a delay between CBF and cortical oxygenation changes.[43] In our study, we found the $T2_{pCSF}$ to be associated with (regional) CBF which brings support for the oxygenation hypothesis. More so, the $T2_{pCSF}$ explained more variance in disease severity than CBF. We hypothesize that $T2_{pCSF}$ may be less sensitive to rapid physiological changes if it reflects the interplay between CBF, cerebrovascular reactivity, oxygen delivery and oxygen consumption rather than a sole component. Additional analyses and future studies are required to test this hypothesis.

Given that $T2_{pCSF}$ had a stronger association with disease severity than CBF, it is interesting to evaluate its value against other established dementia biomarkers. For this purpose, we assessed the association between $T2_{pCSF}$ and atrophy, another well-known marker of disease severity. As expected, a correlation between the two measures was found: the $T2_{pCSF}$ increased with partial volume threshold increases. This shows the effect of partial volume on the obtained T2 value, and the importance of selecting an ap-

propriate partial volume threshold. Unexpectedly, the association between the $T2_{pCSF}$ and global atrophy remained stable for each threshold. Therefore, we think that the relationship between the $T2_{pCSF}$ and atrophy (also) originates from underlying dementia pathology rather than the solely being the effect of partial volume on T2 quantification. For the interpretation of atrophy level in mild cognitive impairment is complicated by age-related variability, the $T2_{pCSF}$ may offer complementary information to facilitate early identification of pathological aging.[44] Indeed, the $T2_{pCSF}$ was able to differentiate patients with dementia/MCI from patients with subjective cognitive impairment, whereas global atrophy could differentiate patients with dementia from MCI/subjective cognitive impairment patients.

An ideal imaging marker for dementia should be associated with either future cognition or with the cognitive domains most predictive of dementia conversion. Therefore, it is promising that the $T2_{pCSF}$ was associated with verbal memory, which in a recent meta-analysis was identified as the best predictor for conversion to dementia from MCI.[28] Future studies in larger cohorts should establish its value in the prediction of future cognitive decline and MCI to dementia conversion.

The current study has several limitations. First, the sample size was relatively small, which limited the number of variables included in the regression models and our ability to study subgroups. The group of dementia patients was a mix of patients with Alzheimer's disease, and patients with mixed Alzheimer's and vascular dementia. It is currently unclear whether the association between the $T2_{pCSF}$ and cognition is applicable to all dementia patients. Furthermore, the dependency of $T2_{pCSF}$ on oxygenation was not validated in our cohort, because of the invasiveness of CSF oxygenation measurements. Consequently, the hypothesized relationship between the two measures is founded on the effect of oxygenation on T2 and the relationship between the $T2_{pCSF}$ and CBF rather than on empirical evidence. Albeit that the value of $T2_{pCSF}$ as an imaging marker is not dependent on the validation of this relationship, an understanding of the underlying pathology would provide insight into the marker's utility as well as into the pathogenesis of dementia.

In summary, $T2_{pCSF}$ provided added value over global atrophy and gray matter CBF to assess cognition in a cohort of patients with varying levels of cognitive impairment. We hypothesized a relationship of the $T2_{pCSF}$ imaging marker with cognition in a memory clinical cohort, because of its dependency on oxygenation and thereby cerebrovascular dysfunction. $T2_{pCSF}$ showed a particularly strong association with verbal memory in a regression model that also included global atrophy and CBF. Future studies in larger cohorts should elicit whether it is predictive of decline and disease progression.

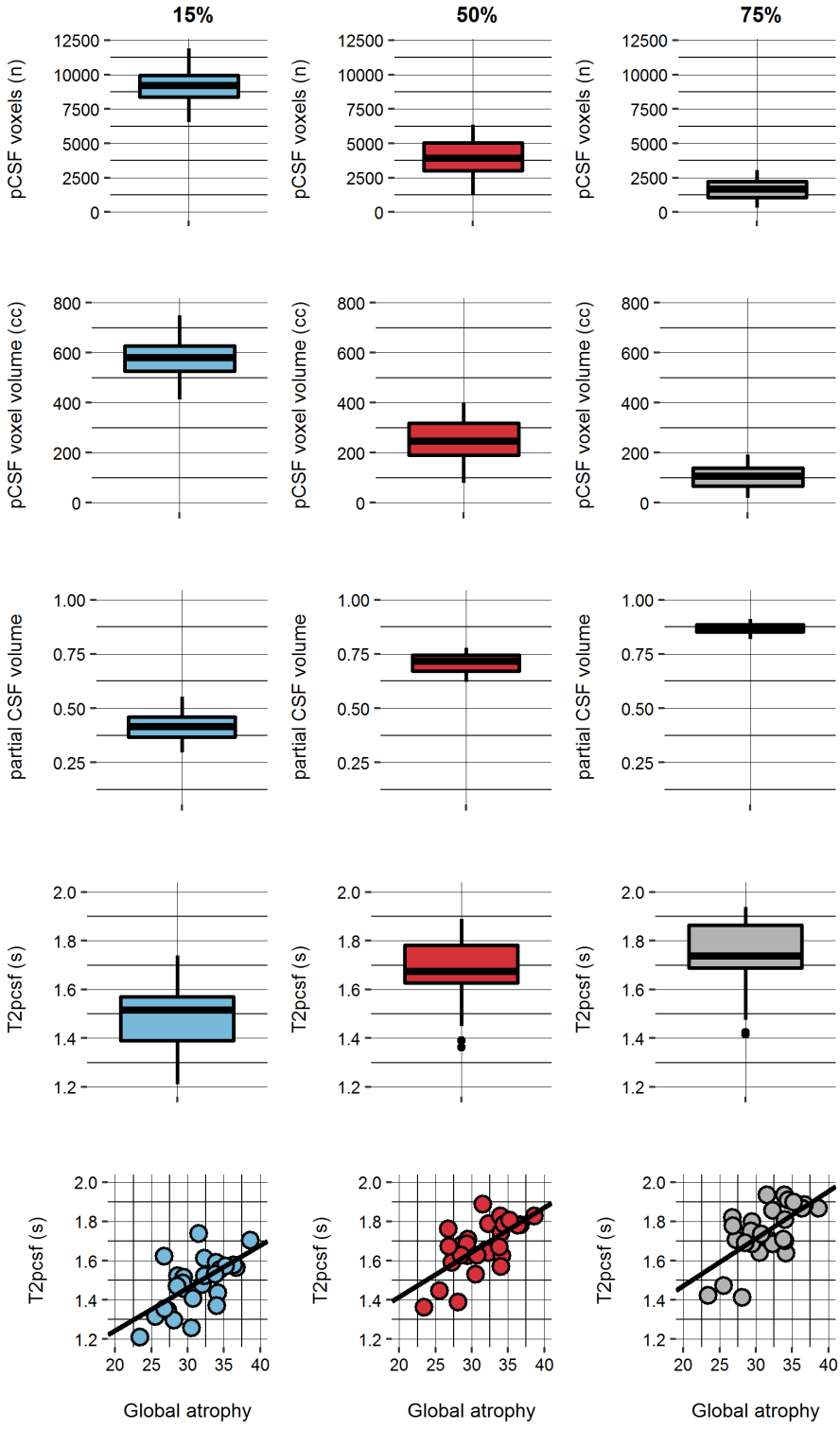
15%
50%
75%
pCSF voxels (n)
12500
10000
7500
5000
2500
0
pCSF voxel volume (cc)
800
600
400
200
0
partial CSF volume
1.00
0.75
0.50
0.25
T2pcsf (s)
2.0
1.8
1.6
1.4
1.2
20
25
30
35
40
Global atrophy

Fig. 3 The effect of partial volume threshold on T2 of peripheral CSF. The left column shows results for a 15% partial volume threshold, the middle column for a 50% threshold, and the right column for a 75% threshold. The first row displays the number of voxels included in the analysis, the second row the volume of the voxels included, the third row the median partial CSF volume of included voxels, the fourth row the T2pCSF of included voxels, and the bottom row the relation between T2pCSF and global atrophy.

Acknowledgements

We acknowledge the following members of the Utrecht Vascular Cognitive Impairment (VCI) Study group, who contributed to the recruitment and evaluation of patients for the Pearl Neurodegenerative Diseases (in alphabetical order by department): University Medical Center Utrecht, the Netherlands, Department of Neurology: G.J. Biessels, L.G. Exalto, O.N. Groeneveld, S.M. Heringa, N. Kalsbeek, J.H. Verwer.; Department of Radiology/Image Sciences Institute: J. de Bresser; Department of Geriatrics: M.E. Emmelot-Vonk, H.L. Koek, J.E. de Wit; Julius Center for Health Sciences and Primary Care: K. Blom; Hospital Diakonessenhuis Zeist, the Netherlands: M. Hamaker, R. Faaij, M. Pleizier, M. Prins, E. Vriens.

References

1. Prince M, Bryce R, Albanese E, Wimo A, Ribeiro W, Ferri CP. The global prevalence of dementia: A systematic review and metaanalysis. *Alzheimer's & dementia*. 2013;9:63-75. e62
2. Sperling RA, Jack CR, Aisen PS. Testing the right target and right drug at the right stage. *Science Translational Medicine*. 2011;3
3. Bruscoli M, Lovestone S. Is mci really just early dementia? A systematic review of conversion studies. *International Psychogeriatrics*. 2004;16:129-140
4. Jack CR, Knopman DS, Jagust WJ, Petersen RC, Weiner MW, Aisen PS, et al. Tracking pathophysiological processes in alzheimer's disease: An updated hypothetical model of dynamic biomarkers. *The Lancet Neurology*. 2013;12:207-216
5. Scheltens P, Launer LJ, Barkhof F, Weinstein HC, van Gool WA. Visual assessment of medial temporal lobe atrophy on magnetic resonance imaging: Interobserver reliability. *Journal of neurology*. 1995;242:557-560
6. Scheltens P, Pasquier F, Weerts JG, Barkhof F, Leys D. Qualitative assessment of cerebral atrophy on mri: Inter-and intra-observer reproducibility in dementia and normal aging. *European neurology*. 1997;37:95-99
7. Initiative tAsDN, Jack CR, Jr, Zeng G, Gunter JL, Bernstein MA, Senjem ML, et al. Brain beta-amyloid measures and magnetic resonance imaging atrophy both predict time-to-progression from mild cognitive impairment to alzheimer's disease. *Brain*. 2010;133:3336-3348
8. Austin BP, Nair VA, Meier TB, Xu G, Rowley HA, Carlsson CM, et al. Effects of hypoperfusion in alzheimer's disease. *Journal of Alzheimer's Disease*. 2011;26:123-133
9. Binnewijzend MAA, Kuijer JPA, Benedictus MR, van der Flier WM, Wink AM, Wattjes MP, et al. Cerebral blood flow measured with 3d pseudocontinuous arterial spin-labeling mr imaging in alzheimer disease and mild cognitive impairment: A marker for disease severity. *Radiology*. 2013;267:221-230
10. Beishon L, Haunton VJ, Panerai RB, Robinson TG. Cerebral hemodynamics in mild cognitive impairment: A systematic review. *Journal of Alzheimer's Disease*. 2017;59:369-385
11. De Vis JB, Peng S-L, Chen X, Li Y, Liu P, Sur S, et al. Arterial-spin-labeling (asl) perfusion mri predicts cognitive function in elderly individuals: A 4-year longitudinal study. *Journal of Magnetic Resonance Imaging*. 2018;48:449-458
12. Eggermont L, Swaab D, Luiten P, Scherder E. Exercise, cognition and alzheimer's disease: More is not necessarily better. *Neuroscience & Biobehavioral Reviews*. 2006;30:562-575
13. Salami A, Wåhlin A, Kaboodvand N, Lundquist A, Nyberg L. Longitudinal evidence for dissociation of anterior and posterior mtl resting-state connectivity in aging: Links to perfusion and memory. *Cerebral Cortex*. 2016;26:3953-3963
14. Wang R, Laveskog A, Laukka EJ, Kalpouzos G, Bäckman L, Fratiglioni L, et al. Mri load of cerebral microvascular lesions and neurodegeneration, cognitive decline, and dementia. *Neurology*. 2018;91:e1487-e1497
15. Knight MJ, Wearn A, Coulthard E, Kauppinen RA. T2 relaxometry and diffusion tensor indices of the hippocampus and entorhinal cortex improve sensitivity and specificity of mri to detect amnestic mild cognitive impairment and alzheimer's disease dementia. *Journal of Magnetic Resonance Imaging*. 2019;49:445-455
16. Passiak BS, Liu D, Kresge HA, Cambronero FE, Pechman KR, Osborn KE, et al. Perivascular spaces contribute to cognition beyond other small vessel disease markers. *Neurology*. 2019;92:e1309-e1321
17. Bouvy WH, van Veluw SJ, Kuijf HJ, Zwanenburg JJ, Kappelle JL, Luijten PR, et al. Microbleeds colocalize with enlarged juxtacortical perivascular spaces in amnestic mild cognitive impairment and early alzheimer's disease: A 7 tesla mri study. *Journal of Cerebral Blood Flow & Metabolism*.0:0271678X19838087
18. De Vis JB, Zwanenburg JJ, van der Kleij LA, Spijkerman JM, Biessels GJ, Hendrikse J, et al. Cerebrospinal fluid volumetric mri mapping as a simple measurement for evaluating brain atrophy. *European Radiology*. 2016;26:1254-1262

19. Lu H, Ge Y. Quantitative evaluation of oxygenation in venous vessels using t2-relaxation-under-spin-tagging mri. *Magnetic Resonance in Medicine*. 2008;60:357-363
20. Spijkerman JM, Petersen ET, Hendrikse J, Luijten P, Zwanenburg JJ. T 2 mapping of cerebrospinal fluid: 3 t versus 7 t. *Magnetic Resonance Materials in Physics, Biology and Medicine*. 2018:1-10
21. Zlokovic BV. Neurovascular pathways to neurodegeneration in alzheimer's disease and other disorders. *Nat Rev Neurosci*. 2011;12:723-738
22. Attems J, Jellinger KA. The overlap between vascular disease and alzheimer's disease - lessons from pathology. *BMC Medicine*. 2014;12:206
23. Aalten P, Ramakers IH, Biessels GJ, de Deyn PP, Koek HL, OldeRikkert MG, et al. The dutch parelsnoer institute - neurodegenerative diseases; methods, design and baseline results. *BMC Neurology*. 2014;14:254
24. Morris JC. The clinical dementia rating (cdr): Current version and scoring rules. *Neurology*. 1993
25. Folstein MF, Folstein SE, McHugh PR. "Mini-mental state": A practical method for grading the cognitive state of patients for the clinician. *Journal of psychiatric research*. 1975;12:189-198
26. Lezak M, Howieson D, Loring D. Neuropsychological assessment. New york: Oxford univer. *Press. E., & JAckuns, C.(1974) The psychology of sex differences. London: Oxford Univer*. 1995;1
27. Brand N, Jolles J. Learning and retrieval rate of words presented auditorily and visually. *The Journal of General Psychology*. 1985;112:201-210
28. Belleville S, Fouquet C, Hudon C, Zomahoun HTV, Croteau J, disease-Quebec CftEIoAs. Neuropsychological measures that predict progression from mild cognitive impairment to alzheimer's type dementia in older adults: A systematic review and meta-analysis. *Neuropsychology Review*. 2017;27:328-353
29. Ashburner J, Barnes G, Chen C, Daunizeau J, Flandin G, Friston K, et al. Spm12 manual. *URL: http://www. fil. ion. ucl. ac. uk/spm/doc/spm12 manual. pdf*. 2016
30. Schmidt P, Gaser C, Arsic M, Buck D, Förschler A, Berthele A, et al. An automated tool for detection of flair-hyperintense white-matter lesions in multiple sclerosis. *Neuroimage*. 2012;59:3774-3783
31. Ashburner J. Computational anatomy with the spm software. *Magnetic Resonance Imaging*. 2009;27:1163-1174
32. Alsop DC, Detre JA, Golay X, Günther M, Hendrikse J, Hernandez-Garcia L, et al. Recommended implementation of arterial spin-labeled perfusion mri for clinical applications: A consensus of the ismrm perfusion study group and the european consortium for asl in dementia. *Magnetic resonance in medicine*. 2015;73:102-116
33. Oguz KK, Golay X, Pizzini FB, Freer CA, Winrow N, Ichord R, et al. Sickle cell disease: Continuous arterial spin-labeling perfusion mr imaging in children. *Radiology*. 2003;227:567-574
34. Alsop DC, Dai W, Grossman M, Detre JA. Arterial spin labeling blood flow mri: Its role in the early characterization of alzheimer's disease. *Journal of Alzheimer's disease : JAD*. 2010;20:871-880
35. Buckner RL, Snyder AZ, Shannon BJ, LaRossa G, Sachs R, Fotenos AF, et al. Molecular, structural, and functional characterization of alzheimer's disease: Evidence for a relationship between default activity, amyloid, and memory. *The Journal of Neuroscience*. 2005;25:7709-7717
36. Tzourio-Mazoyer N, Landeau B, Papathanassiou D, Crivello F, Etard O, Delcroix N, et al. Automated anatomical labeling of activations in spm using a macroscopic anatomical parcellation of the mni mri single-subject brain. *NeuroImage*. 2002;15:273-289
37. Qin Q. A simple approach for three-dimensional mapping of baseline cerebrospinal fluid volume fraction. *Magnetic resonance in medicine*. 2011;65:385-391
38. van der Kleij LA, de Bresser J, Hendrikse J, Siero JC, Petersen ET, Jill B. Fast csf mri for brain segmentation; cross-validation by comparison with 3d t1-based brain segmentation methods. *PloS one*. 2018;13:e0196119
39. Brittain JH, Hu BS, Wright GA, Meyer CH, Macovski A, Nishimura DG. Coronary angiography with magnetization-prepared t2 contrast. *Magnetic resonance in medicine*. 1995;33:689-696
40. R. Core Team. R: A language and environment for statistical computing. 2017
41. Steyerberg EW, Eijkemans MJ, Harrell FE, Habbema JDF. Prognostic modelling with logistic regression analysis: A comparison of selection and estimation methods in small data sets. *Statistics in medicine*.

2000;19:1059-1079
42. Mattsson N, Tosun D, Insel PS, Simonson A, Jack Jr CR, Beckett LA, et al. Association of brain amyloid-ß with cerebral perfusion and structure in alzheimer's disease and mild cognitive impairment. *Brain*. 2014;137:1550-1561
43. van Beek AHEA, Lagro J, Olde-Rikkert MGM, Zhang R, Claassen JAHR. Oscillations in cerebral blood flow and cortical oxygenation in alzheimer's disease. *Neurobiology of Aging*. 2012;33:428.e421-428.e431
44. Fox NC, Schott JM. Imaging cerebral atrophy: Normal ageing to alzheimer's disease. *The Lancet*. 2004;363:392-394

Chapter 9

The effect of physical exercise on cerebral blood flow in Alzheimer's disease

L.A. van der Kleij[1], E.T. Petersen[2], H.R. Siebner[2,3], J. Hendrikse[1], K.S. Frederiksen[4], N.A. Sobol[5], S.G. Hasselbalch[4], E. Garde[2,6]

[1] Department of Radiology, University Medical Center Utrecht, Utrecht, The Netherlands.
[2] Danish Research Centre for Magnetic Resonance, Centre for Functional and Diagnostic Imaging and Research, Copenhagen University Hospital Hvidovre, Hvidovre, Denmark
[3] Department of Neurology, Copenhagen University Hospital Bispebjerg, Copenhagen, Denmark
[4] Danish Dementia Research Centre, Department of Neurology, Rigshospitalet, Copenhagen University Hospital, Copenhagen, Denmark
[5] Musculoskeletal Rehabilitation Research Unit and Institute of Sports Medicine, Copenhagen University Hospital Bispebjerg, Copenhagen, Denmark
[6] Center for Healthy Aging, Faculty of Health and Medical Sciences, University of Copenhagen, Copenhagen, Demark

NeuroImage: Clinical 20 (2018): 650-654

ABSTRACT

In recent years there has been an increasing focus on the relationship between cerebrovascular health, physical exercise and Alzheimer's disease. The aim of the current study was to determine the effect of moderate-to-high-intensity aerobic exercise on cerebral blood flow in patients with mild to moderate Alzheimer's disease. Fifty-one patients were randomized to either usual care or moderate-to-high intensity aerobic exercise for 16 weeks. Exercise had no consistent effect on whole brain or regional cerebral blood flow. Sixteen weeks of exercise are, therefore, not sufficient to produce a consistent increase in cerebral blood flow in a relatively small sample of Alzheimer's patients.

INTRODUCTION

Alzheimer's disease (AD) poses a large burden on our increasingly aging population. In addition to its characteristic Amyloid β and Tau pathology, Alzheimer's disease is also marked by changes in cerebral blood flow (CBF) as AD patients show a 40% decrease in global blood flow compared to healthy controls.[1] A decreased CBF already occurs in individuals with mild cognitive impairment (MCI) before their transition to AD.[2] Certain regions appear to show a particularly decreased CBF in AD, including the precuneus, hippocampus, and posterior cingulate gyrus.[1-3] Interestingly, local hyperperfusion has also been reported despite a global CBF reduction, which has been hypothesized to be a compensatory mechanism.[1]

CBF also provides a method to assess disease severity, as it is associated with cognitive functioning even within a group of AD patients.[4, 5] Moreover, a lower CBF as measured with ASL MRI is related to the rate of future cognitive decline in both healthy elderly individuals and AD patients.[6-10] These findings mark CBF as a potential target for interventions. Interestingly, in healthy individuals the association between age and gray matter CBF is mediated by cardiorespiratory fitness.[11] As well, aerobic exercise has been shown to both mitigate the effect of age on CBF and improve cognition in healthy individuals.[12, 13] Thereby, increasing cardiorespiratory fitness may aid in preventing or slowing pathological cognitive decline by increasing CBF. In earlier studies regular exercise was reported to improve cognitive function and lowering the risk of future MCI and dementia.[14] As well, various studies have shown a beneficial effect of physical exercise on cognition in individuals with dementia.[15]

The aim of the current study was to determine the effect of moderate-to-high-intensity aerobic exercise on cerebral blood flow in patients with Alzheimer's disease (AD).

MATERIALS AND METHODS

The ADEX study (ClinicalTrials.gov no.: NCT01681602) is a multicenter, single-blind, randomized, controlled trial to investigate whether a supervised aerobic exercise program could ameliorate symptoms of AD. The ADEX trial was approved by the The Committees of Biomedical Research Ethics for the Capital Region (Protocol no.: H-3-2011-128) and by the Danish Data Protection Agency (j.no.: 30-0718).

Participants

A total of 200 patients with mild to moderate AD were randomized to either an exercise group or to a control group (usual care). A subgroup of patients underwent brain MRI at baseline and at 16 weeks.[16] All participants recruited at the main three study centers site were asked to participate in the MRI-substudy. Among the inclusion criteria are

a clinical diagnosis of probable AD, a Mini Mental State Examination (MMSE) score of >19,[17] age 50-90 years, stable dose of anti-dementia or mood stabilizing medication. The exclusion criteria include contraindications for physical activity, participation in high intensity physical exercise >2x per week, severe psychiatric disease or alcohol abuse within last 2 years. The inclusion criteria were described in detail earlier.[16]

Intervention

The exercise group underwent 60 minute exercise sessions, three times a week for 16 weeks. All exercise sessions were supervised. The first four weeks consisted of adaptation training for which participants received an *introduction to exercise* session once week, and two exercise sessions a week focusing on building strength (mostly in the legs). The exercise sessions in the subsequent 12 weeks consisted of moderate-to-high intensity aerobic exercise. The intensity of the exercises were adjusted per individual participant to target 70-80% of the heart rate reserve. The exercises were performed on a cross trainer, bicycle and treadmill.

The control group received care as usual.

Imaging protocol

All imaging was performed on a 3T system (Trio, Siemens, Erlangen, Germany). The imaging protocol included a T_1-weighed magnetization-prepared rapid gradient echo (MPRAGE): TR 1550ms, TE 3.04ms, FOV 256x256, 192 slices. A Pulsed Arterial Spin Labeling (PASL) sequence was used to obtain quantitative perfusion measurements with a flow-sensitive alternating inversion recovery (FAIR) labeling scheme, 3D gradient-and-spin-echo (GRASE) multishot readout. PASL provides a method to non-invasively measure cerebral perfusion through the labeling of blood water at the neck region. Images are acquired after a predefined post label delay when the labeled protons have reached the tissue. The parameters of the PASL sequence were: TR 3400ms, TE 19ms, TI 2000ms, FOV 320x160, matrix 64x32, 26 slices, voxel size 5x5x4 mm^3. A Fluid Attenuated Inversion Recovery (FLAIR) sequence was used to calculate white matter hyperintensity (WMH volume). The FLAIR sequence parameters were: TR=6000ms, TE=353ms, TI=2200ms, FOV 256x220x192.

Data processing

To obtain quantitative perfusion maps, the obtained ASL images were processed using IDL 6.1 for Windows (ITT Visual Information Solutions, Boulder, C.O., U.S.A.). The quantitative perfusion maps were registered to the T_1-weighted images that were segmented using FreeSurfer (http://freesurfer.net/fswiki/FreeSurferWiki). Whole brain

CBF was calculated, and five, bilateral regions were selected known to be involved in AD related perfusion changes: the frontal lobe, anterior cingulate cortex (ACC), posterior cingulate cortex (PCC), superior parietal gyrus (SPG) and the precuneus.[1-3] The T_1-weighed images were segmented with FreeSurfer. The PASL images were linearly registered to the MPRAGE space to select the areas for regional CBF analysis (https://surfer.nmr.mgh.harvard.edu/fswiki/). The absolute change in CBF ($CBF_{follow\text{-}up} - CBF_{baseline}$) and relative change in CBF (($CBF_{follow\text{-}up} - CBF_{baseline}$)/$CBF_{baseline}$*100%) were calculated. Areas clearly hyperintense relative to surrounding white matter on both FLAIR and T_2-weighted images were delineated to obtain WMH volume. Local thresholding was applied and WMH volumes for the whole brain were quantified automatically using the Jim image analysis package, Version 6.0, (Xinapse Systems Ltd., Northants, UK, www.xinapse.com). Visual identification and delineation was carried out by a single trained rater blinded to clinical information.

Cognitive and physical outcome measures

The Mini Mental State Examination (MMSE) was administrated at baseline and at 16-week follow-up. VO_2 peak (ml/kg/min) was recorded at both time points using direct breath-by breath cardiopulmonary exercise test (CPET) performed on a graded cycle ergometer. Indirect calorimetry and expired gases were assembled and analyzed using a metabolic measurement system (Jaeger, Master Screen CPX vers. 5.21, Cardinal Health, Germany). VO_2 peak was measured at self- termination of the test and maximal effort was set at RER ≥ 1.05.[18] VO_2 peak was obtained from 34 participants.

Statistical analysis

Statistical analysis was carried out with R (R Foundation for Statistical Computing, Vienna, Austria). Outliers were defined conservatively as values above 4 median absolute deviations (MADs), and they were removed from the results. Given the non-normal distribution, the non-parametric statistical tests Wilcoxon rank-sum test, Wilcoxon signed-rank test and Spearman's correlation were used. Bonferroni correction was used for multiple comparisons.

RESULTS

Fifty-one patients were included in the analysis (Figure 1). Baseline characteristics were similar between the exercise and control group (Table 1). The similarity of the two study arms was also reflected in the baseline whole brain CBF: the median CBF was 39 (interquartile range (IQR) 32 – 42) ml/100g/min and 36 (IQR 31 – 43) for the control and intervention group, respectively.

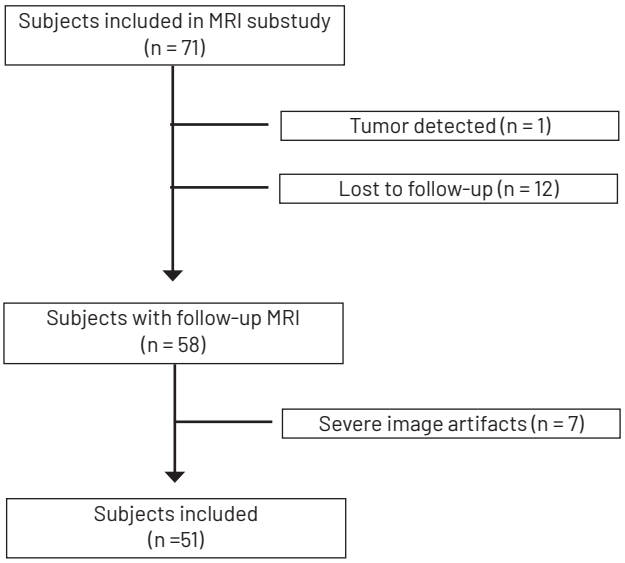

Fig. 1. Flowchart.

Table 1. Baseline characteristics.

	Exercise group (n = 27)	Control group (n = 24)	Difference between study groups
Age (mean±sd)	68±7	69±7	n.s.
Sex (female, %)	37%	41%	n.s.
MMSE (mean±sd)	25±3	25±3	n.s.
WMH (mm^3)	3.5±6.5	4.8±6.1	n.s.
Hypertension	10 (37%)	11 (46%)	n.s.

MMSE = mini mental state examination; WMH = white matter hyperintensities; n.s. = not significant.

After the 16-week intervention the median difference in whole brain CBF was -6 (IQR -1 – 3) ml/100/min for the control group and -4 (IQR 0 – 3) ml/100/min for the intervention group. The change in CBF over the study period did not differ between the control group subjects and exercise group subjects (P>0.05, Figure 2, Table 2) . The effect of exercise on cardiorespiratory fitness was reflected in the VO_2 peak. There was no difference in the VO_2 peak at baseline between the exercise and control arm (24 mL/min/kg (IQR 19 – 29) and 24 mL/min/kg (IQR 23 – 29, respectively)), whereas the VO_2 peak was increased after 16 weeks in the exercise group ($p < 0.01$), but stable in the control group (27 mL/min/kg (IQR 21 – 32) compared to 25 mL/min/kg (IQR 23 – 19)).

Table 2. CBF at baseline and at week 16 follow-up visit for the control group and exercise group

Region	Control group CBF (ml/100g/min)		Exercise group CBF (ml/100g/min)		Difference baseline – follow-up
	baseline	*follow-up*	*baseline*	*follow-up*	
Whole brain	39 (IQR 32 – 42)	37 (IQR 34 – 40)	36 (IQR 31 – 43)	36 (IQR 31 – 41)	*n.s. / n.s.*
Frontal regions	41 (IQR 36 – 44)	41 (IQR 37 – 45)	39 (IQR 34 – 49)	39 (IQR 34 – 44)	*n.s. / n.s.*
ACC	42 (IQR 37 – 45)	42 (IQR 37 – 43)	40 (IQR 34 – 49)	41 (IQR 37 – 46)	*n.s. / n.s.*
PCC	41 (IQR 35 – 47)	38 (IQR 36 – 43)	40 (IQR 33 – 47)	38 (IQR 36 – 42)	*n.s. / n.s.*
SPG	37 (IQR 34 – 41)	36 (IQR 33 – 42)	34 (IQR 30 – 41)	33 (IQR 31 – 37)	*n.s. / n.s.*
Precuneus	44 (IQR 34 – 48)	39 (IQR 36 – 46)	38 (IQR 33 – 46)	40 (IQR 37 – 42)	*n.s. / n.s.*

ACC = anterior cingulate cortex; PCC = posterior cingulate cortex; SPG = superior parietal gyrus; n.s. = not significant

DISCUSSION

Sixteen weeks of moderate-to-high intensity aerobic exercise did not have an effect on cerebral blood flow in a group of patients with mild to moderate Alzheimer's disease. The effect of the exercise intervention on cardiorespiratory fitness (VO_2 peak) did not translate to CBF. This was observed for whole brain as well as for regional CBF in the frontal precuneus. The absence of detectable changes induced by the 16-week exercise intervention is in line with results from other modalities in this study.[18-20] Yet, an effect of exercise has been reported on several neuropsychological and physical function tests in the ADEX trial.[18, 19]

These results demonstrate that although the exercise regime as used in the ADEX trial can positively affect cognition in individuals with Alzheimer's disease, the effect is not reflected in CBF changes. The intensity of the physical exercise program was in line with guidelines for older adults.[21, 22] A strength of this study was the close monitoring of each participant during each exercise session, including individual adjustment to target 70-80% of the heart rate reserve. As such, adherence and proper execution of the exercise program was monitored. A limitation of the study is the length of the intervention, as possibly a longer trial duration would yield different results. Still the optimal duration for such a trial is unknown, and effect of the exercise on cognition in the total population indicates that the length was appropriate for cognitive changes.[19] Several clinically relevant ROIs were selected a priori to monitor the effect of exercise on CBF in AD. The number and location of hypoperfused regions varies among studies, but the

precuneus and posterior cingulate cortex are consistently found hypoperfused on ASL MRI in AD.[23-25] Both regions were included in the analyses of the current study.

The negative results might be due to mild to moderate AD diagnosis of the participants. The disease may be too advanced to induce any CBF increase, because chronic hypoperfusion is hypothesized to precede neurodegeneration years before symptom onset.[26, 27] Furthermore, hypoperfusion can cause characteristic AD pathology.[28] This suggests that CBF should be targeted in healthy elderly or MCI patients to prevent or postpone AD pathology, whereas in our study population AD pathology had already manifested. As well, the occurrence of mild small vessel disease as indicated by the WMH volumes in our study may limit ability to increase CBF, because it is also associated with decreased CBF.[29] Several studies have shown an effect of exercise on CBF in healthy elderly. For example, an increase in ACC CBF was found after three months of training, whereas no change in whole brain CBF occured in healthy adults (57 – 75 years old) who underwent an exercise intervention comparable to the ADEX trial.[30] In comparison, no change in ACC CBF was found in the current study. An increase in hippcampal CBF but no change in ACC CBF was observed in healthy adults (70 – 85 yeas old) after 4 months of partially unsupervised exercise.[31] The intensity of the training program might also affect study results, as no change in CBF was found in healthy adults (64 – 78 years old) who underwent an aerobic exercise program of with less training time per session (30-60 min).[32] In addition, a longer training period may be required to see results in patients with advanced disease. Therefore, future studies should consider a longer intervention or patients with less advanced disease.

Cerebral blood flow has been linked to disease severity as measured with the MMSE in MCI and AD patients,[2] and a possible cause for the CBF reduction seen in this patient population is amyloid deposition in the cerebral blood vessels.[3] Amyloid β is a vasoconstrictor, and may through this reduce CBF.[3] Alternatively, the lowered CBF may reflect lower metabolic demand due to tissue damage or, conversely, tissue damage may be caused by lower CBF.[1]. As such, the question of causality remains unanswered.[33] It is, however, clear that vascular risk factors play an important role in neurodegeneration.[33] In the current study, vascular risk factors did not differ between the two study arms. Interestingly, a more active lifestyle of APOE-e4 allele carriers has been associated with lower cerebral amyloid β deposition.[34] In the ADEX trial, no effect was found of the 16 week exercise program on amyloid β concentrations in the cerebral spinal fluid.[20]

In summary, the results indicate that there may not be an effect of exercise on cerebral blood flow in individuals with mild to moderate AD. An alternative explanation is that 16 weeks may be too brief for detectable effects with ASL MRI in this relatively small sample.

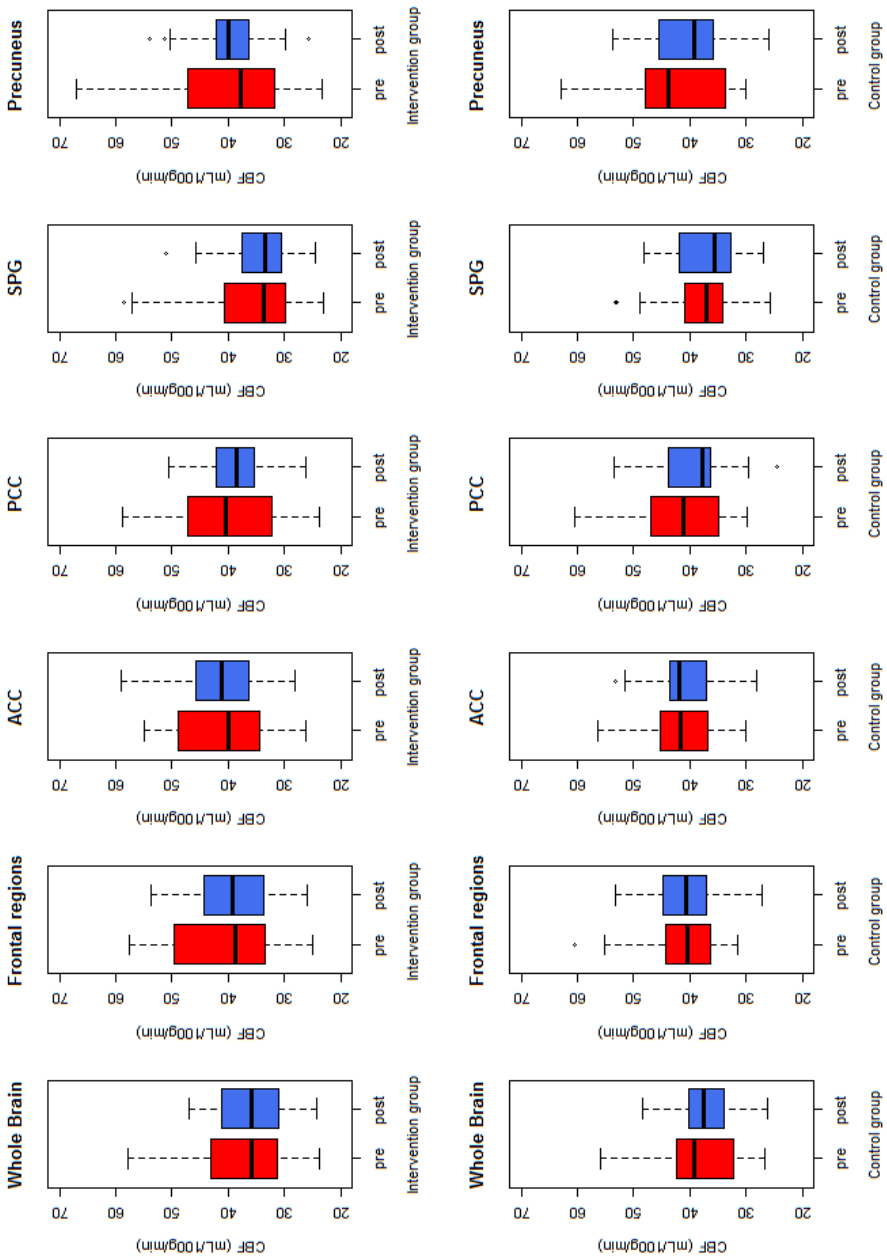

Fig. 2. Change in absolute CBF value (mL/100g/min) for whole brain , frontal regions, anterior cingulate cortex (ACC), posterior cingulate cortex (PCC), superior parietal gyrus (SPG), and the precuneus.

REFERENCES

1. Austin BP, Nair VA, Meier TB, Xu G, Rowley HA, Carlsson CM, et al. Effects of hypoperfusion in alzheimer's disease. *Journal of Alzheimer's disease : JAD*. 2011;26 Suppl 3:123-133
2. Binnewijzend MA, Kuijer JP, Benedictus MR, van der Flier WM, Wink AM, Wattjes MP, et al. Cerebral blood flow measured with 3d pseudocontinuous arterial spin-labeling mr imaging in alzheimer disease and mild cognitive impairment: A marker for disease severity. *Radiology*. 2013;267:221-230
3. J.P. van Osch M, Lu H. Arterial spin labeling perfusion mri in alzheimer's disease. *Current Medical Imaging Reviews*. 2011;7:62-72
4. Eggermont L, Swaab D, Luiten P, Scherder E. Exercise, cognition and alzheimer's disease: More is not necessarily better. *Neuroscience and biobehavioral reviews*. 2006;30:562-575
5. Tosun D, Schuff N, Jagust W, Weiner MW. Discriminative power of arterial spin labeling magnetic resonance imaging and ¹⁸f-fluorodeoxyglucose positron emission tomography changes for amyloid-β-positive subjects in the alzheimer's disease continuum. *Neurodegenerative Diseases*. 2016;16:87-94
6. Benedictus MR, Leeuwis AE, Binnewijzend MAA, Kuijer JPA, Scheltens P, Barkhof F, et al. Lower cerebral blood flow is associated with faster cognitive decline in alzheimer's disease. *European Radiology*. 2017;27:1169-1175
7. Xekardaki A, Rodriguez C, Montandon M-L, Toma S, Tombeur E, Herrmann FR, et al. Arterial spin labeling may contribute to the prediction of cognitive deterioration in healthy elderly individuals. *Radiology*. 2014;274:490-499
8. Wolters FJ, Zonneveld HI, Hofman A, van der Lugt A, Koudstaal PJ, Vernooij MW, et al. Cerebral perfusion and the risk of dementia: A population-based study. *Circulation*. 2017
9. De Vis JB, Peng S-L, Chen X, Li Y, Liu P, Sur S, et al. Arterial-spin-labeling (asl) perfusion mri predicts cognitive function in elderly individuals: A 4-year longitudinal study. *Journal of Magnetic Resonance Imaging*.0
10. Chao LL, Buckley ST, Kornak J, Schuff N, Madison C, Yaffe K, et al. Asl perfusion mri predicts cognitive decline and conversion from mci to dementia. *Alzheimer disease and associated disorders*. 2010;24:19-27
11. Zimmerman B, Sutton B, Low K, Fletcher M, Tan CH, Schneider-Garces N, et al. Cardiorespiratory fitness mediates the effects of aging on cerebral blood flow. *Frontiers in Aging Neuroscience*. 2014;6
12. Lucas SJ, Ainslie PN, Murrell CJ, Thomas KN, Franz EA, Cotter JD. Effect of age on exercise-induced alterations in cognitive executive function: Relationship to cerebral perfusion. *Experimental gerontology*. 2012;47:541-551
13. Ainslie PN, Cotter JD, George KP, Lucas S, Murrell C, Shave R, et al. Elevation in cerebral blood flow velocity with aerobic fitness throughout healthy human ageing. *The Journal of physiology*. 2008;586:4005-4010
14. Ahlskog JE, Geda YE, Graff-Radford NR, Petersen RC. Physical exercise as a preventive or disease-modifying treatment of dementia and brain aging. *Mayo Clinic proceedings*. 2011;86:876-884
15. Groot C, Hooghiemstra AM, Raijmakers PG, van Berckel BN, Scheltens P, Scherder EJ, et al. The effect of physical activity on cognitive function in patients with dementia: A meta-analysis of randomized control trials. *Ageing research reviews*. 2016;25:13-23
16. Hoffmann K, Frederiksen KS, Sobol NA, Beyer N, Vogel A, Simonsen AH, et al. Preserving cognition, quality of life, physical health and functional ability in alzheimer's disease: The effect of physical exercise (adex trial): Rationale and design. *Neuroepidemiology*. 2013;41:198-207
17. Folstein MF, Folstein SE, McHugh PR. "Mini-mental state". A practical method for grading the cognitive state of patients for the clinician. *Journal of psychiatric research*. 1975;12:189-198
18. Sobol NA, Hoffmann K, Frederiksen KS, Vogel A, Vestergaard K, Braendgaard H, et al. Effect of aerobic exercise on physical performance in patients with alzheimer's disease. *Alzheimer's & dementia : the journal of the Alzheimer's Association*. 2016;12:1207-1215
19. Hoffmann K, Sobol NA, Frederiksen KS, Beyer N, Vogel A, Vestergaard K, et al. Moderate-to-high in-

tensity physical exercise in patients with alzheimer's disease: A randomized controlled trial. *Journal of Alzheimer's disease : JAD*. 2016;50:443-453
20. Steen Jensen C, Portelius E, Siersma V, Høgh P, Wermuth L, Blennow K, et al. Cerebrospinal fluid amyloid beta and tau concentrations are not modulated by 16 weeks of moderate- to high-intensity physical exercise in patients with alzheimer disease. *Dementia and Geriatric Cognitive Disorders*. 2016;42:146-158
21. Paterson DH, Warburton DE. Physical activity and functional limitations in older adults: A systematic review related to canada's physical activity guidelines. *International Journal of Behavioral Nutrition and Physical Activity*. 2010;7:38
22. Nelson ME, Rejeski WJ, Blair SN, Duncan PW, Judge JO, King AC, et al. Physical activity and public health in older adults: Recommendation from the american college of sports medicine and the american heart association. *Medicine and science in sports and exercise*. 2007;39:1435-1445
23. Alsop DC, Dai W, Grossman M, Detre JA. Arterial spin labeling blood flow mri: Its role in the early characterization of alzheimer's disease. *Journal of Alzheimer's disease : JAD*. 2010;20:871-880
24. Schroeter ML, Stein T, Maslowski N, Neumann J. Neural correlates of alzheimer's disease and mild cognitive impairment: A systematic and quantitative meta-analysis involving 1351 patients. *NeuroImage*. 2009;47:1196-1206
25. Sierra-Marcos A. Regional cerebral blood flow in mild cognitive impairment and alzheimer's disease measured with arterial spin labeling magnetic resonance imaging. *International Journal of Alzheimer's Disease*. 2017;2017:10
26. Daulatzai MA. Cerebral hypoperfusion and glucose hypometabolism: Key pathophysiological modulators promote neurodegeneration, cognitive impairment, and alzheimer's disease. *Journal of Neuroscience Research*. 2017;95:943-972
27. Hays CC, Zlatar ZZ, Wierenga CE. The utility of cerebral blood flow as a biomarker of preclinical alzheimer's disease. *Cellular and Molecular Neurobiology*. 2016;36:167-179
28. Koike MA, Garcia FG, Kitazawa M, Green KN, LaFerla FM. Long term changes in phospho-app and tau aggregation in the 3xtg-ad mice following cerebral ischemia. *Neuroscience Letters*. 2011;495:55-59
29. Shi Y, Thrippleton MJ, Makin SD, Marshall I, Geerlings MI, de Craen AJM, et al. Cerebral blood flow in small vessel disease: A systematic review and meta-analysis. *Journal of Cerebral Blood Flow & Metabolism*. 2016;36:1653-1667
30. Chapman S, Aslan S, Spence J, DeFina L, Keebler M, Didehbani N, et al. Shorter term aerobic exercise improves brain, cognition, and cardiovascular fitness in aging. *Frontiers in Aging Neuroscience*. 2013;5
31. Burdette J, Laurienti P, Espeland M, Morgan A, Telesford Q, Vechlekar C, et al. Using network science to evaluate exercise-associated brain changes in older adults. *Frontiers in Aging Neuroscience*. 2010;2
32. Flodin P, Jonasson LS, Riklund K, Nyberg L, Boraxbekk CJ. Does aerobic exercise influence intrinsic brain activity? An aerobic exercise intervention among healthy old adults. *Frontiers in Aging Neuroscience*. 2017;9
33. de la Torre JC. Is alzheimer's disease a neurodegenerative or a vascular disorder? Data, dogma, and dialectics. *The Lancet. Neurology*. 2004;3:184-190
34. Head D, Bugg JM, Goate AM, Fagan AM, Mintun MA, Benzinger T, et al. Exercise engagement as a moderator of the effects of apoe genotype on amyloid deposition. *Archives of neurology*. 2012;69:636-643

Part III

Methods

Arterial spin labeling, CSF MRI, and brain volumetric analysis

Chapter 10

ASL: Blood Perfusion Measurement Using Arterial Spin Labelling

L.A. van der Kleij[1] and E.T. Petersen[2,3]

[1] Department of Radiology, University Medical Centre Utrecht, Utrecht University, The Netherlands.

[2] Danish Research Centre for Magnetic Resonance, Centre for Functional and Diagnostic Imaging and Research, Copenhagen University Hospital Hvidovre, Denmark

[3] Centre for Magnetic Resonance, DTU Elektro, Technical University of Denmark, Kgs Lyngby, Denmark

Quantitative MRI of the Brain. CRC Press, 2018. 283-302.

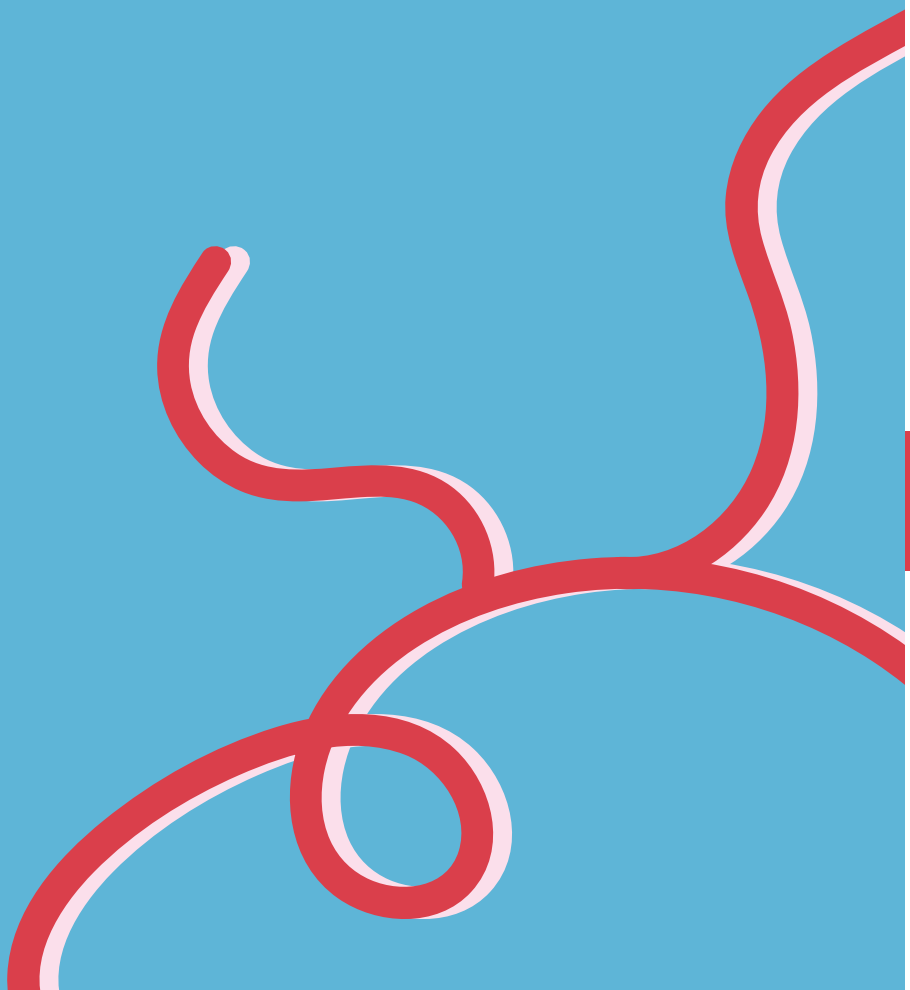

Abstract

Cerebral perfusion is a tightly regulated process to ensure that the metabolic demand of the brain is met at all times. As such, perfusion measurements offer insight in the function, and possible dysfunction, of the brain. Arterial spin labeling is a non-invasive MRI technique which uses magnetically labeled blood water as an endogenous tracer to measure perfusion. It can quantify a wide range of hemodynamic parameters, which together with its non-invasiveness makes it a valuable tool both for research and clinical settings. For example, in acute stroke ASL can provide information on whole brain perfusion, perfusion territories, and arterial transit time.

This chapter provides theoretical background and practical guidance for each stage of an ASL experiment. First, an overview is given on the possibilities of different sequences, after which we look into the acquisition parameters that provide optimal image quality. Once good-quality data is acquired, we discuss the options to convert the images to a quantitative measure of cerebral blood flow while minimizing artifacts. Lastly, the current state of the technique and future perspectives are discussed.

1 Introduction

The vascular system ensures a sufficient supply of oxygen and nutrients to the tissue, while at the same time it removes waste, transports heat, hormones and other messengers throughout the body. This complex transport system thereby ensures the homeostasis of the body and its organs. The steady state nutritive delivery of blood to the tissue's capillary bed is termed *perfusion*. Imaging modalities that can accurately measure perfusion for diagnostic purposes, e.g., to assess whether an ischemic organ is viable or not, are therefore of vital importance. Perfusion imaging modalities includes positron emission tomography (PET), single-photon emission computerized tomography (SPECT), computed tomography (CT), and magnetic resonance imaging (MRI). These methods are typically all in conjunction with the injection of an intravenous tracer. Clinically, MRI is a popular tool for perfusion imaging, due to the additional ability of obtaining structural images with superior soft tissue contrast that is often needed for evaluation of the patient. Two MRI perfusion approaches exist; the first being bolus tracking after the injection of an exogenous endovascular tracer, whereas the second technique called arterial spin labeling (ASL) relies on magnetically labeled water protons as an endogenous tracer. Arterial Spin Labeling is particularly appealing because the injection of a contrast agent can be avoided, which is important in patients with kidney failure or in the pediatric population. In addition, MRI does not involve radiation and this combined with the complete non-invasiveness of ASL makes it a forceful tool for perfusion studies of healthy volunteers and in patient groups requiring repetitive follow-ups. Arterial Spin Labeling was invented in 1992 (Williams *et al.*, 1992). Yet for many years, it remained a research tool for the few, partly due to hardware and software constraints but mainly due to a rather low signal-to-noise ratio (SNR) and a consequently poor robustness of the technique. The interplay in recent years between refined hardware solutions and optimized sequences have elevated ASL into widespread use, particularly within the neuroscience field while clinical use is also rapidly increasing.

This chapter will focus on the different implementations of ASL and how to quantify perfusion from the acquired data, including the problems and pitfalls potentially experienced during the process. Then we revisit research and clinical applications of ASL. Finally, we will look into the future directions for ASL.

2 Perfusion Imaging

2.1 Terminology and units

Blood flows via the arteries and through the smaller arterioles into the capillary bed. It is the blood delivery at this level, which enables the exchange of oxygen and nutrients

to the tissue, we call perfusion. The study of the fluid dynamics of the blood is termed hemodynamics, while the study of the actual flow properties of blood and its elements is termed hemorheology. Both naturally influence the actual perfusion, but in perfusion imaging we aim to be independent of the underlying hemodynamic system and the underlying blood composition in our perfusion estimate. Cerebral blood flow (CBF) is the primary parameter we use to describe perfusion and it has the unit of *ml of blood per 100g of tissue per min*, or [ml/100g/min]. This measure is a rate [s^{-1}] rather than a volume-flux [m^3/s], which is convenient because our techniques measure CBF in voxels of arbitrary volume. In addition to CBF, one often finds other parameters mentioned in the perfusion imaging literature. These includes cerebral blood volume (CBV), which is a dimensionless parameter [%] or [ml/100g], describing the fraction of blood within a voxel and the mean transit time (MTT) which is the average time [s] it takes the blood to traverse the vasculature of the voxel. These are also important clinical parameters, probing the status of the underlying hemodynamic system. For instance, an increased CBV in a patient with large-vessel disease could suggest that auto regulation has dilated the vessels in order to maintain sufficient CBF to the affected tissue.

2.2 Quantification principles

Two types of tracer exist for tracking blood perfusion of the tissue; freely diffusible tracers and intravascular tracers. Freely diffusible tracers, which exit the intravascular space unhindered upon arrival to the tissue's vascular bed, diffusing freely through the brain's otherwise very selective blood-brain-barrier. Freely diffusible tracers such as nitrous oxide (N_2O) was used by the early pioneers (Kety and Schmidt, 1948). Their distribution throughout the full tissue volume causes the MTT to be on the order of minutes at normal physiological flow rates of 40-60 [ml/100g/min] for the brain, thereby allowing ample time for the dynamic arterial and venous blood sampling typically needed for quantification using Fick's principle:

$$\frac{dC_t(t)}{dt} = CBF \cdot \left(C_a(t) - C_v(t)\right) \quad [1]$$

where $C_t(t)$, $C_a(t)$ and $C_v(t)$ are the concentrations of tracer in the tissue, arterial and venous blood respectively.

Intravascular tracers on the other hand, remain in the vasculature due to their relatively large molecular structure, which limits their distribution volume to the vascular volume. Contrary to the freely diffusible tracer, the distribution of intravascular tracers offers an opportunity of measuring CBV in addition to CBF. The central volume theorem states that the ratio between distribution volume and flow is equal to the mean transit time (Hence, for intravascular tracers, MTT=CBV/CBF). Accordingly, if any two

parameters are known, we can calculate the remaining one. The gadolinium-based bolus tracking experiment (Ostergaard *et al.*, 1996) exploits this by estimating the tracer concentration by means of MRI during its first passage of both the arterial and the tissue space. Knowing both the arterial input function $C_a(t)$ and the tissue concentration curve $C_t(t)$, R(t)·CBF is calculated using deconvolution:

$$C_t(t) = CBF \cdot \int_0^t C_a(\tau) R(t-\tau) d\tau \quad \text{[eq 2]}$$

where R(t) is the residue function describing the fraction of contrast remaining in the system at time t after arrival, and it is therefore a decaying function with R(0) =1. The result of the deconvolution; R(t)·CBF, equals CBF at t=0. In addition, the area under the tissue concentration curves allows the assessment of CBV:

$$CBV = \frac{\int_{-\infty}^{\infty} C_t(t) dt}{\int_{-\infty}^{\infty} C_a(t) dt} \quad \text{[eq 3]}$$

The two tracer techniques described above form the basis of the applied perfusion techniques of today. Hybrid solutions exist in the case where restricted leakage or permeability to the tracer exists, which can be quantified by means of the appropriate modeling of R(t)(Tofts and Kermode, 1991). Which scheme Arterial Spin Labeling in fact belongs to is somewhat ambivalent, as we will come back to later.

3 Arterial Spin Labeling: acquisition schemes

The basic ASL perfusion measurement consists of two parts, the 'label' and 'control'. By subtracting the label from the control, the stationary tissue signal is eliminated and the resulting difference map DM becomes proportional to the blood inflow from the label region and thereby it reflects local perfusion (Figures 1 and 2). The first is a 'label' part where the magnetization of the inflowing blood has been manipulated, typically by inverting or saturating it prior to the subsequent post labeling delay (PLD) and final image readout. The second part is the 'control' part, where essentially nothing is done to the inflowing blood, the images are "just" acquired with similar conditions as for the label experiment. The difference signal DM(t) depends on the underlying flow kinetics (Figure 3) and at which time (PLD) it was sampled. Often a single PLD is used, chosen such that the labeled blood spins had enough time to reach the capillaries within the voxels of interest, before image acquisition. Other sequences acquire data at multiple PLDs to allow sampling the entire kinetic curve and through this a more quantitative perfusion estimate. As DM is approximately 1% of the full signal, it requires averaging of multiple label-control pairs to gain a sufficient signal-to-noise ratio (SNR).

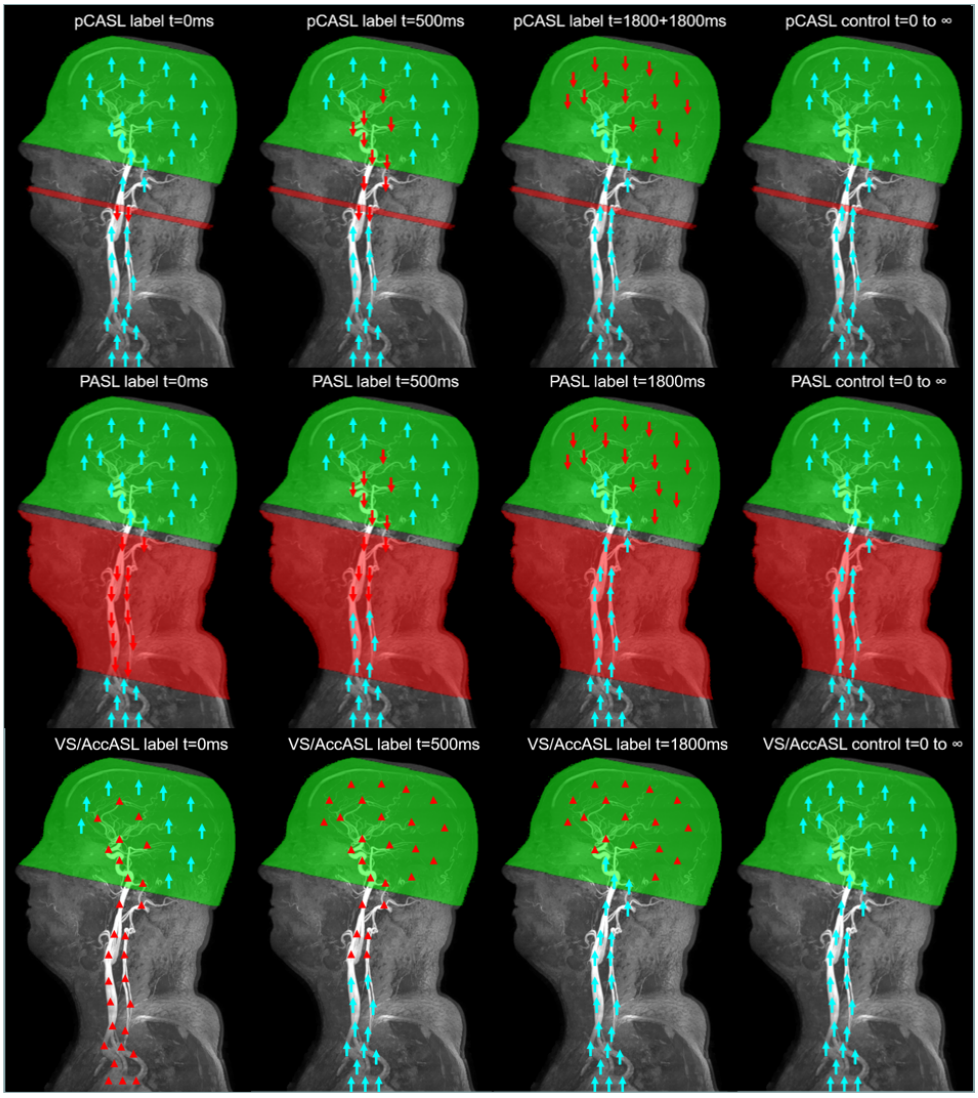

Fig. 1. Upper row: pCASL labeling in a plane located perpendicular to the feeding vessels in the neck. The label plane is kept "on" for typically 1800ms during which time the blood passing through the label plane is inverted. Subsequently, a post labeling delay (PLD) of 1800ms is applied to allow the labeled blood to clear from the vasculature and reach the tissue before imaging. During the control experiment on the right, the blood magnetization is kept undisturbed and otherwise the experiment is similar to the label experiment. Subtraction of control-label cancels the static tissue signal and leave us with the magnetization difference ΔM caused by perfusion. **Middle row:** PASL labels a slab of blood in the neck region at a single instance of time (10-15ms) after which the PLD is inserted before acquisition. To get a well-defined bolus duration in a PASL experiment, a QUIPSSII saturation pulse can be applied within the label region. It has to be applied before the trailing edge of the bolus leave the label region, e.g. at 500ms depicted in the figure. **Bottom row:** VSASL or AccASL labels blood above a certain velocity or acceleration threshold, respectively. Thereby, the labeling also occurs within the imaging region itself, resulting in a very short arterial transit time. In these techniques, the label module cause a saturation, rather than an inversion. Throughout the figure: blue arrow represents non-inverted blood while red arrows or triangles represents inverted and saturated blood, respectively. Red areas are the spatial selective regions while the green area is the imaging region.

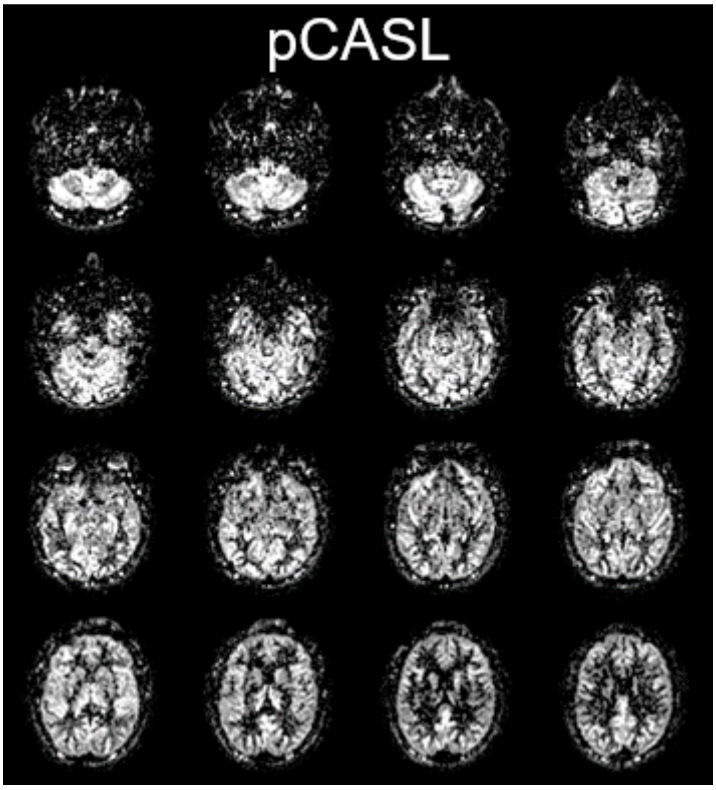

Fig. 2. Example of the resulting ΔM perfusion maps obtained using the pCASL sequence in a healthy volunteer.

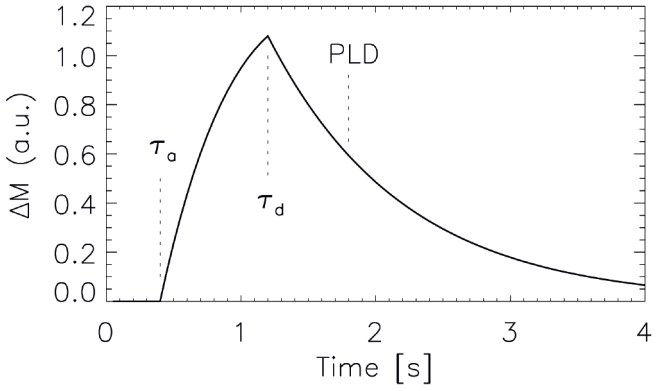

Fig. 3. A kinetic model for PASL assuming fast exchange and therefore a single well-mixed compartment. Having acquired data from multiple PLDs, the cerebral blood flow (CBF), arterial transit time (ATT, marked as τ_a in the figure) as well as the bolus duration (τ_d-τ_a) can be fitted using Eq. 7. If only a single PLD is acquired, one aims at placing it late enough to ensure that the entire bolus has arrived and Eq. 9 is subsequently used for quantification.

A large range of ASL techniques are described in the literature, but they can essentially be categorized into four main types based on how they spatially label the blood. The four types are 1) Continuous ASL, a plane-selective method, 2) Pulsed ASL, a slab-selective method, 3) Velocity and Acceleration selective ASL which are vascular-selective and finally 4) Territorial ASL which is vessel-selective. They will be discussed in detail next, but regardless of the chosen labeling approach, the readout scheme used and whether a single or multiple PLDs are sampled is not different between the methods.

3.1 Continuous ASL (plane-selective)

The first labeling category is called continuous ASL or CASL. As the name suggests, the inflowing blood is continuously labelled in a label plane below the imaging region (Figure 1). It is based on a continuous flow-driven adiabatic inversion of the blood water while it passes the label plane, a method that was previously used for angiography (Dixon *et al.*, 1986). Subsequently it was applied as a method for non-invasive perfusion imaging (Williams *et al.*, 1992), the first of its kind. The typical CASL sequence applies a continuous low amplitude radiofrequency (RF) pulse while applying a magnetic field gradient in the flow direction. By optimizing the RF amplitude and gradient strength such that they match the average flow velocity of the feeding vessel, a labelling efficiency α, in the range of 70– 90% (Zhang *et al.*, 1993; Trampel *et al.*, 2004) can be obtained. A typical label duration is 1.5 to 2 seconds, after which a PLD of a similar duration is applied, to ensure that the trailing edge of the generated bolus will arrive to the tissue before the readout. However, with respect to the image slice, such a long off-resonance labelling pulse causes saturation of the macromolecular pool within the image region, similarly to magnetization transfer (MT) imaging (Henkelman *et al.*, 1993). If this effect is not entirely replicated in the control experiment, the artificial signal intensity difference caused by magnetization transfer will cause an over estimation of the perfusion. Various approaches have been proposed to overcome this, ranging from the use of localized labeling coils to the application of two closely spaced inversion planes during the control experiment. Small external labeling coils with a limited RF field only covering the feeding vessels of the neck, avoid MT effects within the brain region (Zhang *et al.*, 1995). On the other hand, the double adiabatic inversion approach (Alsop and Detre, 1998) aims at keeping the inflowing blood untouched by inverting and reinverting the blood while at the same time keeping the RF power and frequency offset similar to that of the label experiment. Still, CASL provokes issues with the RF amplifiers and the application of long lasting pulses at a 100% duty cycle. Recently an elegant solution to this was proposed (Dai *et al.*, 2008). It is called pseudo continuous ASL or pCASL and it relies on an RF pulse train in combination with varying gradients which together ensure the same flow-driven adiabatic inversion as in the CASL ex-

periment. A great benefit besides the more amplifier-friendly duty cycle, is the fact that the control experiment is achieved simply by switching the polarity of every other pulse in the pulse label train (Figure 4a). This ensures similar magnetization transfer effects between the label and control experiment while leaving the inflowing blood undisturbed. For these reasons, this technique has attracted great interest and it is without doubt the preferred ASL technique today.

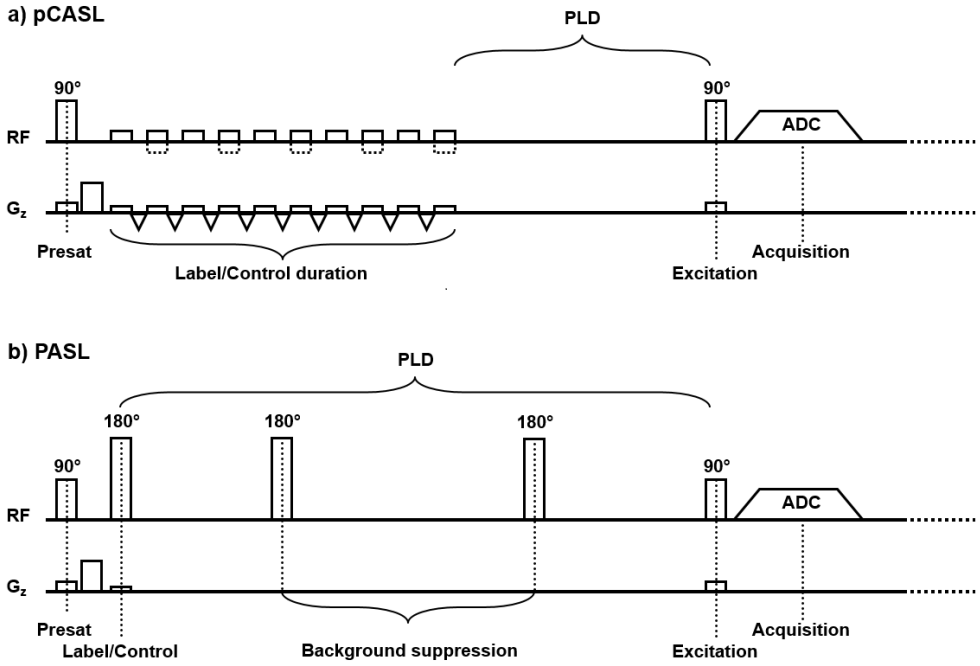

Fig. 4. a) Schematic of the pCASL sequence, which starts with a pre-saturation of the image region to avoid any spin history. Subsequently a train of pulses and gradients that ensure a flow driven adiabatic inversion of the blood passing the label plane performs the pseudo-continuous labeling. For the control experiment, every other pulse phase is toggled by 180° (dotted lines in the pulse train) to cancel the labeling while keeping magnetization transfer effects similar to the label experiment. Then the post labeling delay (PLD) is added before the final excitation and readout (ADC = Analogue to Digital Conversion). b) Schematic of the PASL sequence. Again, a pre-saturation is applied to the image region prior to labeling which is done using an approximately 10 cm wide slab selective inversion in the neck region. The control experiment does not invert the blood, but it aims to keep the magnetization transfer effects similar in the two experiments. In the PASL sequence, two global selective background suppression pulses are displayed which aim at nulling the static tissue signal of e.g. gray and white matter at the time of the excitation pulse, while keeping the ΔM signal undisturbed. This can also be applied in the pCASL sequence and it is an efficient technique to make the sequence more robust to motion and physiological noise. Using background suppression, it is ideally only the perfusion-weighted signal, ΔM, which is measured and therefore subtraction issues originating from the static tissue are avoided.

3.2 Pulsed ASL (slab-selective)

The second labeling category is called pulsed ASL or PASL. Here a slab of typically 10-15 cm of blood is inverted in the neck region at a single instance in time (Figure 1), often using an adiabatic slab-selective inversion pulse (Edelman *et al.*, 1994). Depending on the velocity of the blood in the feeding vessels, the generated bolus has a typical temporal duration of 0.5 to 0.8s, but contrary to CASL, the exact duration is not known. Subsequently, a PLD of a similar duration as used in CASL is applied, to ensure that the trailing edge of the generated bolus will arrive to the tissue before the readout (Figure 4b). Again, off-resonance labeling pulses cause saturation of the signal in the imaging region through magnetization transfer; therefore, the control experiment has to be matched in this regard, similar to the CASL sequence. In fact, the wide variety of PASL sequences described in the literature (E. T. Petersen *et al.*, 2006) mainly differ in how they deal with this compensation. Two main PASL labeling approaches exist. One uses the original slab selection proximal to the image slices proposed by (Edelman *et al.*, 1994), which since has been refined in many versions to circumvent MT issues (Wong *et al.*, 1997; Golay *et al.*, 1999). The second approach, proposed independently by two groups (Kim, 1995; Kwong *et al.*, 1995), centers both the label and inversion slab directly on the image region. By only varying the slab thickness between the label and control experiment, the MT effects cancel out. In today's PASL sequences, the MT effect is however negligible due to the application of a pre-saturation pulse scheme which saturates the static tissue in the imaging region prior to the labeling pulse.

Compared to the CASL sequences, PASL typically obtains a higher inversion efficiency of above 95%. However, the bolus duration is limited by the inversion slab thickness and the blood velocity in the arteries. A slab thickness above 15cm is typically not feasible due to the physical extent of the body coil used for labeling. In addition, unlike in CASL where the bolus is generated in a narrow plane, in PASL the trailing edge of the bolus travels longer than the leading edge, resulting in additional T_1 relaxation of the inverted blood. Altogether, this results in CASL being superior to PASL in terms of SNR. PASL did have some advantage over CASL in terms of ease of implementation, but the popularity of PASL was waned since the introduction of pCASL which is just as easy to implement on the existing scanner hardware as PASL. However, as we will see in later sections, there are some benefits of PASL when it comes to sampling at multiple time-points.

3.3 Velocity and Acceleration selective ASL (vascular-selective)

The third labeling category is not spatially selective in the traditional sense, but rather, the labeling depends on the motion of the blood within the vasculature

(Figure 1). Two such approaches exist, the first one being velocity selective ASL or VSASL, where the blood moving faster than a predefined velocity threshold – typically set in the range of 1-4 cm/s – is saturated by a velocity selective labeling pulse (Wong *et al.*, 2006; Wu and Wong, 2007). During the control experiment, a similar velocity selective labeling pulse module is applied but with a very high or infinite velocity threshold. This causes all the blood to remain undisturbed, while still compensating for direct saturation effects caused by the pulses. An appropriate post labeling delay is applied before the readout as in CASL and PASL. The generated label has approximately half the amplitude as compared to CASL and PASL due to a saturation effect rather than an inversion, which would result in a lower SNR in the perfusion estimates. However, VSASL has the great advantage of labeling inside the image region itself, which means that the bolus arrives to the tissue roughly instantaneously after labeling. The very short arterial transit time (ATT) minimizes the T_1 relaxation of the blood bolus prior to arrival to the tissue. As a result, SNR is gained as compared to CASL and PASL where ATTs up to 1s are commonly observed. In healthy volunteers, VSASL has a performance just below pCASL whereas in patients with long ATT, VSASL outperforms pCASL (Qiu *et al.*, 2012; Schmid *et al.*, 2015).

The second approach works in a similar manner; however, instead of targeting the velocity, it is the acceleration and/or the deceleration of the moving blood that determines the saturation effect. Acceleration selective ASL or AccASL thereby targets both the accelerating and decelerating blood caused by the cardiac cycle, but also velocity changes caused by anatomical changes of the vasculature (Schmid *et al.*, 2014, 2016). Such deceleration exists for instance at the transition from arterioles down to the capillaries, where the blood flow slows down to very low velocities. This technique seems to label the blood even closer to the tissue than VSASL while still labeling the larger vasculature (Schmid *et al.*, 2016) resulting in an increased SNR as compared to VSASL. While the initial AccASL studies looked promising (Schmid *et al.*, 2014, 2015, 2016), with regards to SNR, further studies are needed to establish CBF estimation accuracy.

The MRI vendors do currently not provide VSASL or AccASL sequences, but processing can be done using existing processing pipelines described below.

3.4 Territorial ASL (vessel-selective)

The fourth and last labeling category is aimed at labeling the individual feeding blood vessels to obtain information about the extent of the perfusion territories they feed (Hartkamp *et al.*, 2013). As such, territorial ASL or TASL provides direct clinical information about cerebral blood flow as well as about changes in the perfu-

sion territories. These changes can for example occur as a result of arteriosclerosis obstructing a vessel. The original approach was based on PASL with a dedicated pencil beam (Davies and Jezzard, 2003) or selection slab (Hendrikse *et al.*, 2004) covering the vessel of interest. More recently, the pCASL labeling scheme was adapted to allow a sinusoidal spatial variation of the labeling efficiency within the pCASL labeling plane (Wong, 2007). Flow territory maps of the brain's main feeding vessels can be generated by scanning a series of different orientations and spatial frequencies (Figure 5). This method has also been adapted for selective labeling of a single vessel at a time, even inside the brain (Helle *et al.*, 2010), based on an earlier CASL approach using similar principles (Werner *et al.*, 2005). The MRI vendors does currently not provide TASL sequences and processing of territorial data is done using own tools or tools made available by the provider of the sequence.

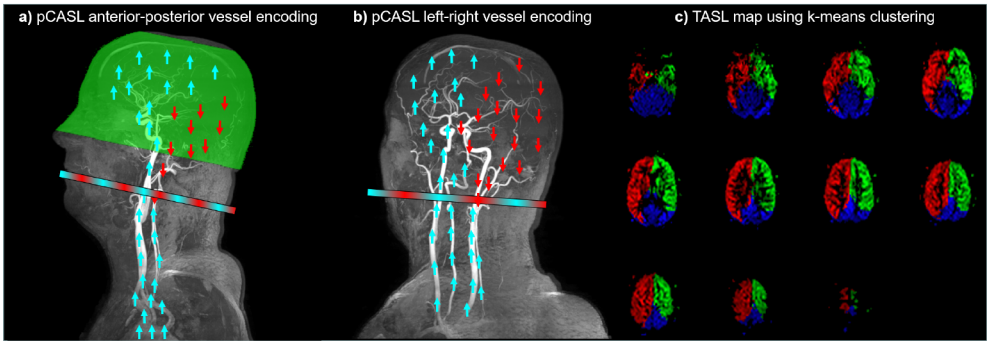

Fig. 5. By applying time varying gradients within the labeling plane during the pCASL labeling train, spatially varying (sinusoidal) label efficiency is achieved. a) Encoding in anterior-posterior direction allows labeling of the vertebral arteries while keeping the carotids unaffected. b) Encoding in left-right direction allows labeling of the right carotid and vertebral artery, while the left side is kept undisturbed. c) Territorial ASL map based on k-means clustering of three different encoding directions as well as the standard label and control. This combination allows robust planning free TASL.

3.5 Controlling the acquired ASL signal

All the above-mentioned labeling categories have the freedom to choose any readout method available, to scan with or without vascular signal crushers, or to scan with or without background suppression. An overview of the recommended acquisition parameters for a basic ASL study in both healthy and patients are provided in Table 1. Following these guidelines will ensure data acquisition in line with the recommendations from the current ASL consensus paper (Alsop *et al.*, 2015). Several software packages are available for ASL processing, including FSL-BASIL (Chappell *et al.*, 2009), and the MATLAB based ASLtbx (Wang *et al.*, 2008) and the ASAP toolbox (Mato Abad *et al.*, 2016). These can directly deal with quantification of pCASL and PASL data and adjusted to process VSASL and AccASL data.

Table 1. Suggested acquisition parameters

Parameter	What and why
Field strength	**3T** if available because it provides higher SNR than 1.5T, and in addition the T_1 of blood is longer at higher field strength which also improves the SNR.
Hardware	**Body coil** for RF transmission. **Parallel imaging** using 8 or more receive coils for a fast read-out with a typical speed up factor of 2-3.
Sequence	**pCASL** because it is made available by all vendors and it is the current workhorse for ASL due to a very good SNR. If possible to adjust, one should aim at an average labeling gradient of 1 mT/m, a slice-selective labeling gradient of 10 mT/m and an average B_1 of 1.5 mT. For quantification, one needs a proton density weighted or M_0 map in addition to the actual ASL scan. This is typically a scan without labeling, with a long TR (>5s) and otherwise using the same matrix, TE etc. as in the pCASL scan, to keep the distortions the same in the two images.
Label Duration	A label duration of **1800 ms** is recommended.
Post Labeling Delay	The **PLD** should be long enough for the labeled blood water to reach the tissue, yet short enough to avoid an unacceptable signal loss due to T_1 decay of the blood. For clinical scanning, a PLD of **2000 ms** is recommended, while it can be reduced to **1800 ms** in healthy adult subjects below 70 years of age, if needed. Multiple PLDs enable determination of ATT.
Background suppression	Background suppression is strongly **recommended**, because it reduces noise from, for example, motion. However, always remember to acquire an M_0 scan without background suppression for the subsequent quantification.
Spatial resolution	**3-4 mm** in plane resolution with a slice thickness of **4-8 mm for sufficient SNR.**
Readout	**3D** gradient echo and spin echo**, 3D** stack of spirals or **multi-slice 2D EPI**. 3D multi-shot (4 or more shots) sequences are often preferred for standard clinical assessment. Multi-slice EPI is recommended for functional ASL studies because the readout matches the often-accompanied BOLD acquisition and they can be done as single shot, that is, within each TR. In fact, the control image can provide simultaneous BOLD contrast if background suppression is switched off. Current single-shot 3D readout options have an unacceptable point-spread function for any clinical or functional evaluation. Both the TR and TE should be chosen shortest possible for the given sequence.
Planning of the labeling plane	Often the label plane is fixed at a predefined distance below the image stack. If possible, the labeling plane should be placed perpendicular to the feeding arteries (carotid and vertebral arteries) with the aid of a fast phase contrast angiogram.

SNR = signal-to-noise ratio; RF = radiofrequency; ASL = arterial spin labelling; pCASL = pseudo-continuous ASL; ATT = arterial transit time; EPI = echo planar imaging; BOLD = blood oxygen level dependent.

3.5.1 Background suppression

ASL considers difference images DM, where the signal is in the order of 1% of the equilibrium signal of the tissue. The small DM introduces a challenge to avoid artifacts in the form of severe subtraction errors should the subject move even slightly between subsequent label and control acquisitions. These typically manifest as very high inten-

sity signals at the edge of the brain, but also between interfaces of different tissues. Four solutions exist:

1) *Prospective motion correction*, which updates the image slab in the event of motion. This is available as a navigator based approach or with external tracking, e.g. using optics.

2) *Retrospective motion correction*, where the volumes are realigned before the subtraction is more common and it is included in most processing pipelines. A limitation is that small disturbances in the deformation and steady-state signal still exist between the corrected label-control pairs, in particular where 2D multi-slice readout is used. In addition, for 3D sequences where multiple shots typically are used to fill the entire k-space, the impact of motion occurs within the volume acquisition which makes retrospective correction impossible.

3) *Background suppression* offers a robust solution for this issue. By nulling the static tissue signal at the time of the readout (Dixon *et al.*, 1991), only the DM signal is sampled, making the technique much more robust to motion and physiological noise (Ye, Frank, *et al.*, 2000). Motion will in this case blur the resulting DM map, rather than destroying it with severe motion artifacts. The principle relies on the application of up to several global inversion pulses applied appropriately during the post labeling delay as depicted in Figure 4b. Each inversion pulse allows the suppression of one tissue type or T_1 value. This technique turns out to be crucial for segmented 3D acquisitions in ASL. While prospective motion correction can be combined with background suppression, retrospective motion correction has limited success due to the very low signal intensity in suppressed images.

4) Outlier detection methods are typically part of the ASL processing pipeline where the control-label pairs that are considered outliers are discarded. This could be based on temporal signal variation, but it can also be based on the magnitude of rotation and translation obtained from the retrospective motion correction. This enables rescue of datasets where severe artifacts contaminated a few subtraction pairs and which otherwise would render the overall perfusion image useless if they were included in the average.

3.5.2 Bolus saturation

For the PASL, VSASL and AccASL labeling schemes, we do not have control over the temporal duration of the bolus, as it is the case in CASL where it is predefined. This poses a problem when we subsequently want to quantify CBF, because an unknown bolus duration will introduce an error in the estimate. Therefore, these techniques should employ bolus saturation schemes that, after a predefined time from labeling, cut off the trailing edge of the bolus. In PASL a well-defined bolus duration is assured by ap-

plying a saturation slab within the label region approximately 5-800ms after labeling (or control) assuming that all the feeding vessels still contained label inside the saturation region at the time it was applied. In Figure 1 middle row, it would correspond to the application of a saturation of the red label region at around 500ms after labeling. This is often referred to as QUIPSSII (Wong *et al.*, 1998). A similar approach can be applied for VSASL and AccASL. However here it is the actual label module which is applied to saturate the blood in both the label and the control experiment. If multiple PLDs is acquired, an alternative to the bolus saturation schemes is to fit the bolus duration as a parameter in the fit as will be discussed later.

3.5.3 Vascular crushers

In addition to motion and physiological noise, another artifact needs consideration at the time of acquisition. It is the potential signal contamination from the feeding arterial vessels. The definition of perfusion is the blood delivery rate to the tissue's capillary bed and, as such, it does not include the signal from the larger arterial vessels, which may or may not feed other regions outside the observed voxel. Arterial signal contamination can be limited by choosing a post labeling delay long enough to ensure that the blood has cleared from the arterial compartment by the time of acquisition. However, if the CBF quantification relies on data from multiple PLDs it would often be necessary to spoil the arterial signal, which is especially prominent at short PLDs. This is done by applying bipolar crusher gradients, which dephase the signal in faster moving vessels based on their velocity (Ye *et al.*, 1997). They are typically applied right after the excitation pulse and prior to the readout. Alternatively, it can be a dedicated crusher module similarly to the label module of VSASL, which is applied prior to the excitation pulse for both the label and the control experiment. An alternative is to keep the vascular signal and include it into the kinetic model (Chappell *et al.*, 2009).

3.5.4 The readout

The chosen readout is independent of the labeling scheme and the choice therefore relates to questions such as what resolution is needed and what underlying point-spread function is allowed. This again needs to be considered with respect to overall SNR, whether vascular crushers are needed and whether multiple readouts are needed within each repetition time.

The traditional readouts were multi slice 2D echo planar imaging (EPI) and spiral, which both have the ability of whole brain coverage in a very short time of 400-600ms. These techniques have the benefit that vascular crushers are easily implemented between the excitation and the readout. As well, they allow repeated low flip-angle readouts, also called a Look-Locker readout. The Look-Locker readout enables the acquisition of multiple PLDs within each repetition time (TR) (Günther *et al.*, 2001), which facilitates fitting of the entire kinetic curve (Figure 3). This approach is most feasible for PASL be-

cause here the labeling takes place in the order of few milliseconds and as a result the sampling can start before the label arrives to the image region. Recently, the fast 3D readout sequences, including 3D gradient echo and spin echo (Günther *et al.*, 2005) and 3D stack-of-spirals (Ye, Frank, *et al.*, 2000), have gained great popularity, because they offer improved SNR and reduced susceptibility artifacts compared to 2D EPI readouts. They rely on interleaving an EPI or a spiral readout, respectively, within a turbo-spin-echo readout. The benefit is a large SNR due to the larger 3D excitation volume rather than single slices. A benefit of these particular 3D sequences over other 3D sequences such as fast spin echo and gradient echo is that the time of excitation is well defined at the point of the initial 90° excitation pulse. This not only makes quantification easier, but it also enhances the effect of background suppression that is critical for these sequences. To avoid excessive blurring, the acquisition is split into 4-8 segments. Even a small degree of motion between these different segments acquired several seconds apart would cause severe image artifacts, was it not for background suppression.

4 Arterial Spin Labeling: quantification

4.1 Kinetic modelling approaches

Having acquired the ASL images with appropriate sequence parameters, that is, without contamination from magnetization transfer, vascular artifacts or motion as discussed above, we are left with a perfusion weighted image ΔM. To convert it to a quantitative measure of cerebral blood flow in [ml/100g/min] we need to apply some sort of kinetic modeling, because ΔM's relation to perfusion depends on various other local and global parameters. These include arrival time, tissue relaxation parameters of both blood and tissue as well as their equilibrium magnetization, bolus duration and inversion efficiency. The complexity of the applied model also needs to be considered in relation to the data acquired, e.g. whether multiple PLDs or only a single PLD were sampled and so forth.

4.1.1 Single compartment

The simplest and most common approach is to view the ASL signal as originating from a single compartment system, that is, the situation where the labeled blood exchanges instantaneously with the tissue compartment upon arrival to the capillary bed. The Bloch equation describing the change in MR signal over time can then be modified to:

$$\frac{dM_t(t)}{dt} = \frac{M_{t,0} - M_t(t)}{T_{1t}} + CBF \cdot \left(M_a(t) - M_v(t)\right) \quad \text{[eq 4]}$$

where M_t, $M_{t,0}$, M_a and M_v are the tissue-, equilibrium-, arterial- and venous-magnetiza-

tion, respectively, and T_{1t} is the relaxation time of the tissue. Because we assume a fast exchange regime, M_v is equal to the tissue magnetization corrected by differences in the water content also described by the blood-brain partition coefficient I, such that $M_v = M_t/I$. Notice the similarity of Eq. [4] to Eq. [1] and, indeed, when considering the water as freely diffusible, ASL quantification is similar to the early nitrous oxide method with the main difference being that ASL quantification is done on a voxel wise basis rather than as a whole brain measure. Many elaborate analytical solutions have been proposed over the years (Kwong *et al.*, 1995; Calamante *et al.*, 1996) for converting DM into CBF, taking into account differences in T_1 between tissue and blood, accounting for the arterial transit time t_a and the actual bolus duration t_b.

Buxton's model is a general kinetic model for ASL (Buxton *et al.*, 1998), which describes DM based on the convolution integral in Eq. [2] and it includes the effect of T_1 decay:

$$\Delta M(t) = 2 \cdot M_{a,0} \cdot CBF \cdot \int_0^t c(\tau) r(t-\tau) m(t-\tau) d\tau \quad \text{[eq 5]}$$

where $M_{0,a}$ is the equilibrium magnetization in a blood filled voxel, *c(t)* is the delivery function or fractional arterial input function (AIF), *r(t-t)* is the residue function describing the fraction of labeled spins arriving to a voxel at time *t*, that still remains within the voxel at time *t*. The magnetization relaxation term *m(t-t)* quantifies the longitudinal magnetization fraction of labeled spins arriving to the voxel at time *t* that remains at time *t*. Solving this for PASL and assuming single compartment kinetics and plug flow is done by setting:

$$c(t) = \begin{cases} 0, & t < \tau_a \\ \alpha \bullet e^{-t \cdot R_{1a}}, & \tau_a \le t < \tau_d \\ 0, & t \ge \tau_d \end{cases}$$

$$r(t) = e^{-\frac{t \cdot CBF}{\lambda}}$$

$$m(t) = e^{-t \cdot R_{1t}} \quad \text{[eq 6]}$$

where R_{1a} and R_{1t} are the relaxation rates for arterial blood and tissue, respectively and a is the inversion efficiency. The trailing edge t_d of the bolus is equal to the arterial transit time t_a plus the bolus duration t_b. This result in a stepwise-defined function:

$$\Delta M(t) = \begin{cases} 0, & t < \tau_a \\ \dfrac{-2 \cdot \alpha \cdot M_{a,0} \cdot CBF}{\delta R} \cdot e^{-t \cdot R_{1a}} \cdot (1 - e^{(t-\tau_a) \cdot \delta R}), & \tau_a \le t < \tau_d \\ \dfrac{-2 \cdot \alpha \cdot M_{a,0} \cdot CBF}{\delta R} \cdot e^{-\tau_d \cdot R_{1a}} \cdot (1 - e^{\tau_b \cdot \delta R}) \cdot e^{-(t-\tau_d) \cdot R_{1app}}, & t \ge \tau_d \end{cases}$$

[eq 7]

where , $dR = R_{1a} - R_{1app}$ and $R_{1app} = R_{1t} + CBF/l$, also called the apparent tissue relaxation rate. If one wants to solve it for CASL, then c(t) in Eq. [6] simply lacks the additional T_1 decay during the bolus duration, that is, $\alpha \cdot e^{-t \cdot R1a}$ becomes $\alpha \cdot e^{-taR1a}$. If multiple post labeling delays are sampled, this would be the simplest kinetic model to fit and as it can be seen, various parameters such as the arterial transit time t_a, blood-tissue partition coefficient l, $M_{a,0}$, R_{1a} and R_{1t} all need to be estimated or measured in order to obtain quantitative CBF values.

Nevertheless, most clinical ASL examinations today are performed using pCASL or PASL at a single PLD. The current consensus (Alsop *et al.*, 2015) is to simplify the quantification to:

$$\mathrm{CBF} = \frac{6000 \cdot \lambda \cdot \Delta M \cdot e^{PLD \cdot R_{1a}}}{2 \cdot \alpha \cdot T_{1a} \cdot M_{t,0} \cdot (1 - e^{-\tau_b \cdot R_{1a}})} \quad \text{[eq 8]}$$

and

$$\frac{6000 \cdot \lambda \cdot \Delta M \cdot e^{PLD \cdot R_{1a}}}{2 \cdot \alpha \cdot \tau_b \cdot M_{t,0}} \text{ [ml/100g/min] for PASL [9]}$$

In this approach, it is assumed that the label only decays with T_1 of blood and that no blood leaves the voxel. This means, that we consider it as a slow exchange system and, correspondingly, that blood stays in the vascular bed during the experimental time of an ASL experiment of a few seconds. Even if exchange of the label to the tissue occurs, the introduced errors due to differences in T_1 are expected to be small, in grey matter at least (Parkes and Tofts, 2002). . By ensuring that the PLD is rather long, on the order of 2 s, one can assume that there will be negligible error due to unknown arterial transit time, for a relatively normal range of transit times (i.e. < 2 s) seen in most subjects not suffering from vascular disease. If the transit times are abnormally long due to pathology, CBF quantification will lose accuracy. On perfusion maps this is reflected by the presence of vascular artifacts. The factor of 6000 ensures the conversion from

[ml/g/s] into the usual [ml/100g/min].

4.1.2 Multi compartment

Aquaporin water channels selectively transfer water molecules back and forth through the blood-brain-barrier or the capillary wall. This causes a restricted exchange of the labeled water from the vasculature to the tissue, and a single compartment model may not be the best description of the system. In practice, it means that the water remains longer in the vasculature and as a result the signal decays with T_1 of blood rather than that of tissue for a longer period of time. This results in an underestimation of CBF. Various flavors of multi-compartment approaches have been proposed to correct for the effect of restricted permeability (St Lawrence *et al.*, 2000; Zhou *et al.*, 2001; Parkes and Tofts, 2002). The system then has a permeability-surface product incorporated in a two or more compartment system, much like for dynamic contrast enhanced perfusion imaging (Tofts and Kermode, 1991). In general, the biggest limitation of these more advanced kinetic models is that they require data at several different PLDs with a good SNR in order to fit the additional parameters. This is currently hard to achieve within clinically realistic scanning times and the approaches are therefore rarely used in clinical studies. Nevertheless, these techniques will potentially become more feasible and maybe even necessary for accurate CBF quantification at ultra-high field of 7T or above where the SNR is increased and the T_1 and T_2 relaxation parameters differ more between arterial and venous blood compared to 1.5T and 3T.

4.1.3 Model free

An alternative to kinetic modeling is to use a sampling scheme where both the tissue signal curve and the arterial input curve is acquired (Esben Thade Petersen *et al.*, 2006). This offers information about the arterial input function or $2 \cdot M_{a,0} \cdot c(t)$ in Eq. 5, while having acquired the tissue signal DM(t) permits to calculate the tissue residue function r(t)m(t) in Eq. 5 by means of deconvolution. This is similar to the dynamic susceptibility contrast perfusion method (Ostergaard *et al.*, 1996) where CBF is extracted from the peak of the resulting residue function, knowing that r(0)m(0) equals 1 by definition. A great advantage of this 'model free' approach is the fact that no prior assumptions about the underlying kinetic modeling, such as whether a single or multiple compartment system is needed.

In arterial spin labeling, the AIF can be extracted locally by considering the arterial signal on a voxel-by-voxel basis. This is achieved by interleaving two ASL experiments with acquisition at multiple PLDs, one with and one without vascular crushers. The extraction of AIF comes at the cost of a 33% increase in acquisition time due to the combination of two experiments (Esben Thade Petersen *et al.*, 2006; Petersen *et al.*, 2010). In the non-crushed experiment, the difference signal $DM_{ncr}(t)$ consists of the tissue signal DM(t) plus $DM_{art}(t)$ which is the arterial contribution in a given voxel. The

crushed experiment, on the other hand gives a difference signal DM_{cr} which is equal to the desired tissue signal DM(t). The needed information $2 \cdot M_{a,0} \cdot c(t)$ therefore lays in $DM_{art}(t)$ which is isolated through subtraction ($DM_{ncr}(t) - DM_{cr}(t)$). Because $DM_{art}(t)$ originates from the arterial blood volume (aBV) and not a pure arterial voxel as expected for $2 \cdot M_{a,0} \cdot c(t)$, a scaling of the area under the curve is needed. The sequence used, is a PASL sequence with QUIPSSII bolus saturation and a Look-Locker multi PLD readout. In this sequence the bolus area is known to be $2 \cdot M_{a,0} \cdot a \cdot t_b$ and scaling can therefore be done accordingly prior to the deconvolution. It also facilitates the assessment of the aBV on a voxel-by-voxel basis using the relationship:

$$aBV = \frac{\int_0^\infty \cdot M_{art}(t) \cdot e^{t/T_{1a}} dt}{2 \cdot M_{a,0} \cdot \tau_b \cdot \alpha} \quad \text{[eq 10]}$$

This technique gives additional information to CBF in the form of aBV and ATT, which can be extracted from the multiple PLD acquisition, as we will see below.

4.2 Parameter estimation

For perfusion quantification, we need knowledge about other parameters than the initially acquired DM, such as the equilibrium magnetization, bolus shape and arrival time, all depending on the complexity of the kinetic modeling in use. Table 2 highlights the usual processing steps which are used and the typical parameters assumptions used for quantification.

4.2.1 Blood and tissue equilibrium magnetization and relaxation times

Regardless of the chosen labeling scheme and modelling approach, the amplitude of the equilibrium magnetization $M_{a,0}$ is always required for absolute quantification. It can in theory be extracted from a 100% blood filled voxel; however, due to a typically low and unknown blood fraction within the individual voxels it is hard to extract in practice. Instead, we typically measure tissue proton density, and we rely on the known differences between the water content of blood and tissue, which is the blood-brain partition coefficient l, giving the relationship $M_{a,0} = M_{t,0}/l$. The tissue proton density or equilibrium magnetization is easy to estimate from a scan with a long repetition time and otherwise similar readout as for the ASL acquisition. The currently used blood-brain partition coefficient was established by H_2O^{15} PET (Herscovitch and Raichle, 1985) with whole brain l=0.9 ml/g, gray matter l_g=0.98 ml/g and white matter l_w=0.82. Typically, the single whole brain value is used, as tissue classification is not always available and it has been shown that spatial variation exists also within a single tissue type (Roberts *et al.*, 1996). Although $M_{a,0}$ ought to be a single global parameter, this method will have a spatial variation depending on $M_{t,0}$. This turns out to be a benefit, because it automat-

ically includes correction for differences in coil sensitivity and other inhomogeneities across the brain which otherwise would need to be corrected separately. An alternative approach is to use a global $M_{t,0}$ and l which essentially would avoid the error due to the spatial variation in lambda. However, it will not correct the coil inhomogeneities, which differs between scanners and scan sessions and therefore is harder to control, making the former approach the preferred method of choice.

Having established $M_{a,0}$ by assuming l and measuring $M_{t,0}$, the relaxation time of blood T_{1a} is likewise needed for any quantification. Most often, it is taken as a general value across the population with a value of 1650ms at 3T (Alsop *et al.*, 2015). This approach does, in fact, introduce an error because it depends on the subject's current hematocrit (Varela *et al.*, 2011; Zhang *et al.*, 2013; De Vis *et al.*, 2014). Therefore, a better approach is to measure T_1 of blood in the individual subjects using a separate scan, or if blood samples exist, convert hematocrit into T_{1a}. The T_1 of tissue is mainly used in more advanced quantification schemes with several PLD, where information about both $M_{t,0}$ and T_{1t} automatically exists. If background suppression is used, both parameters must be extracted from a separate scan.

4.2.2 Arterial transit time (ATT)

The actual time it takes for the blood to travel from the label region to the voxel of interest is called the arterial transit time (ATT) or t_a in the formulas above. In multiple PLD acquisition it is fitted as part of the quantification, using e.g. Eq. 7, but it can also be estimated by searching for the rising edge of the tissue curve. In the single PLD methods it is impossible to estimate ATT and one relies on acquisition at long PLDs assumed to be longer than both the bolus duration t_b and ATT together. In such case, the error is be negligible, as compared to the general errors from other sources such as in the estimates of $M_{a,0}$ and T_{1a}.

4.2.3 Bolus shape, dispersion and decay

The shape of the bolus or AIF has an impact on the quantification. In this case, it is mainly the multi PLD methods that are sensitive to dispersion of the bolus, whereas the single PLD methods are relatively insensitive, as long as the condition PLD > $t_a + t_b$ is fulfilled. Dispersion models can be integrated in the kinetic model fit (Hrabe and Lewis, 2004), and in the model free approach the shape is measured in all voxels with a large enough aBV (Esben Thade Petersen *et al.*, 2006).

5 Arterial Spin Labeling: applications

Arterial Spin Labeling has gained great popularity as a research tool, in particular within the field of neuroscience. Recently, robust techniques such as the pCASL sequence have become generally available on most systems, either as a clinical package from the

vendor or as shared sequences between research sites. This has allowed researchers to add valuable perfusion information to their studies in addition to the standard structural and functional images by adding a few minutes long ASL scan. In the following section, we will revisit some of these applications ranging from basic neuroscience to clinical studies. It is not an exhaustive list as there are more than 2000 ASL publications registered in PubMed today (2017) and the numbers are rapidly increasing.

5.1 Neuroscience

The complete noninvasiveness of ASL makes it a preferable choice for monitoring perfusion changes in many neuroscience applications. Neuronal activation, which particularly increases cerebral metabolic rate of oxygen ($CMRO_2$), is accompanied by a regional increase in CBF to ensure sufficient supply of oxygen to the mitochondria. The classical method for mapping neuronal activation with MRI is called blood oxygen level dependent (BOLD) contrast (Ogawa *et al.*, 1990). As the name suggests, the observed signal changes due to neuronal activation result from T_2^* changes caused by alterations in blood oxygen saturation within the voxel. Changes in the oxygen saturation originate from a complex interplay of changes in $CMRO_2$, CBF and CBV and hence the BOLD signal is hard to interpret. Arterial spin labeling can likewise detect neuronal activation by quantitatively measuring the regional CBF changes. The quantitative aspect makes functional ASL more reproducible over time and between subjects than BOLD (Detre and Wang, 2002; Wang, Aguirre, *et al.*, 2003). Also, the signal is better localized to the activated area (Duong *et al.*, 2001) as opposed to BOLD, where strong signal changes also occur in draining venous vessels further away from the activated region although this effect is field strength dependent. Neuronal activation paradigms have many flavors with the simplest being a block design, meaning with repeated "on" and "off" conditions of up to several minutes in length and where the activation could consist of a simple visual checkerboard or finger tapping, or far more complex cognitive paradigms. A continuous signal sampling is therefore required for the subsequent regression analysis and, similar to BOLD, this can be done for ASL by analyzing subsequent control-label pairs. Contrary to BOLD, where the optimum block duration is 16s due to drift, then the quantitative nature of ASL makes very long block duration of up to days (Wang, Aguirre, *et al.*, 2003) possible. This allow the study of different cognitive paradigms where there is interest in a certain 'state' that may vary slowly in time or the impact of a slow acting drug.

However, there is a penalty in the temporal resolution compared to BOLD due to the required post labeling delay and the need to collect control-label pairs. Neither BOLD nor ASL directly map the $CMRO_2$ change caused by the neuronal activation. Calibrated BOLD tackles this issue with a new imaging scheme where the two approaches are combined and $DCMRO_2$ is extracted using a biophysical model of the CBF and BOLD

signal (Hoge *et al.*, 1999; Chiarelli *et al.*, 2007; Bulte *et al.*, 2012; J. B. De Vis *et al.*, 2015). An additional global CBF challenge is needed, typically a part where CO_2-enriched air is inhaled causing the baseline CBF to increase while $CMRO_2$ stays more or less constant (Figure 6). A caveat of this approach is the fact that the setup is more complicated and harder to perform in some sensitive subjects and, therefore, efforts are made to simplify the calibration (Blockley *et al.*, 2012) to avoid the hypercapnia challenge.

Arterial spin labeling is therefore becoming an important tool, which helps to disentangle the complex behavior of the brain both for gaining a better understanding of the physiological events accompanying activation but also for the cognitive neuroscience field aiming at a better understanding of how the brain processes events.

5.2 Clinical

Most neuronal diseases carry a perfusion aspect, such as stroke and large vessel disease, dementia, and cancer. For example, Alzheimer's disease is marked by hypoperfusion (Austin *et al.*, 2011) whereas high-grade brain tumors are characterized by hyperperfusion (Dangouloff-Ros *et al.*, 2016). Perfusion images can aid in the diagnosis or follow-up of these pathologies. Moreover, the brain has the most advanced auto regulative system for maintaining sufficient perfusion, at all times, also during neuronal activation (Jill B. De Vis *et al.*, 2015). An example of this is the dilation of blood vessels to increase perfusion in response to hypercapnia (elevated CO_2 levels). ASL provides important complementary information to the standard structural MR images. The pediatric population where ionizing radiation and contrast agents should be avoided where possible is in particular benefitting from ASL. Several studies have been performed in neonates (De Vis *et al.*, 2016) and kids (Oguz *et al.*, 2003; Wang, Licht, *et al.*, 2003; Dangouloff-Ros *et al.*, 2016) with various diseases for whom there are no good alternatives available for a whole brain perfusion assessment, especially for the neonates. Arterial spin labeling has also been applied in aging studies (Parkes *et al.*, 2004; J. B. De Vis *et al.*, 2015) and in neurodegenerative diseases where it becomes increasingly apparent that perfusion plays a significant role (Mak *et al.*, 2012; Fernández-Seara *et al.*, 2015; Leeuwis *et al.*, 2016) and regional differences can easily be detected in group analysis between different diseases. Perfusion is an indirect marker of metabolism and indeed the observed areas of hypoperfusion in these patients agree reasonably well with fluorodeoxyglucose (FDG) PET, a direct measure of metabolism (Haller *et al.*, 2016). However, an ongoing quest is how to sufficiently improve the sensitivity to allow robust discrimination between the subtle variations in perfusion patterns on an individual subject basis, which is needed for clinical diagnosis and disease monitoring (Collij *et al.*, 2016). Another area where ASL has proven versatile is in the field of cerebrovascular diseases where ASL does not only provide perfusion information, but it also provides information regarding the extent of the feeding vascular territories (Hartkamp *et al.*,

2013). If in addition, a scan is performed before and after the injection of acetazolamide (Bokkers *et al.*, 2010), the cerebrovascular reserve can be assessed as well. Therefore, ASL can provide a comprehensive clinical picture of the hemodynamic status of stroke patients (Hernandez *et al.*, 2012; Wang *et al.*, 2013) and patients with large vessel disease (Figure 7) (Chng *et al.*, 2008; Hendrikse *et al.*, 2009; Bokkers *et al.*, 2016). For cancer, ASL can also aid in cancer staging (Yang *et al.*, 2016) and the detection of treatment response. Particularly the challenge of distinguishing between radiation necrosis and recurrent tumor (Ye *et al.*, 2016) are ongoing clinical ASL research topics. Perfusion assessment using ASL is done in many other brain diseases such as epilepsy, migraine and psychiatric disorders and the recent review paper by (Haller *et al.*, 2016) gives a comprehensive overview of current clinical applications of ASL in the brain.

6 Image quality and quantification quality

6.1 Pitfalls

A few things need to be kept in mind when interpreting ASL perfusion maps in the clinic or for research purposes.

First, it must be realized that the generated label has a limited lifespan lasting in the order of a few seconds, whereas a gadolinium tracer does not clear significantly within the typical experimental time of several minutes. The consequence of this will mainly affect images from patients with compromised flow due to a stenosis or an occlusion, which results in collateral perfusion via alternative routes and thereby causes very long transit times. If the ATT is longer than the single acquired PLD, then the region will appear dark or with no perfusion at all, making it impossible to quantify the flow. However, in a clinical setting the information can be combined with diffusion and structural images, usually available in such patients, to help determine if it is a very late arrival or no flow, e.g., due to an infarct. Sequences using multiple PLD are less sensitive to prolongation of ATT. However, the prolongation can be so large that ASL would not stand a chance. In intermediate cases, the signal can appear bright in the larger vasculature, suggesting that it is on its way but at the time of sampling it still did not reach the parenchyma.

Second, motion artifacts can destroy ASL perfusion maps. They are often seen as rings in the periphery of the brain with large intensities. If it is present in the final map and you are still at the scanner, repeat the scan. If offline, inspect the individual label-control pairs to see whether discarding a few pairs where the gross motion occurred potentially can save the data.

Third, if using pCASL, keep an eye on the labeling efficiency. This technique is sensitive

to accurate B_0 in the label region and the vessels should be perpendicular to the label plane. Both can vary between the different target vessels and should reduced flow appear in an entire perfusion territory, be suspicious before drawing your conclusions. Again, try to redo the positioning of the label plane and if possible the shim, too. If the observation persists, compare the perfusion map with other clinical images, particularly an angiogram, to confirm the observed phenomenon.

Last but not least, while it is common practice to use a single hematocrit and therefore T_1 of blood for quantification throughout the population (Alsop *et al.*, 2015), it does mean care should be taken when comparing different populations where the hematocrit varies between the groups. This is particularly problematic in the neonatal population where there are large variations between subjects depending on the time since birth (Varela *et al.*, 2011; De Vis *et al.*, 2014), but also in for example patients with the sickle cell disease (Václavů *et al.*, 2016). Therefore, to obtain quantitative perfusion in these populations, one must assess blood T_1 either directly via MRI or indirectly via a hematocrit measurement from the blood with subsequent conversion into T_1.

6.2 Quality assurance and normal perfusion values

In addition to the factors described above, image quality of ASL images also depends on the functionality of the system and the functionality of the coils. Therefore, regular checks of the system and coils are essential to ensure high quality ASL data. In addition to the weekly vendor specific quality assurance (QA), one should consider a stability test in a standardized phantom such as the one proposed by the FBIRN (Greve *et al.*, 2011). The introduction of up to 64 channel receive coils on clinical systems makes it harder to detect failure of the individual coils and therefore testing the SNR of the individual receive elements over time could be considered, if the system allows it.

Even with a stable system, differences in the quantified perfusion between systems and sequences may still be observed. Scanning the same subjects using the standard vendor provided ASL sequences not only results in differences in the global perfusion values, but they also have spatial variations from region to region (Mutsaerts *et al.*, 2015). This scenario improves by implementing near-identical sequences on the scanners with similar label module, readout and resolution (Mutsaerts *et al.*, 2015), but these sequences are not readily available on all systems. Global perfusion values could be calibrated between ASL sequences, sites and vendors using a gold standard flow phantom for ASL. However, the spatial variations caused by hardware and readout will still be an issue and, similar to other perfusion imaging modalities, the term "normal" perfusion values hardly exist. It is therefore important to acquire a matching control group at each site, also in multi-center studies. In other words, one should determine the "normal" perfusion value for the given set-up. The perfusion values reported in the

literature vary primarily between 30-80 ml/100g/min for gray matter, but it is hard to pinpoint what the value should be even for a given sequence.

Finally, cerebral perfusion depends on a range of factors, including various pathologies, age and gender. Aging is associated with a decline in CBF (Parkes *et al.*, 2004; Liu *et al.*, 2012) and women have been found to have a higher CBF and shorter ATT compared to men (Petersen *et al.*, 2010; Liu *et al.*, 2012). The influence of atrophy is of concern when interpreting data in for instance Alzheimer's patients versus age matched controls, or between young and old subjects. In these cases the question often arises whether a flow reduction is simply due to increased partial volume of CSF, due to general tissue atrophy, or if in fact the gray and white matter perfusion is reduced as well. Methods exist for correcting for partial volume based on structural information (Asllani *et al.*, 2008; Ahlgren *et al.*, 2014); however there is no real consensus on when it should be applied, if at all! In addition, baseline CBF fluctuates and is easily affected by medication and substances such as caffeine, which has been found to decrease whole-brain perfusion by about 20% (Haller *et al.*, 2013).

7 Reproducibility

7.1 Validation and Reproducibility studies

Both for clinical and research purposes, it is important to know how robust the method is and how well it compares to the established methods. For ASL, validation studies have been carried out in animals (Walsh *et al.*, 1994; Ewing *et al.*, 2003) using radioactive microspheres and ^{14}C-iodoantipyrine autoradiography and in humans (Ye, Berman, *et al.*, 2000; Heijtel *et al.*, 2014, 2016; Fan *et al.*, 2016) using PET. Good correlations are observed, both at baseline and during a vascular challenge, which is promising for the quantitative usage of ASL in both clinical and research settings.

Arterial spin labeling has also proven reproducible in several test-retest studies of various ASL techniques (Petersen *et al.*, 2010; Gevers *et al.*, 2011; Mutsaerts *et al.*, 2014, 2015; Wu *et al.*, 2014). Both the intra- and inter-subject coefficient-of-variation of approximately 10 and 15%, respectively, are fully in line with that of the ^{15}O-PET studies (Fan *et al.*, 2016).

7.2 Consensus papers

Recently, a consensus paper aimed at directing vendors, researchers as well as clinicians towards a set of standard ASL sequences was published (Alsop *et al.*, 2015). This paper makes a good reference for the minimum requirements needed for perfusion studies performed both clinically and in research. Access to similar ASL sequences

with default parameters across vendors will allow a faster harmonization of the clinical results to the benefit for the entire field. Still, research may involve more elaborate ASL versions, which then typically must be implemented by the researcher, as is the case today.

8 Arterial Spin Labeling: the future

The future for ASL looks bright, the number of clinical research studies using ASL is rapidly increasing and clinical use is picking up! The reproducibility is good and consensus has been reached on how to perform the basic PASL and pCASL experiments. At the same time, a range of advanced new techniques continue to emerge.

8.1 New methodologies

Arterial spin labeling is an extremely versatile method as we have seen above: it allows not only measurement of CBF, but also ATT, aBV and it can give territorial information. New approaches for improving CBF quantitation have been developed, such as the Hadamard encoded pCASL sequence (Teeuwisse *et al.*, 2014; von Samson-Himmelstjerna *et al.*, 2016) which facilitates time efficient mapping of ATT and CBF within the same sequence scan using a Hadamard encoding matrix. Another recent approach for making time efficient collection of CBF, ATT and aBV information is the Turbo QUASAR sequence which relies on the generation of a train of boluses with continuous sampling in between (Petersen *et al.*, 2013).

However, the story does not end here, and advanced sequences keep emerging from the ASL technique. By separating the blood in the sagittal sinus using a PASL labeling approach together with a series of T_2-preparation pulses (Lu and Ge, 2008), global venous oxygenation can be determined, which together with whole brain perfusion information allows the assessment of global $CMRO_2$. This opened for an entire field of ASL-based oxygenation techniques where recent developments aim at separating the vascular compartment from the tissue on a voxel by voxel level in order to assess oxygen extraction (Bolar *et al.*, 2011; Guo and Wong, 2012) or oxygen saturation of the tissue (Alderliesten *et al.*, 2016). Magnetic Resonance Fingerprinting has also been applied to ASL potentially allowing estimation of more parameters from within a single scan (Su *et al.*, 2016) another new direction within ASL imaging aiming to acquire more robust perfusion estimates in shorter acquisition times.

8.2 Concluding remarks

The last decade has seen great progress in the ASL technique. Robust sequences such as the pCASL sequence combined with great technical advances, such as 3-tesla MR

scanners and 16 or more parallel receive channels, have paved the way for robust perfusion evaluation for both clinical and research purposes. The users have gained a noninvasive, accurate and repeatable imaging method for quantitative perfusion.

References

Ahlgren A, Wirestam R, Petersen ET, Ståhlberg F, Knutsson L. Partial volume correction of brain perfusion estimates using the inherent signal data of time-resolved arterial spin labeling. NMR Biomed. 2014; 27: 1112–1122.

Alderliesten T, De Vis JB, Lemmers PMA, van Bel F, Benders MJNL, Hendrikse J, et al. T2-prepared velocity selective labelling: A novel idea for full-brain mapping of oxygen saturation. NeuroImage 2016; 139: 65–73.

Alsop DC, Detre JA. Multisection cerebral blood flow MR imaging with continuous arterial spin labeling. Radiology 1998; 208: 410–416.

Alsop DC, Detre JA, Golay X, Günther M, Hendrikse J, Hernandez-Garcia L, et al. Recommended implementation of arterial spin-labeled perfusion MRI for clinical applications: A consensus of the ISMRM perfusion study group and the European consortium for ASL in dementia. Magn. Reson. Med. 2015; 73: 102–116.

Asllani I, Borogovac A, Brown TR. Regression algorithm correcting for partial volume effects in arterial spin labeling MRI. Magn. Reson. Med. 2008; 60: 1362–1371.

Austin BP, Nair VA, Meier TB, Xu G, Rowley HA, Carlsson CM, et al. Effects of hypoperfusion in Alzheimer's disease. J. Alzheimers Dis. JAD 2011; 26 Suppl 3: 123–133.

Blockley NP, Griffeth VEM, Buxton RB. A general analysis of calibrated BOLD methodology for measuring CMRO2 responses: comparison of a new approach with existing methods. NeuroImage 2012; 60: 279–289.

Bokkers RPH, De Cocker LJ, van Osch MJP, Hartkamp NS, Hendrikse J. Selective Arterial Spin Labeling: Techniques and Neurovascular Applications. Top. Magn. Reson. Imaging TMRI 2016; 25: 73–80.

Bokkers RPH, van Osch MJP, van der Worp HB, de Borst GJ, Mali WPTM, Hendrikse J. Symptomatic carotid artery stenosis: impairment of cerebral autoregulation measured at the brain tissue level with arterial spin-labeling MR imaging. Radiology 2010; 256: 201–208.

Bolar DS, Rosen BR, Sorensen AG, Adalsteinsson E. QUantitative Imaging of eXtraction of oxygen and TIssue consumption (QUIXOTIC) using venular-targeted velocity-selective spin labeling. Magn. Reson. Med. 2011; 66: 1550–1562.

Bulte DP, Kelly M, Germuska M, Xie J, Chappell MA, Okell TW, et al. Quantitative measurement of cerebral physiology using respiratory-calibrated MRI. NeuroImage 2012; 60: 582–591.

Buxton RB, Frank LR, Wong EC, Siewert B, Warach S, Edelman RR. A general kinetic model for quantitative perfusion imaging with arterial spin labeling. Magn. Reson. Med. 1998; 40: 383–396.

Calamante F, Williams SR, van Bruggen N, Kwong KK, Turner R. A model for quantification of perfusion in pulsed labelling techniques. NMR Biomed. 1996; 9: 79–83.

Chappell MA, Groves AR, Whitcher B, Woolrich MW. Variational Bayesian Inference for a Nonlinear Forward Model. Trans Sig Proc 2009; 57: 223–236.

Chiarelli PA, Bulte DP, Gallichan D, Piechnik SK, Wise R, Jezzard P. Flow-metabolism coupling in human visual, motor, and supplementary motor areas assessed by magnetic resonance imaging. Magn. Reson. Med. 2007; 57: 538–547.

Chng SM, Petersen ET, Zimine I, Sitoh Y-Y, Lim CCT, Golay X. Territorial arterial spin labeling in the assessment of collateral circulation: comparison with digital subtraction angiography. Stroke J. Cereb. Circ. 2008; 39: 3248–3254.

Collij LE, Heeman F, Kuijer JPA, Ossenkoppele R, Benedictus MR, Möller C, et al. Application of Machine Learning to Arterial Spin Labeling in Mild Cognitive Impairment and Alzheimer Disease. Radiology 2016; 281: 865–875.

Dai W, Garcia D, de Bazelaire C, Alsop DC. Continuous flow-driven inversion for arterial spin labeling using pulsed radio frequency and gradient fields. Magn. Reson. Med. 2008; 60: 1488–1497.

Dangouloff-Ros V, Deroulers C, Foissac F, Badoual M, Shotar E, Grévent D, et al. Arterial Spin Labeling to Predict Brain Tumor Grading in Children: Correlations between Histopathologic Vascular Density and Perfusion MR Imaging. Radiology 2016; 281: 553–566.

Davies NP, Jezzard P. Selective arterial spin labeling (SASL): perfusion territory mapping of selected feeding arteries tagged using two-dimensional radiofrequency pulses. Magn. Reson. Med. 2003; 49: 1133–1142.

De Vis JB, Alderliesten T, Hendrikse J, Petersen ET, Benders MJNL. Magnetic resonance imaging based noninvasive measurements of brain hemodynamics in neonates: a review. Pediatr. Res. 2016; 80: 641–650.

De Vis JB, Hendrikse J, Bhogal A, Adams A, Kappelle LJ, Petersen ET. Age-related changes in brain hemodynamics; A calibrated MRI study. Hum. Brain Mapp. 2015; 36: 3973–3987.

De Vis JB, Hendrikse J, Groenendaal F, de Vries LS, Kersbergen KJ, Benders MJNL, et al. Impact of neonate haematocrit variability on the longitudinal relaxation time of blood: Implications for arterial spin labelling MRI. NeuroImage Clin. 2014; 4: 517–525.

De Vis JB, Petersen ET, Bhogal A, Hartkamp NS, Klijn CJM, Kappelle LJ, et al. Calibrated MRI to evaluate cerebral hemodynamics in patients with an internal carotid artery occlusion. J. Cereb. Blood Flow Metab. Off. J. Int. Soc. Cereb. Blood Flow Metab. 2015; 35: 1015–1023.

Detre JA, Wang J. Technical aspects and utility of fMRI using BOLD and ASL. Clin. Neurophysiol. Off. J. Int. Fed. Clin. Neurophysiol. 2002; 113: 621–634.

Dixon WT, Du LN, Faul DD, Gado M, Rossnick S. Projection angiograms of blood labeled by adiabatic fast passage. Magn. Reson. Med. 1986; 3: 454–462.

Dixon WT, Sardashti M, Castillo M, Stomp GP. Multiple inversion recovery reduces static tissue signal in angiograms. Magn. Reson. Med. 1991; 18: 257–268.

Duong TQ, Kim DS, Uğurbil K, Kim SG. Localized cerebral blood flow response at submillimeter columnar resolution. Proc. Natl. Acad. Sci. U. S. A. 2001; 98: 10904–10909.

Edelman RR, Siewert B, Darby DG, Thangaraj V, Nobre AC, Mesulam MM, et al. Qualitative mapping of cerebral blood flow and functional localization with echo-planar MR imaging and signal targeting with alternating radio frequency. Radiology 1994; 192: 513–520.

Ewing JR, Wei L, Knight RA, Pawa S, Nagaraja TN, Brusca T, et al. Direct comparison of local cerebral blood flow rates measured by MRI arterial spin-tagging and quantitative autoradiography in a rat model of experimental cerebral ischemia. J. Cereb. Blood Flow Metab. Off. J. Int. Soc. Cereb. Blood Flow Metab. 2003; 23: 198–209.

Fan AP, Jahanian H, Holdsworth SJ, Zaharchuk G. Comparison of cerebral blood flow measurement with [15O]-water positron emission tomography and arterial spin labeling magnetic resonance imaging: A systematic review. J. Cereb. Blood Flow Metab. Off. J. Int. Soc. Cereb. Blood Flow Metab. 2016; 36: 842–861.

Fernández-Seara MA, Mengual E, Vidorreta M, Castellanos G, Irigoyen J, Erro E, et al. Resting state functional connectivity of the subthalamic nucleus in Parkinson's disease assessed using arterial spin-labeled perfusion fMRI. Hum. Brain Mapp. 2015; 36: 1937–1950.

Gevers S, van Osch MJ, Bokkers RPH, Kies DA, Teeuwisse WM, Majoie CB, et al. Intra- and multicenter reproducibility of pulsed, continuous and pseudo-continuous arterial spin labeling methods for measuring cerebral perfusion. J. Cereb. Blood Flow Metab. Off. J. Int. Soc. Cereb. Blood Flow Metab. 2011; 31: 1706–1715.

Golay X, Stuber M, Pruessmann KP, Meier D, Boesiger P. Transfer insensitive labeling technique (TILT): application to multislice functional perfusion imaging. J. Magn. Reson. Imaging JMRI 1999; 9: 454–461.

Greve DN, Mueller BA, Liu T, Turner JA, Voyvodic J, Yetter E, et al. A Novel Method for Quantifying Scanner Instability in fMRI. Magn. Reson. Med. 2011; 65: 1053–1061.

Günther M, Bock M, Schad LR. Arterial spin labeling in combination with a look-locker sampling strategy: inflow turbo-sampling EPI-FAIR (ITS-FAIR). Magn. Reson. Med. 2001; 46: 974–984.

Günther M, Oshio K, Feinberg DA. Single-shot 3D imaging techniques improve arterial spin labeling perfusion measurements. Magn. Reson. Med. 2005; 54: 491–498.

Guo J, Wong EC. Venous oxygenation mapping using velocity-selective excitation and arterial nulling. Magn. Reson. Med. 2012; 68: 1458–1471.

Haller S, Rodriguez C, Moser D, Toma S, Hofmeister J, Sinanaj I, et al. Acute caffeine administration impact

on working memory-related brain activation and functional connectivity in the elderly: a BOLD and perfusion MRI study. Neuroscience 2013; 250: 364–371.
Haller S, Zaharchuk G, Thomas DL, Lovblad K-O, Barkhof F, Golay X. Arterial Spin Labeling Perfusion of the Brain: Emerging Clinical Applications. Radiology 2016; 281: 337–356.
Hartkamp NS, Petersen ET, De Vis JB, Bokkers RPH, Hendrikse J. Mapping of cerebral perfusion territories using territorial arterial spin labeling: techniques and clinical application. NMR Biomed. 2013; 26: 901–912.
Heijtel DFR, Mutsaerts HJMM, Bakker E, Schober P, Stevens MF, Petersen ET, et al. Accuracy and precision of pseudo-continuous arterial spin labeling perfusion during baseline and hypercapnia: a head-to-head comparison with 150 H_2O positron emission tomography. NeuroImage 2014; 92: 182–192.
Heijtel DFR, Petersen ET, Mutsaerts HJMM, Bakker E, Schober P, Stevens MF, et al. Quantitative agreement between [(15)O]H2O PET and model free QUASAR MRI-derived cerebral blood flow and arterial blood volume. NMR Biomed. 2016; 29: 519–526.
Helle M, Norris DG, Rüfer S, Alfke K, Jansen O, van Osch MJP. Superselective pseudocontinuous arterial spin labeling. Magn. Reson. Med. 2010; 64: 777–786.
Hendrikse J, van der Grond J, Lu H, van Zijl PCM, Golay X. Flow territory mapping of the cerebral arteries with regional perfusion MRI. Stroke 2004; 35: 882–887.
Hendrikse J, Petersen ET, Chèze A, Chng SM, Venketasubramanian N, Golay X. Relation between cerebral perfusion territories and location of cerebral infarcts. Stroke J. Cereb. Circ. 2009; 40: 1617–1622.
Henkelman RM, Huang X, Xiang QS, Stanisz GJ, Swanson SD, Bronskill MJ. Quantitative interpretation of magnetization transfer. Magn. Reson. Med. 1993; 29: 759–766.
Hernandez DA, Bokkers RPH, Mirasol RV, Luby M, Henning EC, Merino JG, et al. Pseudocontinuous arterial spin labeling quantifies relative cerebral blood flow in acute stroke. Stroke 2012; 43: 753–758.
Herscovitch P, Raichle ME. What is the correct value for the brain—blood partition coefficient for water? J. Cereb. Blood Flow Metab. Off. J. Int. Soc. Cereb. Blood Flow Metab. 1985; 5: 65–69.
Hoge RD, Atkinson J, Gill B, Crelier GR, Marrett S, Pike GB. Linear coupling between cerebral blood flow and oxygen consumption in activated human cortex. Proc. Natl. Acad. Sci. 1999; 96: 9403–9408.
Hrabe J, Lewis DP. Two analytical solutions for a model of pulsed arterial spin labeling with randomized blood arrival times. J. Magn. Reson. San Diego Calif 1997 2004; 167: 49–55.
Kety SS, Schmidt CF. The nitrous oxide method for the quantitative determination of cerebral blood flow in man: Theory, procedure and normal values. J. Clin. Invest. 1948; 27: 476–483.
Kim SG. Quantification of relative cerebral blood flow change by flow-sensitive alternating inversion recovery (FAIR) technique: application to functional mapping. Magn. Reson. Med. 1995; 34: 293–301.
Kwong KK, Chesler DA, Weisskoff RM, Donahue KM, Davis TL, Ostergaard L, et al. MR perfusion studies with T1-weighted echo planar imaging. Magn. Reson. Med. 1995; 34: 878–887.
Leeuwis AE, Benedictus MR, Kuijer JPA, Binnewijzend MAA, Hooghiemstra AM, Verfaillie SCJ, et al. Lower cerebral blood flow is associated with impairment in multiple cognitive domains in Alzheimer's disease. Alzheimers Dement. J. Alzheimers Assoc 2017; 13(5), 531–40.
Liu Y, Zhu X, Feinberg D, Guenther M, Gregori J, Weiner MW, et al. Arterial spin labeling MRI study of age and gender effects on brain perfusion hemodynamics. Magn. Reson. Med. 2012; 68: 912–922.
Lu H, Ge Y. Quantitative evaluation of oxygenation in venous vessels using T2-Relaxation-Under-Spin-Tagging MRI. Magn. Reson. Med. 2008; 60: 357–363.
Mak HKF, Chan Q, Zhang Z, Petersen ET, Qiu D, Zhang L, et al. Quantitative assessment of cerebral hemodynamic parameters by QUASAR arterial spin labeling in Alzheimer's disease and cognitively normal Elderly adults at 3-tesla. J. Alzheimers Dis. JAD 2012; 31: 33–44.
Mato Abad V, García-Polo P, O'Daly O, Hernández-Tamames JA, Zelaya F. ASAP (Automatic Software for ASL Processing): A toolbox for processing Arterial Spin Labeling images. Magn. Reson. Imaging 2016; 34: 334–344.
Mutsaerts HJMM, van Osch MJP, Zelaya FO, Wang DJJ, Nordhøy W, Wang Y, et al. Multi-vendor reliability of arterial spin labeling perfusion MRI using a near-identical sequence: implications for multi-center studies. NeuroImage 2015; 113: 143–152.

Mutsaerts HJMM, Steketee RME, Heijtel DFR, Kuijer JPA, van Osch MJP, Majoie CBLM, et al. Inter-vendor reproducibility of pseudo-continuous arterial spin labeling at 3 Tesla. PloS One 2014; 9: e104108.

Ogawa S, Lee TM, Kay AR, Tank DW. Brain magnetic resonance imaging with contrast dependent on blood oxygenation. Proc. Natl. Acad. Sci. U. S. A. 1990; 87: 9868–9872.

Oguz KK, Golay X, Pizzini FB, Freer CA, Winrow N, Ichord R, et al. Sickle cell disease: continuous arterial spin-labeling perfusion MR imaging in children. Radiology 2003; 227: 567–574.

Ostergaard L, Weisskoff RM, Chesler DA, Gyldensted C, Rosen BR. High resolution measurement of cerebral blood flow using intravascular tracer bolus passages. Part I: Mathematical approach and statistical analysis. Magn. Reson. Med. 1996; 36: 715–725.

Parkes LM, Rashid W, Chard DT, Tofts PS. Normal cerebral perfusion measurements using arterial spin labeling: reproducibility, stability, and age and gender effects. Magn. Reson. Med. 2004; 51: 736–743.

Parkes LM, Tofts PS. Improved accuracy of human cerebral blood perfusion measurements using arterial spin labeling: accounting for capillary water permeability. Magn. Reson. Med. 2002; 48: 27–41.

Petersen ET, De Vis JB, van den Berg CAT, Hendrikse J. Turbo-QUASAR: a signal-to-noise optimal arterial spin labeling and sampling strategy. ISMRM 21st Annual Meeting & Exhibition in Salt Lake City, USA, #2146. 2013.

Petersen ET, Lim T, Golay X. Model-free arterial spin labeling quantification approach for perfusion MRI. Magn. Reson. Med. 2006; 55: 219–232.

Petersen ET, Mouridsen K, Golay X, all named co-authors of the QUASAR test-retest study. The QUASAR reproducibility study, Part II: Results from a multi-center Arterial Spin Labeling test-retest study. NeuroImage 2010; 49: 104–113.

Petersen ET, Zimine I, Ho Y-CL, Golay X. Non-invasive measurement of perfusion: a critical review of arterial spin labelling techniques. Br. J. Radiol. 2006; 79: 688–701.

Qiu D, Straka M, Zun Z, Bammer R, Moseley ME, Zaharchuk G. CBF measurements using multidelay pseudocontinuous and velocity-selective arterial spin labeling in patients with long arterial transit delays: comparison with xenon CT CBF. J. Magn. Reson. Imaging JMRI 2012; 36: 110–119.

Roberts DA, Rizi R, Lenkinski RE, Leigh JS. Magnetic resonance imaging of the brain: blood partition coefficient for water: application to spin-tagging measurement of perfusion. J. Magn. Reson. Imaging JMRI 1996; 6: 363–366.

von Samson-Himmelstjerna F, Madai VI, Sobesky J, Guenther M. Walsh-ordered hadamard time-encoded pseudocontinuous ASL (WH pCASL). Magn. Reson. Med. 2016; 76: 1814–1824.

Schmid S, Ghariq E, Teeuwisse WM, Webb A, van Osch MJP. Acceleration-selective arterial spin labeling. Magn. Reson. Med. 2014; 71: 191–199.

Schmid S, Heijtel DFR, Mutsaerts HJMM, Boellaard R, Lammertsma AA, Nederveen AJ, et al. Comparison of velocity- and acceleration-selective arterial spin labeling with [15O]H2O positron emission tomography. J. Cereb. Blood Flow Metab. Off. J. Int. Soc. Cereb. Blood Flow Metab. 2015; 35: 1296–1303.

Schmid S, Petersen ET, Van Osch MJP. Insight into the labeling mechanism of acceleration selective arterial spin labeling. MAGMA. 2017; 30(2): 165–74.

St Lawrence KS, Frank JA, McLaughlin AC. Effect of restricted water exchange on cerebral blood flow values calculated with arterial spin tagging: a theoretical investigation. Magn. Reson. Med. 2000; 44: 440–449.

Su P, Mao D, Liu P, Li Y, Pinho MC, Welch BG, et al. Multiparametric estimation of brain hemodynamics with MR fingerprinting ASL. Magn. Reson. Med. 2016

Teeuwisse WM, Schmid S, Ghariq E, Veer IM, van Osch MJP. Time-encoded pseudocontinuous arterial spin labeling: basic properties and timing strategies for human applications. Magn. Reson. Med. 2014; 72: 1712–1722.

Tofts PS, Kermode AG. Measurement of the blood-brain barrier permeability and leakage space using dynamic MR imaging. 1. Fundamental concepts. Magn. Reson. Med. 1991; 17: 357–367.

Trampel R, Jochimsen TH, Mildner T, Norris DG, Möller HE. Efficiency of flow-driven adiabatic spin inversion under realistic experimental conditions: a computer simulation. Magn. Reson. Med. 2004; 51: 1187–1193.

Václavů L, van der Land V, Heijtel DFR, van Osch MJP, Cnossen MH, Majoie CBLM, et al. In Vivo T1 of Blood Measurements in Children with Sickle Cell Disease Improve Cerebral Blood Flow Quantification from Arterial Spin-Labeling MRI. AJNR Am. J. Neuroradiol. 2016; 37: 1727–1732.

Varela M, Hajnal JV, Petersen ET, Golay X, Merchant N, Larkman DJ. A method for rapid in vivo measurement of blood T1. NMR Biomed. 2011; 24: 80–88.

Walsh EG, Minematsu K, Leppo J, Moore SC. Radioactive microsphere validation of a volume localized continuous saturation perfusion measurement. Magn. Reson. Med. 1994; 31: 147–153.

Wang DJJ, Alger JR, Qiao JX, Gunther M, Pope WB, Saver JL, et al. Multi-delay multi-parametric arterial spin-labeled perfusion MRI in acute ischemic stroke - Comparison with dynamic susceptibility contrast enhanced perfusion imaging. NeuroImage Clin. 2013; 3: 1–7.

Wang J, Aguirre GK, Kimberg DY, Roc AC, Li L, Detre JA. Arterial spin labeling perfusion fMRI with very low task frequency. Magn. Reson. Med. 2003; 49: 796–802.

Wang J, Licht DJ, Jahng G-H, Liu C-S, Rubin JT, Haselgrove J, et al. Pediatric perfusion imaging using pulsed arterial spin labeling. J. Magn. Reson. Imaging JMRI 2003; 18: 404–413.

Wang Z, Aguirre GK, Rao H, Wang J, Fernández-Seara MA, Childress AR, et al. Empirical optimization of ASL data analysis using an ASL data processing toolbox: ASLtbx. Magn. Reson. Imaging 2008; 26: 261–269.

Werner R, Norris DG, Alfke K, Mehdorn HM, Jansen O. Continuous artery-selective spin labeling (CASSL). Magn. Reson. Med. 2005; 53: 1006–1012.

Williams DS, Detre JA, Leigh JS, Koretsky AP. Magnetic resonance imaging of perfusion using spin inversion of arterial water. Proc. Natl. Acad. Sci. U. S. A. 1992; 89: 212–216.

Wong EC. Vessel-encoded arterial spin-labeling using pseudocontinuous tagging. Magn. Reson. Med. 2007; 58: 1086–1091.

Wong EC, Buxton RB, Frank LR. Implementation of quantitative perfusion imaging techniques for functional brain mapping using pulsed arterial spin labeling. NMR Biomed. 1997; 10: 237–249.

Wong EC, Buxton RB, Frank LR. Quantitative imaging of perfusion using a single subtraction (QUIPSS and QUIPSS II). Magn. Reson. Med. 1998; 39: 702–708.

Wong EC, Cronin M, Wu W-C, Inglis B, Frank LR, Liu TT. Velocity-selective arterial spin labeling. Magn. Reson. Med. 2006; 55: 1334–1341.

Wu B, Lou X, Wu X, Ma L. Intra- and interscanner reliability and reproducibility of 3D whole-brain pseudo-continuous arterial spin-labeling MR perfusion at 3T. J. Magn. Reson. Imaging JMRI 2014; 39: 402–409.

Wu W-C, Wong EC. Feasibility of velocity selective arterial spin labeling in functional MRI. J. Cereb. Blood Flow Metab. Off. J. Int. Soc. Cereb. Blood Flow Metab. 2007; 27: 831–838.

Yang S, Zhao B, Wang G, Xiang J, Xu S, Liu Y, et al. Improving the Grading Accuracy of Astrocytic Neoplasms Noninvasively by Combining Timing Information with Cerebral Blood Flow: A Multi-TI Arterial Spin-Labeling MR Imaging Study. AJNR Am. J. Neuroradiol. 2016; 37: 2209–2216.

Ye FQ, Berman KF, Ellmore T, Esposito G, van Horn JD, Yang Y, et al. H(2)(15)O PET validation of steady-state arterial spin tagging cerebral blood flow measurements in humans. Magn. Reson. Med. 2000; 44: 450–456.

Ye FQ, Frank JA, Weinberger DR, McLaughlin AC. Noise reduction in 3D perfusion imaging by attenuating the static signal in arterial spin tagging (ASSIST). Magn. Reson. Med. 2000; 44: 92–100.

Ye FQ, Mattay VS, Jezzard P, Frank JA, Weinberger DR, McLaughlin AC. Correction for vascular artifacts in cerebral blood flow values measured by using arterial spin tagging techniques. Magn. Reson. Med. 1997; 37: 226–235.

Ye J, Bhagat SK, Li H, Lup X, Wang B, Liu L, et al. Differentiation between recurrent gliomas and radiation necrosis using arterial spin labeling perfusion imaging. Exp. Ther. Med. 2016; 11: 2432–2436.

Zhang W, Silva AC, Williams DS, Koretsky AP. NMR measurement of perfusion using arterial spin labeling without saturation of macromolecular spins. Magn. Reson. Med. 1995; 33: 370–376.

Zhang W, Williams DS, Koretsky AP. Measurement of rat brain perfusion by NMR using spin labeling of arterial water: in vivo determination of the degree of spin labeling. Magn. Reson. Med. 1993; 29: 416–421.

Zhang X, Petersen ET, Ghariq E, De Vis JB, Webb AG, Teeuwisse WM, et al. In vivo blood T(1) measurements

at 1.5 T, 3 T, and 7 T. Magn. Reson. Med. 2013; 70: 1082–1086.
Zhou J, Wilson DA, Ulatowski JA, Traystman RJ, van Zijl PC. Two-compartment exchange model for perfusion quantification using arterial spin tagging. J. Cereb. Blood Flow Metab. Off. J. Int. Soc. Cereb. Blood Flow Metab. 2001; 21: 440–455.

Chapter 11

Fast CSF MRI for brain segmentation; cross-validation by comparison with 3D T_1-based brain segmentation methods

L.A. van der Kleij[1*], J. de Bresser[1], J. Hendrikse[1], J.C.W. Siero[1,2], E.T. Petersen[3,4], J.B. De Vis[5]

[1] Department of Radiology, University Medical Center Utrecht, Utrecht, The Netherlands
[2] Spinoza Center for Neuroimaging, Amsterdam, The Netherlands
[3] Danish Research Center for Magnetic Resonance, Center for Functional and Diagnostic Imaging and Research, Copenhagen University Hospital Hvidovre, Hvidovre, Denmark
[4] Center for Magnetic Resonance, DTU Elektro, Technical University of Denmark, Kgs Lyngby, Denmark.
[5] National Institute of Neurological Disorders and Stroke, National Institutes of Health, Bethesda, Maryland, USA

PloS one 13.4 (2018): e0196119

Abstract

Objective: In previous work we have developed a fast sequence that focusses on cerebrospinal fluid (CSF) based on the long T_2 of CSF. By processing the data obtained with this CSF MRI sequence, brain parenchymal volume (BPV) and intracranial volume (ICV) can be automatically obtained. The aim of this study was to assess the precision of the BPV and ICV measurements of the CSF MRI sequence and to validate the CSF MRI sequence by comparison with 3D T_1-based brain segmentation methods.

Materials and methods: Ten healthy volunteers (2 females; median age 28 years) were scanned (3T MRI) twice with repositioning in between. The scan protocol consisted of a low resolution (LR) CSF sequence (0:57min), a high resolution (HR) CSF sequence (3:21min) and a 3D T_1-weighted sequence (6:47min). Data of the HR 3D-T_1-weighted images were downsampled to obtain LR T_1-weighted images (reconstructed imaging time: 1:59 min). Data of the CSF MRI sequences was automatically segmented using in-house software. The 3D T_1-weighted images were segmented using FSL (5.0), SPM12 and FreeSurfer (5.3.0).

Results: The mean absolute differences for BPV and ICV between the first and second scan for CSF LR (BPV/ICV: 12±9/7±4cc) and CSF HR (5±5/4±2cc) were comparable to FSL HR (9±11/19±23cc), FSL LR (7±4, 6±5cc), FreeSurfer HR (5±3/14±8cc), FreeSurfer LR (9±8, 12±10cc), and SPM HR (5±3/4±7cc), and SPM LR (5±4, 5±3cc). The correlation between the measured volumes of the CSF sequences and that measured by FSL, FreeSurfer and SPM HR and LR was very good (all Pearson's correlation coefficients >0.83, R^2 .67-.97). The results from the downsampled data and the high-resolution data were similar.

Conclusion: Both CSF MRI sequences have a precision comparable to, and a very good correlation with established 3D T_1-based automated segmentations methods for the segmentation of BPV and ICV. However, the short imaging time of the fast CSF MRI sequence is superior to the 3D T_1 sequence on which segmentation with established methods is performed.

Introduction

Brain volume measurements on magnetic resonance (MR) images is often used as an etiological and prognostic biomarker.[1,2] Alzheimer's disease is a well-known example of a disease characterized by progressive atrophy over the years.[3] Brain volumetrics can also help to monitor the effect of multiple sclerosis treatment.[4] Although qualitative assessment of brain volume is still often used, especially in clinical practice, automatic brain volume measurements have the benefit of providing precise, quantitative brain volume estimates. Widespread use of brain volume measurements in clinical research and clinical practice is hindered by the required 3D T_1-weighted MRI sequence as it has a long scan time (typically >6min). In addition, the long scan time makes it susceptible to motion artefacts. The 3D T_1-weighted sequence is aimed at T_1 contrast, which gives good contrast between gray matter and white matter while CSF appears dark on the images. Recently, we discovered that data of a fast (<1-3min) cerebrospinal fluid (CSF) MRI sequence[5] can be processed to enable brain volume measurements.[6] This short scan time of the CSF sequence is a considerable advantage over the 3D T_1-weighted sequence and this facilitates a more widespread use of brain volume measurements.[6] The CSF MRI sequence is a 2D sequence with a multislice EPI readout that enables mapping of the T_1 and T_2 of CSF. The CSF MRI sequence relies on the longer transverse (T_2) and longitudinal (T_1) relaxation rate of the CSF compared to surrounding tissues and allows segmentation of the CSF and brain parenchymal volume (BPV). The obtained images with the CSF MRI sequence show no contrast between gray matter and white matter, and a good contrast between CSF and brain parenchyma. In a previous study, we showed a good correlation between the CSF MRI sequence and qualitative brain atrophy scores, and a good correlation with brain parenchymal volume (BPV) measured by FMRIB Software Library (FSL) in a simple feasibility study.[6] However, the precision of our proposed CSF MRI brain segmentation method has not been assessed nor has it been validated against other 3D T_1-weighted methods (such as FSL, FreeSurfer and SPM). The aim of this study was to assess the precision of the BPV and intracranial volume (ICV) measurements of the CSF MRI sequence and to validate the CSF MRI sequence by comparison with 3D T_1-based brain segmentation methods.

Material and methods

Participants

For this study ten healthy volunteers (2 females, 8 males) were recruited with a median age of 28 years (range 24-41). Participants were recruited between 2-9-2015 and 22-9-2015, and all participants completed the scan protocol. Recruitment was performed on the university campus. Subjects who demonstrated interest in participating in MR research were approached and screened for MR eligibility. Of the 10 subjects who were

approached, all subjects were MRI eligible. This study was approved by the Medical Ethical Committee of the University Medical Center Utrecht under protocol number NL39070.041.11. All participants provided written informed consent.

MR imaging and data processing

MR imaging was performed on a 3 Tesla Philips Achieva System (Philips, Best, The Netherlands) with a quadrature body coil as transmitter and an 8-channel head coil as a signal receiver. The MRI scan protocol consisted of the following sequences: a low resolution (LR) and a high resolution (HR) CSF MRI sequence, and a high resolution 3D T_1-weighted sequence. To assess the precision, the scan protocol was performed twice with repositioning of the subjects in between both scans (scan 1 and scan 2). The data of the 3D T_1-weighted sequence was also downsampled to the voxel size of the HR CSF MRI sequence.

CSF MRI sequence

As described earlier (for details, see supplemental material in [6], the CSF MRI sequence consists of three parts: a magnetization reset (global non-selective saturation pulse followed by a time delay of 6000ms), a T_2-preparation, and a readout part (multi-slice echo planar imaging (EPI) readout).[5] For the T_2-preparation part, a Malcolm Levitt's CPD (MLEV) T_2-preparation scheme was used with a τ_{CPMG} of 70 ms and 0, 4, 8 and 16 refocusing pulses resulting in effective TEs (eTEs) of 0, 280, 560, and 1120 ms (Figure 1).

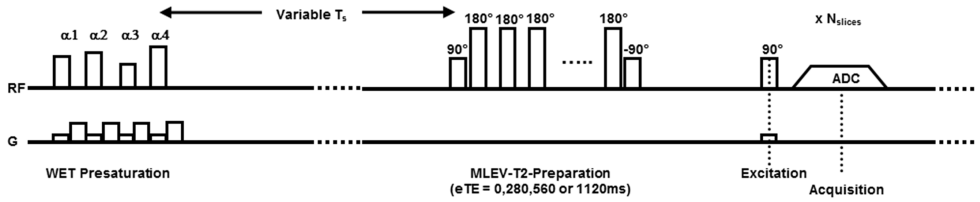

Fig. 1. The CSF MRI sequence. After presaturation and T_s the signal strength depends on T_1 decay to ensure an equal magnetization at the start of each MLEV-T_2 preparation. The MLEV-T_2 preparation with a varying amount of refocusing pulses allows the mapping of T_2 decay. Variation of time T_s in combination with a fixed number of refocusing pulses allow the mapping of T_1 decay. A short T_s is used to determine signal decay. Multi-slice echo planar imaging is used for the readout at each effective echo time.

To compensate for the offset caused by different acquisition times in the multi-slice EPI readout, the different eTE encodings were acquired both with and without an inversion pulse, which was added right after the T_2-preparation module. The final TR of the sequence was 6261 ms. The scan parameters of the low/high resolution CSF MRI sequence were: scan matrix 80x80/240x240, FOV 240x240x161 mm^3/240x240x161 mm^3, voxel size 3.0x3.0x7.0 mm^3/1.0x1.0x3.5 mm^3, SENSE factor 2.5/2.5, number of

slices 23/46, scan time 0:57 min/3:21 min.

Data of the CSF MRI sequences was fully automatically processed using IDL 6.1 for Windows (ITT Visual Information Solutions, Boulder, CO, U.S.A.).

First, signal decay curves were obtained for each voxel from which a voxelwise estimation of the T_2 of the CSF was performed using the following formula:

$$S\left(eTE,T_a\right)-S\left(T_a\right)=A\cdot e^{\frac{-eTE}{T_{2,CSF}}} \quad \text{Eq.1}$$

$$A=M_0\cdot\left(1-e^{\frac{-T_s}{T_{1,CSF}}}\right)\cdot e^{\frac{-T_a}{T_{1,CSF}}}$$

where $S(T_a)$ is the signal recovery at time T_a, the constant A is the recovered magnetization at time T_s after the non-selective saturation pulse, $T_{1,CSF}$ and $T_{2,CSF}$ are the longitudinal and transverse relaxation of the CSF. Second, the M_0 of the voxels were obtained by extrapolating the T_2 of the CSF to the intersect at eTE=0 ms. From this, the actual volume fraction of CSF (CSF_{vf}) in a voxel is obtained by relating the M_0 of a voxel to the M_0 of reference voxels. Only last 3 echo times are used to extrapolate the M_0 of CSF in order to exclude parenchymal tissue. The reference voxels free of partial volume are automatically selected based on a histogram analysis of signal intensities. The CSF volume was based on the CSF M_0 map which was smoothed with a 7mm Gaussian filter. The signal value at 99.5% of the nonzero histogram was used to determine the reference voxels filled with CSF. The upper 0.5% of values were discarded to avoid artificially high reference values caused by noise. Third, total CSF volume (Vcsf) was obtained by multiplying the volume fraction by the voxel size (mm^3).

$$CSF_{VF}=\frac{S\left(eTE=0\right)}{S_{ref}\left(eTE=0\right)} \quad \text{Eq.2}$$

Fourth, based on the first acquired echo (eTE = 0) of the CSF MRI sequence which includes both parenchymal and CSF signal, the intracranial volume (ICV) was measured. A conservative brain extraction (BET) mask from FSL[7] was applied to the CSF map to remove the skull and eyes. The CSF map and skull stripped (BET) eTE = 0 images were added and subsequently smoothed with a Gaussian filter of 3mm. Then, the threshold of any signal above 3% of the resulting histogram was assigned to the ICV. The assignment of voxels to the ICV was binary (Figure 2). The brain parenchymal volume was calculated from the difference between the ICV and total CSF volume.

The postprocessing time was 1 minute for the low resolution CSF MRI sequence (CSF LR), and it was 25 minutes for the high resolution CSF MRI sequence (CSF HR).

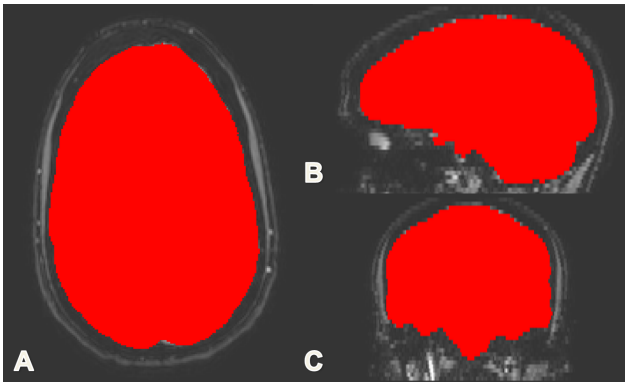

Fig. 2. The ICV derived from the CSF MRI sequence. Example of the ICV in an axial (A), saggital (B) and coronal (C) slice. The mask resulting from the BET application to the CSF data is shown in red. The raw CSF data is shown in gray-scale in the background.

3D T1-weighted sequence and 3D T1-based segmentation methods

MR imaging parameters of the HR 3D-T_1-weighted MRI sequence were; matrix size 256x256, FOV 232x256x192, voxel size 1.0x1.0x1.0 mm^3, TR = 8187ms, TE = 4.5ms, scan time 6:47 min. The data were downsampled to LR 3D-T_1-weighted images with a resolution similar to the CSF HR MRI sequence through registration to the CSF HR images: voxel size 1.0x1.0x3.5 mm^3, scan time 1:59 min (MeVis Medical Solutions AG, Bremen, Germany, version 2.7). The 3D T_1-weighted images were used for brain segmentation by FMRIB Software Library 5.0 (FSL), FreeSurfer (5.3.0) and Statistical Parametric Mapping 12 (SPM).

FSL

FSL is software created by the Analysis Group, FMBRIB, Oxford, UK. In FSL, Structural Image Evaluation using Normalization of Atrophy Cross-sectional (SIENAX) was used to obtain brain volumes normalized for skull size.[8, 9] The –B option was used for bias field correction and neck clean up.[10] The brain extraction tool was used to strip non-brain tissue and the f-parameter was set at 0.2, because the best overall results were obtained with this setting as tested by visual inspection. In SIENAX, both the skull and extracted brain were registered to standard space to allow the calculation of (peripheral) CSF volume and the removal of structures such as the eyes with a probabilistic map.[8] The gray matter and white matter were taken together to obtain the BPV. The CSF was added to the BPV to obtain the ICV.

FreeSurfer

FreeSurfer is open source software developed by the Athinoula A. Martinos Center for Biomedical Imaging, Harvard-MIT, Boston. The volume-based stream consists of five steps, including registration to standard space and skull stripping.[11] In Freesurfer, each

voxel is assigned to a certain structure. The probability of the voxel belonging to a particular structure is modulated by the neighboring voxels, because they are expected to belong to the same structure.[10] Automated brain segmentation in FreeSurfer (surfer.nmr.mgh.harvard.edu) was performed using the standard settings (recon-all –all). BPV and ICV were obtained from the stats file that becomes available after segmentation (asegstats2table).

SPM

SPM12 is developed by the Wellcome Department of Cognitive Neurology, Institute of Neurology, Queen Square, London.[12] Neck slices were removed in FSL to preprocess the images. Brain volumes were obtained from the pre-processed images with the 'Segment' function (http://www.fil.ion.ucl.ac.uk/spm). This function uses the Unified Segmentation algorithm, which combines image registration, tissue classification and bias correction.[13] As such, both the signal intensity of the voxel and the location through registration with tissue probability maps determines the probability of a voxel belonging to a certain tissue class. The recommended default settings were used. As such, the number of Gaussians for white matter and gray matter were set from one to two. The ICV and BPV were calculation from the obtained gray matter, white matter and CSF volumes.

Statistical analysis

Statistical analysis was carried out with R (R Foundation for Statistical Computing, Vienna, Austria).

Precision

For both BPV and ICV the precision was calculated by the mean (absolute) differences between the measurements of scan 1 and scan 2 for the CSF sequences and the 3D T_1-based methods (FSL, FreeSurfer, SPM). The mean difference between the results of scan 1 and scan 2 reflects whether a systematic bias exists in the test-retest measurements. The mean absolute difference reflects the total test-retest volume error between the results of scan 1 and 2. Wilcoxon signed rank tests were used to evaluate whether there was a significant difference between the test-retest measurements. Bland-Altman plots were used to visualize these differences.[14] Precision was compared between the CSF sequences and the 3D T_1-based methods.

Comparison between methods

The absolute volumes of BPV and ICV between the CSF sequences and the 3D T_1-based methods (FSL, FreeSurfer, SPM) were evaluated for significant differences (Wilcoxon signed rank). To test for correlation between the CSF sequences and the 3D T_1-based

methods, Pearson's correlation coefficients were calculated. Bland-Altman plots comparing the volumes obtained with the CSF sequence with those of the 3D T_1-based methods were used to visualize differences. The results from the first scan were used for the Bland-Altman plots. The degree of variance was calculated (R^2) with 90% confidence intervals (CI).

Results

All segmentations of all methods were considered of good quality (see Figure 3 for an example).

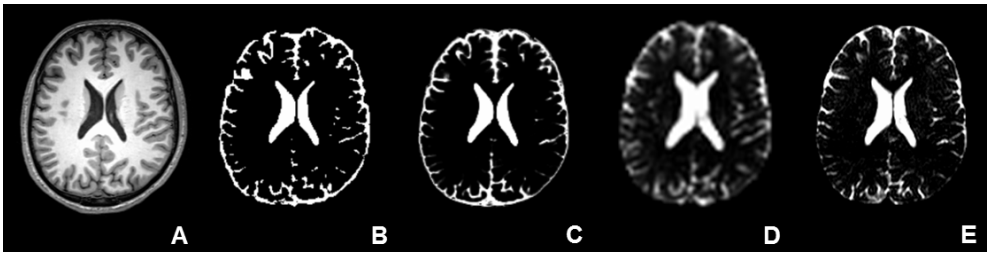

Fig. 3. All CSF measurements for all methods in each subject . One slice from subject 8 from A) the HR T_1-weighted image (downsampled images have the same in-plane resolution); B) 3D T_1-weighted FSL HR; C) 3D T_1-weighted SPM HR; D) postprocessed CSF LR; E) postprocessed CSF HR . No image is presented for FreeSurfer, because FreeSurfer uses the determinant of the transformation matrix to estimate ICV rather than distinguishing the skull from peripheral CSF.

BPV

Precision

Figure 4 shows all BPV measurements for all methods in each subject. Table 1 shows the mean BPV for the first and second scan and the mean (absolute) differences between measurements on these scans for each of the methods in cc. The mean difference is the average of all test-retest differences to indicate whether there is a bias between the two measurements. The mean absolute difference is the average of the absolute test-retest differences, and it provides a measure of precision as it contains the cumulative error. The BPV measured on the first and second scan were not significantly different within each method ($p>0.05$). The mean differences for BPV between the first and second scan for the CSF LR (-7±14 cc) and CSF HR (2±7 cc) sequences were in the range of those for FSL HR (-2±15 cc), FSL LR (4±7 cc), FreeSurfer HR (1±6 cc), FreeSurfer LR (1±12 cc), SPM HR (2±5 cc), and SPM LR (-2±6 cc). The mean absolute differences for BPV between scans were comparable for the CSF HR sequence (5±5 cc) and FSL HR (9±11 cc), FSL LR (7±4 cc), FreeSurfer HR (5±2 cc), FreeSurfer LR (9±8 cc), SPM HR (5±3 cc), and SPM LR (5±4 cc) but the CSF LR (12±9 cc) showed somewhat larger mean absolute differences than FreeSurfer HR and SPM HR and LR. The Bland-Altman plots comparing the BPV obtained at the first scan versus that of the second scan for the CSF MRI sequence and the HR 3D T_1-based methods are shown in Figure 5.

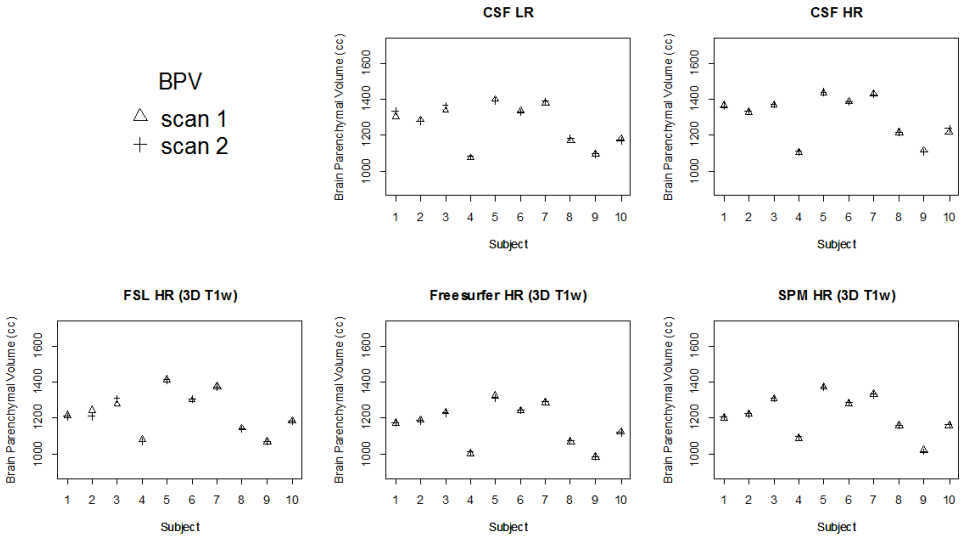

Fig. 4. All BPV measurements for all methods in each subject. CSF LR = CSF low resolution MRI scan; CSF HR = CSF high resolution MRI scan.

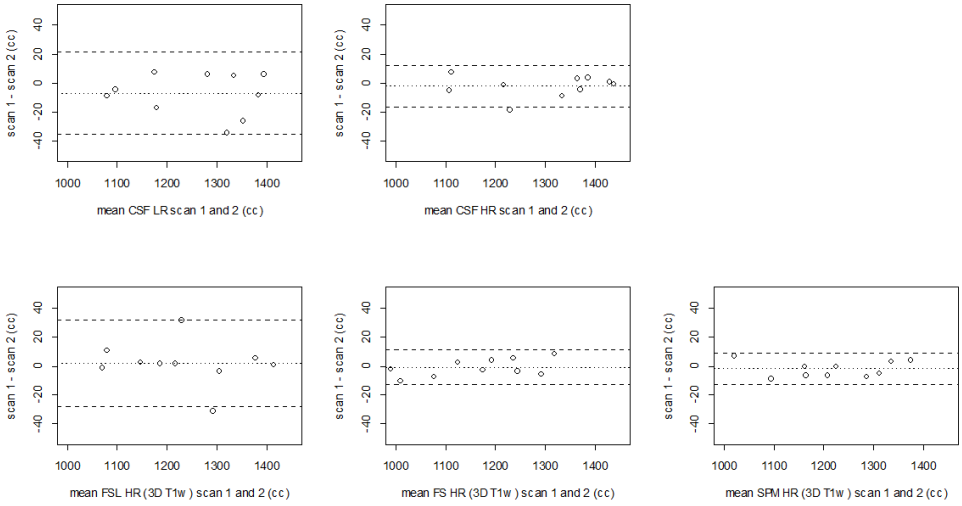

Fig. 5. Bland Altman plots for precision of BPV per method. CSF LR, CSF HR (top row), FSL, FreeSurfer and SPM (bottom row). The dashed lines represent the limits of agreement (mean difference ±1.96*SD of the differences). CSF LR = CSF low resolution MRI scan; CSF HR = CSF high resolution MRI scan; FS = FreeSurfer.

The Bland-Altman plots from the downsampled 3D T_1 sequence are shown in S2 Figure. The mean in the Bland-Altman plots should be close to 0, indicating that there is a small absolute difference between scan 1 and scan 2 within methods. The mean was close to 0 for all methods. The limits of agreement in the Bland-Altman plots should be narrow, indicating a good precision. The limits of agreement were most narrow for SPM HR (-13 – 9 cc) and FreeSurfer HR (-13 – 11 cc), and SPM LR (-11 – 15).

.

Table 1. Precision of BPV and ICV for CSF LR, CSF HR and automated segmentation methods with downsampled data

	CSF LR (cc)	CSF HR (cc)	FSL HR (cc)
BPV			
Scan 1	1255±111	1296±117	1231±109
Scan 2	1262±112	1298±116	1229±112
Mean difference between scans	-7.0±13.9	1.9±7.0	-2.2±14.5
Mean absolute difference between scans	12.4±9.4	5.3±4.9	9.2±11.4
ICV			
Scan 1	1481±130	1499±137	1598±136
Scan 2	1481±129	1500±136	1595±14
Mean difference between scans	0.0±7.8	1.2±4.3	-3.6±29.5
Mean absolute difference between scans	6.9±3.7	3.9±2.1	18.5±23.3

Value s represent means±SD in cc. CSF LR = CSF low resolution MRI scan; CSF HR = CSF high resolution with a resolution equal to the CSF HR image: 1x1x3.5 mm^3

Comparison between methods

The CSF sequences measured significantly higher BPV compared to the HR 3D T_1-based methods (FSL HR, FreeSurfer HR, SPM HR), except for CSF LR versus FSL HR (Table 2). The CSF HR sequence measured a significantly higher BPV than FreeSurfer LR (S1 Table). However, both the CSF LR and CSF HR measurements of BPV showed a very good correlation with the 3D T_1-based segmentation methods (all Pearson's correlation coefficients >0.93; Table 2, S1 Table). The Bland-Altman plots comparing the BPV obtained with the CSF sequences with those of the 3D T_1-based methods are shown in Fig 6. The mean in the Bland-Altman plots should be close to 0, indicating that there is a small absolute difference between the CSF sequences and the 3D T_1-based methods. In the Bland-Altman plots, the mean was closest to 0 for CSF LR/FSL LR (-2 cc), CSF LR/SPM LR (11 cc), and CSF LR/FSL HR (24 cc), CSF HR/FSL LR (39 cc) and CSF LR/SPM HR (39 cc), (Fig 6). The limits of agreement in the Bland-Altman plots should be narrow, indicating a small variation in measurements between the CSF sequences and the 3D T_1-based methods. The limits of agreement were the most narrow for CSF LR/FreeSurfer HR (49 – 133 cc) , CSF LR/FreeSurfer LR (35 – 130), CSF HR/FreeSurfer HR (79 – 185 cc), and CSF LR/FSL LR (-61 – 56) (Fig 6). The degree of variance was comparable between all measures (R^2 0.88 – 0.97, Table 2).

ICV

Precision

Fig 7 shows all ICV measurements for all methods in each subject. Table 1 shows the mean ICV for the first and second scan, and the mean (absolute) differences between

FreeSurfer HR (cc)	SPM HR (cc)	FSL LR (cc)	FreeSurfer LR[a] (cc)	SPM LR (cc)
1164±109	1216±105	1257±108	1172±110	1244±116
1165±106	1218±105	1261±104	1173±101	1242±118
0.9±5.7	2.0±5.3	3.8±7.3	1.2±11.7	-1.9±6.2
5.1±2.6	5.0±2.7	7.2±4.1	9.0±7.5	5.0±4.1
1555±251	1513±135	1690±145	1707±151	1497±123
1567±253	1515±140	1691±141	1714±152	1494±122
11.8±10.4	2.4±7.4	0.9±7.6	6.6±14.1	-3.4±4.5
13.5±8.2	4.3±6.5	6.0±4.7	11.8±10.2	5.0±2.7

MRI scan. [a]The automated segmentations were performed n downsampled (LR) T_1-weighted scans with

measurements on these scans for each of the methods. The ICVs measured on the first and second scan were not significantly different within each method ($p>0.05$), except for SPM LR ($p<0.05$). The mean differences for ICV between scans of the CSF LR (0±8 cc) and CSF HR (1±4 cc) sequences were smaller than for the 3D T_1-based brain segmentation methods (Table 1). For ICV, the mean absolute differences between scans of the CSF LR (7±4 cc) and CSF HR (4±2 cc) sequences were small and within the range of FSL

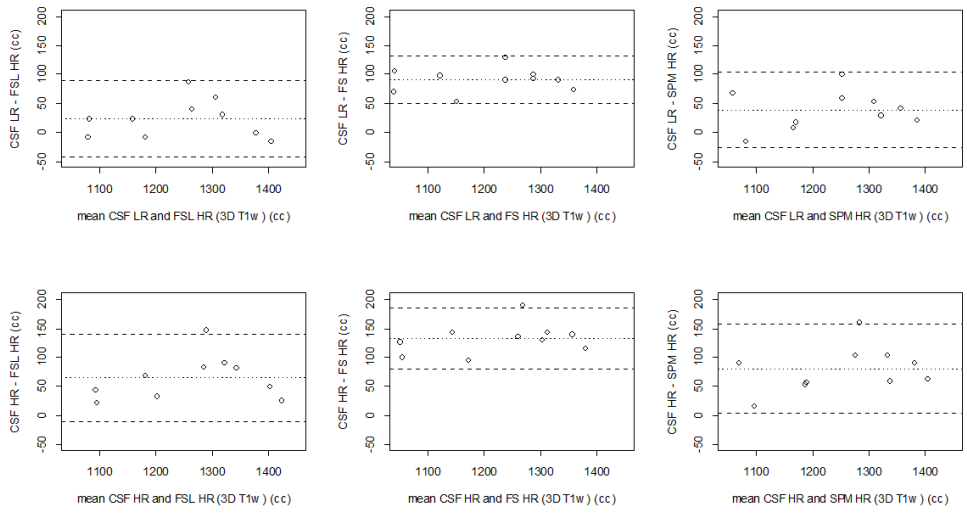

Fig 6. Bland Altman plots for the comparison of BPV between the CSF MRI sequences and the 3D T_1-based brain segmentation methods. The dashed lines represent the limits of agreement (mean difference ±1.96*SD of the differences). CSF LR = CSF low resolution MRI scan; CSF HR = CSF high resolution MRI scan; FS = FreeSurfer.

HR (19±23 cc), FSL LR (6±5 cc), FreeSurfer HR (14±8 cc), FreeSurfer LR (12±10), SPM HR (4±7 cc), and SPM LR (5±3 cc). The Bland-Altman plots comparing the ICV obtained at the first scan versus that of the second scan for all methods are shown in Figure 8. In the Bland-Altman plots, only FreeSurfer HR showed a mean that was somewhat further away from 0. The limits of agreement were most narrow for CSF HR (-10 – 8 cc), and SPM LR (-6 – 13 cc).

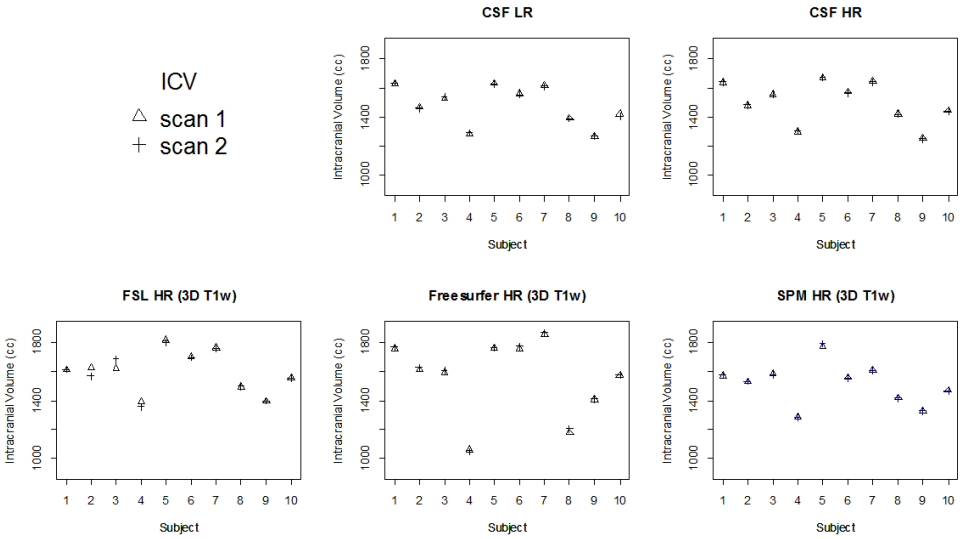

Fig. 7. All ICV measurements for all methods in each subject. CSF LR = CSF low resolution MRI scan; CSF HR = CSF high resolution MRI scan.

Comparison between methods

The CSF sequences measured somewhat lower ICV compared to the HR 3D T_1-based methods (FSL, FreeSurfer, SPM), but this was only significantly different for the CSF sequences versus FSL ($p<0.05$). The CSF sequences measured a lower ICV than FSL LR and FreeSurfer LR ($p<0.05$). There was a good to very good correlation for ICV measurements between the CSF sequences and the 3D T_1-based methods (all Pearson's correlation coefficients >0.83, Table 2, S1 Table). The Bland-Altman plots comparing the ICV obtained with the CSF sequences with those of the 3D T_1-based methods are shown in Figure 9 and in S6 Figure. In the Bland-Altman plots, the mean was closest to 0 for CSF HR/SPM LR (1 cc), CSF HR/SPM (-14 cc), CSF LR/SPM LR (-17 cc), and CSF LR/SPM HR (-32 cc). The limits of agreement were the most narrow for CSF HR/FreeSurfer LR (-264 – -153 cc), CSF LR/FreeSurfer LR (-296 – -157 cc), CSF HR/FSL LR (-276 – -106 cc), CSF LR/FSL LR (-298 – -120 cc), and CSF LR/SPM LR (-109 – 76 cc) . The degree of variance was comparable between all measures (R^2 0.84-0.92), except for FreeSurfer (R^2 0.67 – 0.75, Table 2).

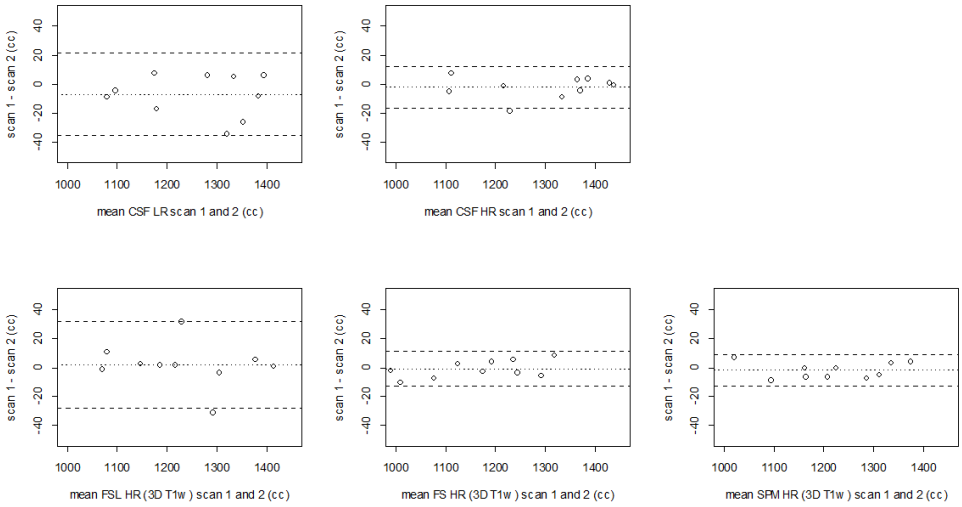

Fig. 8. Bland Altman plots for precision of ICV per method. CSF LR, CSF HR (top row), FSL, FreeSurfer and SPM (bottom row). The dashed lines represent the limits of agreement (mean difference ±1.96*SD of the differences). CSF LR = CSF low resolution MRI scan; CSF HR = CSF high resolution MRI scan; FS= FreeSurfer.

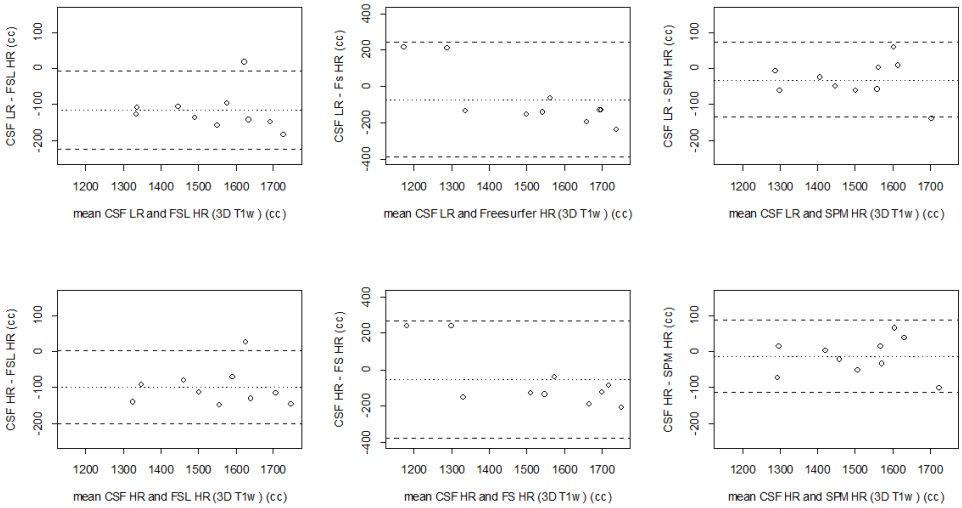

Fig. 9. Bland Altman plots for the comparison of ICV between the CSF MRI sequences and the 3D T_1-based brain segmentation methods. The dashed lines represent the limits of agreement (mean difference ±1.96*SD of the differences). CSF LR = CSF low resolution MRI scan; CSF HR = CSF high resolution MRI scan; FS = FreeSurfer.

Table 2. Correlation between the CSF MRI sequences and the HR 3D T_1-based brain segmentation methods.

	Scan 1		
Correlation tested	*Mean Δvolume (cc)*	*Pearson's Correlation Coefficient*	*R^2(90% CI)*
CSF LR BPV			
FSL HR	24±32	.98	.92 (.77-.97)
FreeSurfer HR	91±20*	.96	.97 (.88-.99)
SPM HR	39±32*	.96	.92 (.75-.96)
CSF HR BPV			
FSL HR	65±37*	.95	.90 (.70-.97)
FreeSurfer HR	132±25*	.98	.95 (.82-.99)
SPM HR	80±37*	.95	.90 (.65-.96)
FSL HR BPV			
FreeSurfer HR	67±18	.99	.97 (.95-.99)
SPM HR	15±24	.98	.95 (.85-.98)
Freesurfer HR BPV			
SPM	-52±21	.98	.96 (.91-.98)
CSF LR ICV			
FSL HR	-117±52*	.93	.86 (.44-.99)
FreeSurfer HR	-74±153	.86	.75 (.49-.90)
SPM HR	-32±50	.92	.86 (.48-.94)
CSF HR ICV			
FSL HR	-99±49*	.93	.87 (.49-.98)
FreeSurfer HR	-56±155	.84	.70 (.38-.88)
SPM HR	-14±48	.94	.88 (.53-.93)
FSL HR ICV			
FreeSurfer HR	43±152	.86	.73 (.49-.87)
SPM HR	85±39	.96	.92 (.75-.97)
Freesurfer HR ICV			
SPM HR	42±158	.83	.69 (.41-.86)

CSF LR = CSF low resolution MRI scan; CSF HR = CSF high resolution MRI scan *$p < 0.05$

	Scan 2		
	Mean Δvolume (cc)	*Pearson's Correlation Coefficient*	*R^2(90% CI)*
	33±40*	.94	.88 (.64-.96)
	97±31*	.96	.92 (.75-.97)
	44±38*	.94	.88 (.60-.96)
	69±37*	.95	.90 (.75-.97)
	133±22*	.98	.97 (.88-.99)
	80±35*	.95	.91 (.72-.96)
	64±20	.98	.97 (.92-.99)
	11±26	.97	.95 (.86-.97)
	-53±21	.98	.96 (.91-.98)
	-114±54*	.92	.85 (.47-.99)
	-86±157	.86	.74 (.52-.88)
	-34±56	.92	.84 (.42-.92)
	-95±50*	.94	.87(.53-.98)
	-67±159	.83	.69 (.40-.87)
	-15±52	.93	.86 (.53-.92)
	28±151	.86	.74 (.48-.88)
	79±42	.95	.91 (.73-.96)
	52±160	.82	.67 (.33-.86)

Discussion

This study demonstrates that the proposed CSF MRI sequences perform similarly in terms of precision (test-retest) and obtained volumes as conventional 3D T_1-weighted MRI sequences in the assessment of BPV and ICV, but with a much shorter scan time. The automated segmentation methods performed similarly for high resolution and downsampled 3D T_1-weighted data for BPV and ICV. Furthermore, an excellent correlation was found between the BPVs and ICVs obtained with the CSF MRI sequences and those obtained with the 3D T_1-weighted MRI sequences using FSL, FreeSurfer and SPM.

The precision and performance of commonly used MRI-based segmentation methods varies across different methods and also varies dependent on the application.[15-17] The observed precision of our CSF MRI sequences were in line with these previous studies of commonly used brain segmentation methods. As was expected, the CSF HR sequence showed a slightly higher precision than the CSF LR sequence. The CSF sequences even showed a markedly higher precision for ICV than FSL in this study. This is caused by the limited contrast on 3D T_1-weighted images between the tabula interna of the skull and the dura mater on one side, and the CSF on the other side.[18] As a result, the ICV that is calculated on 3D T_1-weighted images can be troublesome and several segmentation methods show difficulties in calculating the ICV.[18-20] Especially FreeSurfer has been shown earlier to perform less well than other methods for ICV.[15, 16] In this study, the mean absolute difference for ICV is two-to-four times lower for the two CSF sequences than for FSL and FreeSurfer, indicating a better precision.

The short imaging time of 57 seconds is a major advantage of the CSF LR sequence over 3D T_1 based methods, because it facilitates an easy addition of this sequence to a scan protocol. The 3D T_1-weighted sequence used in our study had a scan time of nearly 7 minutes and this scan could thus be avoided when a high-resolution T_1- weighted scan is not necessary to answer any of the other clinical or research questions. Nowadays, shorter 3D T_1-weighted sequences that still provide sufficient image quality for most radiology exams are available, and we simulated the precision of such a sequence by downsampling the data of the high resolution T_1-weighted sequence. The results of this analysis demonstrated that global measures from automated segmentation methods – BPV and ICV – are not sensitive to a somewhat lower scan quality. The precision of our LR CSF sequence was similar to the precision of both the HR and LR T_1-weighted sequence, but then with a scan time half of the scan time of the LR T_1-weighted sequence. Another strength of our CSF sequences is the good contrast between the skull and CSF, which is often limited in 3D T_1-weighted images. This leads to an very good precision of our CSF sequences for ICV. A limitation of our CSF sequences is that there is almost no contrast between the white and gray matter. Consequently, both gray and white matter atrophy and cortical thickness cannot be distinguished. Another limitation of the CSF LR and HR sequences could be that the obtained volumes are not

similar to the volumes obtain with SPM, FreeSurfer or FSL. However, this also holds for comparisons across these 3D T1-based segmentation methods.[15, 16] More importantly, we have shown that there is an excellent correlation between the estimated volumes from the CSF sequences and the 3D T1-based methods.

The purpose of this paper was to cross-validate the CSF MRI sequences for volume estimates. Future work could focus on further image processing of the CSF images such that regional brain atrophy can be determined. This would allow detection of different patterns of brain atrophy. This is a useful addition, as several diseases are marked by a characteristic pattern of brain atrophy, for example frontotemporal dementia.[21] The postprocessing time of 1 minute could also be further decreased in future studies to enable an easier implementation in clinical practice. In addition, the CSF sequences could be further validated in cohorts of patients with more brain abnormalities and variations in brain pathology. The CSF sequence might provide information about the CSF. For example, the $T_{2,}$ of CSF may be related to oxygen partial pressure.[5, 22]

In conclusion, both CSF MRI sequences have a precision comparable to, and a very good correlation with established 3D T_1-based automated segmentations methods for segmentation of BPV and ICV. However, the short imaging time of the fast CSF MRI sequence is superior to the 3D T_1-weighted sequence on which segmentation with established methods is performed.

References

1. Pasquier F, Leys D, Weerts JG, Mounier-Vehier F, Barkhof F, Scheltens P. Inter- and intraobserver reproducibility of cerebral atrophy assessment on mri scans with hemispheric infarcts. *Eur Neurol*. 1996;36:268-272
2. Scheltens P, Leys D, Barkhof F, Huglo D, Weinstein HC, Vermersch P, et al. Atrophy of medial temporal lobes on mri in "probable" alzheimer's disease and normal ageing: Diagnostic value and neuropsychological correlates. *J Neurol Neurosurg Psychiatry*. 1992;55:967-972
3. Frisoni GB, Fox NC, Jack CR, Scheltens P, Thompson PM. The clinical use of structural mri in alzheimer disease. *Nat Rev Neurol*. 2010;6:67-77
4. Giorgio A, De Stefano N. Clinical use of brain volumetry. *J Magn Reson Imaging*. 2013;37:1-14
5. Qin Q. A simple approach for three-dimensional mapping of baseline cerebrospinal fluid volume fraction. *Magn Reson Med*. 2011;65:385-391
6. De Vis JB, Zwanenburg JJ, van der Kleij LA, Spijkerman JM, Biessels GJ, Hendrikse J, et al. Cerebrospinal fluid volumetric mri mapping as a simple measurement for evaluating brain atrophy. *Eur Radiol*. 2016;26:1254-1262
7. Smith SM. Fast robust automated brain extraction. *Human brain mapping*. 2002;17:143-155
8. Smith SM, Zhang YY, Jenkinson M, Chen J, Matthews PM, Federico A, et al. Accurate, robust, and automated longitudinal and cross-sectional brain change analysis. *Neuroimage*. 2002;17:479-489
9. Smith SM, Jenkinson M, Woolrich MW, Beckmann CF, Behrens TEJ, Johansen-Berg H, et al. Advances in functional and structural mr image analysis and implementation as fsl. *Neuroimage*. 2004;23:S208-S219
10. Zhang YY, Brady M, Smith S. Segmentation of brain mr images through a hidden markov random field model and the expectation-maximization algorithm. *Ieee T Med Imaging*. 2001;20:45-57
11. Fischl B, Salat DH, Busa E, Albert M, Dieterich M, Haselgrove C, et al. Whole brain segmentation: Automated labeling of neuroanatomical structures in the human brain. *Neuron*. 2002;33:341-355
12. Ashburner J. Computational anatomy with the spm software. *Magn Reson Imaging*. 2009;27:1163-1174
13. Ashburner J, Friston KJ. Unified segmentation. *Neuroimage*. 2005;26:839-851
14. Bland JM, Altman DG. Statistical methods for assessing agreement between two methods of clinical measurement. *Lancet*. 1986;1:307-310
15. Heinen R, Bouvy WH, Mendrik AM, Viergever MA, Biessels GJ, de Bresser J. Robustness of automated methods for brain volume measurements across different mri field strengths. *PloS one*. 2016;11:e0165719
16. de Bresser J, Portegies MP, Leemans A, Biessels GJ, Kappelle LJ, Viergever MA. A comparison of mr based segmentation methods for measuring brain atrophy progression. *Neuroimage*. 2011;54:760-768
17. de Boer R, Vrooman HA, Ikram MA, Vernooij MW, Breteler MM, van der Lugt A, et al. Accuracy and reproducibility study of automatic mri brain tissue segmentation methods. *Neuroimage*. 2010;51:1047-1056
18. Mendrik AM, Vincken KL, Kuijf HJ, Breeuwer M, Bouvy WH, de Bresser J, et al. Mrbrains challenge: Online evaluation framework for brain image segmentation in 3t mri scans. *Comput Intell Neurosci*. 2015;2015:813696
19. Malone IB, Leung KK, Clegg S, Barnes J, Whitwell JL, Ashburner J, et al. Accurate automatic estimation of total intracranial volume: A nuisance variable with less nuisance. *Neuroimage*. 2015;104:366-372
20. Sargolzaei S, Sargolzaei A, Cabrerizo M, Chen G, Goryawala M, Pinzon-Ardila A, et al. Estimating intracranial volume in brain research: An evaluation of methods. *Neuroinformatics*. 2015;13:427-441
21. Kitagaki H, Mori E, Yamaji S, Ishii K, Hirono N, Kobashi S, et al. Frontotemporal dementia and alzheimer disease: Evaluation of cortical atrophy with automated hemispheric surface display generated with mr images. *Radiology*. 1998;208:431-439
22. Zaharchuk G, Busse RF, Rosenthal G, Manley GT, Glenn OA, Dillon WP. Noninvasive oxygen partial pressure measurement of human body fluids in vivo using magnetic resonance imaging. *Academic radiology*. 2006;13:1016-1024

Appendix

S1 Table. Correlation between the CSF MRI sequences and the LR 3D T_1-basedbrain segmentation methods.

	Scan 1		
Correlation tested	*Mean Δvolume (cc)*	*Pearson's Correlation Coefficient*	*R^2(90% CI)*
CSF LR BPV			
FSL LR	-2±28	.97	.93 (.84-.97)
FreeSurfer LR	83±23	.98	.96 (.82-.99)
SPM LR	11±36	.95	.90 (.76-.95)
CSF HR BPV			
FSL LR	39±35	.95	.91 (.77-.96)
FreeSurfer LR	124±30*	.97	.94 (.74-.99)
SPM LR	52±40	.94	.89 (.68-.95)
FSL LR BPV			
FreeSurfer LR	89±19	.98	.96 (.88-.98)
SPM LR	17±33	.95	.90 (.75-.95)
Freesurfer LR BPV			
SPM LR	-72±32	.96	.92 (.82-.97)
CSF LR ICV			
FSL LR	-209±43*	.96	.92 (.63-.97)
FreeSurfer LR	-227±34*	.98	.96 (.87-.99)
SPM LR	-17±45	.94	.88 (.62-.94)
CSF HR ICV			
FSL LR	-191±41*	.96	.92 (.70-.96)
FreeSurfer LR	-209±27*	.99	.97 (.90-.99)
SPM LR	1±47	.94	.89 (.66-.93)
FSL LR ICV			
FreeSurfer LR	-18±39	.97	.93 (.83-.96)
SPM LR	192±30*	.99	.97 (.90-.99)
Freesurfer LR ICV			
SPM LR	210±58*	.93	.87 (.57-.92)

CSF LR = CSF low resolution MRI scan; CSF HR = CSF high resolution MRI scan. * $p < 0.05$

	Scan 2		
	Mean Δvolume (cc)	*Pearson's Correlation Coefficient*	*R^2(90% CI)*
	1±39	.94	.88 (.62-.96)
	89±35	.95	.91 (.64-.98)
	20±40	.94	.89 (.65-.94)
	37±33	.96	.92 (.76 -.97)
	125±29*	.97	.95 (.79 -.99)
	56±38	.95	.90 (.76-.96)
	88±17	.99	.97 (.92-.99)
	19±37	.95	.91 (.73-.95)
	-69±34	.96	.93 (.80-.97)
	-191±39*	.95	.91 (.63-.98)
	-214±31*	.97	.94 (.81-.98)
	6±46	.94	.88 (.64-.94)
	-191±39*	.96	.92 (.68-.97)
	-214±31*	.98	.97 (.88-.99)
	6±46	.94	.89 (.67-.93)
	-23±36	.97	.95 (.86-.98)
	197±31*	.98	.97 (.84-.99)
	220±56*	.94	.89 (.70-.94)

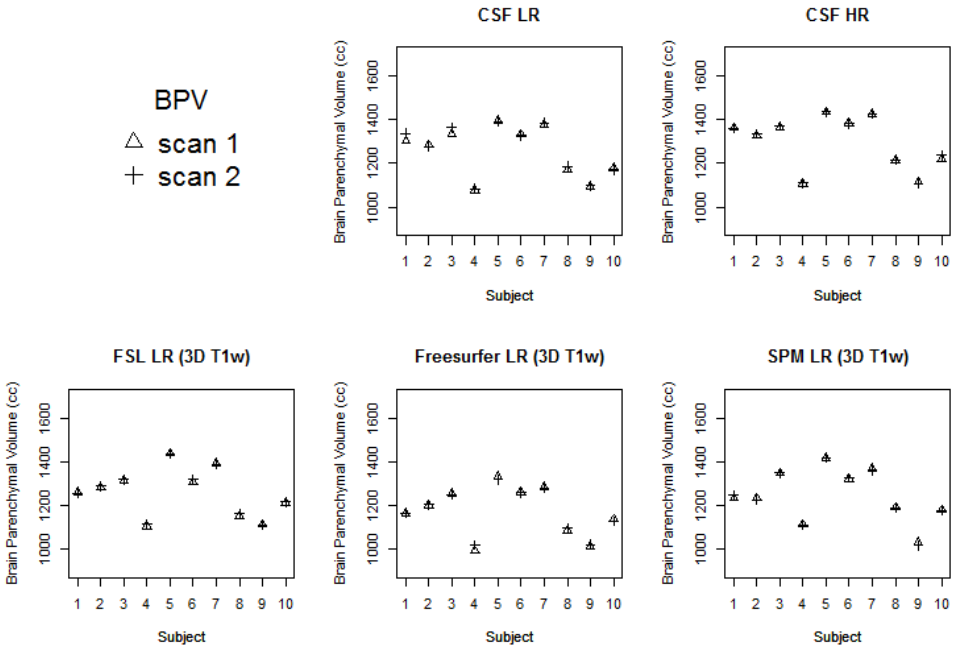

S1 Fig. All BPV measurements for all methods in each subject. CSF LR = CSF low resolution MRI scan; CSF HR = CSF high resolution MRI scan.

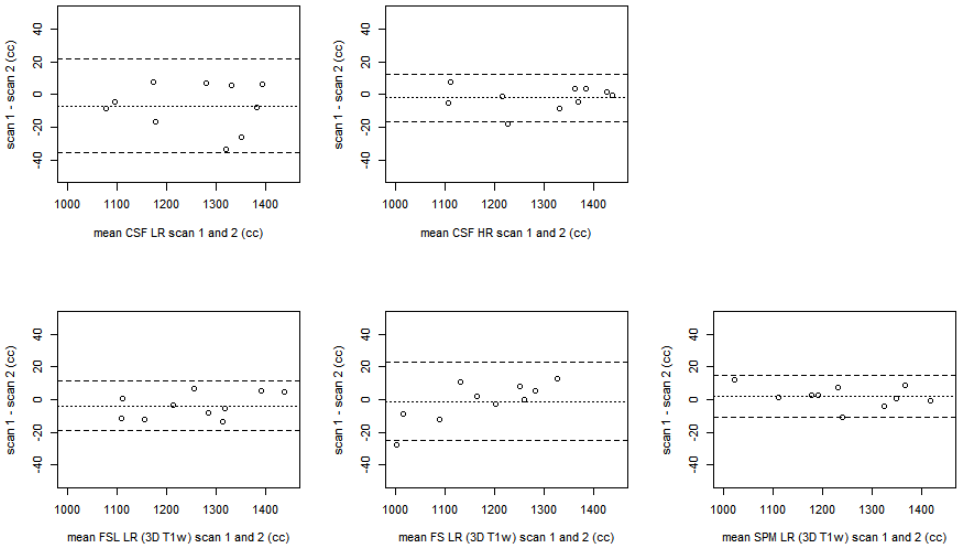

S2 Fig. Bland Altman plots for precision of BPV per method. CSF LR, CSF HR (top row), FSL LR, FreeSurfer LR, and SPM LR (bottom row). The dashed lines represent the limits of agreement (mean difference ±1.96*SD of the differences). LR = low resolution, downsampled scan. CSF LR = CSF low resolution MRI scan; CSF HR = CSF high resolution MRI scan; FS = FreeSurfer.

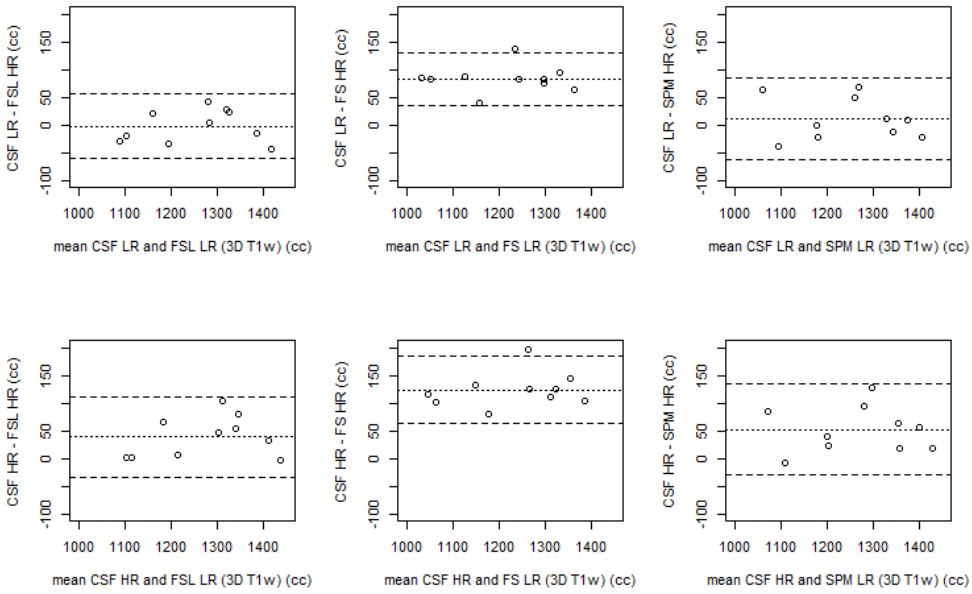

S3 Fig. Bland Altman plots for the comparison of BPV between the CSF MRI sequences and the downsampled (LR) 3D T_1-based brain segmentation methods. The dashed lines represent the limits of agreement (mean difference ±1.96*SD of the differences). CSF LR = CSF low resolution MRI scan; CSF HR = CSF high resolution MRI scan; FS = FreeSurfer.

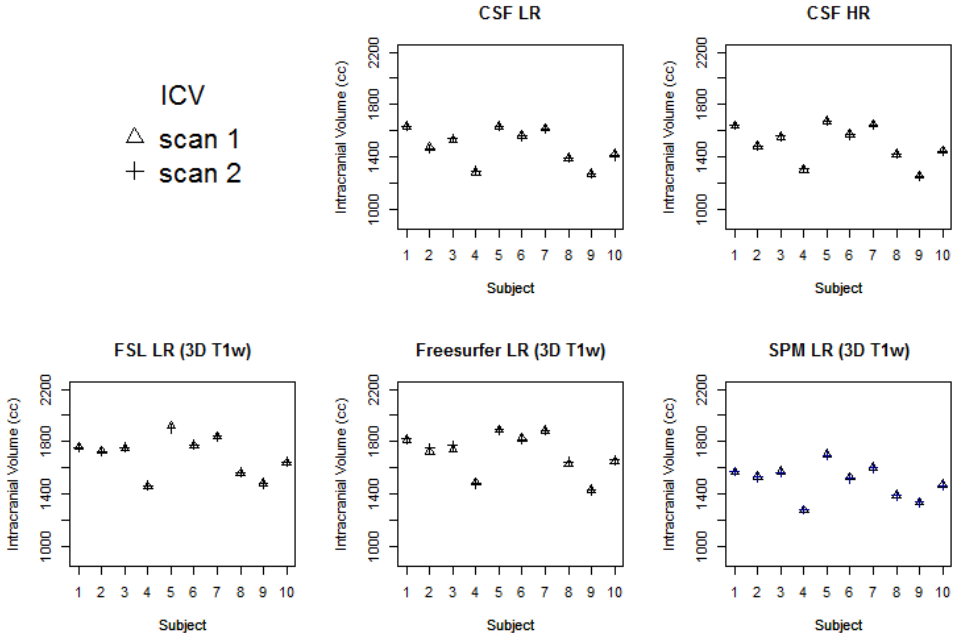

S4 Fig. All ICV measurements for all methods in each subject. CSF LR = CSF low resolution MRI scan; CSF HR = CSF high resolution MRI scan.

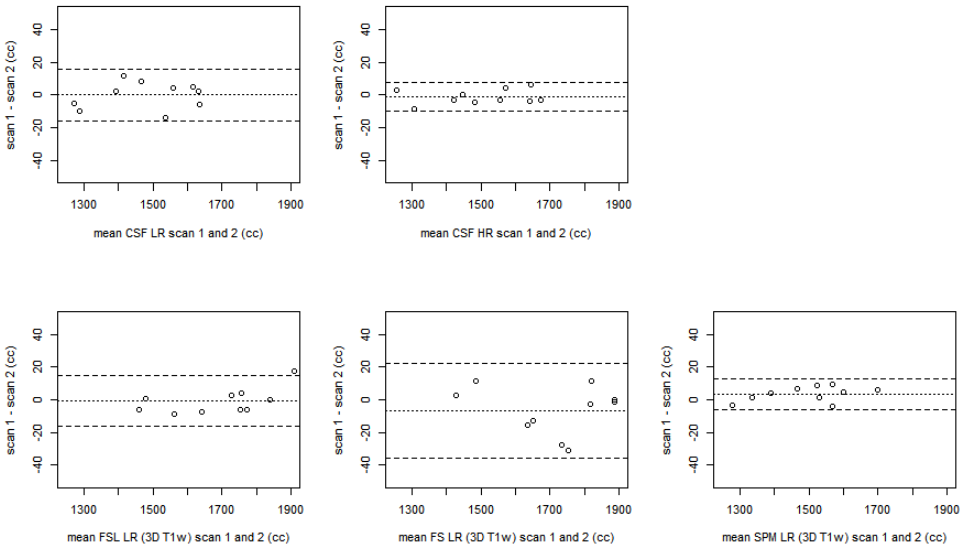

S5 Fig. Bland Altman plots for precision of ICV per method. CSF LR, CSF HR (top row), FSL LR, FreeSurfer LR, and SPM LR (bottom row). CSF LR, CSF HR (top row), FSL LR, FreeSurfer LR, and SPM LR (bottom row). The dashed lines represent the limits of agreement (mean difference ±1.96*SD of the differences). LR = low resolution, downsampled scan. CSF LR = CSF low resolution MRI scan; CSF HR = CSF high resolution MRI scan; FS = FreeSurfer.

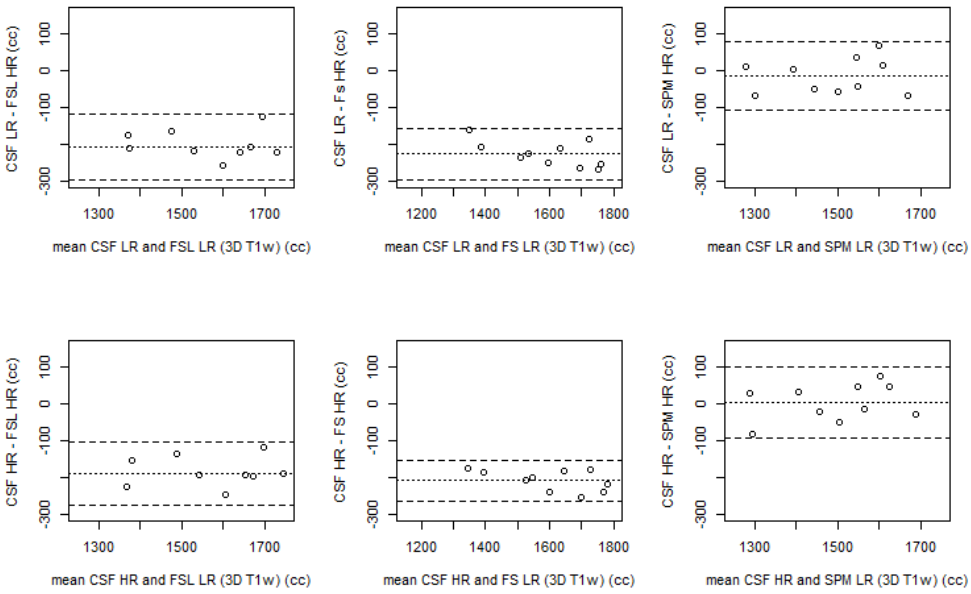

S6 Fig. Bland Altman plots for the comparison of ICV between the CSF MRI sequences and the downsampled (LR) 3D T_1-based brain segmentation methods. The dashed lines represent the limits of agreement (mean difference ±1.96*SD of the differences). CSF LR = CSF low resolution MRI scan; CSF HR = CSF high resolution MRI scan; FS = FreeSurfer.

Chapter 12

Arterial CO_2 pressure changes during hypercapnia are associated with changes in brain parenchymal volume

L.A. van der Kleij[1], J.B. De Vis[2], J. de Bresser[3], J. Hendrikse[1], J.C.W. Siero[1,4]

[1] Department of Radiology, University Medical Center Utrecht, Utrecht University, Utrecht, The Netherlands
[2] National Institute of Neurological Disorders and Stroke, National Institutes of Health, Bethesda, Maryland, USA
[3] Department of Radiology, Leiden University Medical Center, Leiden, The Netherlands
[4] Spinoza Center for Neuroimaging, Amsterdam, The Netherlands

Submitted manuscript

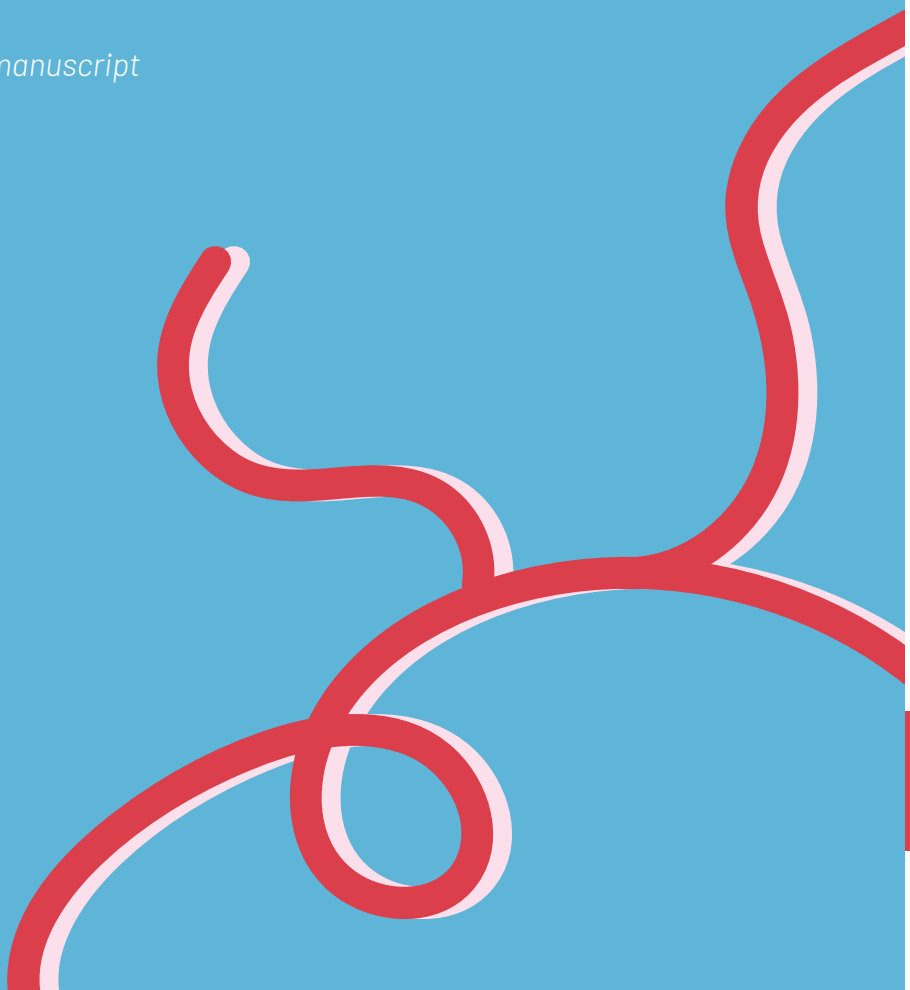

Abstract

The Monro-Kellie hypothesis states that volume changes in any intracranial component (blood, brain tissue, CSF) should be counterbalanced by a co-occurring opposite change to maintain intracranial pressure within the fixed volume of the cranium. Hypercapnia causes an increase in cerebral blood volume through dilation of the cerebral vasculature. In this feasibility study, we investigate the Monro-Kellie hypothesis' application to structural MRI in observing compensating intracranial volume changes during hypercapnia. Seven healthy subjects (median 32 (24–64) years old; 43% female) underwent a $3DT_1$-weighted structural MRI (3T) under normocapnia and hypercapnia. Intracranial tissue volumes were computed from the acquired $3DT_1$-weighted scans. In accordance with the Monro-Kellie hypothesis, the significant increase in measured brain parenchymal volume (+6.0ml; IQR +4.5 – +8.5; *P*=0.02) during hypercapnia co-occurred with a decrease in intracranial cerebrospinal fluid (-10.0 ml; IQR -13.5 – -6.5; *P*=0.03). The results of this study convey several implications for interpreting volumetric MRI results and potential applications: blood volume changes either caused by disorders, anesthesia or medication can affect outcome of brain volumetric studies. In addition, besides probing tissue displacement, the approach described in this study may assess the brain's cerebrovascular reactivity and ability to displace CSF, a potential pathophysiological target of interest for clinical research.

Introduction

The cerebral vasculature plays a critical role in maintaining an optimal supply of cerebral blood flow (CBF) to the brain. This is dependent on cerebral autoregulation and cerebrovascular reactivity (CVR). Autoregulation refers to the mechanism to adjust cerebral perfusion pressure in order to maintain a stable cerebral blood flow, whereas CVR is the brain's capacity to change vessel diameter in response to a vasoactive stimulus. Such vasoactive stimuli are lowered pH, which induces vasodilation directly, and CO_2, which induces vasodilation both directly and indirectly.[1]

Dilation of the cerebral arteries, arterioles and capillaries prompts an increase in cerebral blood volume (CBV) and CBF.[2,3] An increase in CBV is accompanied by an outflow of cerebrospinal fluid (CSF) to the spinal canal in order to maintain intracranial pressure within the fixed volume formed by the cranium and dura mater as postulated by Burrow's correction of the Monro-Kellie doctrine (Figure 1).[4] As well, CSF can drain to the venous sinuses through the subarachnoid villi. Changes in CBV occur constantly as a response to the cardiac cycle, respiratory cycle, fluctuations in blood gases and locally in response to changes in neural activation.[5-7] CBV also changes in response to respiratory acidosis and metabolic acidosis induced in disease or experimental settings. In experimental settings, the most commonly used vasoactive stimulus is an increase in the partial arterial pressure of CO_2 ($PaCO_2$) by means of a hypercapnic breathing challenge. In these cases the vasodilatory response is larger than, for example, during the cardiac cycle. Consequently, CBV and CSF volume changes are also expected to be a multitude larger.

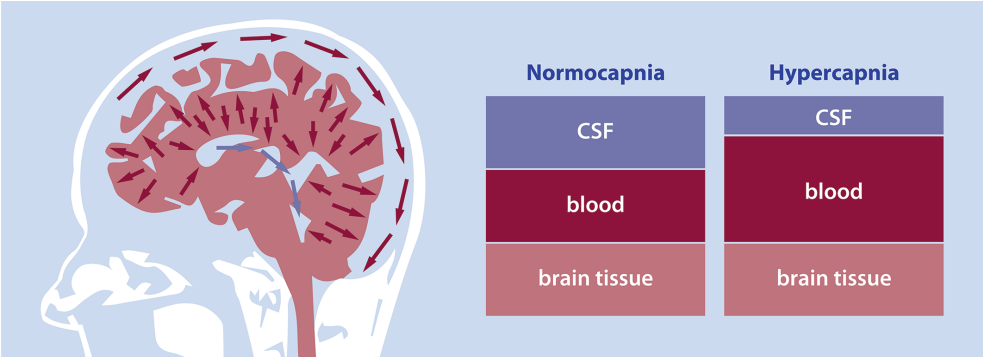

Fig. 1. A schematic illustration of the Monro-Kellie doctrine. The Monro-Kellie doctrine describes the dynamic relationship between the intracranial cerebrospinal fluid (CSF), blood and brain volumes to maintain intracranial pressure. The left panel displays the CSF displacement invoked by an increased cerebral blood volume during hypercapnia. As well, flow in the superior sagittal sinus is shown. Here, CSF is absorbed in the subarachnoid villi. The middle panel is an illustration of the intracranial compartment during normoxic normocapnia (NC). The right panel shows the intracranial volume during hypercapnia (HC), when blood volume increases and CSF volume decreases.

The CBV should be taken into account in longitudinal and cross-sectional studies investigating brain volume, as changes in CBV can impact cerebral tissue volume measurements. Intracranial tissue volumes are typically obtained using T_1-weighted structural images. Since the longitudinal relaxation times (T_1) of gray matter and blood at 3T are similar,[8] blood signals from within gray matter are indiscernible from gray matter tissue signals. Therefore, CBV changes can cause a considerable change in segmented gray matter volume.[8-10] Moreover, a change may occur in partial volume of gray matter relative to the surrounding white matter, which can confound tissue class assignment at tissue borders. As such, changes in (baseline) $PaCO_2$ can affect measured tissue volumes on T_1-weighted images.[10]

Hypercapnia is commonly assumed to predominantly affect gray matter volume measures. Accordingly, observed cortical thickness is increased during hypercapnia.[10] Following the Monro-Kellie hypothesis, we hypothesize that compensating volume changes should be observed in brain parenchymal and CSF volumes on structural MRI in response to cerebral blood volume increases during hypercapnia. In this feasibility study, we investigate the hypothesis' application to structural MRI in observing compensating intracranial volume changes during hypercapnia.

Methods

Participants

Eight healthy volunteers (median age 29 years, range 24 - 64 years) were imaged on a 3 tesla MRI system with an 8-channel head receive coil in August 2015 (Philips Medical Systems, Best, The Netherlands). The study was approved by the Medical Ethical Committee of the University Medical Center Utrecht under protocol number NL39070.041.11. All participants provided written informed consent. Subjects included in this study had two consecutive 3DT1 Magnetization Prepared Rapid Gradient Echo (MPRAGE) scans as part of their imaging protocol: the first scan was performed during normoxic normocapnia (NC) as a baseline scan and the second scan during normoxic hypercapnia (HC). The subjects were not repositioned between scans. All volunteers completed the scan protocol.

Imaging protocol

The acquisition parameters of the 3DT1 MPRAGE were: sagittal 3D inversion-recovery turbo field echo (IR-TFE) were voxel size 1x1x1 mm^3, FOV 240x240x180 mm^3, matrix size 240x240, TR/TE/TI 8/3.2/950 ms, flip angle 10°, 191 Hz readout bandwidth per pixel, shot-interval 2100 ms, SENSE factor 2, acquisition time 3:11 min.

Respiratory challenge

End-tidal O2 (EtO_2) and CO_2 ($EtCO_2$) were controlled using a computer-controlled rebreathing method (RespirAct™, Thornhill Research Inc., Toronto, Canada), which closely match $PaCO_2$ and PaO_2 in healthy volunteers.[11] Subjects were fitted with a sealed mask to prevent air leakage (Tegaderm film, 3M, Maplewood, MN, USA). Sensor lines connected to the face mask and the monitor provided continuous monitoring of breathing pressure and EtO_2 / $EtCO_2$. Before the subjects entered the scanner, a test run was performed in supine position to establish the subject's baseline EtO_2, $EtCO_2$, tidal volume and respiratory rate. These values were then used as input for the NC and HC blocks. The HC challenge consisted of a boxcar stimulus in which $EtCO_2$ was targeted 10 mmHg above a subject's resting baseline $EtCO_2$ over a period of 4:30 min. The 3DT1 MPRAGE scan was started one minute after the hypercapnic stimulus onset.

Image processing

Longitudinal image analysis was performed with the CAT12 toolbox (http://www.neuro.uni-jena.de/cat/) as an extension of SPM12,[12] because of its high accuracy[13] for obtaining gray matter, white matter and CSF volume. Segmentation quality was assessed visually as 'adequate' or 'poor' (L.A.v.d.K.). The intracranial volume was defined as the sum of CSF, gray matter and white matter volumes; and the BPV as the sum of gray matter and white matter volumes. Ventricular volumes were obtained with the ROI CAT12 modality that uses the neuromorphometrics atlas (Neuromorphometrics Inc, http://Neuromorphometrics.com).

Statistical analysis

Statistical analysis was performed in R version 3.4.3.[14] Absolute volume changes were defined as Vol_{HC} - Vol_{NC} (ml), and relative volume changes were defined as: (Vol_{HC} - Vol_{NC} / Vol_{NC})*100%. Volumes between conditions were compared using a wilcoxon signed-rank test. A non-parametric test was chosen because of the small sample size.

Results

Segmentation quality was deemed poor in one out of eight subjects due to excessive motion during hypercapnia. Consequently, seven subjects were included in the volumetric analysis. The median age of the included patients was 32 years (range 24 – 64) and 43% was female. Baseline characteristics are presented in Table 1. The median mmHg $EtCO_2$ increase was 8.68 (IQR 6.77 – 9.60) mmHg (P = 0.02), and no significant change in EtO_2 was observed (P = 0.156).

Table 1. Baseline characteristics and end-tidal CO_2 values†

Subject	Age	Sex	NC $EtCO_2$ (mmHg)	HC $EtCO_2$ (mmHg)	Δ$EtCO_2$ (mmHg)	NC EtO_2 (mmHg)	HC EtO_2 (mmHg)	ΔEtO_2 (mmHg)
1	64	M	36	49	13	113	113	0
2	34	M	32	39	7	111	118	8
3	25	F	33	39	6	111	113	2
4	24	F	36	45	10	107	108	1
5	25	F	37	44	7	107	117	10
6	34	M	28	38	10	119	116	-3
7	32	M	34	42	9	97	109	12
Median (IQR)			*34 (33 - 36)*	*42 (39 – 44)*	*9* (7 - 10)*	*111 (107-112)*	*113 (111 -117)*	*2 (0 – 9)*

$EtCO_2$ = end-tidal CO_2; EtO_2 = end-tidal O_2; NC = normoxic normocapnia; HC = normoxic hypercapnia
†Values are rounded to the nearest integer. Changes are calculated from unrounded data. **P*<0.05.

Median BPV during NC was 1234 ml (IQR 1162 – 1305 ml), which increased by 0.53% (IQR 0.35 – 0.72%) during HC (*P* = 0.02; Table 2). This was an absolute brain volume increase of 6.0 ml (IQR 4.5 – 8.5 ml) (*P* = 0.02) . Gray matter showed a non-significant relative increase of 0.31% (IQR -0.06 – 0.75%; *P* = 0.47), and an absolute volume increase of 2.0 ml (IQR -0.5 – 5.0 ml; *P* = 0.50). In contrast, white matter volume increased by 0.80% (IQR 0.48 – 1.21%; *P* = 0.02), which is an absolute volume increase of 4.0 ml (IQR 2.5 – 7.0ml; *P* = 0.02) (Figure 2). A global decrease in CSF volume (3.4% IQR 2.1 – 4.8%; P = 0.03) was measured with a median change of -10.0 ml (IQR -13.5 – -6.5 ml; P = 0.034) during hypercapnia compared to normocapnia. As well, a decrease in ventricular volume occurred during HC compared to NC: the median relative volume change was -1.59% (IQR -2.84 – -1.14%) and the absolute median volume change was -0.38 ml (IQR -0.26 – -0.53 ml; *P* = 0.02).

Table 2. Absolute volumes under normocapnia and hypercapnia†

	Volumes at NC (ml)	Volumes at HC (ml)	ΔVolume (ml)	P
Intracranial volume	1508 (1493–1587)	1507 (1495–1581)	-3.0 (-1.5–-6.5)	0.271
BPV	1234 (1162–1305)	1243 (1167–1311)	6.0 (4.5–8.5)	0.02*
Gray matter	707 (653–745)	714 (654–740)	2.0 (-0.5–5.0)	0.50
White matter	528 (524–548)	535 (527–554)	4.0 (2.5–7.0)	0.02*
Total CSF	295 (279–318)	285 (267–312)	-10.0 (-13.5–-6.5)	0.03*
Ventricular CSF	17.6 (15.1–22.3)	17.3 (14.8–22.0)	-0.4 (-0.3–-0.5)	0.01*

NC = normocapnia; HC = hypercapnia; BPV = brain parenchymal volume; CSF = cerebrospinal fluid.
†Values are rounded to the nearest integer. Volume changes are calculated from unrounded data.
**P*<0.05. Volumes in median (IQR).

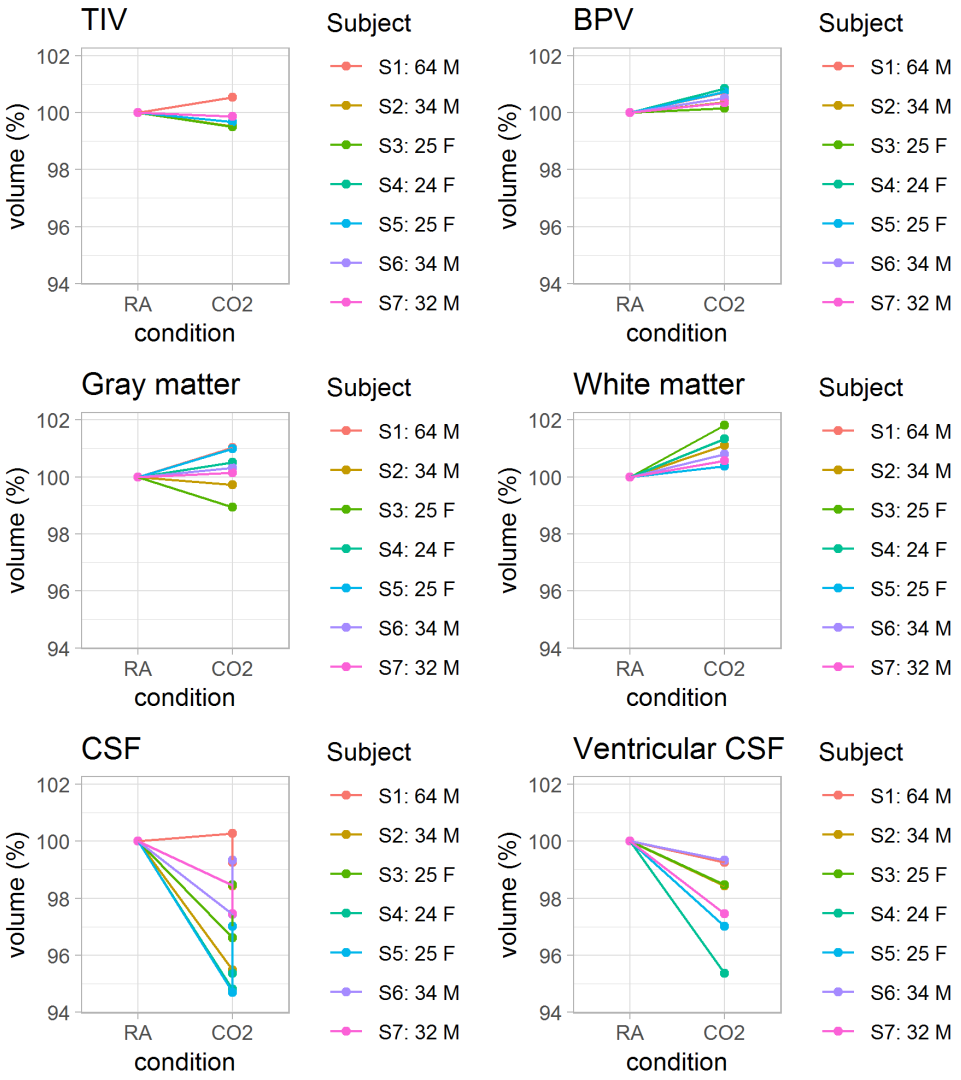

Fig. 2. Relative changes in tissue volume (%). Tissue volume changes during hypercapnia are plotted relative to each volume during normocapnia (RA) (set to 100%) per subject. Subject 1 showed an increase in all measured volumes, which resulted in an estimated intracranial volume increase of 9 ml during hypercapnia (top left image). TIV = total intracranial volume; BPV = brain parenchymal volume; CSF = cerebrospinal fluid.

Discussion

We found an increase in brain parenchymal volume and a decrease in CSF volume on $3DT_1$-weighted MRI during hypercapnia. The results of this study demonstrate the feasibility of widely used, structural MRI sequences to observe volumetric reactivity capability. As well, the results convey several implications for interpreting volumetric MRI results and its potential applications. For instance, diseases and pharmaceutical drugs

with vasoactive properties may influence brain and CSF volume assessment. This can affect longitudinal and cross-sectional study designs, for instance regarding atrophy measurements. Also, segmentation analyses of conventional imaging sequences could be used to infer CVR when a vasodilatory stimulus is given.

A median 6 ml increase in BPV was observed during a +9 mmHg hypercapnia stimulus, which is in agreement with an earlier study reporting on ΔCBV as a response to a +10 mmHg hypercapnia stimulus.[15] $PaCO_2$ and blood pH effects can occur in various contexts, and these results highlight that they warrant careful consideration in the interpretation and analysis of intracranial volumetric data. An increase in $PaCO_2$ and/or a reduction in blood pH can occur in a range of settings aside from a hypercapnic breathing paradigm. As abnormal baseline $PaCO_2$ can affect volume measures [10], awareness of its occurrence is important in the abundant longitudinal and cross-sectional studies that investigate brain volume changes. One example of an acute onset respiratory acidosis is the administration of sedative agents in patients undergoing MRI, or exercise tasks during MRI.[16-18] In addition, respiratory acidosis can occur in restrictive or obstructive lung disease in which impaired respiratory exchange causes CO_2 retention, whereas metabolic acidosis may occur in patients with chronic kidney disease due to impaired H^+ excretion.[19, 20] In cross-sectional studies, differences in $PaCO_2$ could confound volumetric MRI results if one group experienced an increased $PaCO_2$ while the other group(s) did not. In longitudinal studies, .long-term CBV changes related to age and specific pathologies should be regarded.[10] The size of the effects remains to be investigated, but it could have implications for an extensive amount of studies investigating brain volume.

Second, the approach described in this study can be applied as a structural CVR measure. A drawback of our study design is that no data were collected on cerebral blood volume. Therefore, future research is required with CBV measurements along structural CVR to validate the current proof-of-concept study. Structural images are always part of the scan protocol for clinical purposes, and they are readily available even at non-academic hospitals. The $3DT_1$-based approach offers an excellent contrast between brain parenchyma and CSF. Yet it also carries the limitation of low contrast between the CSF, dura mater and skull, thereby limiting the method's ability to detect peripheral CSF volume changes accurately. This makes the sequence suitable for detecting brain volume changes, but less so for the detection of total CSF volume changes as indicated by the variability in obtained intracranial volume. Alternative, short sequences are available to determine CSF volume changes due to hypercapnia.[21] Short imaging time is of particular importance for any sequence used in clinical settings, where CVR assessment can aid in treatment selection and function as a marker of disease severity along with the structural markers.[22, 23] The use of structural images for CVR measurements reduces scan time and cost, because only one additional scan during hypercapnia is appended

to the scan protocol.

Limitations of our study are the relatively small sample size and the homogeneous group of healthy subjects. Subsequent studies should elicit whether this method is also applicable for older individuals and for various patient populations. Also, no quantitative T1 measurements were performed in the current study for comparison with morphological changes. While a study with a comparable hypercapnia challenge did observe an increase in gray matter volume on 7T MRI,[10] no significant increase in gray matter volume was found in our study. Segmentation was performed on a UNI image in that study, which is a T_1-weighted image unaffected by T_2^*, proton density and field inhomogeneities. Whereas this does not affect total brain volume, our observed increase in white matter volume rather than gray matter volume might be explained by these biases. Further, an earlier reported difference in the effect of hypercapnia on T1 in gray matter compared to white matter may contribute to the found changes. A significant decrease in gray matter T1 has been found during hypercapnia, while no significant change occurred in white matter [10]. Therefore, hypercapnia may increase the probability of white matter assignment in voxels at gray - white matter boundaries.[24, 25] Second, earlier work has shown the dilation of cerebral arteries during hypercapnia.[26] A considerable amount of these arteries are co-located with the segmented white matter. As their signal intensity is closer to white matter than gray matter, they can contribute to a higher segmented white matter volume during hypercapnia. Third, the volumetric changes in gray matter and white matter (~3 ml) are close to the threshold of volume changes that can reliably be detected with automatic segmentation.[21] As such, the changes in total brain volume are more informative than the absolute changes in white and gray matter separately. Future studies should investigate the effect of baseline hemodynamic characteristics on brain volume assessments to ensure that they do not confound brain volumetric studies.

In conclusion, we showed that arterial CO_2 pressure changes during hypercapnia are associated with changes in BPV and CSF volume in accordance with the Monro-Kellie hypothesis. The found volume changes highlight the relevance of accounting for hemodynamic parameters when interpreting volumetric MRI studies. The proposed volumetric approach to measure CVR may offer a new marker of intracranial tissue reactivity.

References

1. Yoon S, Zuccarello M, Rapoport R. Pco2 and ph regulation of cerebral blood flow. *Frontiers in Physiology*. 2012;3:365
2. Willie CK, Tzeng Y-C, Fisher JA, Ainslie PN. Integrative regulation of human brain blood flow. *The Journal of Physiology*. 2014;592:841-859
3. Meng L, Gelb AW. Regulation of cerebral autoregulation by carbon dioxide. *Anesthesiology*. 2015;122:196-205
4. Burrows G. *On disorders of the cerebral circulation ; and on the connection between affections of the brain and diseases of the heart*. London: Longman, Brown, Green and Longmans; 1846.
5. Wåhlin A, Ambarki K, Hauksson J, Birgander R, Malm J, Eklund A. Phase contrast mri quantification of pulsatile volumes of brain arteries, veins, and cerebrospinal fluids compartments: Repeatability and physiological interactions. *Journal of Magnetic Resonance Imaging*. 2012;35:1055-1062
6. Balédent O. Imaging of the cerebrospinal fluid circulation. In: Rigamonti D, ed. *Adult hydrocephalus*. Cambridge: Cambridge University Press; 2014:121-138.
7. Piechnik SK, Evans J, Bary LH, Wise RG, Jezzard P. Functional changes in csf volume estimated using measurement of water t2 relaxation. *Magnetic Resonance in Medicine*. 2009;61:579-586
8. Lu H, Clingman C, Golay X, van Zijl PCM. Determining the longitudinal relaxation time (t1) of blood at 3.0 tesla. *Magnetic Resonance in Medicine*. 2004;52:679-682
9. Wright PJ, Mougin OE, Totman JJ, Peters AM, Brookes MJ, Coxon R, et al. Water proton t 1 measurements in brain tissue at 7, 3, and 1.5t using ir-epi, ir-tse, and mprage: Results and optimization. *Magnetic Resonance Materials in Physics, Biology and Medicine*. 2008;21:121
10. Tardif CL, Steele CJ, Lampe L, Bazin PL, Ragert P, Villringer A, et al. Investigation of the confounding effects of vasculature and metabolism on computational anatomy studies. *NeuroImage*. 2017;149:233-243
11. Slessarev M, Han J, Mardimae A, Prisman E, Preiss D, Volgyesi G, et al. Prospective targeting and control of end-tidal co2 and o2 concentrations. *The Journal of Physiology*. 2007;581:1207-1219
12. Ashburner J. Computational anatomy with the spm software. *Magn Reson Imaging*. 2009;27:1163-1174
13. Mendrik AM, Vincken KL, Kuijf HJ, Breeuwer M, Bouvy WH, de Bresser J, et al. Mrbrains challenge: Online evaluation framework for brain image segmentation in 3t mri scans. *Computational Intelligence and Neuroscience*. 2015;2015:813696
14. R Core Team. R: A language and environment for statistical computing. 2017
15. Alderliesten T, De Vis JB, Lemmers PMA, van Bel F, Benders MJNL, Hendrikse J, et al. Simultaneous quantitative assessment of cerebral physiology using respiratory-calibrated mri and near-infrared spectroscopy in healthy adults. *NeuroImage*. 2014;85:255-263
16. Ellison RG, Ellison LT, Hamilton WF. Analysis of respiratory acidosis during anesthesia. *Annals of Surgery*. 1955;141:375-382
17. Clement P, Mutsaerts H-J, Václavů L, Ghariq E, Pizzini FB, Smits M, et al. Variability of physiological brain perfusion in healthy subjects – a systematic review of modifiers. Considerations for multi-center asl studies. *Journal of Cerebral Blood Flow & Metabolism*. 2018;38:1418-1437
18. Querido JS, Sheel AW. Regulation of cerebral blood flow during exercise. *Sports Medicine*. 2007;37:765-782
19. Bruno CM, Valenti M. Acid-base disorders in patients with chronic obstructive pulmonary disease: A pathophysiological review. *Journal of Biomedicine and Biotechnology*. 2012;2012:8
20. Chen W, Abramowitz MK. Metabolic acidosis and the progression of chronic kidney disease. *BMC Nephrology*. 2014;15:55-55
21. van der Kleij LA, de Bresser J, Hendrikse J, Siero JCW, Petersen ET, De Vis JB. Fast csf mri for brain segmentation; cross-validation by comparison with 3d t1-based brain segmentation methods. *PLOS ONE*. 2018;13:e0196119
22. Silvestrini M, Pasqualetti P, Baruffaldi R, Bartolini M, Handouk Y, Matteis M, et al. Cerebrovascular reactivity and cognitive decline in patients with alzheimer disease. *Stroke*. 2006;37:1010-1015

23. Low SW, Teo K, Lwin S, Yeo LLL, Paliwal PR, Ahmad A, et al. Improvement in cerebral hemodynamic parameters and outcomes after superficial temporal artery-middle cerebral artery bypass in patients with severe stenoocclusive disease of the intracranial internal carotid or middle cerebral arteries. *Journal of Neurosurgery*. 2015;123:662-669
24. Glasser MF, Van Essen DC. Mapping human cortical areas in vivo based on myelin content as revealed by t1- and t2-weighted mri. *The Journal of Neuroscience*. 2011;31:11597-11616
25. Bock NA, Hashim E, Janik R, Konyer NB, Weiss M, Stanisz GJ, et al. Optimizing t1-weighted imaging of cortical myelin content at 3.0t. *NeuroImage*. 2013;65:1-12
26. Verbree J, Bronzwaer A-SGT, Ghariq E, Versluis MJ, Daemen MJAP, van Buchem MA, et al. Assessment of middle cerebral artery diameter during hypocapnia and hypercapnia in humans using ultra-high-field mri. *Journal of Applied Physiology*. 2014;117:1084-1089

Chapter 13

General Discussion

The aim of this thesis was to explore applications of three selected, quantitative MRI makers: cerebral perfusion, the T2 of peripheral cerebrospinal fluid (CSF) and volumetric measures. The studied populations share a risk of future decline, where a patient's functional status will either deteriorate, remain stable or recover. In part 1, we used quantitative MRI markers to investigate the impact of aneurysmal subarachnoid hemorrhage (aSAH) and traumatic brain injury (TBI) on the brain. Both conditions are characterized by a relatively young patient population and a substantial proportion of patients with poor functional outcome. In part 2, we investigated the three quantitative MRI markers to distinguish between individuals on the continuum between healthy aging and dementia.

Structural imaging

Summary of findings

In the systematic review and meta-analysis of **chapter 2**, ischemic lesions on diffusion weighted imaging (DWI) were found in about 50% of patients in the acute (≤72 hours) and subacute stages (72 hours – 21 days) after injury. Clinical condition on admission was associated with lesions prevalence in the acute state, whereas differences in aneurysm treatment modality as well as the timing of MRI in the individual studies were associated with subacute lesion prevalence. A probable explanation for the effect of MRI timing on lesion prevalence in the subacute stage is that imaging was performed on different times relative to delayed cerebral brain injury occurrence. Studies that image either during neurological decline or after the high risk window for delayed brain injury will find a higher proportion of patients with lesions than studies that image before onset of delayed brain injury. The prediction interval associated with lesion prevalence ranged from 4% to 96% in the acute stage, and between 20% and 76% in the subacute stage. Wide prediction intervals indicate that the expected proportion of patients with lesions for a new study carries a high degree of uncertainty. **Chapter 3** showed that chronic infarcts and decreased brain volume on MRI are related to poor outcome after aSAH. In agreement with previous research,[1-6] the longitudinal studies in **chapters 4 and 6** demonstrated that brain volume changes commonly ensue after aSAH and traumatic brain injury (TBI). In aSAH patients the median volume change was -2.0% (IQR -3.7 – -0.7%) between 14 days and 6 months, which further decreased between 6 and 18 months. Interestingly, in chapter 4 lesions on DWI/T2-FLAIR around day 14 were not associated with brain volume change, which signals that focal lesions are not predictive of global cerebral volume changes. The progressive decrease in volume between 6 and 18 months to me indicates that the found changes are probably not only due to edema normalization, but reflect true brain volume loss. Following the observed brain volume changes in aSAH, we hypothesized in chapter 6 that traumatic SAH – assessed

on T2*-weighted GRE and T2-FLAIR images – is also associated with larger brain volume changes. In fact, no volume change was observed between 1 and 90 days in TBI patients clear of SAH (-0.4%, IQR -1.8 – 0.9%), whereas the median volume change was -3.2% (IQR -4.8 – -1.3%) in patients with SAH. Unlike the study in aneurysmal SAH patients, we did not obtain additional follow-up measures in the TBI group. However, other studies have showed long-term, continuing brain volume decrease after TBI, which also suggests that the found changes reach beyond edema normalization.[7] In addition, although our results only show a correlation rather than a causal relationship, preclinical evidence exists for a causal relationship between subarachnoid blood and cortical infarctions.[8] Further research is warranted to confirm the relationship between SAH, functional outcome,[9] and brain volume changes. Even though the appearance of traumatic SAH is often subtle on imaging, it may help identify the 1 out of 5 mild TBI patients that experience long-term functional impairment.[10] In summary, the findings in chapter 6 show that SAH may be a factor to take into consideration for treatment decisions after trauma.

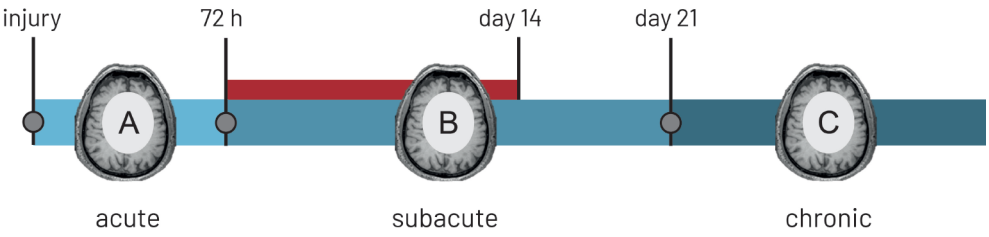

Fig. 1. Disease stages and imaging time points after subarachnoid hemorrhage (time not to scale). The high risk window for delayed brain injury between days 4 and 14 is highlighted in red. At time point A, brain injury can be found due to the initial insult, early brain injury and, if applicable, due to aneurysm securing. At time point B, new injury can arise due to delayed brain injury. At time point C, chronic infarcts and atrophy can be assessed.

Notes on the use of structural imaging

Time of imaging and lesion assessment method can influence outcome

Whereas the same technique – DWI – was used in all studies reviewed in chapter 2, the image assessment differed between studies; some studies in chapter 2's review did not specify DWI lesion evaluation, and only half of studies reported the acquisition of DWI with apparent diffusion coefficient (ADC) maps. Along with the relatively small study samples – median ~35 patients per study – this methodological disparity may partially explain the variable lesion prevalence between studies. DWI can either be interpreted with or without the ADC value and either with or without a joined reading of T2-FLAIR or T2-weighted images. Ideally, ischemic lesions are identified based on combined information from DWI, ADC and T2-FLAIR/T2-weighted imaging, because the signal intensities on the three image types change over the course of days and weeks.[11] In ad-

dition to changed signal intensities, the timing of imaging can also affect found lesion prevalence considering that additional lesions can occur in the first weeks following aSAH due to aneurysm securing, early brain injury and delayed brain injury (Figure 1). Accordingly, imaging at different time points can yield different information (Figure 1).

The effect of cerebral blood volume in brain volumetric studies

Volume measurements from segmented 3DT1-weighted images are a widely used measure in cross-sectional and longitudinal studies. The findings in **chapter 12** emphasize that observed changes in cerebral brain volume can be caused by changes in cerebral blood volume, because blood has a similar T1 to gray matter.[12] Thus, cerebral blood volume can be a confounder in the assessment of brain volume and brain volume changes on 3DT1-weighted images. We found a 6ml increase in measured brain volume in response to blood volume increases provoked by hypercapnia, which is roughly 0.5% of brain volume when assuming an average cerebral volume of 1300ml. Aside from experimental settings, blood volume changes due to respiratory or metabolic acidosis can also occur in a range of clinical settings, for instance in patients scanned under sedation or in patients with chronic kidney disease.[13, 14] As such, it could be helpful in brain volumetric studies to include a cerebral blood volume measurement in cases where significant changes in blood volume are expected.[15, 16]

Nevertheless, the effect of cerebral blood volume changes on 3DT1-based brain volume measurements is not only a nuisance: we propose it can be exploited as an alternative measure of cerebrovascular reactivity (CVR). To confirm this hypothesis, a comparison should be performed with established MRI methods for CVR: blood-oxygenation-level-dependent (BOLD) MRI and arterial spin labeling (ASL) MRI.[17, 18] BOLD and ASL MRI are sensitive methods to detect CVR. ASL MRI provides the added advantage of cerebral blood flow (CBF) measurements, which can contribute valuable information. However, absolute quantification of the CBF CVR responses can be problematic in areas with severely prolonged bolus arrival times. As well, the signal-to-noise ratio is decreased by prolonged arterial transit times, which, for example, typically occurs in aging. In comparison, BOLD signal changes originate from a complex interaction of CBF, cerebral blood volume, and the cerebral metabolic rate of oxygen, and they are dependent on the baseline physiological state including baseline venous oxygenation, oxygen extraction fraction, and CBF.[19] A drawback of structural CVR measurements is a likely lower sensitivity to small changes than ASL and BOLD MRI. An advantage of structural CVR is that structural images are always part of the scan protocol for clinical purposes, and they are readily available even at non-academic hospitals. Additionally, the use of alternative sequences can be explored for structural CVR measurement, such as the CSF MRI sequence described in **chapter 11**. In contrast to 3DT1-weighted images, CSF MRI scans show a high contrast between CSF, dura mater and skull, As such, they could potentially provide a more accurate measure of CSF changes upon vasodilation.

A pitfall of the sequence is that differences in gray and white matter volume changes cannot be observed.

Perfusion imaging

Summary of findings

Cerebral blood flow is modulated by cerebral health and pathology, which makes it a promising quantitative marker to identify patients at risk. Moreover, changes in CBF may precede the manifestation of structural damage. Perfusion imaging on any imaging modality usually involves an injected intravenous tracer, but ASL MRI provides a non-invasive alternative by labeling blood water at the neck level as an endogenous tracer (**chapter 10**). Following a post label delay (PLD), homogeneous perfusion images are acquired when the labeled blood water has reached the capillary bed. If the arterial transit time (ATT) is longer that the PLD, it results in a more heterogeneous perfusion image. Consequently, signal decreases on typically used single PLD images can either indicate regionally decreased CBF or increased ATT.

Apart from an artifact, the degree of perfusion heterogeneity has been proposed as a measure of cerebrovascular health.[20-23] In chapter 4 we found that increased perfusion heterogeneity on day 14 in aSAH patients is associated with long-term brain volume changes. Here, we used two different measures of perfusion heterogeneity: the coefficient of variation (standard deviation / mean perfusion) and the borderzone ratio (borderzone / whole brain perfusion). The borderzone regions are supplied by distal vasculature, so they are inherently more sensitive to hypoperfusion due to ATT increases.[24] Our findings from a relatively small sample are in agreement with the idea that perfusion heterogeneity is tied to perfusion impairment.[21, 24] In chapter 6, perfusion measured within 48 hours after trauma was also associated with brain volume changes, even though its effect on brain volume appeared less pronounced than the presence of traumatic SAH. Specifically, we found a moderate association between brain volume changes following trauma and the mean peak measure from the model-free temporal similarity perfusion (TSP) mapping analysis. Building on these found associations between perfusion and volume change, **chapter 5** describes the protocol of an ongoing phase II randomized controlled trial that investigates the use of acetazolamide in aneurysmal subarachnoid hemorrhage (ASH). Acetazolamide can benefit patients with aSAH through increasing perfusion, reducing cerebrospinal fluid production and reducing cerebral edema. At the time of writing, ten out of 40 projected patients are included in the trial, so no results are discussed in this thesis yet. If the ASH trial is successful in showing the safety and efficacy of acetazolamide after aSAH, a phase III trial should determine its effect on delayed brain injury.[25]

Traditionally, Alzheimer's disease has been viewed as primarily a brain parenchymal problem, but now it has been recognized that vascular pathology can accelerate and aggravate pathology.[26] For example, amyloid β collects around smooth muscle cells of the vessel wall, and can thereby affect vessel function and cerebral perfusion.[27, 28] Moreover, cardiorespiratory fitness has been associated with preserved brain function and structure, which suggests that improved vascular health can promote healthy aging.[29, 30] Indeed, **chapter 7** showed that preventable vascular risk factors and physical fitness are associated with gray matter cerebral blood flow in elderly participants around 65 years old. Here sex-related differences were found regarding the specific vascular risk factors and physical fitness measures that were associated with CBF. Counterintuitively, the group with the lowest cardiorespiratory fitness showed the highest CBF in women. This finding is in agreement with a recent study, and with the idea that higher cerebral blood flow can reflect both good cerebrovascular health and compensatory mechanisms in poor cerebrovascular health.[31, 32] Nevertheless, physical fitness throughout life and physical exercise interventions in healthy elderly have been found to increase regional CBF.[33, 34] Interestingly, the exercise intervention in **chapter 9** was effective in improving cardiorespiratory fitness (VO_2 peak) in patients with Alzheimer's disease, but no effect of physical exercise on CBF was found. Probable explanations for the absence of a CBF change are either the intervention duration or disease state of the participants. I think that the advanced disease stage is the main cause of the lack of an effect. In the main ADEX study, executive function improved only in the participants that best complied with the intervention.[35]

Notes on the use of perfusion imaging

The effect of blood T1 on cerebral blood flow quantification in ASL MRI

The quantification of CBF from ASL MRI images requires either an estimation or measurement of the T1 of blood ($T1_{blood}$).[36] The $T1_{blood}$ value is dependent on hematocrit, and accordingly it can be estimated from hematocrit values with the following formula: $T1_{blood} = 0.52 * \text{hematocrit} + 0.38$.[36] The results of chapter 7 confirmed that $T1_{blood}$ should ideally be individually corrected, because significant differences in quantified CBF were observed after $T1_{blood}$ was corrected for hematocrit. Especially cross-sectional studies are sensitive to this effect, as here CBF differences between groups may be traced to $T1_{blood}$ differences between groups. Yet, also longitudinal studies where $T1_{blood}$ changes are expected should take this effect into account. Aside from obtaining the hematocrit through a venous blood sample, several non-invasive imaging methods exist to determine $T1_{blood}$ within a few seconds to a minute of scan time.[37, 38] These sequences can be especially helpful in cases where hematocrit is not a valid measure of $T1_{blood}$. For example, in sickle cell disease the relationship between hematocrit and $T1_{blood}$ is different, so $T1_{blood}$ estimates from hematocrit deviate from the true value.[39]

Interpretation of absolute and relative cerebral blood flow measurements
Absolute CBF is difficult to compare between studies, since it can differ depending on imaging sequence, post-processing and a wide range of physiological factors.[40] Moreover, a simple rule which states that lower perfusion indicates worse health does not seem sufficient, for it has been shown that increased physical fitness can also be associated with lower CBF.[31] Still, in context of other measures on an individual's health, CBF can provide valuable information. Therefore, relative measures like perfusion heterogeneity may be more consistent and easier to interpret. This is especially applicable when regional perfusion is affected, such as in patients with neoplasms, stroke, or moyamoya disease. Here reference values from healthy tissue can be used for relative CBF and – in case of a multi-delay sequence – arterial transit time.

The effect of noise on study results
ASL MRI is typically associated with high levels of acoustic noise. Particularly when scanning the severely ill patients of chapter 6, but also in patients with dementia of chapter 8, I noticed that the high noise levels associated with MRI are a major contribution to patient discomfort.[41] Discomfort contributed to patient motion during the imaging protocol, which in turn affected image quality. Although motion can be prospectively or retrospectively corrected, minimization of patient motion by improving patient comfort could also be a successful route. Therefore, along faster scanning and higher field strength, the reduction of scanner noise may significantly improve image quality.[42–45]

The $T2_{pCSF}$ parameter

Summary of findings

In **chapter 8** we observed a positive association of $T2_{pCSF}$ with disease severity in a cohort of patients with cognitive decline. This finding is in agreement with previous research from our group in which patients with dementia showed a higher $T2_{pCSF}$ than healthy, elderly control subjects.[46] We propose that the $T2_{pCSF}$ may provide a more comprehensive measure of cerebrovascular dysfunction than CBF due to its dependency on oxygenation. This hypothesis is based on the dependency of $T2_{pCSF}$ on oxygenation, and that oxygen can only enter the peripheral CSF space through diffusion along vessel walls. As such, CSF may provide an indirect measure of tissue oxygenation and oxygen consumption.

From a clinical perspective, a valuable marker in cognitive decline can distinguish between patients with the same disease stage to predict future decline. To illustrate: only 1 in 3 MCI patients will develop dementia, so the other 2 out of 3 patients will remain at a relatively stable level of cognitive impairment. It is paramount to know what a patient's

trajectory will be for the patient and their caregiver(s), for the treating physician and for clinical trials.[47] Interestingly, the T_{2pCSF} marker showed an especially strong association with verbal memory, which as a cognitive domain has been found most predictive of future decline.[48] An interesting finding was that $T2_{pCSF}$ was different in patients with subjective cognitive complaints compared to MCI and dementia patients, but not between MCI and dementia patients. In contrast, global atrophy was different in patients with dementia compared to subjective cognitive decline and MCI patients, but not between subjective cognitive decline and MCI patients. Given this distinction, I hypothesize that it demonstrates the potential of $T2_{pCSF}$ as an earlier marker for neurodegenerative disease than global atrophy.

Notes on the use of $T2_{pCSF}$ mapping

Although the results in chapter 8 are ground for cautious optimism, they should be regarded as a first impression rather than a confirmation of $T2_{pCSF}$'s value in cognitive decline. The study's major limitations are the small sample size and lack of follow-up data. Therefore, no generalizations can be made based on these results. As well, pathology is missing, so we can only speculate on what biological processes are driving the observed $T2_{pCSF}$ differences. Nonetheless, I think the results are sufficiently promising to investigate $T2_{pCSF}$'s ability to distinguish patients with a similar level of cognitive impairment based on their future decline. The short acquisition time of under a minute facilitates an easy addition of the CSF MRI sequence to a scan protocol. As well, aside from $T2_{pCSF}$ measurements, chapter 11 demonstrated that the CSF MRI sequence provides a valid and reliable measure of cerebral atrophy

Short thesis overview

Aneurysmal subarachnoid hemorrhage

- The variability in lesion prevalence between studies can be explained by a) timing of imaging, b) clinical status of included patients, c) image reading approach.
- The high variability in reported lesion prevalence on diffusion weighted imaging in the acute and subacute stage bars an estimate for future studies.
- Long-term brain volume changes of a few percent were common.
- Increased perfusion heterogeneity may help identify patients at risk for large brain volume changes.

Traumatic brain injury

- Brain volume changes were found in patients with a relatively good clinical status, which suggests a worse disease state than clinical symptoms at admission imply.
- Subarachnoid hemorrhage in (mild) traumatic brain injury should be considered as a risk factor and it may present a treatment target.

Ageing – dementia

- Preventable vascular risk factors and physical fitness were associated with cerebral blood flow in elderly individuals.
- A measurement or estimate of $T1_{blood}$ can significantly influence results from ASL MRI studies.
- The CSF MRI sequence provides $T2_{pCSF}$ and atrophy measurements within a minute of scan time.
- The $T2_{pCSF}$ was associated with cognition in a memory clinic cohort.
- 16 weeks of moderate-to-intense exercise did not affect cerebral blood flow in patients with mild or moderate Alzheimer's disease.

Future questions

- Is perfusion heterogeneity in the subacute stage after aneurysmal subarachnoid hemorrhage associated with worse cognitive and functional outcome?
- Is subarachnoid hemorrhage due to trauma associated with worse cognitive and functional outcome?
- Can $T2_{pCSF}$ predict future decline in patients with cognitive impairment?
- How does a 1 year exercise intervention affect cerebral blood flow in elderly volunteers around 65 years old with varying levels of health? (LISA study follow-up)

References

1. Koivisto T, Vanninen R, Hurskainen H, Saari T, Hernesniemi J, Vapalahti M. Outcomes of early endovascular versus surgical treatment of ruptured cerebral aneurysms: A prospective randomized study. *Stroke*. 2000;31:2369-2377
2. Bendel P, Koivisto T, Äikiä M, Niskanen E, Könönen M, Hänninen T, et al. Atrophic enlargement of csf volume after subarachnoid hemorrhage: Correlation with neuropsychological outcome. *American Journal of Neuroradiology*. 2010;31:370-376
3. de Bresser J, Schaafsma JD, Luitse MJ, Viergever MA, Rinkel GJ, Biessels GJ. Quantification of structural cerebral abnormalities on mri 18 months after aneurysmal subarachnoid hemorrhage in patients who received endovascular treatment. *Neuroradiology*. 2015;57:269-274
4. de Bresser J, Vincken KL, Kaspers AJ, Rinkel GJ, Viergever MA, Biessels GJ. Quantification of cerebral volumes on mri 6 months after aneurysmal subarachnoid hemorrhage. *Stroke*. 2012;43:2782-2784
5. Sidaros A, Skimminge A, Liptrot MG, Sidaros K, Engberg AW, Herning M, et al. Long-term global and regional brain volume changes following severe traumatic brain injury: A longitudinal study with clinical correlates. *NeuroImage*. 2009;44:1-8
6. Tate DF, Khedraki R, Neeley ES, Ryser DK, Bigler ED. Cerebral volume loss, cognitive deficit, and neuropsychological performance: Comparative measures of brain atrophy: Ii. Traumatic brain injury. *Journal of the International Neuropsychological Society*. 2011;17:308-316
7. Trivedi MA, Ward MA, Hess TM, Gale SD, Dempsey RJ, Rowley HA, et al. Longitudinal changes in global brain volume between 79 and 409 days after traumatic brain injury: Relationship with duration of coma. *J Neurotrauma*. 2007;24:766-771
8. Hartings JA, York J, Carroll CP, Hinzman JM, Mahoney E, Krueger B, et al. Subarachnoid blood acutely induces spreading depolarizations and early cortical infarction. *Brain*. 2017;140:2673-2690
9. Wardlaw JM, Easton VJ, Statham P. Which ct features help predict outcome after head injury? *Journal of Neurology, Neurosurgery & Psychiatry*. 2002;72:188-192
10. McMahon P, Hricik A, Yue JK, Puccio AM, Inoue T, Lingsma HF, et al. Symptomatology and functional outcome in mild traumatic brain injury: Results from the prospective track-tbi study. *J Neurotrauma*. 2014;31:26-33
11. Thurnher M. Brain ischemia - imaging in acute stroke. *Radiology Assistant*.
12. Tardif CL, Steele CJ, Lampe L, Bazin P-L, Ragert P, Villringer A, et al. Investigation of the confounding effects of vasculature and metabolism on computational anatomy studies. *Neuroimage*. 2017;149:233-243
13. Ellison RG, Ellison LT, Hamilton WF. Analysis of respiratory acidosis during anesthesia. *Annals of surgery*. 1955;141:375
14. Chen W, Abramowitz MK. Metabolic acidosis and the progression of chronic kidney disease. *BMC nephrology*. 2014;15:55
15. Uh J, Lin A-L, Lee K, Liu P, Fox P, Lu H. Validation of vaso cerebral blood volume measurement with positron emission tomography. *Magnetic Resonance in Medicine*. 2011;65:744-749
16. Hua J, Liu P, Kim T, Donahue M, Rane S, Chen JJ, et al. Mri techniques to measure arterial and venous cerebral blood volume. *NeuroImage*. 2019;187:17-31
17. Juttukonda MR, Donahue MJ. Neuroimaging of vascular reserve in patients with cerebrovascular diseases. *Neuroimage*. 2017
18. Smeeing DPJ, Hendrikse J, Petersen ET, Donahue MJ, de Vis JB. Arterial spin labeling and blood oxygen level-dependent mri cerebrovascular reactivity in cerebrovascular disease: A systematic review and meta-analysis. *Cerebrovascular Diseases*. 2016;42:288-307
19. Amemiya S, Kunimatsu A, Saito N, Ohtomo K. Impaired hemodynamic response in the ischemic brain assessed with bold fmri. *Neuroimage*. 2012;61:579-590
20. Bokkers RPH, van Laar PJ, van de Ven KCC, Kapelle LJ, Klijn CJM, Hendrikse J. Arterial spin-labeling mr imaging measurements of timing parameters in patients with a carotid artery occlusion. *American Journal of Neuroradiology*. 2008;29:1698-1703

21. Mutsaerts HJMM, Petr J, Václavů L, van Dalen JW, Robertson AD, Caan MW, et al. The spatial coefficient of variation in arterial spin labeling cerebral blood flow images. *Journal of Cerebral Blood Flow & Metabolism*. 2017;37:3184-3192
22. Dai W, Fong T, Jones RN, Marcantonio E, Schmitt E, Inouye SK, et al. Effects of arterial transit delay on cerebral blood flow quantification using arterial spin labeling in an elderly cohort. *Journal of Magnetic Resonance Imaging*. 2017;45:472-481
23. Lee Y, Kim T. Assessment of hypertensive cerebrovascular alterations with multiband look–locker arterial spin labeling. *Journal of Magnetic Resonance Imaging*. 2018;47:663-672
24. Zaharchuk G, Bammer R, Straka M, Shankaranarayan A, Alsop DC, Fischbein NJ, et al. Arterial spin-label imaging in patients with normal bolus perfusion-weighted mr imaging findings: Pilot identification of the borderzone sign. *Radiology*. 2009;252:797-807
25. Veldeman M, Höllig A, Clusmann H, Stevanovic A, Rossaint R, Coburn M. Delayed cerebral ischaemia prevention and treatment after aneurysmal subarachnoid haemorrhage: A systematic review. *BJA: British Journal of Anaesthesia*. 2016;117:17-40
26. de la Torre JC. Is alzheimer's disease a neurodegenerative or a vascular disorder? Data, dogma, and dialectics. *The Lancet Neurology*. 2004;3:184-190
27. Weller RO, Preston SD, Subash M, Carare RO. Cerebral amyloid angiopathy in the aetiology and immunotherapy of alzheimer disease. *Alzheimer's Research & Therapy*. 2009;1:6
28. Di Marco LY, Farkas E, Martin C, Venneri A, Frangi AF. Is vasomotion in cerebral arteries impaired in alzheimer's disease? *Journal of Alzheimer's Disease*. 2015;46:35-53
29. Boraxbekk C-J, Salami A, Wåhlin A, Nyberg L. Physical activity over a decade modifies age-related decline in perfusion, gray matter volume, and functional connectivity of the posterior default-mode network—a multimodal approach. *Neuroimage*. 2016;131:133-141
30. Ainslie PN, Cotter JD, George KP, Lucas S, Murrell C, Shave R, et al. Elevation in cerebral blood flow velocity with aerobic fitness throughout healthy human ageing. *The Journal of physiology*. 2008;586:4005-4010
31. Intzandt B, Sabra D, Foster C, Desjardins-Crépeau L, Hoge R, Steele CJ, et al. Enhanced fitness relates to reduced cerebrovascular reactivity and perfusion in a sample of very healthy older adults. *bioRxiv*. 2018:444208
32. Luckhaus C, Flüß MO, Wittsack H-J, Grass-Kapanke B, Jänner M, Khalili-Amiri R, et al. Detection of changed regional cerebral blood flow in mild cognitive impairment and early alzheimer's dementia by perfusion-weighted magnetic resonance imaging. *Neuroimage*. 2008;40:495-503
33. Thomas BP, Yezhuvath US, Tseng BY, Liu P, Levine BD, Zhang R, et al. Life-long aerobic exercise preserved baseline cerebral blood flow but reduced vascular reactivity to co2. *Journal of Magnetic Resonance Imaging*. 2013;38:1177-1183
34. Chapman SB, Aslan S, Spence JS, DeFina LF, Keebler MW, Didehbani N, et al. Shorter term aerobic exercise improves brain, cognition, and cardiovascular fitness in aging. *Frontiers in aging neuroscience*. 2013;5:75
35. Hoffmann K, Sobol NA, Frederiksen KS, Beyer N, Vogel A, Vestergaard K, et al. Moderate-to-high intensity physical exercise in patients with alzheimer's disease: A randomized controlled trial. *Journal of Alzheimer's Disease*. 2016;50:443-453
36. Lu H, Clingman C, Golay X, Van Zijl PC. Determining the longitudinal relaxation time (t1) of blood at 3.0 tesla. *Magnetic Resonance in Medicine: An Official Journal of the International Society for Magnetic Resonance in Medicine*. 2004;52:679-682
37. Varela M, Hajnal JV, Petersen ET, Golay X, Merchant N, Larkman DJ. A method for rapid in vivo measurement of blood t1. *NMR in Biomedicine*. 2011;24:80-88
38. Li W, Liu P, Lu H, Strouse JJ, van Zijl PCM, Qin Q. Fast measurement of blood t1 in the human carotid artery at 3t: Accuracy, precision, and reproducibility. *Magnetic Resonance in Medicine*. 2017;77:2296-2302
39. Václavů L, van der Land V, Heijtel DFR, van Osch MJP, Cnossen MH, Majoie CBLM, et al. In vivo t1 of blood measurements in children with sickle cell disease improve cerebral blood flow quantification

from arterial spin-labeling mri. *American Journal of Neuroradiology*. 2016;37:1727
40. Clement P, Mutsaerts H-J, Václavů L, Ghariq E, Pizzini FB, Smits M, et al. Variability of physiological brain perfusion in healthy subjects–a systematic review of modifiers. Considerations for multi-center asl studies. *Journal of Cerebral Blood Flow & Metabolism*. 2018;38:1418-1437
41. McJury PhD M, Shellock PhD FG. Auditory noise associated with mr procedures: A review. *Journal of Magnetic Resonance Imaging*. 2000;12:37-45
42. Pierre EY, Grodzki D, Heismann B, Aandal G, Gulani V, Sunshine J, et al. Making mri scanning quieter: Optimized tse sequences with parallel imaging. *MAGNETOM Flash*. 2013;5:30-34
43. Alibek S, Vogel M, Sun W, Winkler D, Baker CA, Burke M, et al. Acoustic noise reduction in mri using silent scan: An initial experience. *Diagnostic and Interventional Radiology*. 2014;20:360
44. Corcuera-Solano I, Doshi A, Pawha PS, Gui D, Gaddipati A, Tanenbaum L. Quiet propeller mri techniques match the quality of conventional propeller brain imaging techniques. *American Journal of Neuroradiology*. 2015;36:1124-1127
45. Heismann B, Ott M, Grodzki D. Sequence-based acoustic noise reduction of clinical mri scans. *Magnetic Resonance in Medicine*. 2015;73:1104-1109
46. De Vis J, Zwanenburg J, van der Kleij L, Spijkerman J, Biessels G, Hendrikse J, et al. Cerebrospinal fluid volumetric mri mapping as a simple measurement for evaluating brain atrophy. *European radiology*. 2016;26:1254-1262
47. Mitchell AJ, Shiri-Feshki M. Rate of progression of mild cognitive impairment to dementia – meta-analysis of 41 robust inception cohort studies. *Acta Psychiatrica Scandinavica*. 2009;119:252-265
48. Belleville S, Fouquet C, Hudon C, Zomahoun HTV, Croteau J. Neuropsychological measures that predict progression from mild cognitive impairment to alzheimer's type dementia in older adults: A systematic review and meta-analysis. *Neuropsychology review*. 2017;27:328-353

Appendices

Nederlandse samenvatting

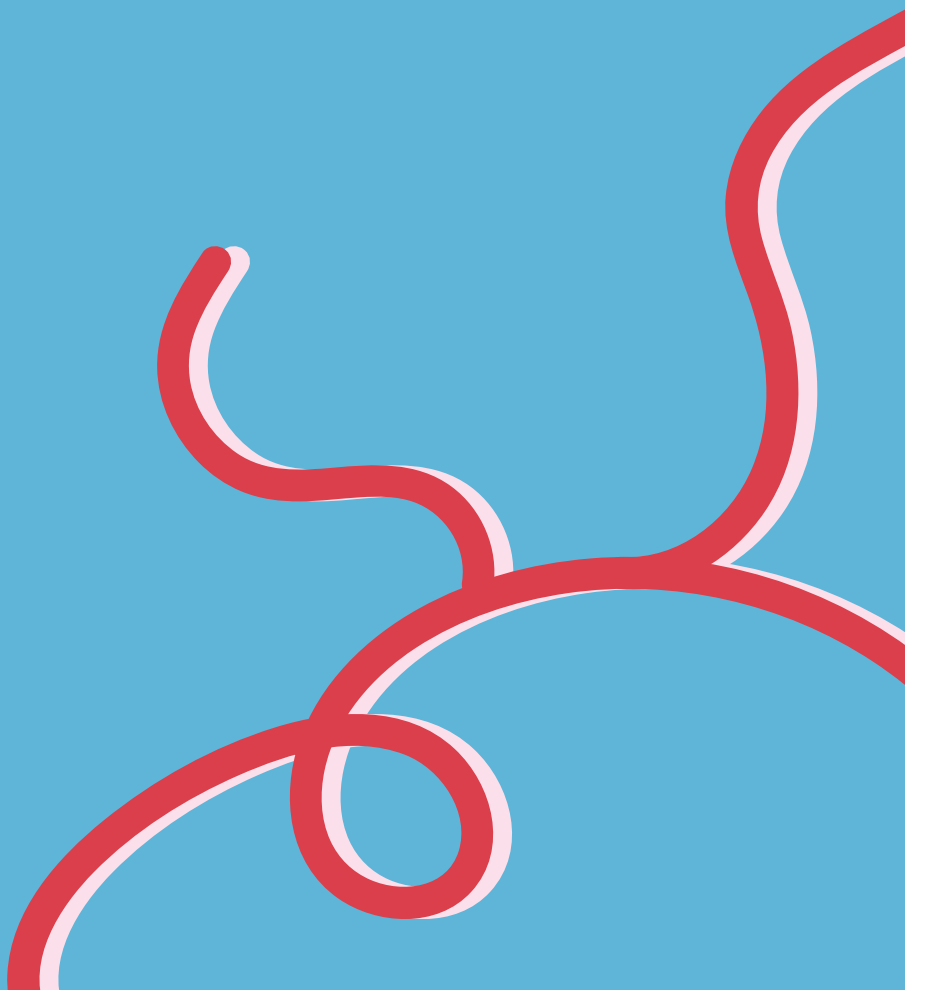

Het maken van beelden met magnetic resonance imaging (MRI) stelt ons in staat om binnen het levende menselijke lichaam te kijken. Ten opzichte van andere medische beeldvormingstechnieken blinken MRI-scans uit in het superieure contrast tussen verschillende type zachte weefsels; zo zijn in het brein de witte stof en de grijze stof duidelijk van elkaar te onderscheiden. Een ander voordeel van MRI is dat zowel de hersenstructuur als de hersenfunctie in beeld kunnen worden gebracht. Dankzij onophoudelijke ontwikkelingen en innovaties aan de hardware en de scansequenties blijven de mogelijkheden van MRI groeien.

MRI-beelden kunnen zowel kwalitatief als kwantitatief worden geanalyseerd en beoordeeld. In de dagelijkse patiëntenzorg wordt doorgaans een kwalitatieve beoordeling gemaakt door de radioloog. Een kwalitatieve beoordeling wordt op het oog gedaan en is daarom relatief snel, omdat het geen aanvullende beeldverwerking vereist. Kwalitatieve beoordelingen kunnen worden verwerkt in gevalideerde, semi-kwantitatieve scores om de bevindingen te categoriseren. Zo kan de mate van witte stof afwijkingen worden geplaatst op een score van 0 tot 3, waarmee de relatieve ernst kan worden aangegeven.[1] Een kwalitatieve beeldanalyse is vatbaar voor inter- en intrabeoordeler variatie, omdat ze afhankelijk is van de interpretatie en expertise van de beoordelaar. Dit betekent dat de beoordeling af kan wijken als dezelfde persoon de beelden op een ander tijdspunt beoordeelt (intrabeoordeelaar variatie) en dat de beoordelingen kunnen afwijken als twee personen hetzelfde beeld beoordelen (interbeoordelaar variatie). In vergelijking met een kwalitatieve aanpak vereist een kwantitatieve analyse weliswaar extra beeldverwerking, maar het maakt ook een objectievere en nauwkeurigere beoordeling, de identificatie van subtiele beeldaspecten, en het poolen van data mogelijk. In dit proefschrift heb ik me gericht op drie geselecteerde kwantitatieve MRI-markers: de cerebrale doorbloeding, de transversale relaxatietijd (T2) van het perifere hersenvocht (*cerebrospinal fluid*, $T2_{pCSF}$) en breinvolume metingen. Breinvolume metingen en de cerebrale doorbloeding worden momenteel al veelvuldig gebruikt voor verschillende toepassingen. De $T2_{pCSF}$ is daarentegen een nieuwe marker die (nog) niet gebruikt wordt voor klinische toepassingen. Ik heb mij verder toegespitst op twee ziektebeelden die worden gekenmerkt door een slechte prognose: de subarachnoïdale hersenbloeding en cognitieve stoornissen/dementie. De onderzochte MRI-markers kunnen bijdragen aan een verbeterd inzicht in beide ziektebeelden en ze kunnen mogelijk patiënten identificeren die een groter risico lopen op toekomstige achtergang. Tenslotte zijn metingen van de cerebrale bloeding gebruikt als uitkomstmaat in gerandomiseerd klinisch interventieonderzoek.

Deel 1

Aneurysmatische subarachnoïdale bloeding

Deel 1 van dit proefschrift is gericht op toepassingen van de drie MRI-markers voor patiënten met een subarachnoïdale bloeding (SAB). Hoofdstukken 2 – 5 zijn toegespitst op een specifiek subtype, namelijk de aneurysmatische subarachoïdale bloeding (aSAB). Een aSAB wordt veroorzaakt door het barsten van een aneurysma, een uitstulping van de vaatwand, waardoor er bloed de ruimte instroomt onder het spinnewebvlies (arachnoidea) dat de hersenen omhult (Figuur 1).

Een SAB treft een relatief jonge populatie – de gemiddelde leeftijd is ongeveer 55 jaar – en draagt een slechte prognose: slechts 70% van de patiënten overleeft de eerste 90 dagen, en 60% van de overlevende patiënten kan een volledig zelfstandig dagelijks bestaan voortzetten.[2-4] Zelfs de patiënten die weer volledig zelfstandig functioneren ervaren dikwijls blijvende cognitieve klachten en een verminderde kwaliteit van leven.[5] Samengenomen zorgen aSAB's voor een grote last op patiënten, hun zorgverleners en de maatschappij. Niet alle risicofactoren die samenhangen met een slechtere uitkomst zijn te behandelen, zoals een hogere leeftijd van de patiënt of een grotere omvang van de bloeding.[6] Het ziekteverloop biedt echter ruimte voor preventieve behandelingen, omdat een deel van de hersenschade zich pas dagen of weken na de bloeding ontwikkelt. Het verloop na een SAB kan worden opgedeeld in grofweg drie fases vanaf het tijdstip van bloeding: de acute fase (≤72 uur), de subacute fase (72 uur – dag 21) en de chronische fase (>21 dagen). Ongeveer een kwart van de aSAB patiënten ontwikkelt aanvullende, vertraagde hersenschade in de subacute fase; dit vindt meestal plaats tussen dag 4 en 14 na het barsten van het aneurysma.[7-9]

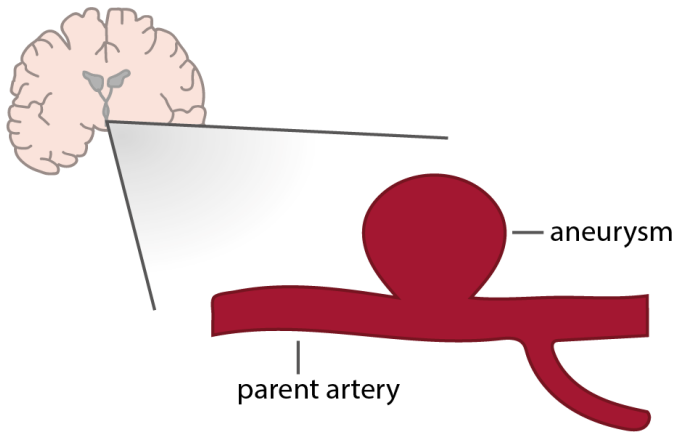

Fig. 1. Schematische weergave van een cerebraal, ballonvormig aneurysma. Een aneurysma bevindt zich meestal aan de onderkant van de hersenen bij de cirkel van Willis.

Voordat we kijken naar toepassingen voor de kwantitatieve MRI-markers, hebben we in de systematische reviews van hoofdstukken 2 en 3 de aanwezige hersenschade in elke fase in beeld gebracht. In **hoofdstuk 2** hebben we gekeken naar hersenschade door zuurstofgebrek (ischemische laesies) op diffusie-gewogen MRI-beelden. Diffusie-gewogen MRI is gevoelig voor vroege hersenschade, omdat het de daaraan verbonden verminderde mobiliteit van water detecteert.[10] Uit een meta-analyse van 13 studies werd vastgesteld dat ongeveer de helft van de patiënten ischemische laesie heeft in de acute (≤72 uur) en subacute (72 uur – 21 dagen) fases na een hersenbloeding. De klinische status bij binnenkomst in het ziekenhuis was gerelateerd aan laesies in de acute fase, terwijl het type aneurysma behandeling en de dag van de MRI-scan ten opzichte van de hersenbloeding gerelateerd waren aan de aanwezigheid van laesies in de subacute fase. In **hoofdstuk 3** laten we zien dat chronische infarcten en een verminderd breinvolume op MRI-scans samenhangen met een slechtere uitkomst na een aSAB (Figuur 2).

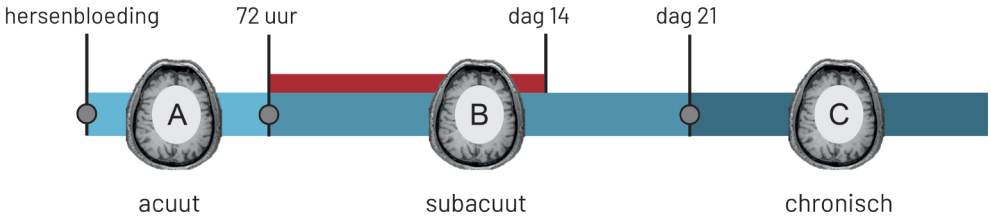

Fig. 2. Ziektestadia en tijdspunten voor beeldvorming na een subarachnoïdale bloeding (tijd niet op schaal). Op tijdpunt A kan hersenschade worden gevonden die het directe gevolg is van het barsten van het aneurysma, *early brain injury (EBI)* en, indien van toepassing, schade door de aneurysma behandeling. Op tijdspunt B kan zogenaamde *vertraagde* hersen*schade* worden aangetroffen. De periode met het hoogste risico voor vertraagde hersenschade is aangegeven met een rode markering tussen dag 4 en 14. Op tijdspunt C kunnen chronische infarcten en atrofie worden beoordeeld. Atrofie is het 'krimpen' van het brein door het afsterven van hersencellen.

Het doel van **hoofdstuk 4** was om te bepalen welke kenmerken in de acute en subacute fases een hoger risico meedragen voor langdurig verminderd breinvolume na een aSAB. We onderzoeken in deze studie het verband tussen perfusie heterogeniteit rond dag 14, klinische variabelen en breinvolume veranderingen tussen dag 14, 6 maanden en 18 maanden. Perfusie heterogeniteit betekent dat het brein niet gelijkmatig wordt doorbloed op de MRI-beelden, wat kan duiden op een verstoorde doorbloeding. Deze studie is gebaseerd op een aangetoonde correlatie tussen perfusie heterogeniteit, vertraagde schade (subacuut) en een slechte functionele uitkomst na een aSAB.[11, 12] Functionele uitkomst geeft mate van beperking aan die iemand ondervindt in het dagelijks functioneren. Het volumeverlies vanaf dag 14 was rond de 2% na 6 maanden en rond de 3.2% na 18 maanden. Hoofdstuk 4 laat zien dat perfusie heterogeniteit is gerelateerd aan een hogere mate van breinvolumeverlies. Aangezien er geneesmiddelen bestaan die de cerebrale doorbloeding verhogen, interpreteren we deze bevindingen als een mogelijk aangrijppunt om langdurige schade te beperken. **Hoofdstuk 5** beschrijft het

studieprotocol van een lopende fase II studie (*ASH-studie)* waarin we de effectiviteit en veiligheid van het medicijn acetazolamide onderzoeken bij behandeling van een aSAB. We veronderstellen dat acetazolamide aSAB patiënten kan helpen op drie manieren: het kan (1) de doorbloeding van het brein verhogen, (2) de productie van het hersenvocht verlagen en (3) cerebraal oedeem verminderen.[13-18]

Traumatisch hersenletsel

In **hoofstuk 6** passen we de bevindingen van hoofdstuk 4 toe in een andere studiepopulatie: patiënten met traumatisch hersenletsel (*traumatic brain injury, TBI*). Milde klinische symptomen na het letsel geven geen garantie op een volledig herstel, dus enkel de klinische status bij ziekenhuisopname is onvoldoende om te bepalen welke patiënten langdurig hinder zullen ondervinden van het trauma.[19] Een belangrijke onderzoeksvraag is daarom welke factoren zijn gerelateerd aan grotere chronische hersenschade. TBI en aSAB patiënten hebben een aantal overeenkomsten, waardoor we verwachtten dat de opgedane kennis van aSAB toegepast kan worden in TBI-patiënten. Ten eerste zijn patiënten met traumatisch hersenletsel ook relatief jong met een gemiddelde leeftijd van 60 (Verenigde Staten), hoewel net als bij aSAB mensen van alle leeftijden worden getroffen.[20] Ten tweede hebben ook TBI patiënten vaak een langdurig verminderd breinvolume. Ten derde is een verstoorde hersendoorbloeding gebruikelijk na TBI, en eerder onderzoek laat een verband zien tussen een gestoorde hersendoorbloeding in de acute en subacute fase en een chronisch verminderd breinvolume.[21, 22] Ten slotte is de aanwezigheid van subarachnoïdaal bloed gerelateerd aan een slechte functionele uitkomst.[23] Het verband tussen subarachnoïdaal bloed en breinvolume verlies na TBI is echter nog niet eerder aangetoond. In dit hoofdstuk laten we zien dat het breinvolume verlies tussen 1 en 90 dagen na trauma rond de 0.5% ligt voor TBI patiënten zonder subarachnoïdaal bloed, maar dat het rond de 3% is voor patiënten met subarachnoïdaal bloed. Onze resultaten tonen geen oorzakelijk verband aan, al bestaat er bewijs uit preklinische studies voor een causaal verband tussen subarachnoïdaal bloed en hersenschade. Aanvullende onderzoek is nodig om een mogelijk oorzakelijk verband aan te tonen tussen subarachnoïdaal bloed en verslechterde functionele uitkomst na traumatisch hersenletsel. De implicatie hiervan kan zijn dat hoewel subarachnoïdaal bloed doorgaans subtiel is op hersenscans, het kan bijdragen aan de identificatie van de 1 op 5 milde TBI patiënten die langdurige beperkingen ondervindt na traumatisch hersenletsel.

Deel 2

Het spectrum tussen cognitief gezond ouder worden en dementie

In slechts 160 jaar is de hoogste levensverwachting wereldwijd voor vrouwen gestegen van 45 jaar (Zweden) tot 85 jaar (Japan).[24, 25] Deze verhoogde levensverwachting betekent niet automatisch dat de oudere jaren worden doorgebracht in goede gezondheid: meer mensen krijgen te maken met ouderdomsziekten zoals dementie. [26, 27] Dit betekent dat de verouderende wereldbevolking een grote uitdaging vormt voor de 21e eeuw.[24] Het tweede deel van dit proefschrift onderzoekt de drie kwantitatieve MRI-markers voor patiënten in het spectrum dat loopt van gezonde ouderdom tot dementie.

Factoren die invloed hebben op de mate van gezond ouder worden kunnen worden opgedeeld in drie brede categorieën: fysiologisch, cognitief/mentaal en sociaal/steunnetwerk.[28] De hoofdstukken in dit proefschrift zijn gericht op de fysiologische factoren die samenhangen met (gezonde) ouderdom. Gedurende de levensloop zorgen verschillen in deze factoren voor een brede spreiding in de gezondheid tussen individuen met dezelfde chronologische leeftijd; een fenomeen dat wordt aangeduid als een verschil in biologische leeftijd.[29] Biologische leeftijd wordt gedefinieerd als verschillen in gezondheid en levensverwachting onder mensen met dezelfde chronologische leeftijd.[30] De studiepopulatie van **hoofdstuk 7** gaf ons de kans om verschillen te onderzoeken tussen thuiswonende ouderen met ongeveer dezelfde leeftijd: alle vrijwilligers waren tussen de 62 en 70 jaar oud.[31] Zo konden we de relatie onderzoeken van risicofactoren voor vaatziekten en fysieke fitheid met de cerebrale doorbloeding, zonder verstoring door het effect van leeftijd. Voor mannen en vrouwen waren er verschillende variabelen gerelateerd aan de cerebrale doorbloeding. Een onverwachte bevinding was dat in vrouwen de groep met de slechtste conditie de hoogste cerebrale doorbloeding hadden. Dit komt echter overeen met het idee dat een hoge doorbloeding van het brein zowel een teken kan zijn van goede cerebrovasculaire gezondheid als van compensatoire mechanismen binnen een staat van slechte cerebrovasculaire gezondheid.[32, 33] Desondanks is aangetoond dat het behouden van een goede fysieke conditie gedurende de levensloop en sportinterventies in gezonde ouderen zorgen voor een relatief hoge cerebrale doorbloeding.[34, 35]

In de volgende twee hoofdstukken stappen we over van een 'gezonde' oudere populatie naar studiepopulaties met cognitieve stoornissen om klinische toepassingen van de MRI-markers te onderzoeken. Meerdere studies hebben aangetoond dat cerebrale atrofie en cerebrale doorbloeding zijn gerelateerd aan de ernst van de ziekte en toekomstige cognitieve achteruitgang.[36-38] Wij verwachtten dat, net als de cerebrale doorbloeding, de $T2_{pCSF}$ kan wijzen op een verlaagde cerebrale energiebehoefte en cerebrovasculair disfunctioneren. Deze hypothese is gebaseerd op een eerdere studie

van onze onderzoeksgroep waarin een hogere $T2_{pCSF}$ werd gevonden in ouderen met dementie in vergelijking met gezonde ouderen.[39] Onze verklaring hierover is dat dit wordt veroorzaakt door een lagere zuurstofspanning van het perifere hersenvocht in de groep ouderen met dementie. In **hoofdstuk 8** onderzoeken we of $T2_{pCSF}$ extra informatie geeft ten opzichte van cerebrale atrofie en de cerebrale doorbloeding om ziekte ernst te bepalen in een cohort van patiënten die waren doorverwezen naar een geheugenpolikliniek.[40] We vonden hier een positief verband tussen $T2_{pCSF}$ met de ernst van de cognitieve stoornis, wat in overeenstemming is met onze eerdere studie. Vanuit een klinisch perspectief is het waardevol om een marker te hebben die toekomstige cognitieve achteruitgang kan voorspellen. Ter illustratie: enkel 1 uit 3 patiënten gediagnosticeerd met *Mild Cognitive Impairment (MCI)* ontwikkelt dementie, dus de andere 2 MCI patiënten zullen redelijke stabiel blijven in hun cognitieve klachten.[41] Het is van groot belang om te weten wat het ziekteverloop zal zijn voor de patiënt, de mantelzorger(s), de behandeld arts en klinisch geneesmiddelen onderzoek. In hoofdstuk 8 hebben we geen vervolgdata, dus we kunnen hier geen uitspraken over doen. Om de daadwerkelijke waarde van $T2_{pCSF}$ vast te stellen is daarom een grotere studie vereist die de patiënten over langere tijd volgt.

Hoofdstuk 9 onderzoekt het effect van 16 weken matig-tot-intensief sporten in patiënten met de ziekte van Alzheimer.[42] Onze resultaten laten zien dat hoewel de sportinterventie de conditie verbeterde van de proefpersonen, dit niet werd vertaald naar een verhoging van de cerebrale doorbloeding. Mogelijke verklaringen hiervoor zijn ofwel de lengte van de sportinterventie – mogelijk te kort om een effect te bereiken – of de vergevorderde ziekte van de proefpersonen. Persoonlijk denk ik dat de vergevorderde ziekte de belangrijkste verklaring is voor het afwezige effect. In de hoofdstudie werd alleen in de proefpersonen die het beste het sportprogramma volgende een vooruitgang gezien op bepaalde cognitieve domeinen.[43]

Deel 3

Methoden

De hoofdstukken in deel drie beschrijven gebruikte methoden in dit proefschrift. **Hoofdstuk 10** kan worden benut als naslagmateriaal voor metingen van de cerebrale doorbloeding met arterial spin labeling (ASL) MRI. ASL is een non-invasieve manier om de cerebrale doorbloeding te meten door gebruik te maken van ter nekhoogte gelabeld bloed als endogene tracer.[44] Dit hoofdstuk biedt een praktisch overzicht van ASL en laat verschillende onderzoeks- en klinische toepassingen zien. **Hoofdstuk 11** kan gebruikt worden als naslagwerk voor de hersenvocht (*CSF*) sequentie en de brein segmentatie software pakketten die worden gebruikt in dit proefschrift. Hier tonen we aan dat afgezien van de $T2_{pCSF}$ marker beschreven in hoofdstuk 8, de korte MRI-sequentie (1 minuut) ook kan worden gebruikt voor intracraniële volumemetingen. We laten zien dat de precisie en betrouwbaarheid van de verkregen volumes met de CSF MRI-sequentie vergelijkbaar zijn met conventionele segmentatiemethodes gebaseerd op 3DT1-gewogen beelden. **Hoofdstuk 12** onderzoekt de mogelijkheden van structurele MRI om breinvolume veranderingen te detecteren gedurende hypercapnie. Hypercapnie – verhoogde CO_2 niveaus in het bloed – zorgt voor het uitzetten van de vaten (vasodilatatie) en hiermee vergroot het cerebraal bloedvolume. [45] Burrow's correcte van de Monro-Kellie hypothese stelt dat een verhoging in het cerebrale bloedvolume gepaard gaat met wegvloeien van hersenvocht uit de schedel om een gelijkmatige intracraniële druk te behouden.[46] Geïnspireerd op de Monro-Kellie hypothese hebben we veranderingen gemeten in grijze stof, witte stof en het hersenvocht als reactie op bloedvolumeveranderingen gedurende hypercapnie. Het breinvolume nam toe met 6ml, wat gelijk staat aan ongeveer 0.6% van het totale breinvolume. Dit is te verklaren door het feit dat bloed een gelijksoortige signaalintensiteit heeft als het brein op 3DT1-gewogen beelden.[47] Het effect van bloedvolume op breinvolume metingen is van belang, omdat het kan voorkomen in een wijd scala aan omstandigheden; bijvoorbeeld anesthesie kan een effect hebben op het cerebrale bloedvolume.[48] Zodoende kan het nuttig zijn om bloedvolume metingen toe te voegen in breinvolumestudies waarin aanzienlijke verschillen in bloedvolume worden verwacht.[49, 50]

Een beknopt proefschrift overzicht

Aneurysmatische subarachnnoïdale bloeding

- De uiteenlopende gevonden laesieprevalentie tussen studies kan worden verklaard door a) het tijdstip van beeldvorming, b) klinische status bij ziekenhuisopname en c) de manier waarop de laesies zijn beoordeeld.
- Er kan geen nauwkeurige schatting worden gemaakt van het aantal te verwachten laesies in toekomstig onderzoek wegens de uiteenlopende laesieprevalentie op diffusie-gewogen MRI-beelden in de acute en subacute fases.
- Op de lange termijn zijn breinvolume veranderingen van een paar procent gebruikelijk.
- Verhoogde heterogeniteit van de cerebrale doorbloeding kan mogelijk helpen om patiënten te identificeren die het risico lopen op grotere breinvolume veranderingen.

Traumatisch hersenletsel

- Veranderingen in het breinvolume traden op in patiënten met een relatieve goede klinische status, wat duidt op ernstiger letsel dan de symptomen bij ziekenhuisopname suggereren.
- De aanwezigheid van subarachnoïdaal bloed bij traumatisch hersenletsel zou mee moeten worden genomen als risicofactor in toekomstig onderzoek en kan het doelwit zijn van behandeling.

Veroudering – dementie

- Te voorkomen risicofactoren voor vaatziekten en fysieke fitheid zijn geassocieerd met de cerebrale doorbloeding in oudere personen.
- Een meting of schatting van $T1_{bloed}$ kan een significant effect hebben op de resultaten van ASL MRI studies.
- De CSF MRI-sequentie toegespitst op het afbeelden van hersenvocht verschaft $T2_{pCSF}$ en atrofie metingen met slechts een minuut scantijd.
- De $T2_{pCSF}$ is gerelateerd aan cognitie in een studiecohort uit een geheugenpolikliniek.
- 16 weken matig-tot-intensief sporten had geen effect op de cerebrale doorbloeding in patiënten met milde tot matig-ernstige ziekte van Alzheimer.

Openstaande vragen voor vervolgonderzoek

- Is perfusie heterogeniteit in de subacute fase na een aneurysmatische subarachnoïdale bloeding geassocieerd met een slechtere cognitieve en functionele uitkomst?
- Is een subarachnoïdale bloeding bij traumatisch hersenletsel geassocieerd met een slechtere cognitieve en functionele uitkomst?
- Kan de $T2_{pCSF}$ toekomstige achteruitgang voorspellen in patiënten met een cognitieve stoornis?
- Hoe beïnvloed een sportinterventie van 1 jaar de cerebrale doorbloeding in vrijwilligers rond de 65 jaar? (LISA studie vervolg, data reeds verzameld)

Referenties

1. Fazekas F, Chawluk JB, Alavi A, Hurtig HI, Zimmerman RA. Mr signal abnormalities at 1.5 t in alzheimer's dementia and normal aging. *American journal of roentgenology*. 1987;149:351-356
2. Anderson C, Hankey G, Jamrozik K, Dunbabin D. Epidemiology of aneurysmal subarachnoid hemorrhage in australia and new zealand: Incidence and case fatality from the australasian cooperative research on subarachnoid hemorrhage study (across). *Stroke*. 2000;31:1843-1850
3. Vergouwen MDI, Jong-Tjien-Fa AV, Algra A, Rinkel GJE. Time trends in causes of death after aneurysmal subarachnoid hemorrhage. *A hospital-based study*. 2016;86:59-63
4. Zacharia BE, Hickman ZL, Grobelny BT, DeRosa P, Kotchetkov I, Ducruet AF, et al. Epidemiology of aneurysmal subarachnoid hemorrhage. *Neurosurgery Clinics*. 2010;21:221-233
5. Passier P, Visser-Meily J, van Zandvoort M, Rinkel G, Lindeman E, Post M. Predictors of long-term health-related quality of life in patients with aneurysmal subarachnoid hemorrhage. *NeuroRehabilitation*. 2012;30:137-145
6. Rosengart Axel J, Schultheiss Kim E, Tolentino J, Macdonald RL. Prognostic factors for outcome in patients with aneurysmal subarachnoid hemorrhage. *Stroke*. 2007;38:2315-2321
7. van Gijn J, Kerr RS, Rinkel GJE. Subarachnoid haemorrhage. *The Lancet*. 2007;369:306-318
8. Roos YBWEM, de Haan RJ, Beenen LFM, Groen RJM, Albrecht KW, Vermeulen M. Complications and outcome in patients with aneurysmal subarachnoid haemorrhage: A prospective hospital based cohort study in the netherlands. *Journal of Neurology, Neurosurgery & Psychiatry*. 2000;68:337-341
9. Connolly ES, Rabinstein Alejandro A, Carhuapoma JR, Derdeyn Colin P, Dion J, Higashida Randall T, et al. Guidelines for the management of aneurysmal subarachnoid hemorrhage. *Stroke*. 2012;43:1711-1737
10. Gass A, Ay H, Szabo K, Koroshetz WJ. Diffusion-weighted mri for the "small stuff": The details of acute cerebral ischaemia. *The Lancet Neurology*. 2004;3:39-45
11. Mustonen T, Koivisto T, Vanninen R, Hänninen T, Vapalahti M, Hernesniemi J, et al. Heterogeneity of cerebral perfusion 1 week after haemorrhage is an independent predictor of clinical outcome in patients with aneurysmal subarachnoid haemorrhage. *Journal of Neurology, Neurosurgery & Psychiatry*. 2008;79:1128-1133
12. Lanterna LA, Lunghi A, Martchenko S, Gritti P, Bonaldi G, Biroli F. Cerebral watershed hypoperfusion in subarachnoid hemorrhage: Computed tomography perfusion analysis. 2011;114:961
13. Bokkers RP, van Osch MJ, Klijn CJ, Kappelle LJ, Hendrikse J. Cerebrovascular reactivity within perfusion territories in patients with an internal carotid artery occlusion. *J Neurol Neurosurg Psychiatry*. 2011;82:1011-1016
14. Bartsch P, Swenson ER. Clinical practice: Acute high-altitude illnesses. *N Engl J Med*. 2013;368:2294-2302
15. Jafarzadeh F, Field ML, Harrington DK, Kuduvalli M, Oo A, Kendall J, et al. Novel application of acetazolamide to reduce cerebrospinal fluid production in patients undergoing thoracoabdominal aortic surgery. *Interact Cardiovasc Thorac Surg*. 2014;18:21-26
16. Gao F, Zheng M, Hua Y, Keep RF, Xi G. Acetazolamide attenuates thrombin-induced hydrocephalus. *Acta Neurochir Suppl*. 2016;121:373-377
17. Faraci FM, Mayhan WG, Heistad DD. Vascular effects of acetazolamide on the choroid plexus. *J Pharmacol Exp Ther*. 1990;254:23-27
18. Sturdivant NM, Smith SG, Ali SF, Wolchok JC, Balachandran K. Acetazolamide mitigates astrocyte cellular edema following mild traumatic brain injury. *Scientific Reports*. 2016;6:33330
19. McMahon P, Hricik A, Yue JK, Puccio AM, Inoue T, Lingsma HF, et al. Symptomatology and functional outcome in mild traumatic brain injury: Results from the prospective track-tbi study. *J Neurotrauma*. 2014;31:26-33
20. DiMaggio C, Ayoung-Chee P, Shinseki M, Wilson C, Marshall G, Lee DC, et al. Traumatic injury in the united states: In-patient epidemiology 2000–2011. *Injury*. 2016;47:1393-1403
21. Bendinelli C, Cooper S, Evans T, Bivard A, Pacey D, Parson M, et al. Perfusion abnormalities are frequently detected by early ct perfusion and predict unfavourable outcome following severe traumatic

brain injury. *World Journal of Surgery*. 2017;41:2512-2520
22. Xu Y, McArthur DL, Alger JR, Etchepare M, Hovda DA, Glenn TC, et al. Early nonischemic oxidative metabolic dysfunction leads to chronic brain atrophy in traumatic brain injury. *J Cereb Blood Flow Metab*. 2010;30:883-894
23. Wardlaw JM, Easton VJ, Statham P. Which ct features help predict outcome after head injury? *Journal of Neurology, Neurosurgery & Psychiatry*. 2002;72:188-192
24. World Health Organization. *World report on ageing and health*. World Health Organization; 2015.
25. Oeppen J, Vaupel JW. Broken limits to life expectancy. *Science*. 2002;296:1029-1031
26. Prince M, Bryce R, Albanese E, Wimo A, Ribeiro W, Ferri CP. The global prevalence of dementia: A systematic review and metaanalysis. *Alzheimer's & Dementia*. 2013;9:63-75.e62
27. Ferrucci L, Giallauria F, Guralnik JM. Epidemiology of aging. *Radiologic Clinics of North America*. 2008;46:643-652
28. Hansen-Kyle L. A concept analysis of healthy aging. *Nursing Forum*. 2005;40:45-57
29. Mitnitski A, Howlett SE, Rockwood K. Heterogeneity of human aging and its assessment. *Journals of Gerontology Series A: Biomedical Sciences and Medical Sciences*. 2016;72:877-884
30. Chen BH, Marioni RE, Colicino E, Peters MJ, Ward-Caviness CK, Tsai P-C, et al. DNA methylation-based measures of biological age: Meta-analysis predicting time to death. *Aging (Albany NY)*. 2016;8:1844
31. Eriksen CS, Garde E, Reislev NL, Wimmelmann CL, Bieler T, Ziegler AK, et al. Physical activity as intervention for age-related loss of muscle mass and function: Protocol for a randomised controlled trial (the lisa study). *BMJ Open*. 2016;6:e012951
32. Intzandt B, Sabra D, Foster C, Desjardins-Crépeau L, Hoge R, Steele CJ, et al. Enhanced fitness relates to reduced cerebrovascular reactivity and perfusion in a sample of very healthy older adults. *bioRxiv*. 2018:444208
33. Luckhaus C, Flüß MO, Wittsack H-J, Grass-Kapanke B, Jänner M, Khalili-Amiri R, et al. Detection of changed regional cerebral blood flow in mild cognitive impairment and early alzheimer's dementia by perfusion-weighted magnetic resonance imaging. *Neuroimage*. 2008;40:495-503
34. Thomas BP, Yezhuvath US, Tseng BY, Liu P, Levine BD, Zhang R, et al. Life-long aerobic exercise preserved baseline cerebral blood flow but reduced vascular reactivity to co2. *Journal of Magnetic Resonance Imaging*. 2013;38:1177-1183
35. Chapman SB, Aslan S, Spence JS, DeFina LF, Keebler MW, Didehbani N, et al. Shorter term aerobic exercise improves brain, cognition, and cardiovascular fitness in aging. *Frontiers in aging neuroscience*. 2013;5:75
36. Jack Jr CR, Wiste HJ, Vemuri P, Weigand SD, Senjem ML, Zeng G, et al. Brain beta-amyloid measures and magnetic resonance imaging atrophy both predict time-to-progression from mild cognitive impairment to alzheimer's disease. *Brain*. 2010;133:3336-3348
37. Binnewijzend MA, Kuijer JP, Benedictus MR, van der Flier WM, Wink AM, Wattjes MP, et al. Cerebral blood flow measured with 3d pseudocontinuous arterial spin-labeling mr imaging in alzheimer disease and mild cognitive impairment: A marker for disease severity. *Radiology*. 2013;267:221-230
38. Chao LL, Buckley ST, Kornak J, Schuff N, Madison C, Yaffe K, et al. Asl perfusion mri predicts cognitive decline and conversion from mci to dementia. *Alzheimer Dis Assoc Disord*. 2010;24:19-27
39. De Vis J, Zwanenburg J, van der Kleij L, Spijkerman J, Biessels G, Hendrikse J, et al. Cerebrospinal fluid volumetric mri mapping as a simple measurement for evaluating brain atrophy. *European radiology*. 2016;26:1254-1262
40. Aalten P, Ramakers IH, Biessels GJ, de Deyn PP, Koek HL, OldeRikkert MG, et al. The dutch parelsnoer institute - neurodegenerative diseases; methods, design and baseline results. *BMC Neurology*. 2014;14:254
41. Mitchell AJ, Shiri-Feshki M. Rate of progression of mild cognitive impairment to dementia – meta-analysis of 41 robust inception cohort studies. *Acta Psychiatrica Scandinavica*. 2009;119:252-265
42. Hoffmann K, Frederiksen KS, Sobol NA, Beyer N, Vogel A, Simonsen AH, et al. Preserving cognition, quality of life, physical health and functional ability in alzheimer's disease: The effect of physical exercise (adex trial): Rationale and design. *Neuroepidemiology*. 2013;41:198-207

43. Hoffmann K, Sobol NA, Frederiksen KS, Beyer N, Vogel A, Vestergaard K, et al. Moderate-to-high intensity physical exercise in patients with alzheimer's disease: A randomized controlled trial. *Journal of Alzheimer's Disease*. 2016;50:443-453
44. Williams DS, Detre JA, Leigh JS, Koretsky AP. Magnetic resonance imaging of perfusion using spin inversion of arterial water. *Proceedings of the National Academy of Sciences*. 1992;89:212-216
45. Yoon S, Zuccarello M, Rapoport RM. Pco2 and ph regulation of cerebral blood flow. *Frontiers in physiology*. 2012;3:365
46. Burrows G. *An disorders of the cerebral circulation; and on the connection between affections of the brain and diseases of the heart*. Longman; 1846.
47. Tardif CL, Steele CJ, Lampe L, Bazin P-L, Ragert P, Villringer A, et al. Investigation of the confounding effects of vasculature and metabolism on computational anatomy studies. *Neuroimage*. 2017;149:233-243
48. Ellison RG, Ellison LT, Hamilton WF. Analysis of respiratory acidosis during anesthesia. *Annals of surgery*. 1955;141:375
49. Uh J, Lin A-L, Lee K, Liu P, Fox P, Lu H. Validation of vaso cerebral blood volume measurement with positron emission tomography. *Magnetic Resonance in Medicine*. 2011;65:744-749
50. Hua J, Liu P, Kim T, Donahue M, Rane S, Chen JJ, et al. Mri techniques to measure arterial and venous cerebral blood volume. *NeuroImage*. 2019;187:17-31

Publications

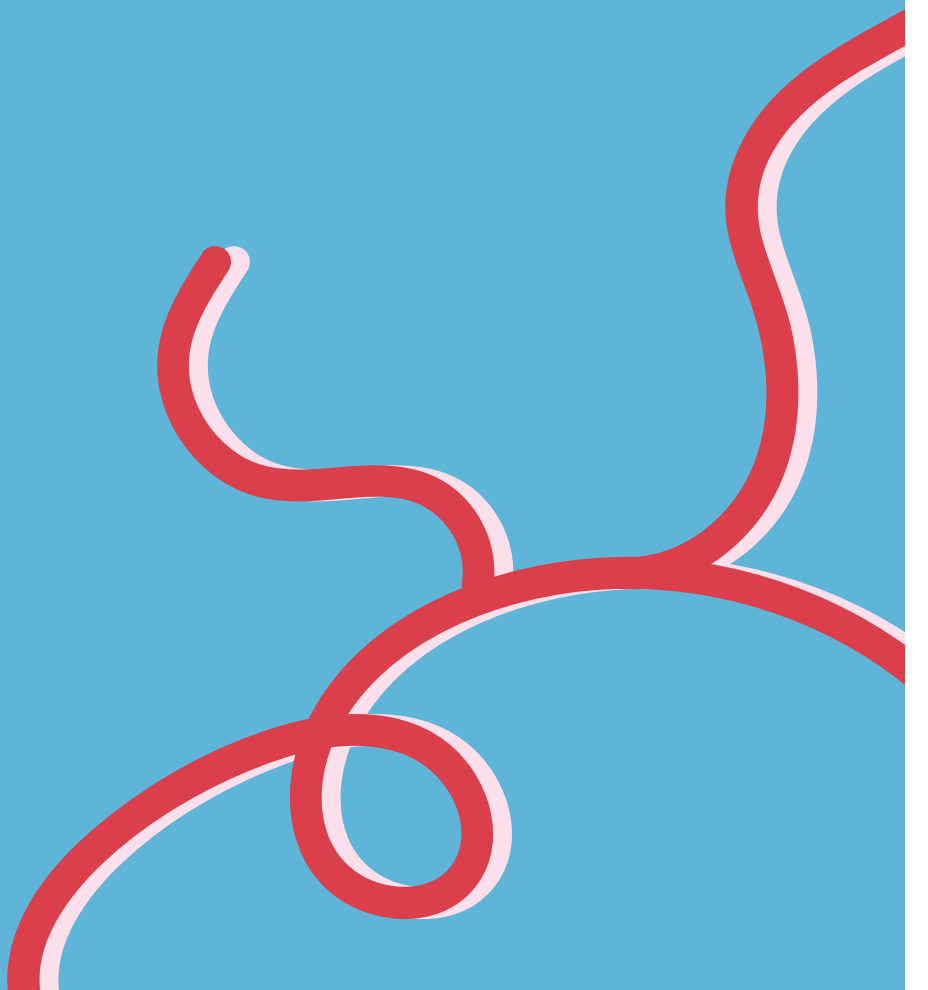

Published manuscripts

van der Kleij, L.A., Petersen, E.T., Siebner, H.R., Hendrikse, J., Frederiksen, K.S., Sobol, N.A., Hasselbalch, S.G., Garde, E. (2018). The effect of physical exercise on cerebral blood flow in Alzheimer's disease. NeuroImage: Clinical, 20, 650-654.

van der Kleij, L.A., & Petersen, E.T. (2018). ASL: Blood Perfusion Measurement Using Arterial Spin Labelling. In Quantitative MRI of the Brain (pp. 283-302). CRC Press.

Van der Kleij, L.A., de Bresser, J., Hendrikse, J., Siero, J.C.W., Petersen, E.T., De Vis, J.B. (2018). Fast CSF MRI for brain segmentation; Cross-validation by comparison with 3D T1-based brain segmentation methods. *PloS one*, *13*(4), e0196119.

Reijmer, Y.D., van den Heerik, M.S., Heinen, R., Leemans, A., Hendrikse, J., de Vis, J.B, **van der Kleij LA,** Lucci C, Hendriks ME, van Zandvoort MJE, Huenges Wajer IMC, Visser-Meily JMA, Rinkel GJE, Biessels GJ, Vergouwen , MDI. (2018). Microstructural White Matter Abnormalities and Cognitive Impairment After Aneurysmal Subarachnoid Hemorrhage. Stroke, 49(9), 2040-2045.

Stehouwer, B.L., **van der Kleij, L.A.,** Hendrikse, J., Rinkel, G.J.E., De Vis, J.B. (2018). Magnetic resonance imaging and brain injury in the chronic phase after aneurysmal subarachnoid hemorrhage: A systematic review. International Journal of Stroke, 13(1), 24-34.

Van Der Kleij, L.A., De Vis, J.B., Olivot, J.M., Calviere, L., Cognard, C., Zuithoff, N.P.A., Rinkel, G.J.E., Hendrikse, J., Vergouwen, M.D.I. (2017). Magnetic resonance imaging and cerebral ischemia after aneurysmal subarachnoid hemorrhage: a systematic review and meta-analysis. Stroke, 48(1), 239-245.

De Vis, J.B., Zwanenburg, J.J., **van der Kleij, L.A.**, Spijkerman, J.M., Biessels, G.J., Hendrikse, J., Petersen, E.T. (2016). Cerebrospinal fluid volumetric MRI mapping as a simple measurement for evaluating brain atrophy. European radiology, 26(5), 1254-1262.

van der Kleij, L.A., Jones, A.R., Steen, I.N., Young, C.A., Shaw, P.J., Shaw, C.E., Leigh, P.N., Turner, M.R., Al-Chalabi, A. (2015). Regionality of disease progression predicts prognosis in amyotrophic lateral sclerosis. Amyotrophic Lateral Sclerosis and Frontotemporal Degeneration, 16(7-8), 442-447.

Submitted manuscripts

L.A. van der Kleij, C. Lucci, T.D. Witkamp, M.D.I. Vergouwen, G.J.E. Rinkel, J. Hendrikse, E.T. Petersen, J.B. De Vis. Subacute perfusion impairment is related to long-term brain parenchymal volume loss after subarachnoid hemorrhage.

L.A. van der Kleij, M.D.I. Vergouwen, I.C. van der Schaaf, J.C.W. Siero, G.J.E. Rinkel, J.B. De Vis, J. Hendrikse. Acetazolamide in aneurysmal Subarachnoid Haemorrhage (ASH): study protocol of a phase II randomized controlled trial.

L.A. van der Kleij, J.B. De Vis, M.C. Restivo, L.C. Turtzo, J. Hendrikse, L.L. Latour. Subarachnoid hemorrhage and cerebral perfusion are associated with brain volume decrease after

traumatic brain injury.

L.A. van der Kleij, J.B. De Vis, J. de Bresser, J. Hendrikse, J.C.W.Siero. Arterial CO2 pressure changes during hypercapnia are associated with changes in brain parenchymal volume.

Manuscripts in preparation

L.A. van der Kleij, N.L. Højland Reislev, C.S. Eriksen, H.R. Siebner, C.-J. Boraxbekk, E.L. Mortensen, M. Kjaer, E. Garde, E.T. Petersen. Is cerebral blood flow affected by preventable vascular risk factors and physical fitness level?.

L.A. van der Kleij, E.T. Petersen, J.H. Verwer, J. Hendrikse, G.J. Biessels, J.B. De Vis. Transverse relaxation time of CSF in the peripheral subarachnoid space reflects cognition in a memory clinic cohort.

Conference presentations (first author only)

Perfusion and brain volume loss after traumatic brain injury. L.A. van der Kleij, J.B. De Vis, M.C. Restivo, C.L. Turtzo, J. Hendrikse, L.L. Latour. ISMRM 27th Annual Meeting, Montreal, Canada, May 11-16, 2019 (digital poster presentation).

I**s cerebral blood flow affected by preventable neurovascular risk factors and physical fitness level?** L.A. van der Kleij, N.L. Højland Reislev, C.S. Eriksen, H.R. Siebner, C.-J. Boraxbekk, E.L. Mortensen, M. Kjaer, E.T. Petersen, E. Garde. ISMRM 27th Annual Meeting, Montréal, Canada, May 11-6,2019 (digital poster presentation).

Lower oxygenation in the peripheral subarachnoid space reflects decreased cerebral blood flow in dementia-related brain structures. L.A. van der Kleij, I.M.J. Kant, G.J. Biessels, J. Hendrikse, E.T. Petersen, J.B. De Vis. ISMRM 26th Annual Meeting, Paris, France, June 16-21, 2018 (oral presentation).

Decreased borderzone perfusion is related to brain parenchymal volume loss after subarachnoid hemorrhage. L.A. van der Kleij, C. Lucci, E.T. Petersen, M.D.I. Vergouwen, G.J.E. Rinkel, J. Hendrikse and J.B. De Vis. ISMRM 25th Annual Meeting, Honolulu, Hawaii, U.S.A., April 22-27, 2017 (multi-media electronic poster presentation).

The effect of physical exercise on cerebral blood flow in Alzheimer's disease. L.A. van der Kleij, E.T. Petersen, H.R. Siebner, J. Hendrikse, K.S. Frederiksen, N.A.Sobol, S.G. Hasselbalch, E. Garde. 2nd Congress of the European Academy of Neurology (EAN), Copenhagen, Denmark, May 28-31, 2016 (digital poster presentation).

Cross-validation of a CSF MRI sequence for calculating brain volume by comparison with brain segmentation methods. L.A. van der Kleij, J. de Bresser, E.T. Petersen, J. Hendrikse, and J.B. De Vis. ISMRM, Singapore, Republic of Singapore, May 7-13, 2016 (poster presentation).

The effect of physical exercise on cerebral blood flow in Alzheimer's disease. L.A. van der Kleij, E.T. Petersen, H.R. Siebner, J. Hendrikse, K.S. Frederiksen, N.A.Sobol, S.G. Hasselbalch, E. Garde. ISMRM, Singapore, Republic of Singapore,May 7-13, 2016 (poster presentation).

Dankwoord

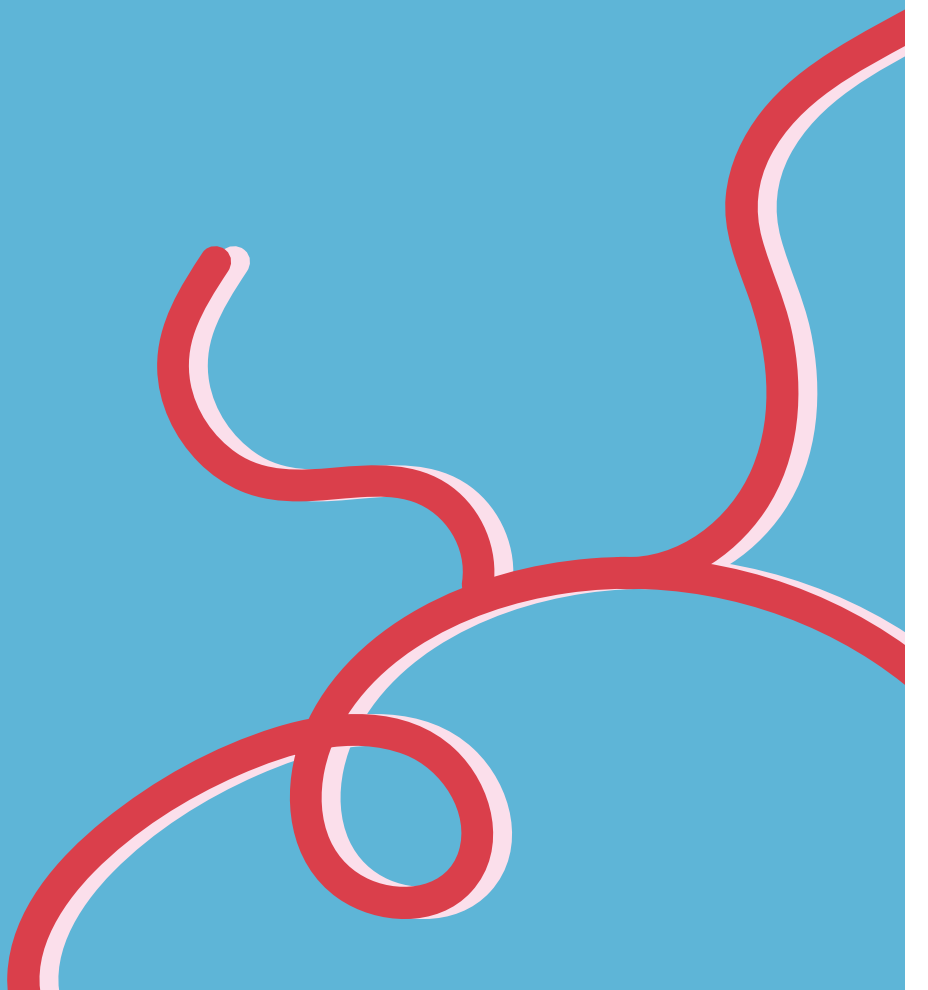

Beste lezer,

Dit proefschrift is tot stand gekomen dankzij vele mensen. In de eerste plaats wil ik de patiënten en vrijwilligers bedanken voor hun deelname aan de studies dit proefschrift. Het onderzoek in dit proefschrift is gedreven door de ambitie om hun vertrouwen om te zetten naar een waardevolle, integere bijdrage aan het wetenschappelijke discours.

Prof. Jeroen Hendrikse, je bezit over een buitengewoon groot enthousiasme en een onuitputtelijke stroom aan ideeën. Achter een ogenschijnlijke nonchalance zitten radertjes die altijd draaien: je bent continu bezig met nieuwe projecten en de onderzoekslijnen van de toekomst. Bovenal ben je ook de man van de verbinding: je kent iedereen – van stagiair tot hoogleraar – en iedereen kent jou. Ondanks je drukke agenda kon ik altijd laagdrempelig bij je terecht, bedankt daarvoor. Ik wil je ook bedanken voor je vrijgevigheid in het delen van mogelijkheden en middelen. Ik heb hierdoor het beste uit mezelf en onze onderzoeksprojecten kunnen halen. Bovenal wil ik je bedanken voor het grote vertrouwen dat je mij vanaf dag één hebt geschonken.

Dr. Jill De Vis, ik had me geen betere co-promotor kunnen wensen. Je bent zowel een uitmuntende, gedreven wetenschapper als een persoonlijk betrokken, bevlogen begeleider. Ik genoot van je ambitie, de snelle en leerzame feedback en de lange skype gesprekken. Na anderhalf jaar vertrok je uit Nederland voor een Amerikaans vervolg van je wetenschappelijke- en medische carrière. Het tijdzoneverschil bleek soms zelfs een voordeel te zijn: 's avonds een stuk wegsturen naar de V.S. en de volgende ochtend door met de verbeterde versie. Buiten de opgebouwde academische band, heb ik genoten van alle mooie momenten samen met jou en Matthew, met jullie bruiloft als hoogtepunt.

Dr. Esben Petersen, you were the technical MRI/ASL expert and the steady, calm rock of my supervision team. I greatly enjoyed our time behind the computer spent coding and having interesting discussions, which were regularly continued over a beer. You taught me a lot through your in-depth knowledge of both technical and clinical concepts. Also a warm thank you to Natalia for making my visits to Denmark extra memorable with the evenings around the family dinner table and in the garden.

Graag wil ik de leden van de beoordelingscommissie bedanken voor de tijd en moeite die zij hebben gestoken in het lezen van dit proefschrift: prof. Klomp, prof. Van Osch, prof. Rinkel, prof. Velthuis en prof. Van der Zwan.

Dit proefschrift is voortgekomen uit een nauwe samenwerking met de afdeling Neurologie. Dr. Mervyn Vergouwen, bedankt voor de fijne samenwerking de afgelopen jaren bij de hoofdstukken over subarachnoïdale bloedingen. Je bent hoofdonderzoeker bij de ASH studie en *senior author* voor hoofdstuk 2, beide uitdagende projecten waarin ik veel van je heb mogen leren. Prof. Gabriel Rinkel bedankt voor je actieve

betrokkenheid bij hoofdstukken 2 – 5, zowel voor de sturing in de praktische uitvoering als je omvangrijke kennis over subarachnoïdale bloedingen. Prof. Geert-Jan Biessels, bedankt voor de leerzame input en interessante discussies die ten grondslag liggen aan hoofdstuk 8. Mijn dank gaat ook uit naar alle (research) verpleegkundigen die de uitvoering van de patiënten studies mogelijk maakten.

Binnen de afdeling Radiologie: beste dr. Jeroen Siero, bedankt voor de aangename samenwerking, je enthousiasme en onvoorwaardelijke hulp. Beste dr. Jeroen de Bresser, bedankt voor je expertise bij de segmentatiehoofdstukken en prettige samenwerking. Beste dr. Irene van der Schaaf, bedankt voor de fijne samenwerking aan de ASH studie. Mijn dank aan de laboraten voor hun hulp bij de (soms uitdagende) scansessies. In het bijzonder wil ik Niels Blanken bedanken, dankzij jouw hulp waren alle scanner gerelateerde uitdagingen zo opgelost.

Mijn dank gaat ook uit naar de mensen van het Trialbureau, het Technisch Cluster, de Multimedia-afdeling, de apotheek Klinisch Geneesmiddelenonderzoek en de secretaresses van het stafsecretariaat.

Dear DRCMR group, thank you the interesting collaborations and hospitality. I remain impressed by the ambitious cohort studies you conduct, which provide valuable data on aging and dementia. I came to love the Danish approach to life, the Copenhagen aesthetic and the Danish pastries. Thank you for making my regular visits so enjoyable.

Dear Prof. Larry Latour, and the NIH group, thank you for my wonderful research stay at the acute cerebrovascular diagnostics unit. I found the group's active dedication to improving patient care through research deeply inspiring. You gave me the warmest introduction to Washington D.C. that I could have hoped for.

Dear Radiology and 7T group, thank you for the past years. Whatever the question, help was always quickly available. I feel lucky to have spent each with you at the UMC offices, and at dinners, bars, sailboats, (exotic) conference locations (…and the list goes on).

Lieve vrienden, bedankt voor alle mooie momenten, de zin en de onzin tijdens dit PhD hoofdstuk. Jullie hebben de afgelopen jaren onvergetelijk gemaakt. For the non-Dutch speaking friends: a massive thank you for sharing and celebrating the ride with me. It has been an incredible few years because of you.

Ten slotte wil ik mijn familie bedanken voor de oneindig liefdevolle en solide basis waarop ik mijn dromen kan bouwen. Als de afgelopen jaren iets hebben bewezen, is dat we samen alles aankunnen.

Lisa Annette van der Kleij was born on the 13th of November 1990 in Den Haag, the Netherlands. She grew up in Nootdorp with her parents Ruud and Marga, and her sister Sabine. After completing secondary school at the Huygenslyceum in Voorburg, she enrolled in the Liberal Arts and Sciences program of University College Utrecht. There, she followed a range of courses with a focus on life sciences, neuroscience and linguistics. As part of the curriculum she completed an exchange semester at Monash University, Melbourne, Australia. In 2012 she obtained her Bachelor of Science degree cum laude. Thereafter she moved to the North-East of Thailand to teach English in the community center of the ISARA foundation and the public school of Banguad, a small village. Next, she moved to London, U.K. to obtain a master's degree in Clinical Neuroscience from the Institute of Psychiatry, Psychology and Neuroscience at King's College. She graduated cum laude (with distinction) in 2014. After graduating, she started her PhD program in January 2015 at the department of Radiology at the University Medical Center Utrecht under the supervision of Dr. De Vis, Dr. Petersen and Prof. Hendrikse. In this work she explored clinical applications of three selected quantitative MRI markers for patients with subarachnoid hemorrhage and in healthy/pathological aging.